SKBF
KBS
TEKNISK
RAPPORT
80-15

Aluminium oxide as an encapsulation material for unreprocessed nuclear fuel waste – evaluation from the viewpiont of corrosion

Final Report 1980-03-19
Swedish Corrosion Institute and its reference group

SVENSK KÄRNBRÄNSLEFÖRSÖRJNING AB / PROJEKT KÄRNBRÄNSLESÄKERHET

POSTADRESS: Kärnbränslesäkerhet, Box 5864, 102 48 Stockholm, Telefon 08-67 95 40

ALUMINIUM OXIDE AS AN ENCAPSULATION MATERIAL FOR UNREPROCESSED NUCLEAR FUEL WASTE - EVALUATION FROM THE VIEWPOINT OF CORROSION

Final Report 1980-03-19

Swedish Corrosion Institute and its reference group

A list of other reports published in this series is attached at the end of this report. Information on KBS technical reports from 1977-1978 (TR 121) and 1979 (TR 79-28) is available through SKBF/KBS.

THE SWEDISH CORROSION INSTITUTE
Einar Mattsson
1980-01-17

DOCUMENTS INCLUDED IN THE REPORT

Final report of the reference group:

ALUMINIUM OXIDE AS AN ENCAPSULATION MATERIAL FOR UNREPROCESSED NUCLEAR FUEL WASTE - EVALUATION FROM THE VIEWPOINT OF CORROSION

- Basis for evaluation of life of aluminium oxide canister for spent fuel. KBS. Appendix A
- Corrosion of aluminium oxide in aqueous solutions - a review of the literature. Roger Carlsson and Sven Karlsson. Appendix B
- Corrosion rate of Al_2O_3 in aqueous solutions from 25-350°C. W S Fyfe. Appendix C
- Studies of the durability of alumina in water. L Hydén. Appendix D
- Residual stresses, defects and calculated life of synthetic corundum canisters. B Larsson. Appendix E
- Calculated life of container of aluminium oxide. J Carlsson. Appendix F
- Statement of comment on ASEA's study entitled "Residual stresses, defects and calculated life of aluminium oxide container". L Hermansson, R Carlsson. Appendix G 1

  Supplementary statement concerning delayed failure in aluminium oxide containers. L Hermansson, R Carlsson. Appendix G 2
- Letter of 1979-03-19. Sh M Wiederhorn. Appendix H
- Life prediction of alumina canisters. A G Evans. Appendix I 1

  Letter of 1979-12-13. A G Evans. Appendix I 2
- Special statement. G Wranglén.

ALUMINA AS CANISTER MATERIAL FOR UNREPROCESSED NUCLEAR WASTE - EVALUATION WITH RESPECT TO CORROSION

Final report 1980-03-19

The Swedish Corrosion Institute and its Reference Group

SUMMARY

To fulfil the requirements of the so-called "Stipulation Law" the Nuclear Fuel Safety Project (KBS) has proposed that spent unreprocessed nuclear fuel shall be disposed of by encapsulation in canisters of high-purity alumina sintered under isostatic pressure. The canisters will have a wall thickness of 100 mm and are to be placed in vertical boreholes extending from horizontal tunnels 500 m below ground in igneous rock. In each borehole one canister is deposited embedded in a quartz sand/ bentonite buffer.

The Swedish Corrosion Institute has been assigned the task of evaluating this proposal from the viewpoint of corrosion and of estimating the life of the canisters under the given conditions. To do this work, the Swedish Corrosion Institute has appointed an expert group of 10 Swedish specialists, mainly from the fields of corrosion and materials technology. The expert group arrived at the following conclusions. With one exception (G. Wranglén) the group was unanimous in its evaluation.

The alumina is not thermodynamically stable in water. In pure water hydration will occur, below 100° C leading to the formation of either $Al(OH)_3$ in the amorphous state or crystalline gibbsite ($Al_2O_3 \cdot 3H_2O$). Corrosion may take place by slow dissolution or flaking off of a surface layer. Various immersion tests showed that the corrosion rate will be less than 0.1 µm/year, probably one or two powers of ten lower.

If the alumina canister in the storage has sufficiently large surface defects and is under sufficiently high mechanical tension the defects may grow slowly into propagating cracks, ultimately leading to fracture, so-called delayed fracture. On the basis of results from fracture

mechanical studies and after introduction of safety factors with respect to possible unknown features of the delayed fracture it was judged possible to eliminate the risk of delayed fracture if the canisters pass the following production control:

- Proof testing at 150 MN/m^2, using acoustic emission technique to ensure that crack growth does not occur during the unstressing cycle.
- Surface acoustic wave examination with respect to surface inclusions, canisters with inclusions larger than 100 µm within a 100 µm deep surface zone being rejected.

Canisters which pass the production control mentioned are estimated to have a life of hundreds of thousands of years, or probably considerably more, under the conditions specified.

It may be questioned whether the very hard production control prescribed is reasonable. As the knowledge of delayed fracture in ceramics will increase, however, it will certainly be possible to relax the conservative requirements.

SWEDISH CORROSION INSTITUTE
1980-03-19

ALUMINIUM OXIDE AS AN ENCAPSULATION MATERIAL FOR UNREPROCESSED NUCLEAR FUEL WASTE - EVALUATION FROM THE VIEWPOINT OF CORROSION

1. BACKGROUND

The Stipulations Act passed by the Swedish Parliament provides that the power producers must demonstrate:

- either how and where an absolutely safe final storage of reprocessed waste can be effected
- or how and where an absolutely safe final storage of the unreprocessed spent nuclear fuel can be effected.

In order to gather data for the final account of the final storage scheme, the Nuclear Fuel Safety Project (Projekt Kärnbränslesäkerhet, KBS) was formed in December of 1976 by the four utility companies that build nuclear power plants in Sweden. Within the framework of this project, the Swedish Corrosion Institute has been commissioned to provide an evaluation and assessment of the corrosion resistance possessed by the encapsulation alternatives proposed by KBS. The present report concerns an assessment of aluminium oxide as an encapsulation material for unreprocessed waste.

In order to fulfil its commitment, the Corrosion Institute has appointed a reference group of specialists, mainly from the field of corrosion and materials. The group also includes a representative from the Swedish Nuclear Power Inspection Board as an observer. The reference group consists of the following members:

Professor E Mattsson	Swedish Corrosion Institute, Chairman
L Ekbom, Lic.Eng.	Swedish Corrosion Institute (now with the National Defence Research Institute)
R Carlsson, Lic.Eng.	Swedish Silicate Research Institute
Chief Eng. T Eckered	Swedish Nuclear Power Inspection Board (observer)
G Eklund, D.Eng.	Institute for Metals Research
Professor I Grenthe	Royal Institute of Technology
Dr. R Hallberg	University of Stockholm
S Henrikson, M.A.	Studsvik Energiteknik AB (now with the Swedish Corrosion Institute)
Prof. N-G Vannerberg	Chalmers University of Technology
Prof. G Wranglén	Royal Institute of Technology

The reference group has based its assessment on studies and calculations carried out both within and outside the group and on statements from and discussions with various experts, especially professor A G Evans of the University of California, Professor W S Fyfe of the University of Western Ontario, Professor Janne Carlsson of the Royal Institute of Technology and Dr. Leif Hermansson of the Swedish Silicate Research Institute.

In arriving at its conclusions, the group has attempted to evaluate the corrosion resistance which would be exhibited by the canister under the given conditions and premises, on the basis of current knowledge. The reference group is in unanimous agreement with the assessments presented in this report, with the exception of Professor Gösta Wranglén, who has submitted a special statement.

2. PREMISES FOR THE ASSESSMENT

KBS has specified the premises for the assessment with respect to geological conditions, the environment surrounding the canister and the function of the buffer mass (appendix A). These premises have been discussed within the reference group. However, it has not been the function of the reference group to judge the correctness of these premises.

2.1 Proposed method of storage

According to the proposal, unreprocessed waste in the form of fuel rods from the reactor are rolled into coils and enclosed in an aluminium oxide canister. The canister is fabricated of aluminium oxide of high purity (> 99.8% Al_2O_3) that has been sintered by means of hot isostatic pressing to a high density (> 99.5% of the theoretical value). Closure of the canister is effected by joining a lid of the same material to the container by means of hot isostatic pressing. The construction of the canister is shown in figure 1. Its outside diameter is 500 mm, length 3 m and wall thickness min 100 mm. The steel shell from the fabrication process may be removed, if desired. The canisters will be fabricated in such a manner that tensile stresses of max. 38 MPa will be created in the outer surface of the canister.

Thermal insulation, for example aluminium silicate fibre, and a supporting block of magnesium oxide are placed in the top of the canister before the canister is sealed with a lid.

The canisters are placed in vertical boreholes emanating from horizontal tunnels in rock 500 m below the ground surface (figure 2). The vertical holes are drilled with a diameter of 1.0 m and a depth of 6.0 m and spaced at intervals of 4.0 m. One canister is deposited in each borehole.

The hole around the canister is filled with a buffer mass. In connection with water seepage into the repository, the buffer material will exert a swelling pressure on the canister which can give rise to tensile stresses in the canister of max. about 10 MPa. However, it is claimed that these tensile stresses disappear completely after water saturation and ground water pressurization.

The intention with the above-described storage method, is to create a number of barriers that prevent radioactive elements from reaching the biosphere. Thus, the more or less slow dissolution of radioactive elements from the waste constitutes an inner barrier, the canister itself and the buffer mass surrounding the canister comprise a second and third barrier, and, finally, the long transport path through the rock constitutes a fourth, outer barrier. The present study concerns only one of these four barriers, namely the canister.

2.2 Composition of the groundwater

The canisters will be surrounded by groundwater. The composition of the groundwater at the depth in question, according to the premises, is given in table 1. Ions that can be incorporated in a hydrated layer on the surface of the canister, such as silicate and magnesium ions, are of interest for corrosion of the aluminium oxide canister. The pH of the groundwater can be assumed to fall within the range pH 7-9, due to the buffering effect of minerals in and around the tunnel system.

When the canisters are deposited and the holes are filled with buffer mass, air will fill the pores and cavities in the buffer mass in the tunnels until the final backfilling of the repository. After the repository has been sealed, the air will dissolve in invading groundwater.

2.3 Groundwater flow

In accordance with the premises, the waste will be emplaced in selected rock with low permeability, i.e. with few and narrow cracks. This means that the flow of water through the rock will only be on the order of 0.1 litre per m^2 of rock and year. The water flow is localized to thin cracks, generally spaced at several metres. Significant increases in the flow of water in the rock can only occur as a result of major disturbances of the rock, e.g. tectonic movements. Water flow strong enough to carry away the buffer material is not expected to occur under any circumstances.

2.4 Buffer

The canister is surrounded by a buffer mass consisting of 90-85% quartz sand and 10-15% bentonite. This buffer is said to perform several functions. It is to constitute a soft, formable bed with good bearing capacity for the canister. It is to reduce the penetration of and distribute evenly the groundwater over the surface of the canister. It is to serve as a chemical buffer against the groundwater and thereby regulate the pH of the water between 8.5 and 9. Finally the buffer is to retard the transport of the species present and the possible leakage of radioactive elements from the canister.

A buffer of the specified composition is said to possess great plasticity and durability. It has low permeability, 10^{-10} - 10^{-13} m/s, i.e. on the same order of magnitude as that of the rock. Upon contact with water, the bentonite swells. This swelling capacity is assumed to provide a guarantee against the formation of cracks in the material. The plasticity of bentonite is documented over geological time periods.

A mixture of 10-20% bentonite and 90-80% quartz sand is used to fill up the tunnels.

2.5 Temperature of the canister

Due to the radioactivity of the waste, heat is generated, raising the temperature of the waste and thereby of the canister and its immediate environment. This heat flux is relatively high at the start, but declines rapidly over the first 100 years. The temperature of the canister at the time of deposition can be selected by adjusting various parameters in connection with deposition.

A maximum temperature at the outer surface of the canister of 70°C has been given for unreprocessed waste, even if the buffer material is dry. After 1000 years, the temperature has dropped to below 50°C. Thanks to the thickness and good thermal conductivity (30-40 W/m, °C) of the canister material, the temperature will be nearly uniform over the entire canister surface.

2.6 Radiolysis

If the groundwater around the canister is exposed to nuclear radiation, radiolysis of the water can take place. This can lead to the formation of, among other things, oxygen and hydrogen. Radiolysis is dependent upon the nature and intensity of the radiation. Calculation of the radiolysis effect has shown that the equilibrium concentrations will not exceed 13 ppb oxygen, 9 ppb hydrogen and 4 ppb hydrogen peroxide. If the formed oxidants react with reducible material, however, new oxidants can be formed by radiolysis until equilibrium is restored.

2.7 Canister life

The reference group has not received any specifications from KBS with regard to the life of the canister.

Most of the activity in the waste from nuclear fuel decays during the first 600 years. This applies to the portion that derives from cesium 137 and strontium 90. The remaining activity decays at a much slower rate, and some persists for millions of years. Some of the radioactivity derives from transuranium elements.

3. CORROSION OF THE ALUMINIUM OXIDE CANISTER

Aluminium oxide occurs in the pure state in nature in the form of the mineral corundum, both in silicon-poor rocks and as erosion remains in sediments and river beds. Geologically speaking, the

mineral is one of the most durable and resistant in existence. The material has a high melting point and hardness and exhibits high corrosion resistance in a neutral aqueous environment.

Ceramic materials produced by sintering possess corrosion properties and strengths that are dependent upon the purity of the material and the sintering procedure. Aluminium oxide produced in the conventional manner normally contains pores and a silicate-bearing binder phase at the grain boundaries. According to the proposed method, the canister is fabricated of high-purity aluminium oxide by means of hot isostatic pressing. This renders the material virtually free from pores and impurities at the grain boundaries. It is known that the corrosion resistance of the material is dependent upon its purity and density (appendix B).

In evaluating the corrosion resistance of the aluminium oxide canisters, the main type of corrosion that must be considered besides general corrosion is stress corrosion cracking or so-called "delayed fracture".

3.1 General corrosion

The aluminium in aluminium oxide exists in its stable oxidation state (III) under outdoor conditions, so that no redox reactions can be expected. However, the oxide is not thermodynamically stable in water, where hydration can occur. Since the canister will be surrounded by water after an initial phase, the hydration reaction on the surface of the aluminium oxide canister and the dissolution of the hydroxide will be decisive in determining the general corrosion of the canister.

Hydration forms reaction products the composition of which is dependent upon the environment (appendix B). In pure water at temperatures below 100 ^{o}C, amorphous aluminium hydroxide or crystalline gibbsite ($Al_2O_3.3H_2O$) is formed. Above 100^{o}C, the mineral boehmite ($Al_2O_3.H_2O$) is formed. However, groundwater contains various ions originating partly from the surrounding rock and partly from the sand-bentonite buffer surrounding the canister. These ions can be incorporated into the aluminium hydroxide layer. In this manner, a film of, for example, silicates with low solubility can form on the surface of the canister, counteracting the reaction with water (appendix B).

The rate at which the aluminium oxide corrodes after the initial hydration depends primarily on the rate at which the hydroxide layer is dissolved. Aluminium is amphoteric, and the dissolution of the oxide is heavily pH-dependent. But its solubility is relatively low within the pH range 3.5-10.5.

Representative leaching tests with aluminium oxide in the environment in question cannot be found in the literature (appendix B). However, a number of such tests have now been carried out for production of data on which the assessment can be based, table 2.

Leaching tests have been carried out at Studsvik at 90°C both in pure water (appendices D 4 and D 5) and in groundwater with and without bentonite (appendix D 2). The test results have been evaluated both gravimetrically and by means of ESCA analysis of the layer of reaction products formed, the ESCA analysis at the Chalmers University of Technology (appendix D 1). The depth to which hydrogen has penetrated into the test material has been determined by means of a nuclear physical method at the University of Uppsala (appendix D 3). Measureable hydration rates were obtained in pure water, while the only changes that could be measured on specimens in groundwater was the growth of mainly $Mg(OH)_2$ layers.

At the University of Umeå leaching tests have been carried out at 80°C in chloride water the pH of which has been adjusted to 8.5 by means of bicarbonate addition, at the University of Umeå (appendix D 6). The leaching rate quickly assumed a constant value. Upon gravimetric determination, the corrosion rate was found to be 68 nm/year, and upon analysis of the dissolved quantity of aluminium by means of a spectrofluorometric method, a value of 16 nm/year was obtained. The difference is assumed to be due to mechanical flaking from the surface. Microcracks in the surface remaining from specimen preparation may be the cause of such flaking. Supplementary measurements at 40°C have revealed corrosion rates on the order of 1 nm/year.

Leaching of crushed aluminium oxide the Soxhlet method at ASEA (appendix C) has given results on the same order of magnitude as those given by the other methods (10-100 nm/year). The higher values appear to be associated with the fact that the surface structure had been disturbed in connection with specimen preparation. By means of a prior ageing of the specimen, is seems possible to obtain a constant corrosion rate (10 nm/year) after a relatively short time.

Professor W S Fyfe has determined the corrosion rate of aluminium oxide made by ASEA. The tests were carried out in an autoclave at a temperature of between 160 and 300°C (appendix C). Pure water and water in equilibrium with quartz and granite, respectively, were used as corrosion agents. The corrosion rate was found to be a linear function of 1/T (figure 3). The corrosion rates determined for natural sapphire (appendix C) as well as the corrosion rates determined at the University of Umeå for ASEA's aluminium oxide in chloride containing water with a pH of 8.5 at 40°C, conform well to the extrapolation of the straight line that was found by Fyfe for the temperature interval 160-300°C. This is worth noting, since the reaction product above 100°C is boehmite and below 100°C amorphous aluminium hydroxide or crystalline gibbsite. Clearly, there is little difference between the activation energies for the corrosion reactions above and below 100°C.

In summary, it can be concluded that measured corrosion rates in pure water are clearly below 100 nm/year within the temperature interval 80-100°C. At lower temperatures, such as those posited for the storage of nuclear fuel waste, the reaction rate is one or two powers of ten lower. In the presence of groundwater, the corrosion rate appears to be reduced to unmeasurable levels. A

significant precipitation of foreign ions then takes place on the aluminium oxide surface. This agrees with the results of calculations, which show that gibbsite has lower solubility than kaolin, with which the groundwater comes into contact (appendix D 7).

In a ceramic material of high purity and without foreign phases at the grain boundaries, conditions for preferential attack at the grain boundaries are not favourable. Certain indications in connection with the nuclear physical investigation at the University of Uppsala, however, point towards preferential hydrogen penetration at the grain boundaries. But the depth of penetration is not greater than the mean corrosion rate determined for the surface as a whole by means of other methods (table 2). Radiolysis is not judged to increase the tendency towards intercrystalline corrosion, since the aluminium oxide is of such high purity, and oxidizable impurities, such as Fe, Mn and Cr, are most probably incorporated in the α-Al_2O_3 structure and not particularly enriched at the grain boundaries. Oxidation of boron at the grain boundaries with the formation of soluble perborates is not thermodynamically possible under the prevailing storage conditions.

3.2 Delayed fracture

All materials contain defects in the form of pores, weakened grain boundaries, inclusions, cracks etc. These defects give rise to stress concentration when the material is subjected to load. Fracture occurs when the stress concentration next to a critical defect reaches the theoretical strength of the material. The defect (crack) then grows rapidly until fracture is a fact.

If the material is subjected to a load lower than a certain critical stress, no rapid crack growth takes place. However, it is known that ceramic materials that are subjected to loads lower than this critical stress can withstand this load for perhaps several years, only to crack suddenly then. This phenomenon is known as delayed fracture (appendix E III). The cause is the fact that non-critical defects present in the material grow slowly under the influence of load and environment to critical size, after which fracture occurs.

Of the different theories posited to explain the mechanisms behind delayed fracture, Charles and Hilligs' model generally seems to be able to explain experimental data best. These researchers assume that crack growth takes place through a chemical reaction between material and water at the tip of the crack. In this reaction, material is dissolved in the water. The activation energy for the reaction is affected by the stress intensity at the tip of the crack. The rate of dissolution is dependent upon such factors as stress, temperature and geometry of the crack tip. The reaction rate is also dependent upon the purity of the material. A threshold level for the stress below which fracture does not occur, regardless of how long a period of time the stress is applied, has been found to exist for some materials. According to the model, the crack tip becomes sharper or more rounded as the crack grows, depending upon the stress state. If the crack tip becomes sharper, i.e. its radius becomes smaller, the crack will grow until the conditions for rapid crack growth are fulfilled. If the stress is low, however,

material around the tip of the crack will also have time to dissolve so that the radius increases. This reduces the stress concentration around the crack tip, which leads to the reaction being inhibited and the crack growth slowing down and perhaps stopping altogether.

The relation between crack propagation velocity (V) and stress intensity (K_I) is given by the equation:

$$V = A.K_I^n \qquad (1)$$

where A and n are constants. The stress intensity factor K_I is dependent upon crack geometry, the load and the shape of the structure. The relation between crack velocity and stress intensity is often depicted graphically in a K-V diagram, which is characterized by three regions I, II and III (figure 4a). The condition for failure is that $K_I = K_{IC}$, where K_{IC} designates the fracture toughness of the material and is a material constant. According to the diagram, the curve veers off towards a lower threshold value K_O, below which delayed fracture does not occur. The existence of such a limit has been established experimentally for glass and for certain ceramic materials. In the case of aluminium oxide, however, the deflection of the curve towards a limiting value K_O takes place at such a low crack propagation velocity ($< 10^{-10}$ ms^{-1}) that it has not been possible to verify this deflection experimentally. On the other hand, no cases are known where the curve has deflected at a low crack propagation velocity towards lower K values, as is shown in principle in figure 4b. In accordance with what is known, it is therefore possible to obtain conservative values of the crack propagation velocity if the portion of the curve's region I that is determined experimentally is extrapolated towards lower values, assuming constant values of n and A.

Since no data have been found in the literature on slow crack growth for Al_2O_3 of the type concerned here with high purity and density, a study of this phenomenon has been carried out at ASEA with this material in an environment of "rock water" (appendix E IV). The study has been carried out with Double Torsion (DT) specimens in accordance with the load-relaxation method. A K-V diagram (region I) for specimens without defects is shown in figure 5; the curves are corrected for various sources of error. A 99.9% one-side confidence limit has been calculated from the test results to be applied in conservative calculations. The constants for this limiting curve have been determined to be the following rounded-off values:

$$n = 210$$
$$\log A = -120.$$

The time to fracture can be determined from the relation between crack propagation velocity and the stress intensity factor (from equation 1), if the initial size of an existing surface crack and the critical crack size are known (appendix E). Vice versa, the largest permissible initial crack can be determined at a given time to fracture and critical crack size. With the aid of the material data determined for Al_2O_3 of high purity and density, the largest permissible initial defect has been calculated for given

time to fracture. The results are shown in figure 6. This figure shows which combinations of maximum permissible initial defect and maximum tensile stress are acceptable in the canister.

The residual stresses in the canister after production have been determined by means of calculation (appendix E I), and the results have been verified through experimental measurement (on a 1/3-scale container) in accordance with the trepanning method (appendix E II). The maximum tensile stress occurs 500-600 mm from the sintering joint for the lid. According to the calculations, the maximum stress at this joint amounts to 30-38 MN/m^2, depending upon the gap between the container and the internal support used in connection with the sealing procedure. According to figure 5, this stress level corresponds to a maximum permissible initial defect, a_1, of about 1.6 mm for a life of 10^6 years.

Unpermitted initial defects can be detected by means of test loading, also known as proof testing. This is done so that the stress in the material is raised to such a high value σ_p (the proof stress) that all defects larger than a_1, lead to fracture. After test loading, no defects larger than a_1 are present in the canisters that passed the test. A relationship can be derived between the time to fracture (t_{min}) for the canister and the stress (σ_a) inherent in it. This relationship can be depicted graphically in a test loading graph containing curves for different values of σ_p / σ_a (Fig. 7) For a time to fracture of 10^6 years and a maximum stress in the material of 38 MN/m^2, a value for σ_p / σ_a of 2.13 is obtained, i.e. a required proof stress of 2.13 x 38 = 81 MN/m^2. If only canisters that have survived a test load of 81 MN/m^2 are used for waste storage, a canister life of 10^6 years can thus be expected.

However, certain doubts concerning the study of delayed fracture reported here (appendices F, G 1, H, I 1), have been expressed by experts, for the following reasons:

a. The KV curves determined experimentally at crack propagation velocities within the interval 10^{-4} - 10^{9} ms^{1} have been extrapolated to a level corresponding to 10^{16} ms^{1} under the assumption that no new mechanism comes into play within the extrapolated interval which could lead to accelerated crack growth. In other words, cases of the type illustrated in figure 4 b have been disregarded in principle, and on good grounds, since no such cases are known.

b. The risk that surface inclusions in the material might react with the surrounding environment, forming reaction products with a greater volume than the original inclusion, has been disregarded. Such reactions could lead to tangential stresses in the material around the inclusion, resulting in the initiation of radial cracks. These cracks could then grow under the influence of the stresses present in the structure. The size of the radial cracks formed in this manner is usually not more than 3 times the size of the inclusion.

L Hermansson and R Carlsson have suggested that five supplementary studies be carried out in order to clear up certain questions (appendix G 1). They have further maintained that until these questions have been cleared up, it is necessary that each canister be subjected to production control by means of test loading at such a high stress (approx. 110 MN/m^2) that all canisters with surface cracks deeper than 0.8 mm are screened out, if a canister life of 10^6 years shall be guaranteed. ASEA has explained that it is not possible at the present time to carry out these supplementary studies, since they are difficult to perform on aluminium oxide with sufficient measuring accuracy and several of the questions are under theoretical study at other laboratories.

Evans has proposed the following harder requirements in order to compensate for the uncertainty factors mentioned above (appendix I 1):

a. By increasing the test load, it is possible to increase the probability that the stress intensity in the material will lie below the threshold value for crack growth even under the influence of unknown mechanisms of crack growth (figure 4b). The test load should therefore be applied at as high a stress as possible, in consideration of the strength of the material. It would be ideal if a σ_p / σ_a ratio of 4 could be achieved, corresponding to a test load of 4 x 38 = 152 MN/m^2. Canisters that can withstand this proof stress would not have surface defects larger than 0.4 mm. The previously mentioned ratio of 2.13 can be regarded as a minimum requirement. It is further necessary to monitor the test loading procedure by recording acoustic emission, even during the unloading phase, in order to ensure that crack growth does not occur.

b. In order to minimize the risk of the creation of microcracks in connection with reacting and swelling surface inclusions, it is proposed that canisters with surface inclusions larger than 100 µm within a 100 µm deep surface zone be classified as unacceptable. Surface inclusions of this type can be detected by means of surface acoustic wave examination of the canister.

(appendix I 1 and I 2).

L Hermansson and R Carlsson (appendix G 2) have questioned the reasonableness of test loading at such a high stress as about 150 MN/m^2. In canisters that had passed such a test, any crack growth velocity would be many orders of magnitude smaller than the rate of general corrosion for the canister. Such precautions could lead to a high rejection rate in canister manufacture. However, as supplementary studies are carried out and increasing knowledge is gained on delayed fracture in ceramics, it should be possible to relax these precautions, leading to less rejection.

4. CONCLUSION

The results obtained indicate that the canister's corrosion rate will be less than 0.1 μm/year, probably one or two powers of ten less.

It would appear to be possible to eliminate the risk of delayed fracture by only accepting canisters that pass the following production control:

- test loading at 150 MN/m^2 with use of the acoustic emission technique for detecting crack growth

- surface control by means of acoustic wave examination for detection of surface inclusions, whereby canisters with surface inclusions larger than 100 μm within a 100 μm deep surface zone are rejected.

A canister made of high-purity Al_2O_3 by means of hot isostatic pressing, with a wall thickness of 100 mm and having passed the above-described production control, is judged to have a life of hundreds of thousands of years and probably considerably longer under the conditions assumed to exist in the repository.

The necessity of such a stringent production control as that described above can be questioned. As more and more knowledge is gained concerning delayed fracture in ceramics, however, it should be possible to relax these precautionary measures.

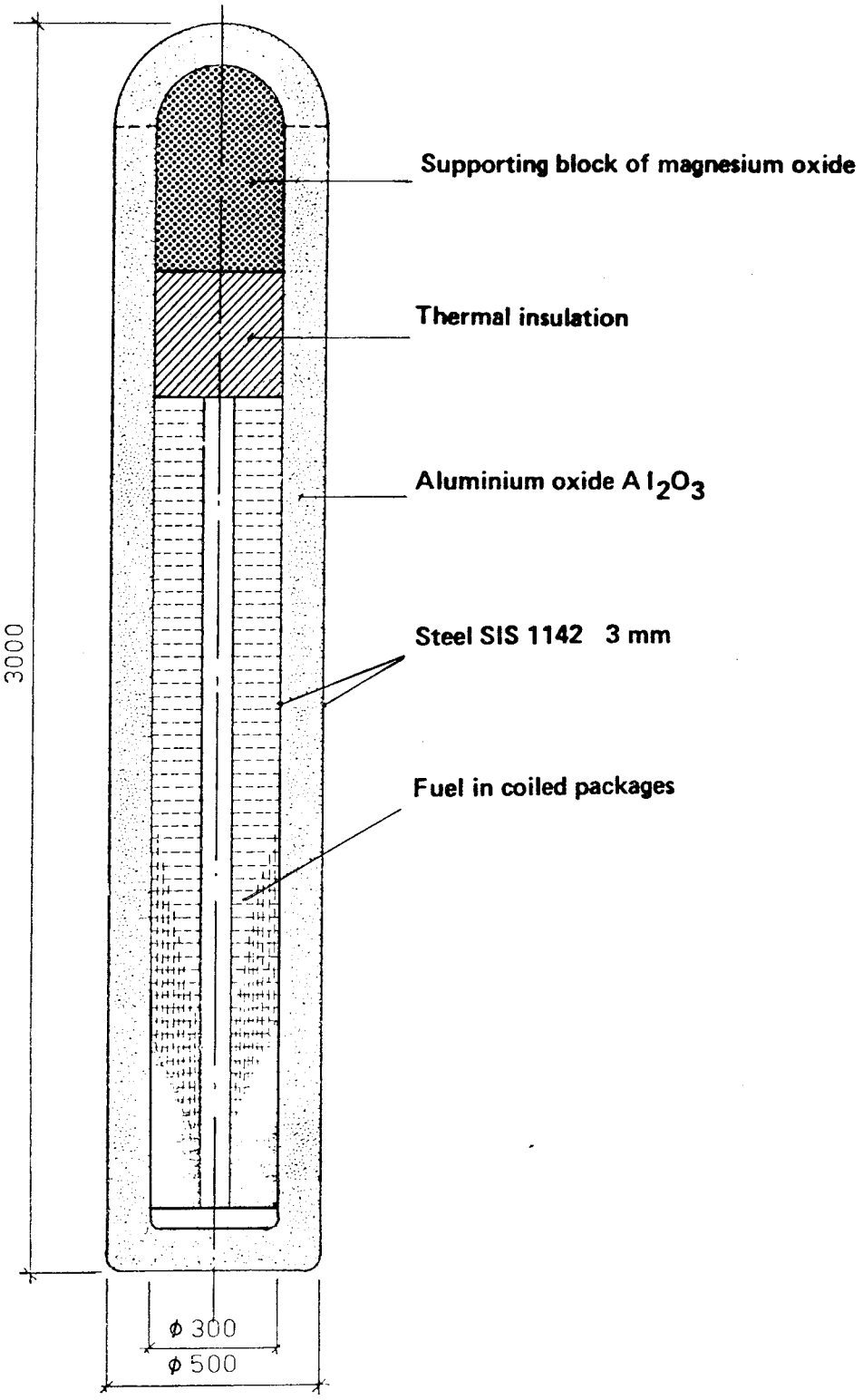

Figure 1. Aluminium oxide canister

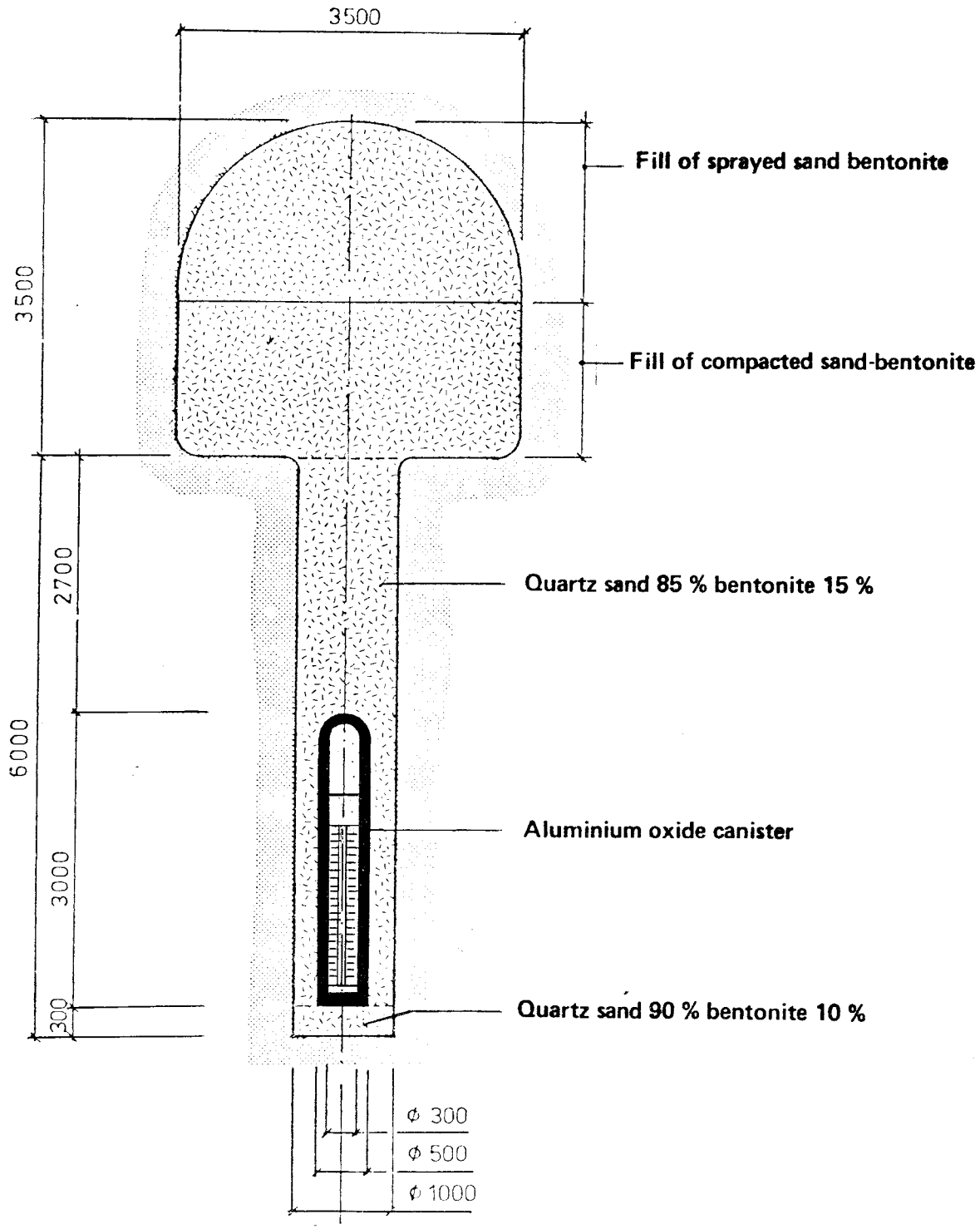

Figure 2. Storage hole after sealing

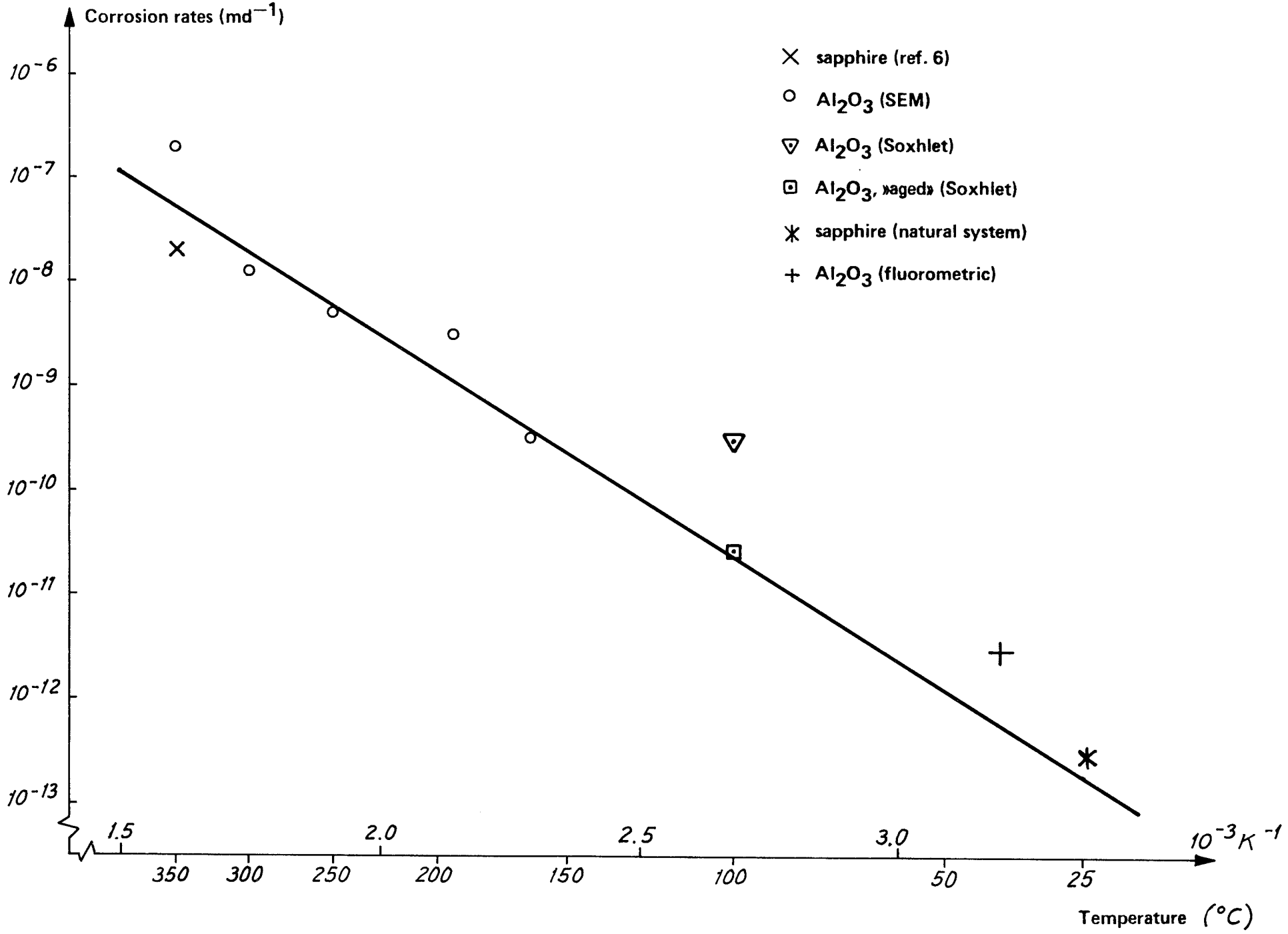

Figure 3. Arrhenius reaction rate curve for Al_2O_3 and natural sapphire. Log corrosion rate vs 1/T.

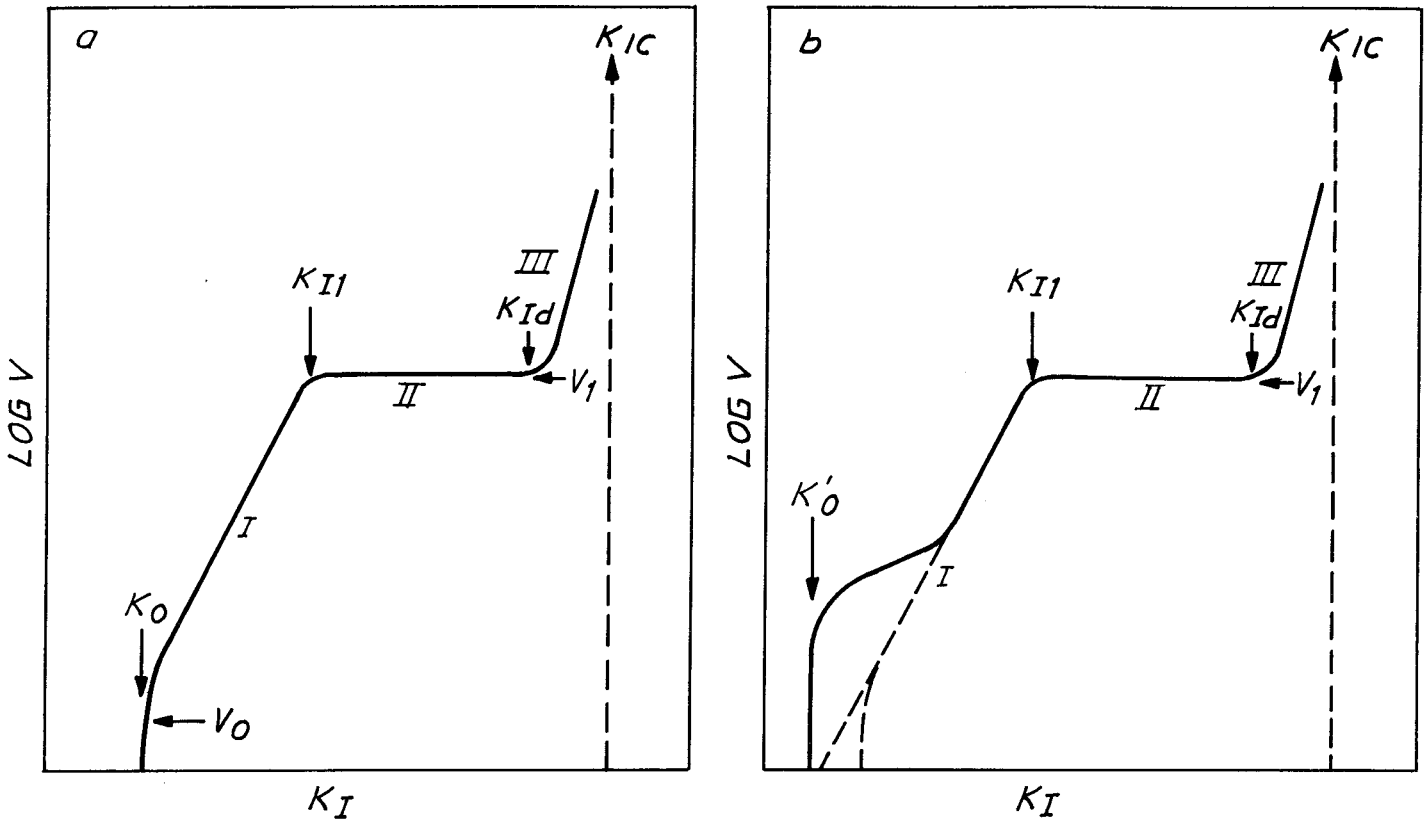

Figure 4. Schematic K-V diagrams

a. According to what is known now

b. With now unknown accelerated cracking mechanism at low crack propagation velocity

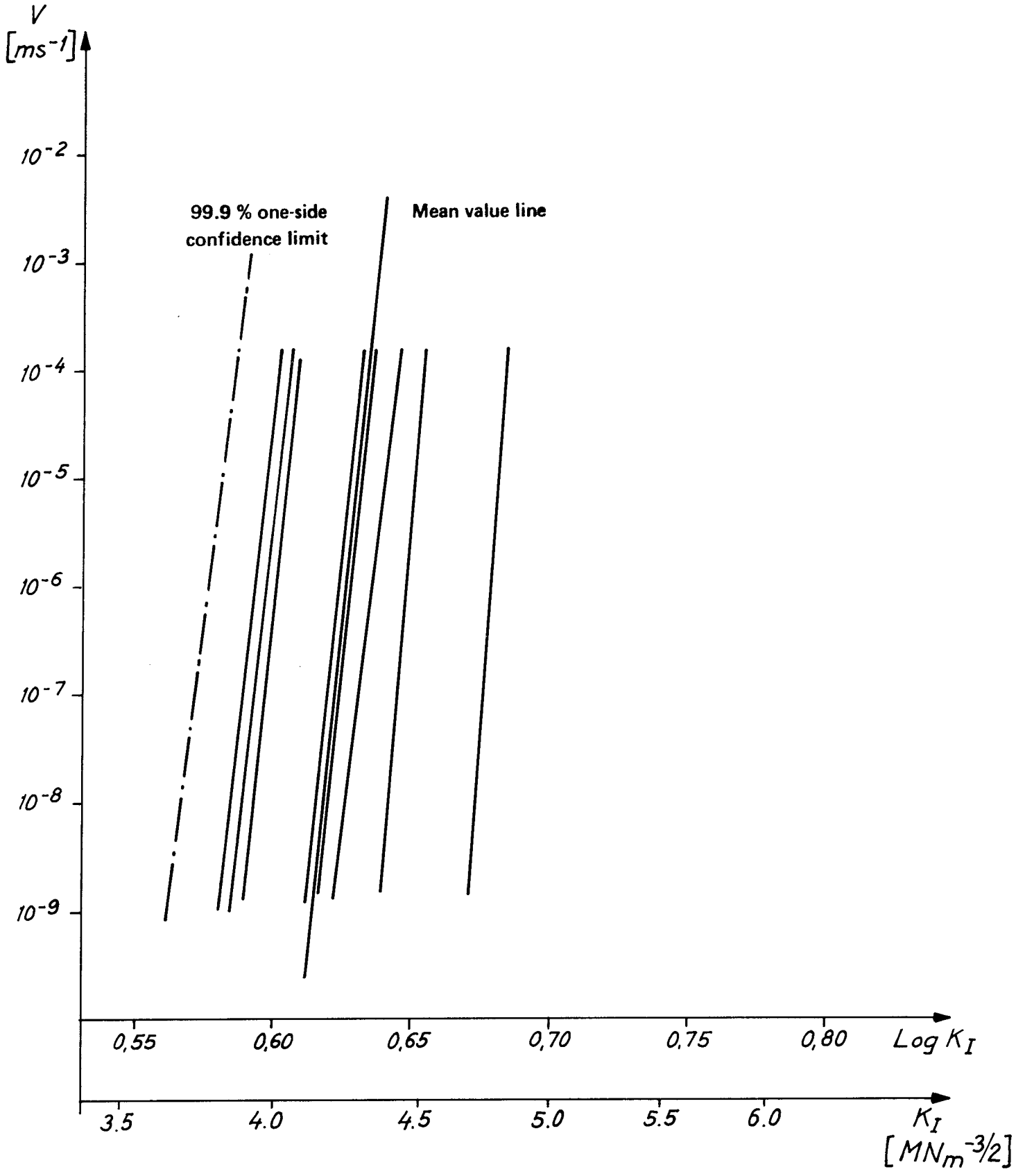

Figure 5. K—V lines for specimens without defects corrected for sources of error.

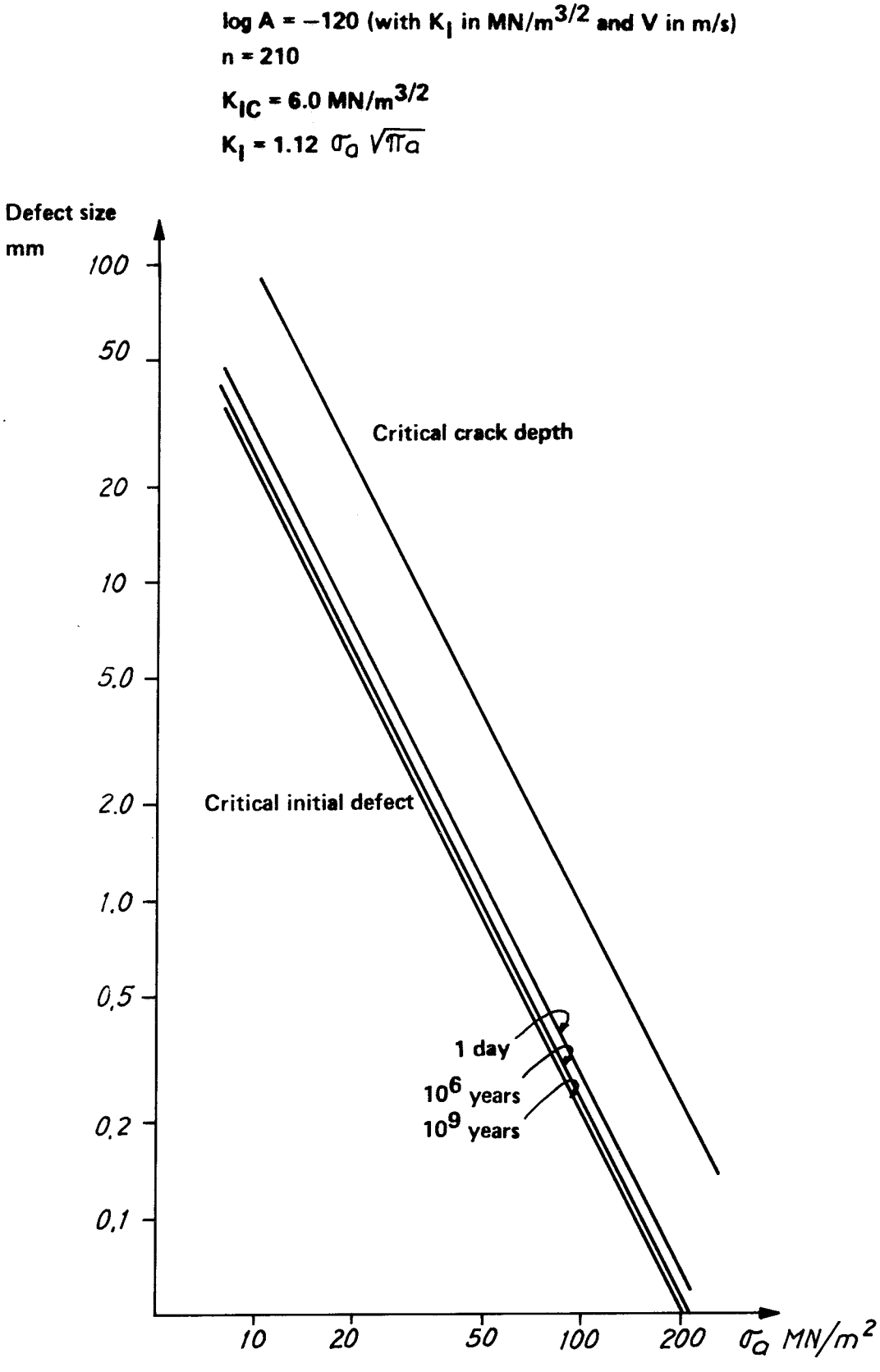

Figure 6. Permitted initial defect
Material data according to appendix E IV

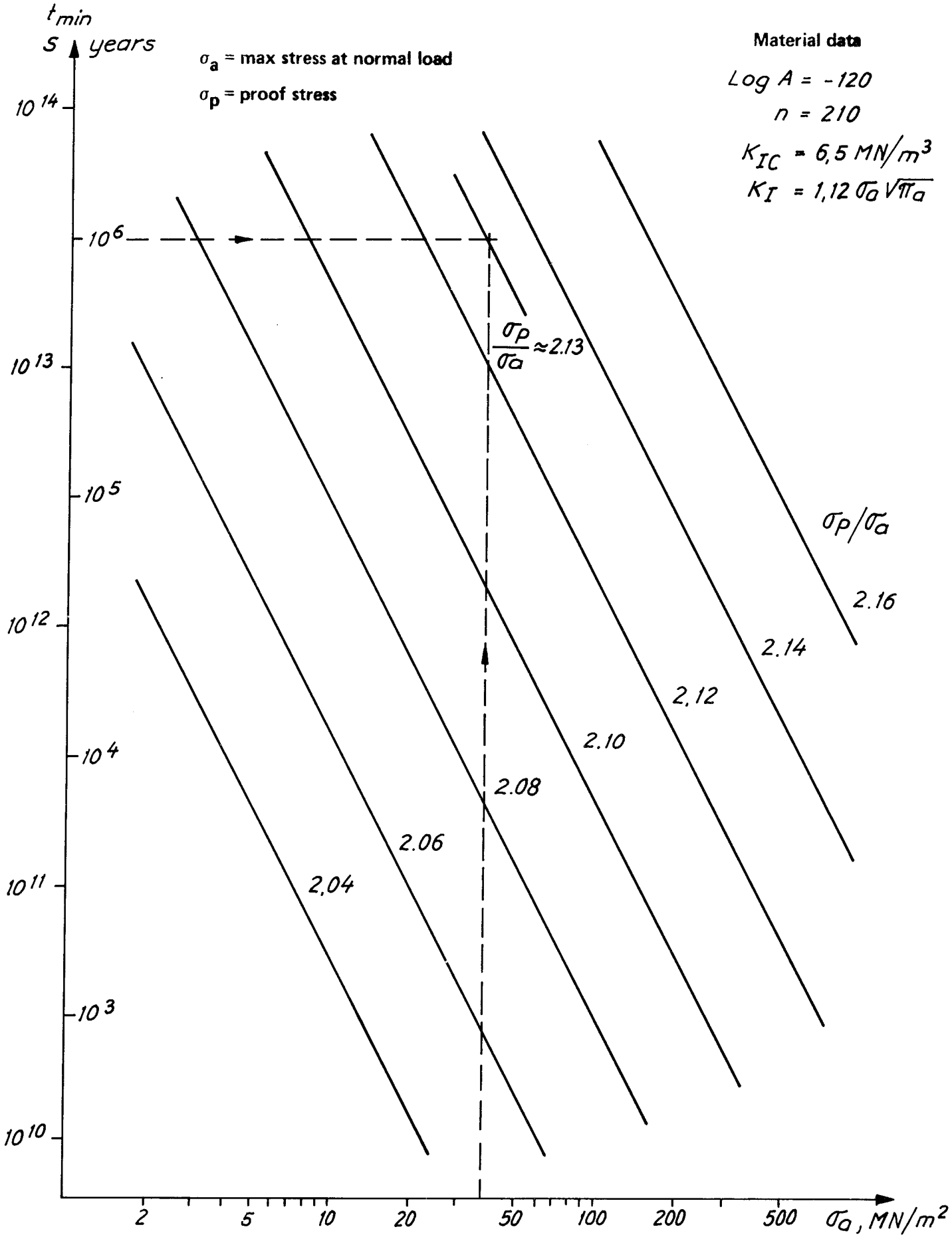

Figure 7. Test loading diagram Minimum time to fracture t_{min} (σ_a, σ_p/σ_a)

Table 1. Groundwater composition

Analysis	Unit	Probable interval	Min.value x)	Max value
Conductivity	S/cm	400-600		1100
pH		7,2-8,5		9,0
$KMnO_4$-consumption	mg/l	20-40		50
COD_{Mn}	"	5-10		12,5
Ca^{2+}	"	25-50	10	60
Mg^{2+}	"	5-20		30
Na^+	"	10-100		100
K^+	"	1-5		10
Fe-tot	"	1-20		30
Fe^{2+}	"	0,5-15		30
Mn^{2+}	"	0,1-0,5		3
HCO_3^-	"	60-400		500
CO_2	"	0-25		35
Cl^-	"	5-50		100
SO_4^{2-}	"	1-15		50
NO_3^-	"	0,1-0,5		2
PO_4^{3-}	"	0,01-0,1		0,5
F^-	"	0,5-2		8
SiO_2	"	5-30		40
HS^-	"	<0,1-1		5
NH_4	"	0,1-0,4		2
NO_2	"	<0,01-0,1		0,5
O_2	"	<0,01-0,07		0,1

x) Estimated probability for that the values will not be lower than the minimum or higher than the maximum is 95%.

PROBABLE COMPOSOSITION OF GROUND WATER IN CRYSTALLINE ROCK AT GREAT DEPTHS

Table 2. Leaching tests with aluminium oxide

Material	Leaching	Evaluation	App.	Conditions				Leaching rate nm/year
				Water type	pH	Temp °C	Time, days	
Crushed Al_2O_3	Soxhlet	Gravimetric	C	Pure	7	100	100	10-100
Al_2O_3 sintered by isostatic pressing	Autoclave	SEM	C	Pure	7	163	58	120
	Stagnant	Gravimetric	D4 D5	Pure	7	90	180	10
	Stagnant	Gravimetric	D4 D5	Pure Buffered	9.3	90	180	12
	Stagnant	H-analysis	D3	Pure	7	90	184	34±9
	Stagnant	H-analysis	D3	Pure	9.3	90	184	22±9
	Flowing	Fluorometric Gravimetric	D6	Bicarbonate, chloride	8.5	80	75	16±1 68±6
	Flowing	Fluorometric	D6	Bicarbonate, chloride	8.5	40	60	1
	Stagnant	Gravimetric	D2	Groundwater, clay	6-10	90	300	x)
	Stagnant	ESCA	D1	Groundwater	8.5	90	268	x)
Kyanite mineral	Natural		C	Groundwater		25	appr. 10^7 years	<0.1

x) Growth of surface layer, mainly $Mg(OH)_2$

APPENDIX A

BASIS FOR EVALUATION OF LIFE OF ALUMINIUM OXIDE CANISTER FOR SPENT FUEL

Specifications of the conditions in a final repository for spent, unreprocessed nuclear fuel are presented below. They are intended to serve as a basis for the Corrosion Institute's evaluation of the service life of the aluminium oxide canister that is to be used for a long-term isolation of the fuel from the groundwater.

1 Final repository

The final repository is situated in selected, low-permeable crystalline rock (granite or gneiss) at a depth of about 500 m.

A number of vertical shafts connect the deposition level with the surface of the ground. At the deposition level, approximately 1 km long tunnels with a cross-sectional area of about 15 m^2 are blasted out at intervals of 25 m. Vertical holes with a diameter of 1.0 m and a depth of 6.0 m are drilled in the bottom of the tunnels at intervals of 4.0 m.

The design of the final repository is illusted by figures 1 and 2. It is assumed that the repository can be kept open for 30-40 years before final backfilling. During the operating life of the repository, waste deposition and the excavation of new storage space will proceed simultaneously. However, these activities will be carried out in such a manner that they will not interfere with each other.

The work sequence for a storage tunnel is basically as follows. The tunnel is blasted out using a method that provides minimum facturing in the surrounding rock.

On the basis of observations on the tunnel walls and in the pilot holes, a decision is made as to which rock formations are to be used for storage and which may have to be excluded due to unsatisfactory quality of the local rock mass.

The canisters are deposited one by one in the prepared storage holes. After all storage holes have been filled, the tunnel can be backfilled, immediately or at a later date.

The tunnels are filled in several stages. The bottom of the tunnel is compacted using the technique already developed for road embankments, earth dams etc. The top part of the tunnel is filled by spraying using the same technique as that used for the reinforcement of tunnels with concrete. A more detailed description is provided in (1).

After all storage tunnels have been filled, the vertical shafts are also backfilled with the same material as is used in the tunnels. The repository can then be abandoned for good.

2 Geohydrological conditions in the repository

2.1 Permeability of the rock, groundwater flow

Test drillings and measurements at three different sites in Sweden to a depth of about 500 m (total of 7 boreholes) have demonstrated that rock with a permeability of around 10^{-9} m/s is available at the intended depth (2).

The hydraulic gradient (i.e. the slope of an isobar surface) at the depth in question is only one or a few promille. At a hydraulic gradient of 3 o/oo and a permeability of 10^{-9} m/s, a flow of 0.1 litre per year is obtained per m^2 cross-section of the rock.

The above conditions pertain to the time before the repository has been excavated and the time after the water table has been established after closure of the repository. During the intervening period, an inflow towards the repository will take place that compensates for drainage pumping and later for recharging of the aquifer. The original flow pattern of the groundwater should be largely restored one hundred years after closure of the repository. Disturbances of the groundwater flow due to heating of the repository are largely negligible.

The storage holes in the repository will, as has already been indicated, not be located in or immediately adjacent to existing zones of weakness in the bedrock, in which any future rock movements will be concentrated. However, stress changes of tectonic origin, e.g. caused by a glaciation, may conceivably give rise to ruptures and minor displacements in the rock around the repository. Only small movements will be involved here , and the buffer material will, thanks to its swelling capacity and plasticity, act as a mechanical cushion for the canisters. Any fractures created by these movements will not be so large that the buffer material is carried away with the groundwater. Hence, the canisters will always be surrounded by conditions of unchanged low permeability.

2.2 Composition of the groundwater

The chemical composition of the groundwater at great depth in the bedrock, which is especially interesting from the viewpoint of corrosion, has been studied by means of analyses of samples taken from approx. 500 m deep boreholes at Forsmark and in the the Finnsjö area in Northern Uppland County. Together with other results from the analysis of groundwater in crystalline bedrock, these analyses give the probable composition of groundwater in the bedrock for the assumed location of the final repository that is presented in subappendix A:1.

3 Buffer material and tunnel fill

The canister is surrounded in its storage hole by a so-called "buffer material", which fills the space between the canister

and the rock wall. The most important functions of the buffer material are to provide mechanical support for the canister and to minimize the groundwater flow in the canister's immediate environment.

The buffer material in the storage holes consists of a mixture of 10-15% bentonite and 85-90% quartz sand. The tunnel fill consists of a mixture of 10-20% bentonite and sand and/or crushed rock.

3.1 Properties of the buffer material

A suitable bentonite that has been studied in detail is mined in an area in Wyoming and South Dakota in the United States. It is derived from a volcanic ash which has been carried by the winds and sedimented in salt water. The main constituent of bentonite is montmorillonite, also called smectite. It is a layer-lattice mineral of the 3-layer type, where the layers are negatively charged due to the substitution of atoms with a lower valence in the positions for the silicon and aluminium atoms. Between the silicate layers are positive counterions, which compensate for the negative charge of the layers. In the material used here, these ions consist largely of sodium.

Upon contact with water, the bentonite swells due to the storage of the water between the silicate layers. If the swelling is restrained by enclosure of the material in a closed volume, a swelling pressure arises that can amount to 10-20 MPa at a low water ratio, and which approaches 0 at a sufficiently high water ratio. At the water ratios that are applicable for the bentonite under the packing conditions for mixtures with quartz material in storage holes, the swelling pressure can amount to a maximum of 1 MPa, and acts together with the external water pressure.

The swelling capacity of the bentonite provides a guarantee against the formation of water-bearing cracks in the material. Permeability is low, 10^{-9} m/s or lower.

Geological evidence exists in support of the stability of the bentonite for millions of years at the temperatures in question (3).

The chemical composition of the bentonite is presented in subappendix A:2. The chemical composition of the sand is presented in subappendix A:3. The pH of water in contact with bentonite/quartz is within the range 8-9 (3).

3.2 The buffer material in the storage holes

A bed of 10% bentonite and 90% quartz material, with a bulk density of 2.1-2.3 t/m^3 at full water saturation, is laid in the bottom of the storage holes. The canister rests on this bed. A mixture of 15% bentonite and 85% quartz with a bulk density of 2.0-2.2 t/m^3 at full water saturation is packed around and above the canister. Permeability is then 10^{-10}-10^{-13} m/s.

4 Aluminium oxide canister

4.1 Material

The canister is made of a commercially available aluminium oxide with a purity > 99.8%, Alcoa A15 Superground with a mean particle size of 2.5 μm and with a composition as given below.

Table. Composition of aluminium oxide

Trace substances	Typical analysis according to manufacturer	Own analysis
Na_2O	0.08%	0.07%
K_2O	data lacking	0.001
SiO_2	0.05	0.012
CaO	0.03	0.011
MgO	0.01	0.017
Fe_2O_3	0.01	0.016
Cr_2O_3	0.0002	< 0.01
MnO	< 0.0015	< 0.01
B_2O_3	< 0.001	< 0.02

4.2 Design

The design of the canister is illustrated by figure 4. The minimum wall thickness is 100 mm. The outside diameter is 500 mm. The steel shells can be removed, if desired.

4.3 Fabrication

Dried aluminium oxide powder packed into a steel container with a lid is subjected to hot isostatic pressing at a pressure of about 100 MPa and a temperature of about 1350°C to a density of 3.97 t/m^3. This is more than 99.5% of the fully compact density. 144 BWR or 174 PWR fuel rods are placed in the container. The canister is also sealed by means of hot isostatic pressing, with a pressure of 100 MPa at about 1350°C in the joint without the part of the canister containing the fuel being heated to more than 900°C. Owing to these uneven temperature conditions, some residual stresses remain after pressing is concluded. Calculations show that tensile stresses in the outer surface of the canister can amount to 30-70 MPa, depending upon the pressing conditions and the relaxation time (4). The canisters will be sealed with a

relaxation time of at least 6 hours and with a gap of 5 mm between the canister wall and the support block, whereby a tensile stress of no more than 38 MPa will arise in the outer surface of the canister (5).

4.4 Mechanical stresses on the aluminium oxide canister

Transport and handling of the canisters will be done in such a manner and under such control that the canister that is deposited cannot have any mechanical damages as a result of accidents during handling. If any accident takes place that could conceivably have led to damages, the waste is encapsulated.

Under the water saturation that takes place in the repository, the canister will be subjected to swelling pressure from the buffer material and external water pressure that can amount to no more than 5-6 MPa. As water is absorbed, uneven swelling pressures can arise, leading to a tensile stress of no more than about 10 MPa, which disappears completely after water saturation and groundwater pressurizing. Movements in the rock are not expected to be of such magnitude as to give rise to any appreciable stresses.

5 Temperature of the canister

Owing to the moderate heat output of the waste (220 W per canister at the time deposition) and the thickness and high thermal conductivity of the canister material, the temperature can be considered to be uniform over the canister surface. However, the temperature varies somewhat between different canisters, partially due to variations in the burnup of the fuel content and partially to where in the repository the canister is placed. Canisters located in the centre of the repository containing fuel of maximum burnup will have the highest temperature. Canister temperature as a function of time for such a canister is shown in figure 5. The graph is based on calculations in three dimensions using a computer program based on the calculated thermal conductivity of bentonite/quartz and on an average value for the thermal conductivity and heat capacity of the bedrock. The thermal conductivity of the buffer material varies with the water ratio from 0.3 W/m^{o}C when it is completely dry to 2.5 W/m^{o}C when it is water-saturated. The temperature at the canister surface remains below 70^{o}C, even if the buffer material is completely dry (7).

6 Radiolysis

The groundwater nearest the canister will be exposed to radiation, which can give rise to radiolysis of the water. Calculations of the radiolysis effect show that equilibrium concentrations will not exceed: for oxygen 13 ppb, for hydrogen 9 ppb and for hydrogen peroxide 4 ppb (6).

References:

1	KBS-1	Handling of spent nuclear fuel and final storage of vitrified high level reprocessing waste. Part III, p 99
2	KBS-1	Handling of spent nuclear fuel and final storage of vitrified high level reprocessing waste. Part II, p 29-33
3	KBS TR-32	Properties of bentonite-based buffer material
4	KBS-2	Handling and final storage of unreprocessed spent nuclear fuel. Appendix 1. Aluminium oxide canister for final storage of spent nuclear fuel. Status report, May 1978.
5	B Larson 78-06-07	Residual stresses, defects and estimated life of container of aluminium oxide (ASEA TR KYBA 78-053).
6	KBS TR-78	Evaluation of radiolysis in groundwater
7	T Tarandi 78-09-06	Temperature distribution in final repository with aluminium oxide canister

78-09-20
AB/LKB

A FIG. 1

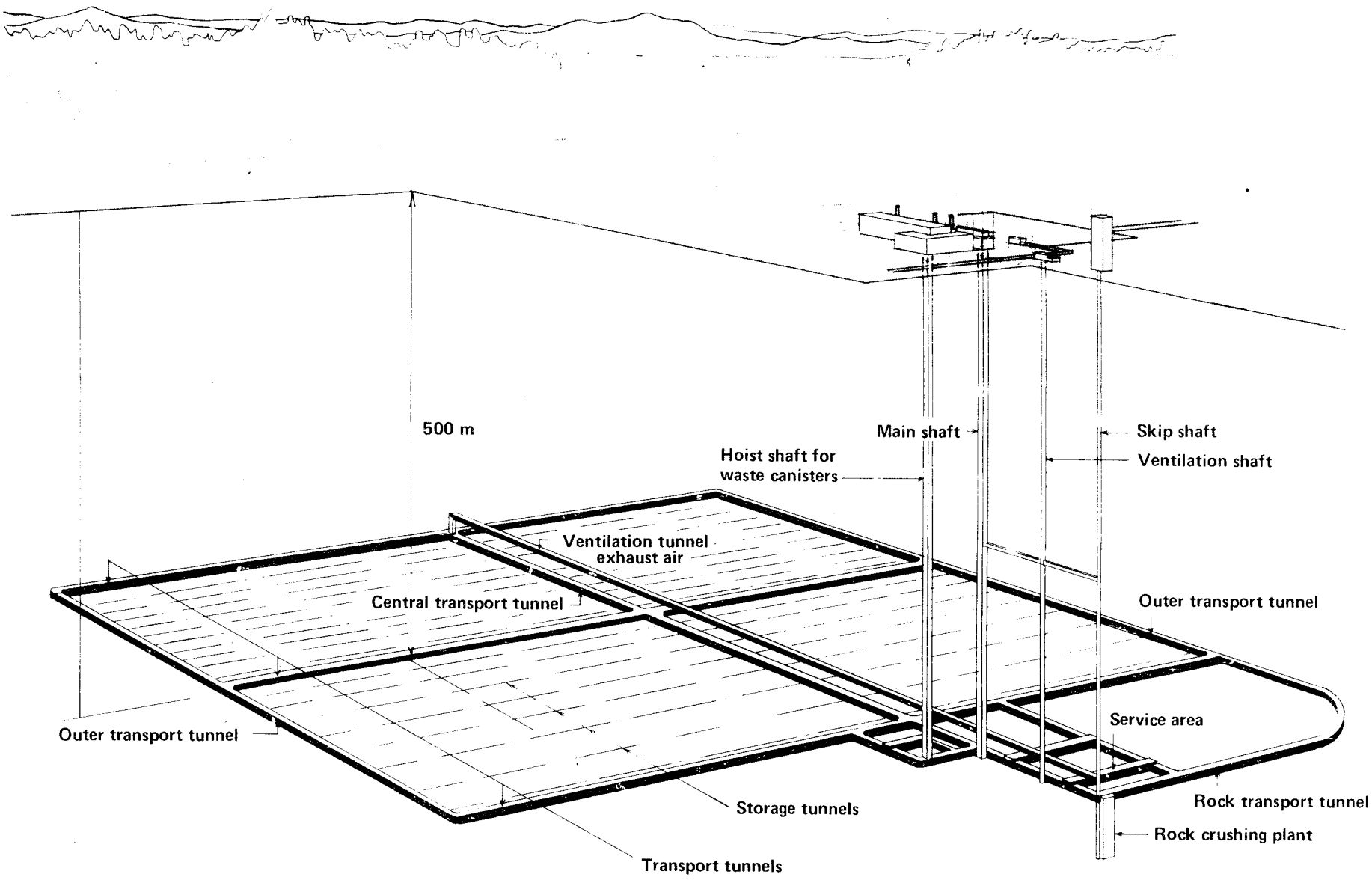
500 m
Main shaft
Skip shaft
Ventilation shaft
Hoist shaft for
waste canisters
Ventilation tunnel
exhaust air
Central transport tunnel
Outer transport tunnel
Outer transport tunnel
Service area
Storage tunnels
Rock transport tunnel
Rock crushing plant
Transport tunnels

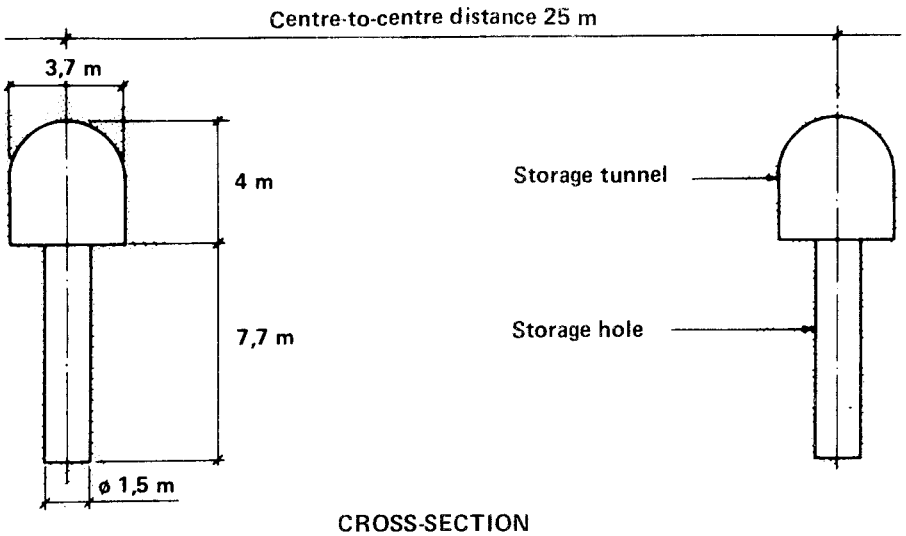

CROSS-SECTION

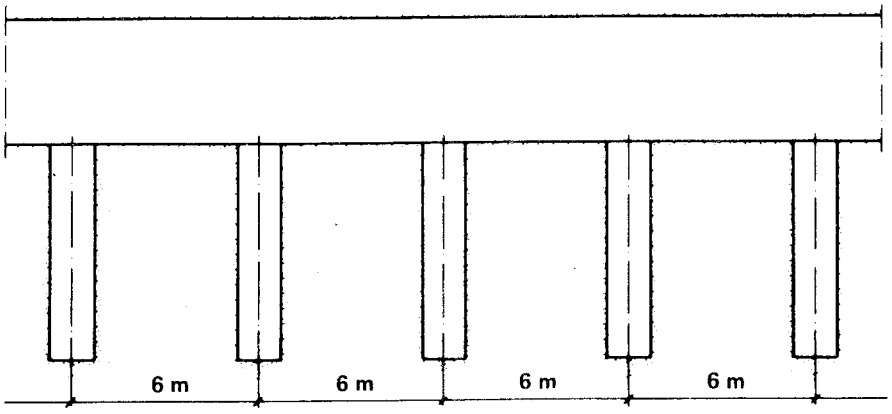

LONGITUDINAL SECTION

A FIG. 2

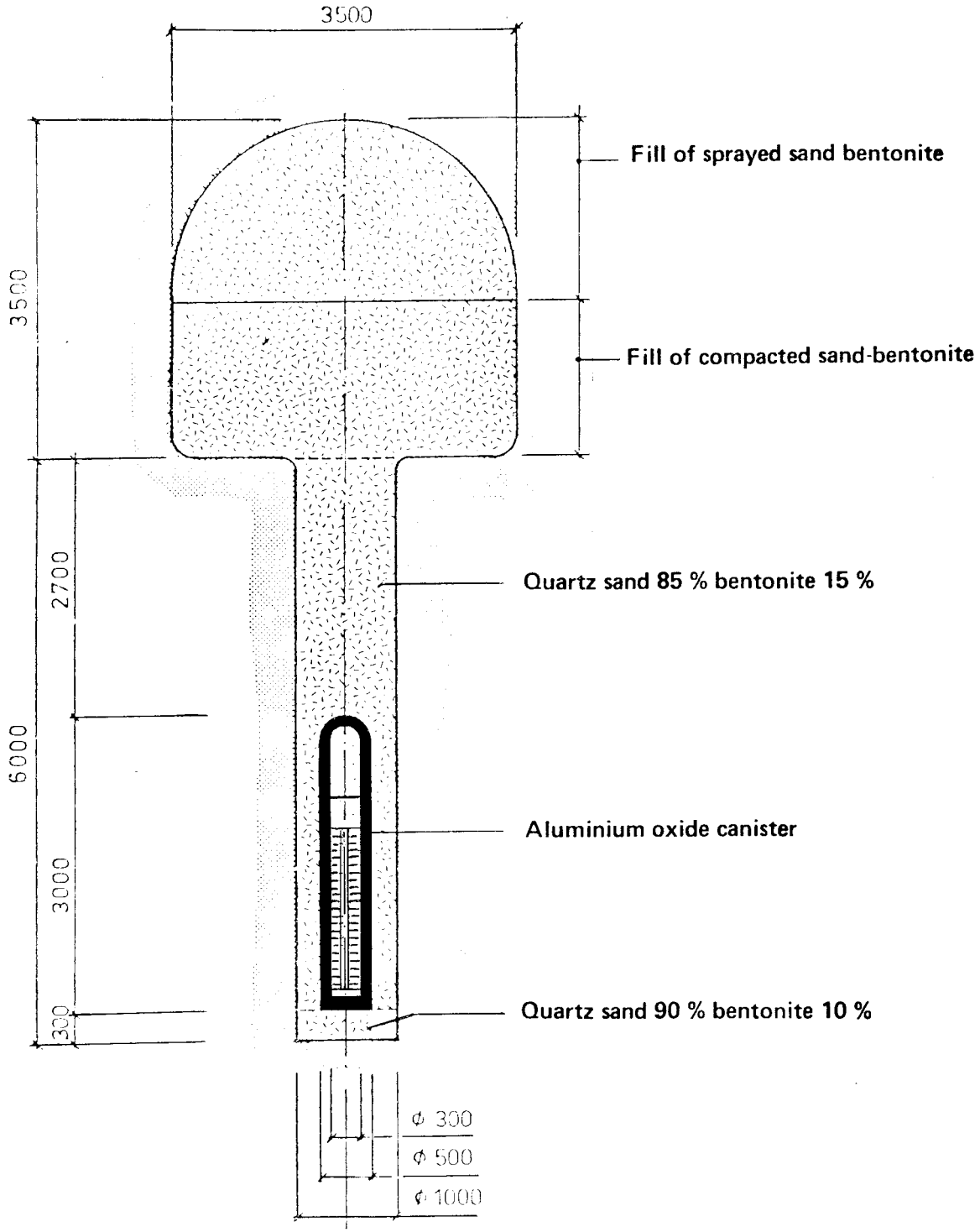

Storage hole after sealing

A FIG. 3

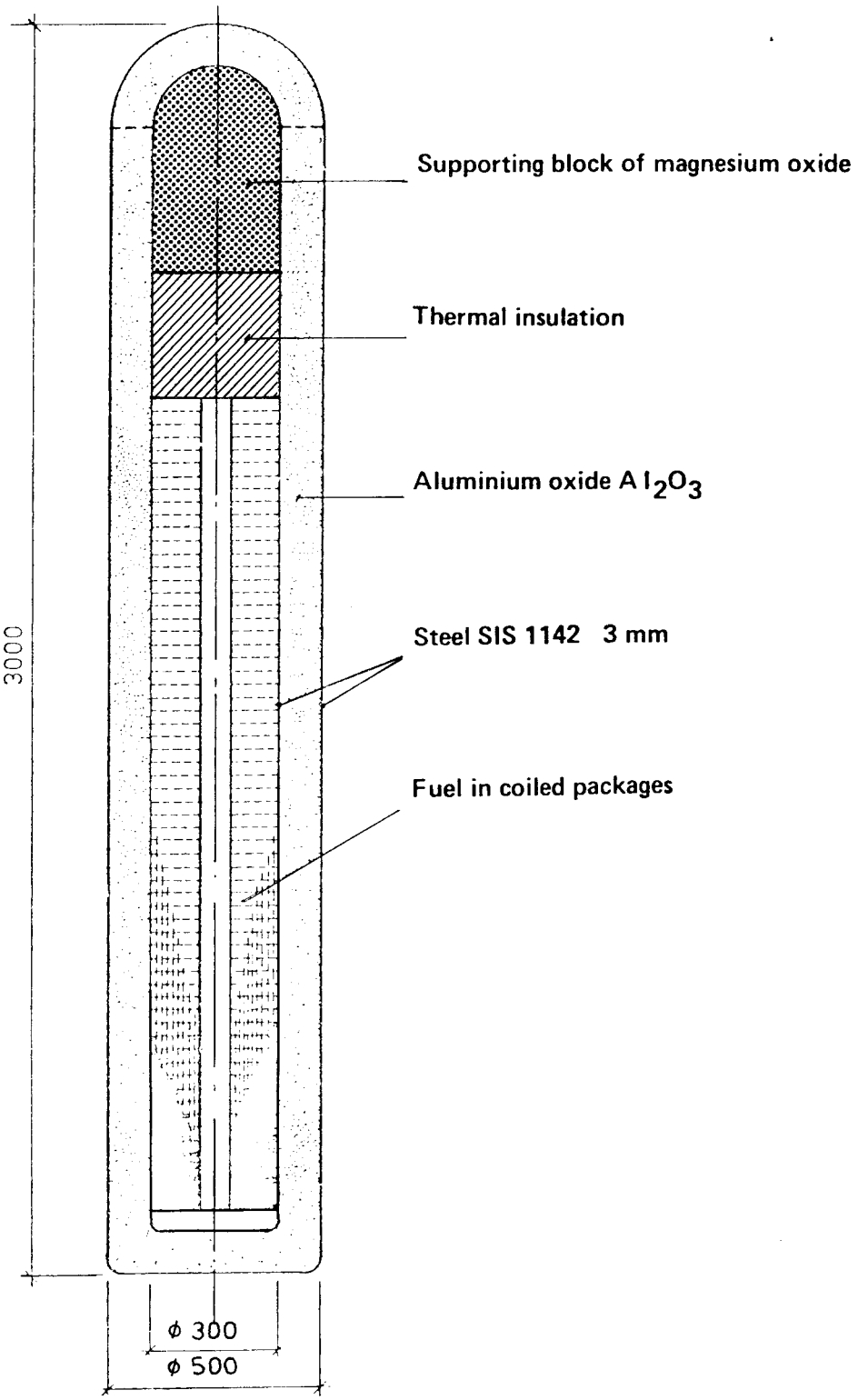

Aluminium oxide canister

A FIG. 4

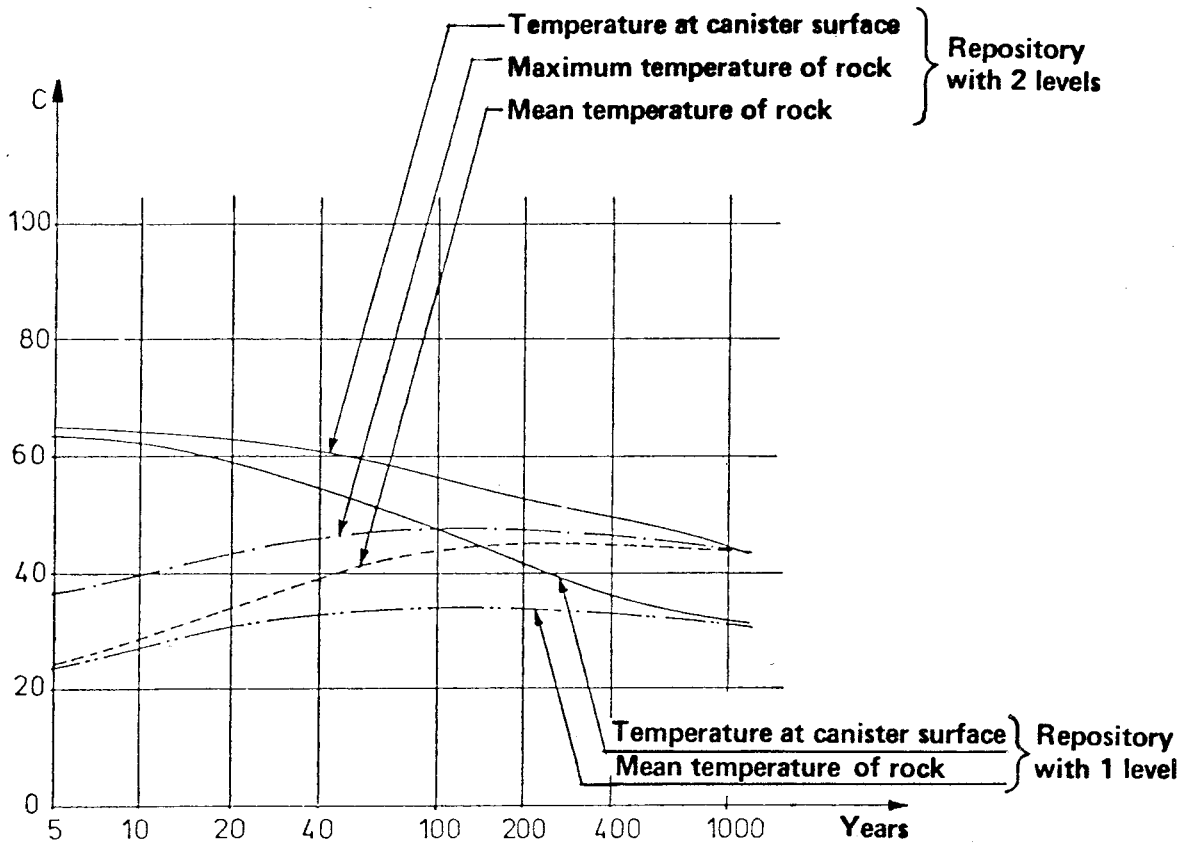

Time following deposition in final repository

VARIATION OF TEMPERATURE AT CENTRE OF FINAL REPOSITORY

A FIG. 5

PROBABLE COMPOSITION OF GROUND WATER IN CRYSTALLINE ROCK AT GREAT DEPTHS

1 Earlier investigations

In KBS Technical Report No 36 a probable composition of groundwater in crystalline rock at great depths was indicated.

The values were based on analyses made of groundwater from various parts of the country, at which values from wells drilled in rock in Uppland with a depth mostly less than 100 m were considered.

After that this table was prepared additional analyses have been made, e.g. at Finnsjön and Stripa, and analyzed at the department of agricultural hydrotechnics of the Royal Institute of Technology in Stockholm, by Gunnar Jacks.

2 Additional investigation

In this additional investigation the results from the new analyses made were considered. In particular it has been considered essential to give the analyses from greater depths a more dominant influence on the selection of a probable interval.

When it has been possible to do so the values have been confined within a more narrow interval than in report No 36.

The table reflects the composition of the groundwater in rock formations which from a geological and hydrological point of view are suitable for a final repository. Such areas can first of all be found under a local watershed.

The results of the analyses show that the intervals selected are realistic.

Of special interest from a corrosion point of view are the values for:

- disolved oxygen
- sulphides
- sulphates
- organic substances

At the assessment of the risk for corrosion due to microbacterial activity the content of nitrates and phosphates is also of interest.

The following general comments may be made on the analyses:

Oxygen

The oxygen content in the groundwater can be expected to be very low. The oxygen has been consumed through biological activity in the groundlayers through which the surface water passes on its way down to the groundwater area.

If Fe^{2+} and sulphides are present in the water, free oxygen will be consumed at the oxidation of these ions. The analyses confirm that the oxygen contents are very low, <0.01 - 0.07 mg/l.

Sulphides

Sulphides can be formed from sulphates through reduction caused by microbacterial activity during the passage of the water through the groundlayer and the rock.

When iron is present the sulphides should appear as iron sulphides with poor solubility.

Analyses made on water from Finnsjön and Stripa have shown contents <0.1 mg/l HS^-. One analysis from Forsmark has shown 5 mg/l but this value may possibly include sulphide present in Fe-sulphide form.

The contents of dissolved sulphides can be expected to be in the interval 0.1 - 1 mg/l.

Sulphate

G Jacks material from wells indicates sulphate contents in the order of magnitude of 15 mg/l, while materials from health authorities have shown contents in the order of 30-40 mg/l.

The analyses of water from great depths show considerably lower sulphate content, in most cases 6-12 mg/l and in some cases still lower values.

The most probable reason for the decrease of the sulphate content with the depth is that sulphate is reduced to sulphides which are then bound to iron as iron sulphide or pyrite. This process has been proved to occur in nature. In deep mines the sulphate content has been found to decrease very much with the depth.

Organic substances

The content of organic substances measured as $KMNO_4$ - consumption is 30-40 mg/l. This corresponds to a chemical oxygen consumption of 7.5 - 10 mg/l and an approximate organic content of about 10 mg/l. The organic substances may be expected to be resistant to biological decomposition

- - - - - - -

The above is an English translation of a document in Swedish dated Stockholm March 7, 1978, by Jan Rennerfelt and Gunnar Jacks.

Analysis	Unit	Probable interval	Min.value x)	Max valu
Conductivity	S/cm	400-600		1100
pH		7,2-8,5		9,0
$KMnO_4$-consumption	mg/l	20-40		50
COD_{Mn}	"	5-10		12,5
Ca^{2+}	"	25-50	10	60
Mg^{2+}	"	5-20		30
Na^+	"	10-100		100
K^+	"	1-5		10
Fe-tot	"	1-20		30
Fe^{2+}	"	0,5-15		30
Mn^{2+}	"	0,1-0,5		3
HCO_3^-	"	60-400		500
CO_2	"	0-25		35
Cl^-	"	5-50		100
SO_4^{2-}	"	1-15		50
NO_3^-	"	0,1-0,5		2
PO_4^{3-}	"	0,01-0,1		0,5
F^-	"	0,5-2		8
SiO_2	"	5-30		40
HS^-	"	<0,1-1		5
NH_4	"	0,1-0,4		2
NO_2	"	<0,01-0,1		0,5
O_2	"	<0,01-0,07		0,1

x) Estimated probability for that the values will not be lower than the minimum or higher than the maximum is 95%.

PROBABLE COMPOSOSITION OF GROUND WATER IN CRYSTALLINE ROCK AT GREAT DEPTHS

PHYSICAL CHARACTERISTICS OF VOLCLAY BENTONITE

The properties of Volclay are those of montmorillonite, a clay mineral of unique characteristics, which constitutes 90% of Volclay substance. Montmorillonite has the approximate chemical formula:

$$[(Al, Fe)_{1.67}Mg_{0.33}]\ Si_4O_{10}(OH)_2(Na, Ca_{0.33})$$

The other 10% consists of minute fragments of other minerals, the most abundant being feldspar. There are small fractions of gypsum, calcium carbonate, and quartz and traces of partially altered volcanic glass, biotite mica, magnetite, limonite, hematite, leucoxene, apatite, zircon, pyrite, titanite, and tremolite.

TYPICAL CHEMICAL ANALYSIS, MOISTURE FREE BASIS

	Percent by Wt. (Varies Between)	
Silica (SiO_2)	58.0	64.0
Alumina (Al_2O_3)	18.0	21.0
Ferric Oxide (Fe_2O_3)	2.5	2.8
Magnesia (MgO)	2.5	3.2
Lime (CaO)	0.1	1.0
Soda (Na_2O)	1.5	2.7
Potash (K_2O)	0.2	0.4
Ferrous Oxide (FeO)	0.2	0.4
Titanium Oxide (TiO_2)	0.1	0.2
Other minor constituents	0.5	0.8
Chemically-held water (H_2O)		5.64
Mechanically-held water (H_2O)		0.00

PARTICLE SIZE

When dispersed in water, Volclay separates into extremely fine particles, as follows:

96% to 97% finer than 44 microns
(No. 325 Standard U.S. Sieve)
93% to 94% finer than 5 microns
87% to 89% finer than 0.5 micron
60% to 65% finer than 0.1 micron

One micron is about 1/25,000 inch. One cubic inch of dry Volclay, when disintegrated in water, is estimated to yield 9500 billion individual flakes, and the total surface area of these particles is about one acre in extent.

GENERAL

Specific gravity—2.7. Actual weight relative to volume depends on the degree of pulverization, the packing and settling of the sample.

pH value of water suspensions is 8.5 to 10.0.

Index of refraction—1.55.

Mohs Hardness—1 to 1.5. Slightly harder than talc.

BASE EXCHANGE

Volclay is noted for its base exchange properties; in a water solution, it gives up sodium and potassium ions and takes in calcium and magnesium ions, thus softening the water slightly. It also enters strongly into base exchange with organic bases, extracting them from solutions of their salts.

The exchangeable metallic bases of average Volclay, determined quantitatively by leaching with ammonium acetate are:

ELEMENT	meg./100 gms.
Sodium	60 to 65
Calcium	15 to 20
Magnesium	5 to 10
Potassium	1 to 5
Sum-corrected for sulphates	85 to 90

Because the exchange ions are affected by many factors, values are somewhat different in different shipments. These values are not guaranteed to exist in any lot or any one shipment.

SWELLING

The rate of swelling depends upon the fineness, grade and on how the bentonite is handled; all grades expand very slowly when water is poured on them, much faster when they are poured into water. Finely powdered Volclay grades absorb water slowly; MX-80 Volclay absorbs it intermediate and specially sized KWK Volclay absorbs water more rapidly.

Volclay absorbs nearly 5 times its weight of water and at full saturation it occupies a volume 12 to 15 times its dry bulk. On drying, it shrinks to its original volume. The swelling is reversible — it can be wetted (swelled) and dried (shrunk) an infinite number of times, if the water used is fairly pure.

It absorbs and swells faster in hot water than cold; it does not swell in alcohol, gasoline and similar liquids; it swells only slightly in solutions of strong chemicals, such as acids, alkalies or salts.

WATER SUSPENSIONS

When mixed with 7 to 10 parts water, it makes gelatinous pastes. With 15 to 20 parts water, it forms milky, flowable sols.

Figures are given showing the consistency (viscosity) of two Volclay suspensions compared with clear water, mixed thoroughly:

	Centipoises
Clear Water	1
5% Volclay (1 Part Volclay to 19 Parts Water)	3 to 8
6-1/4% Volclay (1 Part Volclay to 15 Parts Water)	8 to 25

The sols were tested immediately after stirring; they show higher readings after standing a few hours.

In thinner dilutions — as 1 part Volclay to 99 distilled water — most of the Volclay remains suspended indefinitely. Even in dilutions as low as 1 to 5000, a considerable part does not settle. Distilled water must be used with low Volclay concentrations as the electrolytes in tap water might cause partial flocculation.

Dilute suspensions show Brownian movement — the particles are in motion, colliding and repulsing each other. Heavier slurries exhibit thixotropy, a kind of gelation that occurs when they stand quiescent, but which reverts to fluidity on being shaken or stirred.

EFFECT OF ELECTROLYTES

Particles of Volclay in water carry strong negative charges, causing them to attract and cling to positively charged particles of matter. When neutralized by oppositely charged substances, they floc together, forming spongelike aggregates, and if this occurs in dilute dispersions, the flocs settle. In thicker mixtures, however, as those containing 6% or more of Volclay, the effect of added electrolytes is to increase the viscosity.

Suspensions of Volclay are ordinarily difficult to filter, forming impenetrable cakes which seal off water. One of the effects of neutralizing or flocculating the particles is to make such suspensions more readily filterable.

It follows that all dispersions of Volclay are profoundly affected by electrolytes. The higher the valance of the latter the stronger the effect; monovalent cations are mildly active in causing flocculation, di-valent ones more so and tri-valent ones much more so.

The order of adding electrolytes is important. If an electrolyte is added to a thick slurry in which the Volclay has first been fully hydrated and swelled, the consistency of the slurry will be increased; but if the water is first treated with an electrolyte and the Volclay put in later, the dispersion will be thinner than a mixture of Volclay and clear water.

Temperature of water and time of standing also are factors. Some electrolytes stiffen the slurries temporarily, followed by thinning, after standing days or weeks; others reverse this action.

SORPTION

Montmorillonite unit cells, of the particular kind that constitute Volclay, have the outstanding peculiarity of expanding accordion-like in water. This enlarges the space between the sheets which form the structure and permits the free ingress and egress of ions of various kinds.

The mobility of the flakes when in suspension brings them in close contact with other dissolved and suspended substances. Particles of matter are not only adsorbed onto the surface of the bentonite molecule, but probably also absorbed within its lattice-like structure. The avid sorption of Volclay for other substances — both organic and inorganic — is therefore due to one or more of these factors: great surface area; spongy structure; mobility; base-exchange; strong negative polarity.

BOND STRENGTH

The maximum adherent powers of Volclay in moistened masses with other minerals is exerted when the added moisture is 50% of the weight of the Volclay.

EFFECT OF TEMPERATURE

The properties of Volclay are unaltered at temperatures below 204° C. The chemically held water is progressively driven off when exposed to higher heats for any length of time and is completely gone at 660° C. However, if heated to 537° C. and quickly cooled, its properties are unchanged.

Its swelling properties decrease progressively in the same ratio as the loss of chemically held water.

Softening begins about 1037° C. and fusion occurs at 1337° C.

Volclay imparts to masses of other minerals bonded with it an extraordinary "hot strength", i.e., resistance to load pressure while hot. In the range of temperatures just below the softening point, its "hot strength" far exceeds that of other clays.

MECHANICALLY HELD MOISTURE

Volclay as shipped contains different moisture contents. When exposed to the atmosphere, it slowly gains or loses moisture according to the humidity.

It requires 2 hours at 105° C. to 110° C. to dry it to a moisture-free condition.

KWK VOLCLAY — *fine pellet-size bentonite. Disperses in water much quicker than powder and yields the same, smooth gel.*

SPV VOLCLAY — *powdered bentonite. Mainly for general industrial purposes where bentonite is not mixed with water.*

CHEMICAL COMPOSITION OF THE QUARTZ SAND

The chemical composition of the quartz sand to be used in the final repository appears from the enclosed records which refer to samples of the so called silver sand supplied from Bornholm, Denmark.

The sulfur content in the silver sand is only a few thousands of one percent in according to tests made on eight samples.

ANALYTICA AB

Ångsvägen 4 · Box 6 · 191 21 Sollentuna-Sweden
Telephone 08-96 03 60 · Telex 11285 ANA S

ANALYSINTYG nr 76-16951

Uppdragsgivare

Ahlsell & Ågren AB
Sektion IR, IA, rib
Fack
104 60 STOCKHOLM

Datum 76-05-10 **Ref.:** I. Ahlandsberg

Prov märkt Silversand 95, provnr 1228.

Pb	<10	ppm
Cd	< 5	
As	< 300	
Hg	0.8	
Be	< 1	
Cu	5	
Cr	< 30	
Ni	< 10	
Zn	< 30	
Sn	< 10	
Co	< 10	
Mo	< 10	
Mn	15	
V	<10	
Fe tot	400	

ANALYTICA AB

M. Merseburg

Glasforskningsinstitutet i Växjö

Glasteknisk Utveckling AB

ATTEST 55 V

Ahlsell & Ågren A/S

3700 Rønne
Danmark

Kem analys

1 sand S-17. 4-1-78

SiO_2	98,8	%
Al_2O_3	0,23	
Fe_2O_3	0,20	
Cr_2O_3	0,0011	
CaO	0,04	
Na_2O	0,02	
K_2O	0,10	

1 sand S-36. 4-1-78

SiO_2	99,3	%
Al_2O_3	0,14	
Fe_2O_3	0,11	
Cr_2O_3	0,0002	
CaO	0,01	
Na_2O	0,02	
K_2O	0,05	

1 sand S-55. 4.1.78

SiO_2	99,4	%
Al_2O_3	0,15	
Fe_2O_3	0,10	
Cr_2O_3	< 0,0001	
CaO	0,02	
Na_2O	0,01	
K_2O	0,07	

1 sand S-95. 4.1.78

SiO_2	99,5	%
Al_2O_3	0,14	
Fe_2O_3	0,06	
Cr_2O_3	0,0001	
CaO	0,02	
Na_2O	0,02	
K_2O	0,07	

Växjö 1978-02-03
GLASTEKNISK UTVECKLING AB

S.Linzander

APPENDIX B

SWEDISH SILICATE RESEARCH INSTITUTE
GOTHENBURG

CORROSION OF ALUMINIUM OXIDE IN AQUEOUS SOLUTIONS - A REVIEW OF THE LITERATURE

by
Roger Carlsson and Sven Karlsson

SUMMARY

The following values for general corrosion in aqueous solutions are reported in the literature for material of densely sintered aluminium oxide.

Al_2O_3	Environments	pH	Temp (^oC)	Corrosion (μm/year)	Ref
99.8	H_2O	7.2	ca100	0.2	19
99	H_2O	7	99	4.5	20
99.5	19.2 % Na_2CO_3	12	65	6	21
99	20 % HCl	- 0.7	100	40	22, 24
99	20 % HNO_3	- 0.5	100	20	22, 24
99	20 % H_2SO_4	- 0.3	100	30	22, 24
99	20 % NaOH	14.7	100	< 90	24

The only form of local corrosion in aqueous solutions that is known for Al-oxide, as well as for other oxide-based ceramics, is a type of stress corrosion cracking that can eventually lead to failure ("delayed fracture, static fatigue, subcritical crack growth"). In design sizing using normally obtained flexural strength data, a safety factor of 3 is usually used (30, 46).

INTRODUCTION

This review of the literature concerning corrosion of Al-oxide in aqueous solutions has been limited to temperatures below 100°C. In addition to various handbooks and tabular works, the following reference journals and bibliographies have been examined.

"Gmelins Handbuch der anorganischen Chemie", Al, syst. nr. 35, Teil B (literature covered through 1933)

"Chemical Abstracts" (1951 - June 1977)

"Ceramic Abstracts" (1970 - June 1978)

"British Ceramic Abstracts" (1970 - September 1978)

"Referate" from "Berichte der Deutschen Keramischen Gesellschaft" (1970 - September 1978)

"A bibliography of ceramics and glass" and "Alumina as a ceramic material" ed by Gitzen, W H, American Ceramic Society 1976 and 1970

In addition, a retrospective computer-based literature search has been conducted at the Chalmers University of Technology library for the period 1962-1977.

A complete report of all references found has not been made. Instead, a selection has been made, especially with regard to older literature and monographs.

MODIFICATIONS OF AL-OXIDE

Al-oxide occurs in several different crystalline structures. But of these, only α-Al_2O_3 is stable in a water-free environment. The others are formed by dehydration of Al-hydroxides and all contain a small fraction of hydroxide groups. At temperatures below 600°C, χ, ρ- η -or γ-Al_2O_3 is obtained. These are usually called active Al-oxides and have the composition $Al_2O_3.nH_2O$ ($0<n<0.6$). Dehydration at 900-1000°C gives η-, θ- or δ-Al_2O_3, which are nearly water-free. Finally, at temperatures above 1000°C, the stable water-free form α-Al_2O_3 is obtained irreversibly (1-2).

Certain of the metastable oxides can also be formed through rapid cooling at high temperature in connection with gas phase reactions and plasma spraying.

The mineral corundum consists of α-Al_2O_3. Sintered Al-oxide also consists of α-Al_2O_3.

HYDRATION OF α-Al_2O_3

The system Al_2O_3 - H_2O has been the subject of many equilibrium studies down through the years, and the effect of water on Al-oxide can be considered to have been clearly established (1-8). There are five crystalline Al-hydroxides (table 1), and the particular one that is obtained in a given case depends upon the conditions of formation: temperature, time and environment.

Table 1

Formula	Alternative name	Mineral name
α $Al(OH)_3$	α -trihydrate	gibbsite or hydrargillite
β -$Al(OH)_3$	β -trihydrate	bayerite
$Al(OH)_3$	(structure between α and β)	nordstrandite
α -AlO(OH)	α -monohydrate	boehmite
β -AlO(OH)	β -monohydrate	diaspore

Al-hydroxide also occurs in gel form with an amorphous structure. Gibbsite is the thermodynamically stable phase at temperatures below 90-120°C, and is also the phase which, besides amorphous Al-hydroxide, is normally obtained at these temperatures.

The oxides and hydroxides of aluminium exhibit a strong affinity for polar molecules and readily adsorb a surface layer of water. In an aqueous environment, the oxide is not thermodynamically stable, giving rise to $Al(OH)_3$ either in the amorphous form or as crystalline gibbsite.

ΔG^o for the reaction $Al_2O_3 + 3H_2O = 2Al(OH)_3$ (gibbsite) is 4.2 kcal/mole (9). However, this reaction is extremely slow and α-Al_2O_3 is normally considered to be completely inert in water. Some hydration has, however, been demonstrated, for example through the grinding of fine-grained α-Al_2O_3 (6, 10).

SOLUBILITY OF α-Al_2O_3 AND $Al(OH)_3$ IN AQUEOUS SOLUTIONS

Tables 2 and 3 show equilibrium values measured for α-Al_2O_3 and $Al(OH)_3$, respectively, for solubility in pure water.

Table 2

Temp (°C)	Solubility of Al_2O_3		Ref
	mg/l lsg	M x 10^5	
20	0.94	0.92	11
20	1.04	1.02	11
29	0.98	0.96	12
		1.0	13

Table 3

Temp (°C)	Solubility of $Al(OH)_3$		Ref
	mg/l lsg	M x 10^5	
18		0.1	14
20		1	11
20		1.2	15
ca 20		0.1	16

α-Al_2O_3 is considered to be highly insoluble in acidic and basic solutions, while α-Al_2O_3 exhibits considerable solubility under both acidic and basic conditions (17). Similarly, crystalline $Al(OH)_3$ possesses low solubility and amorphous $Al(OH)_3$ higher solubility in acidic and basic solutions (17).

It can be shown thermodynamically with activity-pH graphs that at equilibrium, the lowest solubility is obtained at pH 5-6, which also agrees with practical values (13, 18). Solubility then increases from pH 7 by approximately one power of ten for each pH unit of increase. At pH 9, solubility is thus about 100 mg Al_2O_3/l, and at pH 9.5 about 300 mg Al_2O_3/l (13).

With regard to the question of solubility in pure water compared with solubility in a groundwater containing additional ions, it can be mentioned that a reduction of solubility from 0.017% in pure water to 0.003-0.009% following the addition of Al_2O_3 is obtained for SiO_2, owing to the formation of insoluble Al silicates. A corresponding reduction takes place for Al_2O_3 as well in the presence of SiO_2 in the solution (25). It has also been found that Mg^{2+} and other polyvalent metal ions are incorporated in layers that reduce the solubility of SiO_2 (26). This can be compared with preliminary ESCA measurements, which show the presence of Si, Mg and Al on surfaces of Al-oxide corroded in groundwater (27).

GENERAL CORROSION OF AL-OXIDE MATERIAL IN AQUEOUS SOLUTIONS

The preceding section showed that the equilibrium concentration for the dissolution of α -Al_2O_3 in pure water is on the order of 1 mg Al_2O_3/l at about 20°C and about 100 mg Al_2O_3/l solution at pH 9. In practice, however, kinetic factors must also be considered, so directly measured corrosion rates under representative environmental conditions are of greater interest. However, no such measurements for the conditions in question here have been reported in the literature. As an extreme case, however, a freely flowing aqueous solution can be chosen. For pulverized material of hot isostatically pressed α -Al_2O_3, ASEA has given corrosion values at about 100°C and pH 7.2 of 0.2 . 10^{-6} g/cm^2 and day, which corresponds to about 0.2 /µm/year (19).

Conversion of the results from an American study (20) where a similar measuring method was used gives a corrosion rate of about 5.10^{-6} g/cm^2 and day at 99°C and pH 7 for a sintered material from Coors Porcelain Co with 99% Al_2O_3. This is equivalent to a corrosion rate of 4.5 /µm/year. The lowest corrosion rate after the Al-oxide was obtained for SiO_2 glass and Pyrex glass. ASEA has also examined similar materials and obtained corrosion rates that are lower than the American values by a factor of 3. Even though the materials and temperature levels have not been identical, ASEA's value for hot isostatically pressed α -Al_2O_3 may be somewhat too low. An increase of the value by a factor of 3 gives 0.6 /µm/year at about 100°C, pH 7 and in a freely flowing solution.

Similar measurements with freely flowing solution have not been found in the literature for higher pH values. In a more stationary environment, a study has been found of sintered Al-oxide with 99.5% Al_2O_3 and the influence of 19.2% Na_2CO_3 in water at 65°C, corresponding to pH 12 (21). The corrosion rate after one day is $6.2.10^{-6}$ g/cm^2 and day, which corresponds to 6/µm/year.

In the conventional sintering and hot pressing of Al-oxide, small quantities of other oxides are used to limit grain growth, among other things. Thus, the addition of MgO gives spinel, mainly at the grain boundaries. In this case, no greater corrosion is obtained at the grain boundaries than in the rest of the material, but such an elevation was found with the addition of SiO_2 (22-23).

Boiling 20% HCl gave a corrosion rate of $\frac{1}{4}.10^{-5}$ g/cm^2 and day for Al-oxide ceramic with 0.2% MgO and 90.10^{-5} g/cm^2 and day for Al-oxide with 3% SiO_2, which corresponds to 40 / m/year and 0.8 mm/year, respectively. For boiling 20% HNO_3 and H_2SO_4, corrosion values equivalent to 20 / m/year and 30 / m/year, respectively, were obtained for the material with only a low MgO content (22). The test periods were 20 days.

Similar data exist for corrosion in strong acids at 100°C (24). A value of less than 10^{-4} g/cm^2 and day is given for 20% NaOH at 100°C, which corresponds to <90 / m/year.

LOCAL CORROSION OF AL-OXIDE MATERIAL IN AQUEOUS SOLUTIONS

For reasons of time, it has not been possible to examine this area in detail.

In an aqueous environment, oxide-based ceramics are always subjected to the form of stress corrosion called static fatigue or delayed fracture. Tensile stresses in the material lead to increased corrosion at the tips of cracks, which then gradually widen and can lead to fracture (28-30).

In addition to chemical corrosion, it is said that delayed fracture can be caused by two other mechanisms. A reduction of the surface energy in the tip of the crack can occur through the adsorption of impurities (31) and a stress can induce diffusion of mobile ions (32). In the presence of water, however, chemical corrosion is always considered to be completely dominant as a cause of delayed fracture (30, 32).

The largest body of experimental data exists for glass, where it is usually figured on the basis of experience that delayed fracture can be avoided with a maximum permissible tensile stress in the material equivalent to 1/3 of the ultimate strength determined in a wet environment, or 20% of the ultimate strength determined in a vacuum (30, 33, 46).

Similar results have been obtained for most ceramics, including materials of sintered Al-oxide (30, 34-55).

REFERENCES

(1) Remy, H: "Treatise on inorganic chemistry", Vol 1, Amsterdam 1956, pp 350-356.

(2) Wade, K and Banister, A J, Chap 12 in "Comprehensive inorganic chemistry" (1973), pp 993-994, 1032-1036.

(3) Torkar, K und Worel, H: Das Zustandsdiagramm des Systems Aluminiumoxyd/Wasser, Monatsh. Chem. 88 739 (1957)

(4) Kennedy, G C, Am. J. Sci. 257, 565 (1959)

(5) Torkar, K und Krischner, H: Neuere Arbeiten über Aluminiumoxyde, Berichte Dt. Ker. Ges. 39 (2) 131 (1962)

(6) Frisch, B: Die Hydratation von α-Aluminiumoxid, Berichte Dt. Ker. Ges. 42 (5) 149 (1965)

(7) Matsushima, S, Kennedy, G C, Akella, J and Haygarth, J, Amer. J. Sci. 265 (1) 34 (1967)

(8) Franz, E D: Das System Al_2O_3 - H_2O bei 25°C und 1 atm Druck im pH-Bereich 5-13, N. Jahrb. Miner. Abhandl. 125 (1) 80 (1975)

(9) Berin - Knacke - Kubaschewski: "Thermochemical Properties of Inorganic Substances", Supplement 1977.

(10) Dawihl, W und Frisch, B: Das System α-Aluminiumoxid - Wasser bei geringen Wasserdampfdrücken, Berichte Dt. Ker. Ges. 44 (2) 44 (1967)

(2a) Kirk-Othmer: "Encyclopedia of Chemical Technology", 3 ed, Vol 2, pp 218-244 (1978)

(11) Remy, H und Kuhlmann, A, Z. anal. Chem. 65, 162, 167 (1924/25)

(12) Busch, W, Z. anorg. Chem. 161, 169 (1927)

(13) Magistad, Chem. and Ind. (2) 1958

(14) Schmäh, H, Z. Naturforsch. 1, 322 (1946)

(15) Jander, G und Ruperti, O, Z. anorg. allg. Chem. 153, 254 (1926)

(16) Fricke, R und Schmäh, H, Z. anorg. allg. Chem. 255, 253 (1948)

(17) "Gmelins Handbuch der anorganischen Chemie" Al, syst. nr. 35, Teil B, pp 97, 115

(18) Freier, R: Aqueous Solutions. Data for Inorganic and Organic Compounds", Vol 2, p 2, Berlin 1978

(19) ASEA: Information in connection with a visit of the Corrosion Institute's reference group to Robertsfors 1977-08-16--17

(20) McCarty, G J and Davidson, M: Ceramic nuclear waste forms: II, A ceramic waste composite prepared by hot pressing, Bull. Amer. Cer. Soc. 55 (2) 190 (1976)

(21) Kertscher, W: Chemische Beständigkeit von Al_2O_3-Keramik, Silikattechnik 22 (8) 266 (1971)

(22) Dawihl, W und Klingler, E: Der Korrosionswiderstand von Aluminiumoxideinkristallen und von gesinterten Werkstoffen auf Aluminiumoxidgrundlage gegen anorganische Säuren, Berichte Dt. Ker. Ges. 44 (1), 1 (1967)

(23) Felten, R P: Einfluss von Zuschlägen auf die Eigenschaften von Aluminiumoxid - eine Literaturübersicht, Sprechsaal 104 1088 (1971)

(24) Heimke, G: Al_2O_3-Oxidkeramik in der chemischen Industrie und im Maschinenbau, Sprechsaal 103, 492 (1970)

(25) Jephcott, C M and Johnston, J H: Arch. Ind. Hyg. and Occupational Med. 1, 323 (1950)

(26) Iler, R K: "The colloid chemistry of silica and silicates", New York 1955, p 16.

(27) Olefjord, I: Preliminära resultat från ESCA-mätningar på korroderad Aloxid ("Preliminary results from ESCA measurements on corroded Al-oxide").

(28) Charles, R J: Static Fatigue of glass, I and II, J. Appl. Phys. 29 (11) 1549 (1958)

(29) Hillig, W B and Charles, R J: "High Strength Materials", New York 1965

(30) Kingery, W D, Bowen H K and Uhlmann D R: "Introduction to Ceramics", 2 ed., New York 1976

(31) Orowan, E: Fatigue of glass under stress, Nature 154 341 (1944)

(32) Quackenbush, C L and Fréchette, V D: Slow fracture of glass in alkanes and other liquids, Materials Science Research, Vol 7 "Surfaces and Interfaces of Glass and Ceramics" ed by Fréchette, V D, La Course, W C and Burdich, V L, New York 1974.

(33) Adamson, B och Backman, H: "Glas i hus" ("Glass in houses") Lund 1975, p 43.

(34) Wiederhorn, S M: Subcritical crack growth in ceramics, "Fracture Mechanics of Ceramics" ed by Bradt, R C, Hasselman, D P H and Lange, F F, New York 1974, Vol 2, p 613.

(35) Freiman, S W, McKinney, K R and Smith, H L: Slow crack growth in polycrystalline ceramics, etc as per ref. (34), p 659.

(36) Chen, C P and Knapp, W J: Fatigue fracture of an alumina ceramic at several temperatures, etc. as per ref. (34), p 691.

(37) Dawihl, W und Klingler, E: Sinterkörper auf Aluminiumoxid-grundlage und die Abhängigkeit ihrer Zeitstandfestigkeit von grenzflächenaktiven Stoffen, Berichte Dt. Ker. Ges. 43 (7) 473 (1966)

(38) Frakes, J T, Brown, S D and Kenner, G H: Delayed failure and ageing of porous alumina in water and physicological media, Bull. Amer. Cer. Soc. 53 (2) 183 (1974)

(39) Gruver, R M, Soffer, W A and Kirchner, H P: Variation of fracture stress with flaw character in 96% Al_2O_3, Bull. Amer. Cer. Soc. 55 (2) 198 (1976)

(40) Bensal, G K, Duckworth, W H and Niesz, D E: Strength-size relations in ceramic materials. Investigation of an alumina ceramic, J. Amer. Cer. Soc. 59 (11/12) 472 (1976)

(41) Chen. C P and Knapp, W J: Delayed fracture of an alumina ceramic, J. Amer. Cer. Soc 60 (1/2) 87 (1977)

(42) Richter, H: Unterkritische Rissausbreitung in keramischen Werkstoffen, Ber. Deut. Ker. Ges. 54 (12) 405 (1977)

(43) Avigdor, D and Brown, S D: Delayed failure of a porous alumina, J. Amer. Cer. Soc. 61 (3/4) 97 (1978)

(44) Ritter, J E Jr and Wulf, S A: Evaluation of proof testing to assure against delayed failure, Bull. Amer. Cer. Soc. 57 (2) 186 (1978)

(45) Swain, M V, Hagan, J T and Field, J E: Indentation induced strength degradation and stress corrosion of tempered glasses, "Fracture Mechanics of Ceramics" ed by Bradt, R C, Hasselman, D P H and Lange, F F, New York 1978, Vol 3, p 231

(46) Wiederhorn, S M: Mechanisms of subcritical crack growth in glass, "Fracture Mechanics of Ceramics" ed by Bradt, R C, Hasselman, D P H and Lange, F F, New York 1978, Vol 4, p 549

(47) McKinnis, C L: Stress corrosion mechanisms in E-glass fiber, etc. as per ref. (46), p 581

(48) Brown, S D: A multibarrier rate process approach to subcritical crack growth, etc. as per ref. (46), p 597

(49) Michalske, T A, Varner, J R and Frechette, V D: Growth of cracks partly filled with water, etc. as per ref (46), p 639

(50) Ritter, J E Jr: Engineering design and fatigue failure of brittle materials, etc. as per ref (46), p 667

(51) Bruce, J G, Gerberich, W W and Koepke, B G: Subcritical crack growth in PZT, etc. as per ref. (46), p 687

(52) Matsui, M, Soma, T and Oda, I: Subcritical crack growth in electrical porcelains, etc. as per ref (46), p 711

(53) Rockar, E M and Pletka, B J: Fracture mechanics of alumina in a simulated biological environment, etc. as per ref. (46), p 725

(54) Pletka, B Jand Wiederhorn, S M: Subcritical crack growth in glass ceramics, etc. as per ref. (46), p 745

(55) Olsen, C E: Static fatigue behavior in chemically strengthened glass, etc. as per ref. (46), p 773

CORROSION RATE OF AL_2O_3 IN AQUEOUS SOLUTIONS FROM 25-350°C

W. S. FYFE

Geology Department, University of Western Ontario, Canada

R. Tegman

ASEA AB, High Pressure Laboratory, Robertsfors, Sweden

Abstract

CORROSION RATE OF AL_2O_3 IN AQUEOUS SOLUTIONS FROM 25-350°C

W. S. Fyfe, Geology Department, University of Western Ontario, Canada and R. Tegman, ASEA AB, High Pressure Laboratory, Robertsfors, Sweden.

The rate of corrosion of both single crystals of corundum and polycrystalline hot isostatically compressed Al_2O_3 are compared. Data based on Soxhlet leaching experiments at 100°C, SEM studies of surface leaching at 160-350°C, and natural corrosion of corundum in soils at 25°C, appear to follow a single Arrhenius reaction rate equation. Corundum and kyanite (Al_2SiO_5) appear to react at similar rates at 100°C and 25°C. Measured corrosion rates vary from 10^{-8} md^{-1} at 350°C to 10^{-13} md^{-1} at 25°C with an energy of activation of 60kJ $mole^{-1}$. A vessel with 10 cm wall thickness of polycrystalline HIP alumina would have a predicted life in excess of 10^7 years.

Introduction

The problems of isolating nuclear waste from the biosphere would be essentially solved if impermeable corrosion resistant containers could be fabricated with life times exceeding a million years. The concept of fabricating such long life "bottles" is quite new in our technology. The importance of such an approach to waste disposal is obvious when we consider other approaches to waste disposal and in particular for the case of deep underground disposal. It is very difficult indeed to predict the permeability of large volumes ($10\ km^3$) of rock and all approaches depending only on the rock barrier are difficult to quantify (1).

When one approaches the problem of corrosion resistant materials there is much to be learned from the behaviour of minerals in natural weathering processes. In particular, we can learn a great deal from environments of tropical weathering where residual lateritic soils are formed. If such environments are considered a list of reactivity of the form:

glass $\gg$ feldspars $\approx$ MgFe silicates $>$ quartz $>$ Al_2O_3, Al_2SiO_5, $ZrSiO_4$ etc $>$ diamond is well established (2).

In general relations appear to exist between chemical complexity of minerals, lattice energies, hardness, melting points etc, but there are no simple rules to predict how a phase will corrode in a natural ground water environment. The beauty of such natural observations in that the times involved in a weathering cycle can be in the order of 10^7 years (3).

Given such data and economical and technological restrictions on fabrication, an obvious choice is Al_2O_3 in the form of corundum. The advances in high temperature, high pressure sintering techniques developed by ASEA make it possible to fabricate large volume containers (4). This paper is concerned with the corrosion characteristics of this polycrystalline material.

Given present thinking on underground storage, the containers might be placed in a common rock or in salt at depths in the range of 0.5 - 2 km where fluid pressures are in the range 50 - - 200 bars and environmental temperatures are in the range 10 - 40°C. The aqueous fluid in the rock will have a chemistry appropriate to the rock and in most respects be similar to normal reduced ground waters (a saturated salt solution for the case of salt). We would emphasize, that given a common rock like granite the normal high content of Na-K feldspars, the fluid phase will be super-saturated with respect to the solution of corundum, i.e. for leaching processes like

$$KAlSi_3O_8(s) \rightarrow K^+(aq) + Si(OH)_4(aq) + Al_2O_3(s)$$

the ΔG will be negative. Corundum should not dissolve.

The stability or corrosion rate of a mineral phase in ground water is normally a function of two types of processes, dissolution and reaction, as illustrated below for corundum:

$$Al_2O_3(s) + aq \rightleftharpoons \text{solution; dissolution}$$

$$\text{e.g. } Al_2O_3(s) + 5\ H_2O(l) \rightleftharpoons 2\ Al(OH)_4^-(aq) + 2\ H^+(aq)$$

$$Al_2O_3(s) + X \rightleftharpoons \text{new phase; reaction}$$

$$\text{e.g. } Al_2O_3(s) + H_2O(l) + SiO_2(s) \rightleftharpoons Al_2Si_2O_5(OH)_4 \text{ (kaolinite)}$$

For corundum, it will be chemical reactions that cause corrosion and the rates of these processes will ultimately limit the life of a container. The material is thermodynamically instable in the water environment but survives because of kinetic factors (c.f. diamond→graphite). The purpose of this paper is to discuss the state of knowledge regarding appropriate corrosion rates.

The Material

Three different preparations of hot isostatically pressed corundum samples were used in these studies. The samples were prepared by preliminary drying at 1100°C at 24 hours. The dried material was loaded into mild steel cannisters and then evacuated at elevated temperature before hot pressing (4). The composition of

the corundum as supplied by Alcoa is shown in Table I, along with the conditions of hot isostatic pressing. Physical properties of the product are also shown in Table I. It should be noted that the density of the product closely approaches that of corundum and it is estimated that porosity is less than 0.5 %. Studies of H_2 diffusion into Al_2O_3 show a very low permeability. Diffusion coefficients in the range $10^{-22} m^2 s^{-1}$ have been reported at temperatures of 230°C (5).

A limited number of comparative experiments were conducted on samples of kyanite (Al_2SiO_5) concentrated in a lateritic weathering profile from Andrelandia, Brazil.

Corrosion Measurements

If a material is to be of interest in the problem of 10^6 year containment, then reasonable wall thicknesses (e.g. 10 cm) must remain at least partially uncorroded. Thus maximum corrosion rates must be in the order of 5 cm in 10^6 year or $1.4 \cdot 10^{-10} md^{-1}$. Thus any technique used to measure corrosion rates must be sensitive to changes of this order of magnitude. Normally accelerated corrosion rates can be studied by increasing temperature but such an approach always presents the normal difficulties of extrapolation to lower temperatures when different mechanisms of reaction, or different reaction products, may be involved.

In the present studies, two methods have been found to yield significant data. In the temperature range 160-350°C, surface corrosion (etching) or the formation of a film of product (boehmite) could be observed by scanning electron microscopy of samples treated in autoclaves. At temperatures near the diaspore-corundum equilibrium point at elevated pressures reaction rates are sufficiently fast that weight changes on single crystals could be used to follow compound formation (6).

It was also found that measurable corrosion rates of materials could be obtained by prolonged leaching in a standard Soxhlet apparatus at 100°C. All such measurements were based on the

weight change of samples.

For scanning electron microscopy (SEM), samples were prepared by diamond cutting small slabs (10x5x2 mm) which were highly polished on one side so that changes to the surface could be readily observed. These samples were placed in small stainless steel vessels and were immersed in pure water (at its saturated vapour pressure) or water in contact with crushed granite.

For Soxhlet experiments of hot isostatically pressed alumina and natural kyanite, samples consisted of crushed material in the size range 250-350 μm. The surface area of typical samples was 400 $cm^2\ g^{-1}$ as determined by standard BET measurements (7). The large surface-volume ratio of the crushed samples is of great advantage when observing slow corrosion rates. Crushed kyanite samples were pre-washed in hydrochloric acid to remove iron oxide stains. With some alumina samples, an attempt has been made to simulate ageing by preheating the crushed material in an autoclave at 140°C for thirty days in a sodium carbonate solution (10 mM CO_3^{-2}, pH 10.5 at 25°C). In most experiments approximately 1 g of crushed sample was contained in a weighed stainless steel screen envelope. Weight changes of the stainless screens were much lower than the observed changes when alumina was present. The Soxhlet leaching procedure was performed at 100°C. The enveloped samples were placed in a glass cup while steam from a boiling water reservoir was condensed and allowed to drip into the cup. The 10 ml cup was drained every sixth minute. The tests were interrupted at regular intervals and weight changes measured. Before weighing all samples were dried at 140°C for 2 hours and cooled in a desiccator. The accuracy of weighing was ± 0.02 mg which corresponds to a 20 % uncertainty in the smallest observed weight changes.

Experiments Observations

Data from the Soxhlet leaching experiments are summarized in Fig. 1. Curve A presents accumulated corrosion depth in nm for

kyanite, curves B and C (essentially identical) for crushed hot isostatically compressed alumina and curve D for "aged" alumina. These data clearly show that kyanite is initially more reactive than alumina but the "steady state" corrosion may be rather similar.

The corrosion rates for the samples of Al_2O_3 with different pretreatment (curves B or C and D) clearly show that the "ageing" process used reduces the final rate of leaching by an order of magnitude.

All samples show a high initial rate of weight loss. This may be attributed to several factors including:

a) initial loss of very fine particles not removed by screening and washing and
b) attack on highly reactive sites caused by grinding or crushing
c) in the case of the aged samples, formation of a thin film of reactive hydrated alumina (this would be expected from comparable SEM data, see below)

It is well known that grinding or crushing processes can activate materials either by causing high dislocation densities or highly reactive points on crystals etc. The study of the low temperature solution of quartz by Morey, Fournier and Rowe (8) nicely illustrates the very long times required for establishing solution equilibria and the influence of ageing processes.

The corrosion curves can be used to provide an indication of the limiting corrosion rates (see Table II). But from consideration of the data it seems reasonable to conclude that the lowest rates will most nearly approach reality. It should be stressed, that in all cases, the alumina content of fluids is below that required for saturation (9). In this case, it is most unlikely, that product films (e.g. boehmite) will form on the crystals and confuse the interpretation of weight changes. This in turn is in accord with

the behaviour shown by the aged alumina material where a reactive hydrated film may have been rapidly dissolved within the first few hours of the Soxhlet leaching test.

Finally, it is obvious from the data of Fig 1, that to observe true steady state corrosion rates in this system at temperatures of 100°C or below, experimental times in the order of years are required. But from the purposes of "life-time" predictions this also implies that, predictions of corrosion rates based on short term data will tend to be pessimistic.

The interpretation of the data based on scanning electron microscopy is more subjective. Experiments have clearly shown, that the preparation and treatment of the polished surface may have significant influence on reactions. For example in Fig 2a and 2b we show alumina surfaces treated with water at 310°C. In the case of 2b, the material had first been cleaned by 5 M HCl for some minutes before autoclaving. This sample is now completely covered by a boehmite film while the untreated sample has only small amounts of this product formed.

In Fig. 3 we show a typical example of a plate treated at 250°C for 20 days in pure water. A product film has formed covering about 10 % of the surface. The average thickness of this product partial layer is in the order of 0.1 μm so that on average, the surface is being transformed at a rate of about $5 \cdot 10^{-9}$ md^{-1}. The significance of such a figure is probably no better than a factor of two.

Figs. 4a-b, (195°C, 30 days) show only incipient development of a product but features of general surface corrosion and corrosion of scratches resulting from the diamond polishing process. The pitting features observed in Fig.4a are almost certainly related to surface effects of polishing. The development of pits is very rapid and erratic and could also partially explain the high rates of initial attack seen in Soxhlet tests. The best polished edges

of slabs often showed no pits. While these data are very approximate a series of values of corrosion rates from typical experiments is shown in Table III.

Finally, we return to the consideration of natural occurrences of corundum and kyanite in nature. Corundum concentrations in soils and sediments have been reported from many situations e.g. Ghana, Thailand, Brazil etc, (see Vol. 1. Dana, System of Mineralogy, 7th ed.) (10). The kyanite used in this study from Andrelandia Brazil, and corundum from Mata Azul, Brazil, occur in thick deeply leached laterite soils. The chemistry of such soils has been discussed by Kronberg et al (3), who on the basis of groundwater chemistry and soil chemistry have derived the duration of weathering. These authors consider that for typical 100 m thick profiles, weathering times are in the order of 10^7 years. From observations of one of these (Fyfe) on the kyanite occurrence at Andrelandia, the crystal sizes (2 x 1 x 0,5 cm) are essentially identical in both unweathered rock and soil. Assuming that not more than 1 mm has corroded, the corrosion rate is in the order of $3 \cdot 10^{-13}$ md^{-1} at surface temperature (25°C). Given all the variables, the error estimates of crystal size cannot be greater than a factor of 2, and similarly for weatering time. The satisfying feature of the above result is that it appears quite reasonable in the light of all other data both for kyanite and corundum (see Fig. 5).

As well as the studies in pure water, some SEM observations were made on "granite-saturated" water and sodium carbonate solutions. On the basis of our data, we see no significant difference between the reaction rate in pure water and granite water or between different batches of alumina. Some experiments indicated that reaction products (at 300°C) were forming in the powdered granite matrix rather than on the alumina surface. But study of surface etching and the behaviour of scratches and the weight changes of the slabs, did not indicate a significantly different rate of

corrosion.

Reaction rates were studied in 1 % and 10 % sodium carbonate solutions. The rates of reaction were accelerated by 3-4 orders of magnitude in these strongly alkaline solutions. Crystallization of boehmite was spectacular (Fig. 6).

Influence of Temperature

Data from all sources discussed in the preceeding sections are shown in Fig. 5 and Table III. These data from widely different sources and different types of samples plot reasonably on a conventional Arrhenius reaction rate curve. From Fig. (5) an activation energy of 60kJ $mole^{-1}$ can be estimated. This value may be compared to the activation energy for the solution of quartz (11) and dissolution of corundum in alkaline solution (12) and could indicate that the rate determining process is related to the processes which lead to the liberation of an Al-O group from the surface of the crystal. At a lower temperature gibbsite is formed rather than boehmite. For the reaction water + boehmite $\rightleftharpoons$ gibbsite the equilibrium temperature is uncertain, but below 100°C (13). The fact that boehmite and gibbsite exist together in nature supports that the equilibrium temperature is rather low and/or that the reaction rates in the system are low. It is evident that the extrapolated rate of hydration at temperatures below the equilibrium temperature do not diminish as fast as above that temperature. This means that an extrapolation below 100°C should not significantly change the conclusions.

Discussion and Conclusions

On the basis of available data, it appears that the corrosion rates of single crystals of corundum, and polycrystalline aggregates formed by hot isostatic pressing are similar. This implies that when these types of aggregates are corroded grain boundary attack does not dominate the corrosion process.

From the corrosion rates shown in Fig. 5, $\approx 10^{-11}$ md^{-1} at 100°C, $\approx 10^{-13}$ md^{-1} at 25°C, it follows that a 10 cm wall, would require between 30 million years at 100°C and 3 billion years at 25°C for total corrosion. While all possible factors involved in the chemical aspects of corrosion in a natural system have not yet been explored, it is clear that this material could be of great interest in long term waste disposal.

REFERENCES

(1) Bredehoeft, A. W., England, D. B., Trask, N. J. and Winograd, I. J. "Geological Disposal of High Radioactive Wastes - Earth-Science Perspectives". Geological Survey Circular 779, 1978.

(2) Krauskopf, K. B. Introduction to Geochemistry. McGraw-Hill, New York, 1967.

(3) Kronberg, B. I., Fyfe, W. S. and Leonardos Jr., O. H. "The Chemistry of some Brazilian Soils: Element Mobility During Intense Weathering". Chem. Geol. (in press) 1978.

(4) Kärnbränslecykelns slutsteg. Slutförvaring av använt kärnbränsle. II Teknisk del. Bilaga 1 (i tryck). KBS, Fack, 102 40 Stockholm.

(5) Fowler, J. D., Chandra, D., Elleman, T. S., Payne, A. W. and Verghese, K. "Tritium Diffusion in Al_2O_3 and BeO". J. Am. Ceram. Soc., 50, (3-4), 155-161, 1977.

(6) Fyfe, W. S. and Hollander, M.A. "Equilibrium Dehydration of Diaspore at Low Temperatures". Am. Jour. Sci., 262, 709-712, 1964.

(7) Chyssler, J. "Specifika ytan (BET-metoden) med Kr som adsorptionsgas". AP-BP-136, 1978. Studsvik Energiteknik AB, S- 611 82 Nyköping, Sweden.

(8) Morey, G. W., Fournier, R. O. and Rowe, J. J. "The Solubility of Quartz in Water in the Temperature Intervals from 25° to 300°C". Geochim. et Cosmochim. Acta, 26, 1029-1043, 1962.

(9) Szabo, Z. G., Csányi, L. J., and Kávai, M. Z. Anal. Chem. 146, 401-414, 1955.

(10) Dana, J. D. and Dana, E. S., The System of Mineralogy, Vol. 1, 7th ed, John Wiley and Sons, New York 1944.

(11) Weill, D. F. and Fyfe, W. S. "The Solubility of Quartz in H_2O in the Range 1000-4000 bars and 400-550°C". Geochim et. Cosmochim, Acta, 28, 1243-1255, 1964.

(12) Rymyantsev, V. V., Role of Adsorbed Water in Hydrothermal Dissolution and Crystallization of Quartz and Corundum". Kristallografiya. 20, (4), 870-872, 1975.

(13) Torkar, K. and Worel, H., Das Zustandsdiagramm des Systems Aluminiumoxyd/Wasser. Mh.Chem. 88, (5), 739-748, 1957.

Table 1. Properties and analysis of alumina

Sample No	M16	M18	M3
Alumina powder (Alcoa)	A15	A15	A16
HIP parameters (^{o}C/h/MPa)	1350/3/150	1400/3/150	1350/4/150
Density (g/cm^{3})	3.963	3.976	3.969
Flexural strength (MPa)	175	350	510
Weibull modulus	9	14	9
Grain size (μm)	up to 100	3-7	5
Trace elements (%)			
Na_2O	0.08		0.09
K_2O	No information available -		
SiO_2	0.05		0.03
CaO	0.03		0.01
MgO	0.01		0.03
Fe_2O_3	0.01		0.01
Cr_2O_3	<0.0002		<0.0002
MnO	<0.0015		<0.0015
B_2O_3	<0.001		<0.001

The differences between the samples are due to different raw materials and pressing cycles. Sample M18 is most representative of the material produced in cannister fabrication and has been used in most of the tests.

Table II. Corrosion rates obtained by Soxhlet leach test. The rates were determined from the tangent to the curves at time indicated.

Material	Accumulated corrosion nm		Corrosion rate (nmd^{-1})	
	60 d	100 d	60 d	100 d
Kyanite	126	140	0.45	0.33
Al_2O_3 (I)	52	67	0.44	0.34
Al_2O_3 (II)	49	-	0.45	-
Al_2O_3 ("aged")	11	-	0.026	-

Table III. Corrosion rates of alumina at different temperatures and test conditions.

Temp °C	Time (days)	Mean Corrosion (m)	Corrosion rate (md^{-1})	Test conditions (Comments)
350	14	$2.8 \cdot 10^{-7}$	$2.0 \cdot 10^{-8}$	Sapphire + $H_2O(l)$ (ref 6)
350	48	$1 \cdot 10^{-5}$	$2.0 \cdot 10^{-7}$	Al_2O_3 + H_2O + granite (s) (SEM)
300	39	$5 \cdot 10^{-7}$	$1.2 \cdot 10^{-8}$	Al_2O_3 + H_2O + SiO_2(s) (SEM)
250	20	$1 \cdot 10^{-7}$	$5.0 \cdot 10^{-9}$	Al_2O_3 + H_2O (SEM)
195	30	$1 \cdot 10^{-7}$	$3.3 \cdot 10^{-9}$	Al_2O_3 + H_2O (SEM)
163	58	$2 \cdot 10^{-8}$	$3.3 \cdot 10^{-10}$	Al_2O_3 + H_2O (SEM)
100	100	-	$3.4 \cdot 10^{-10}$	Al_2O_3 + H_2O (Soxhlet)
100	60	-	$2.6 \cdot 10^{-11}$	Al_2O_3 ("aged") + H_2O (Soxhlet)
25	$\approx 3.6 \cdot 10^9$	$< 1 \cdot 10^{-3}$	$< 2.8 \cdot 10^{-13}$	Nature (ref 3)

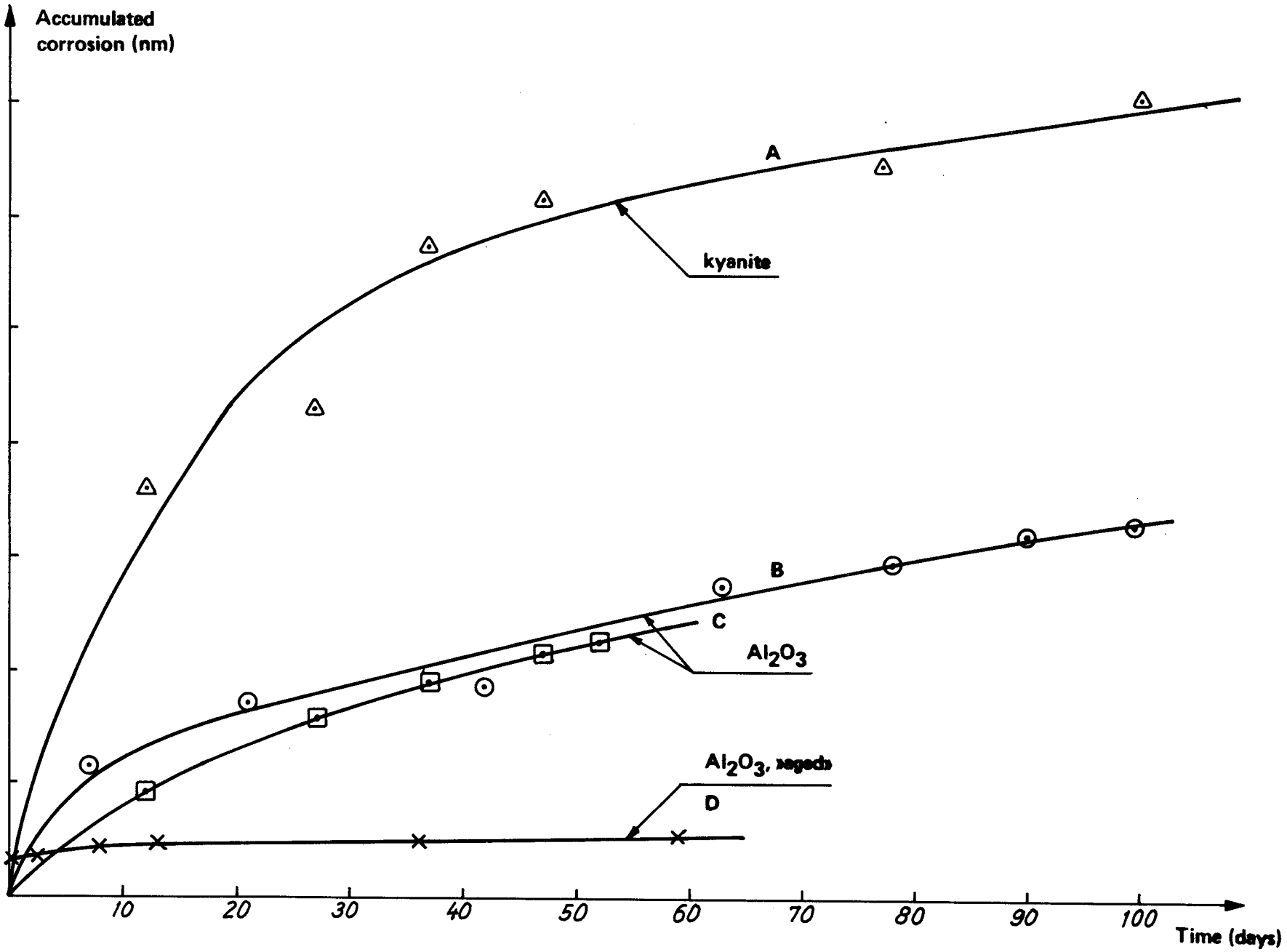

Figure 1. Soxhlet leaching tests of Al_2O_3 and natural kyanite at 100°C.
Accumulated average corrosion depth vs time.

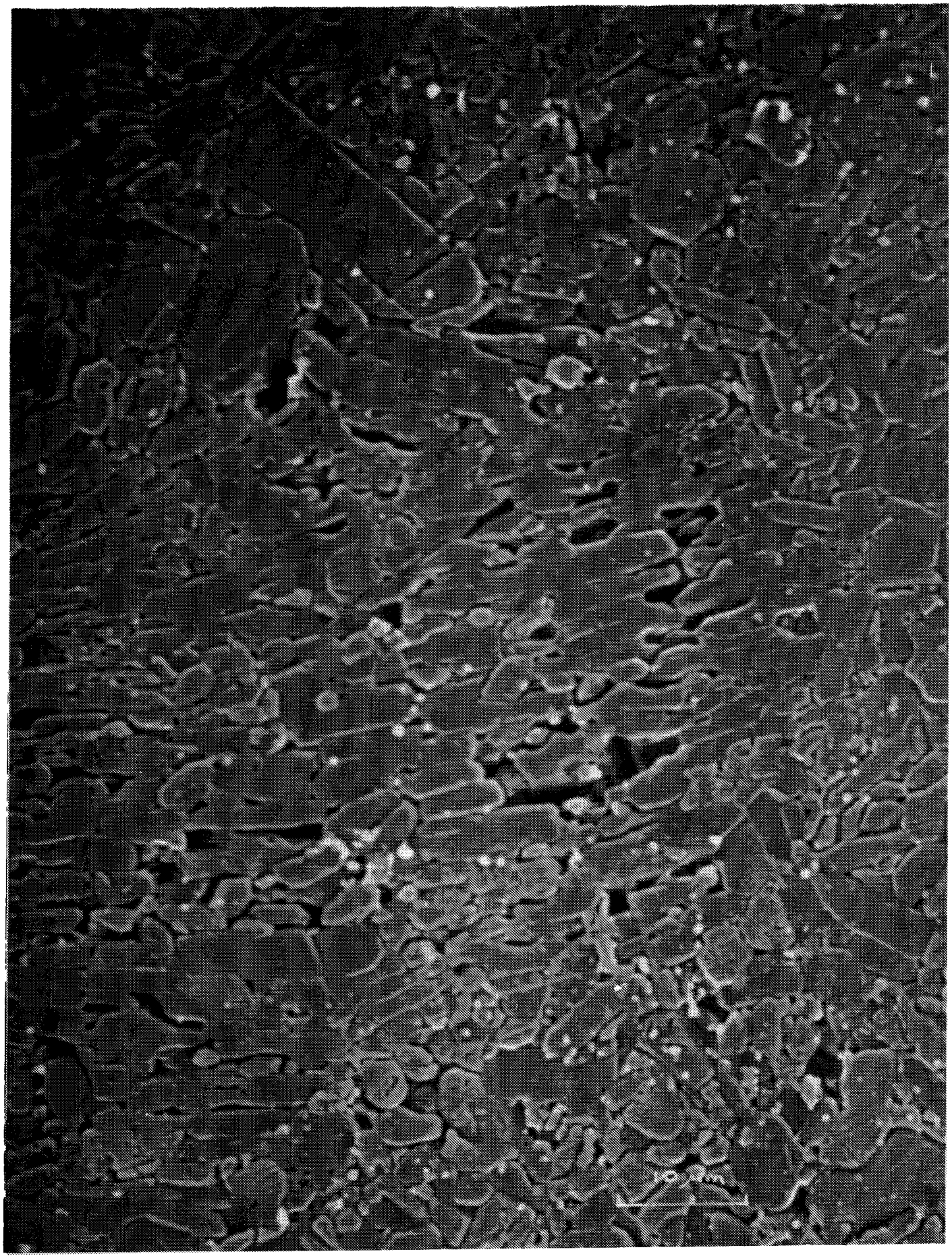

Fig. 2a SEM-photo of Al_2O_3 autoclaved in water at 310°C for 21 days.

Fig. 2b SEM-photo of Al_2O_3 autoclaved in water at 310°C fo:
Surface treated by 5M HCl before autoclaving.

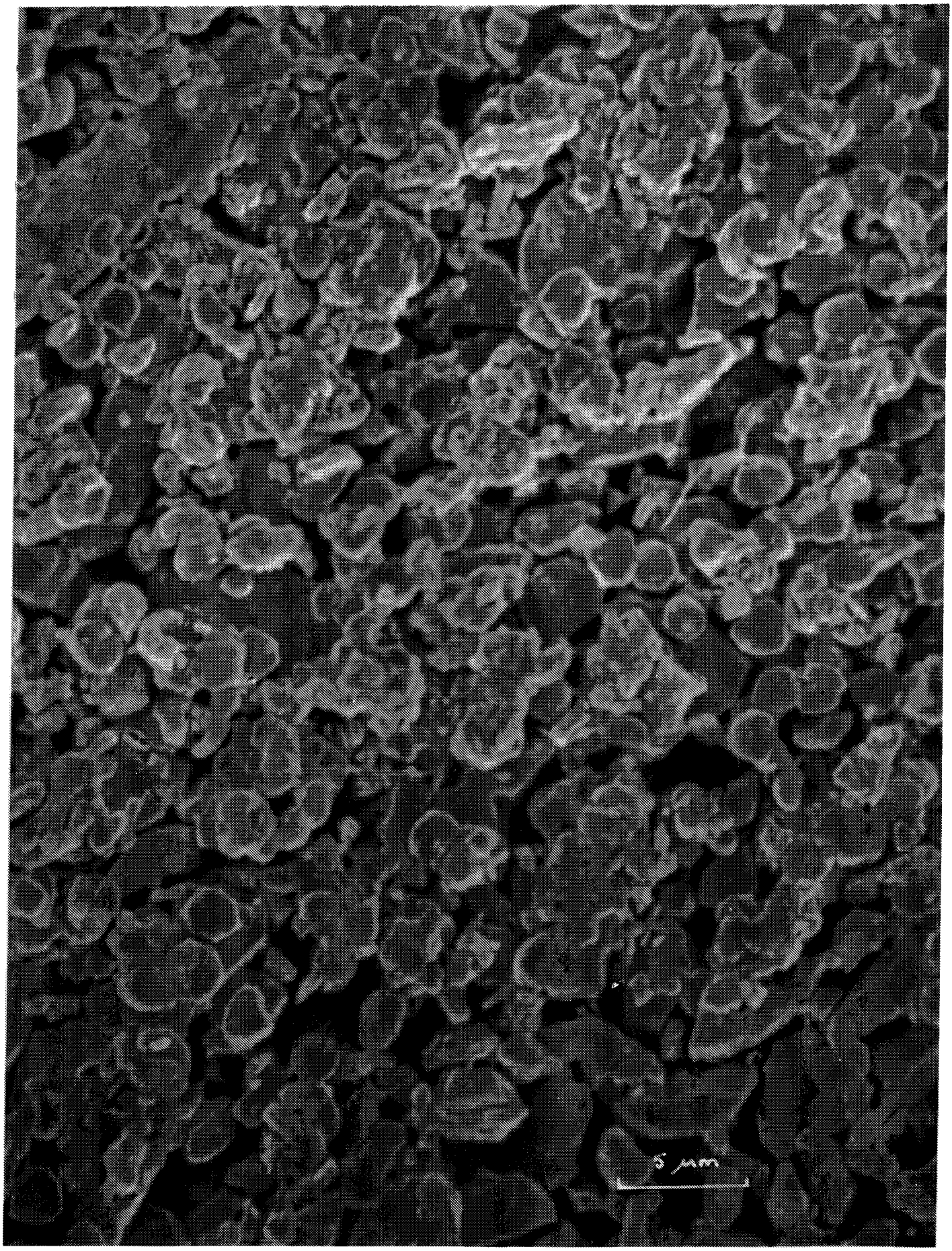

Fig. 3 SEM-photo of Al_2O_3 autoclaved in water at 250°C for 20 days.

Fig. 4a SEM-photo of Al_2O_3 autoclaved in water at 195°C for 30 days.

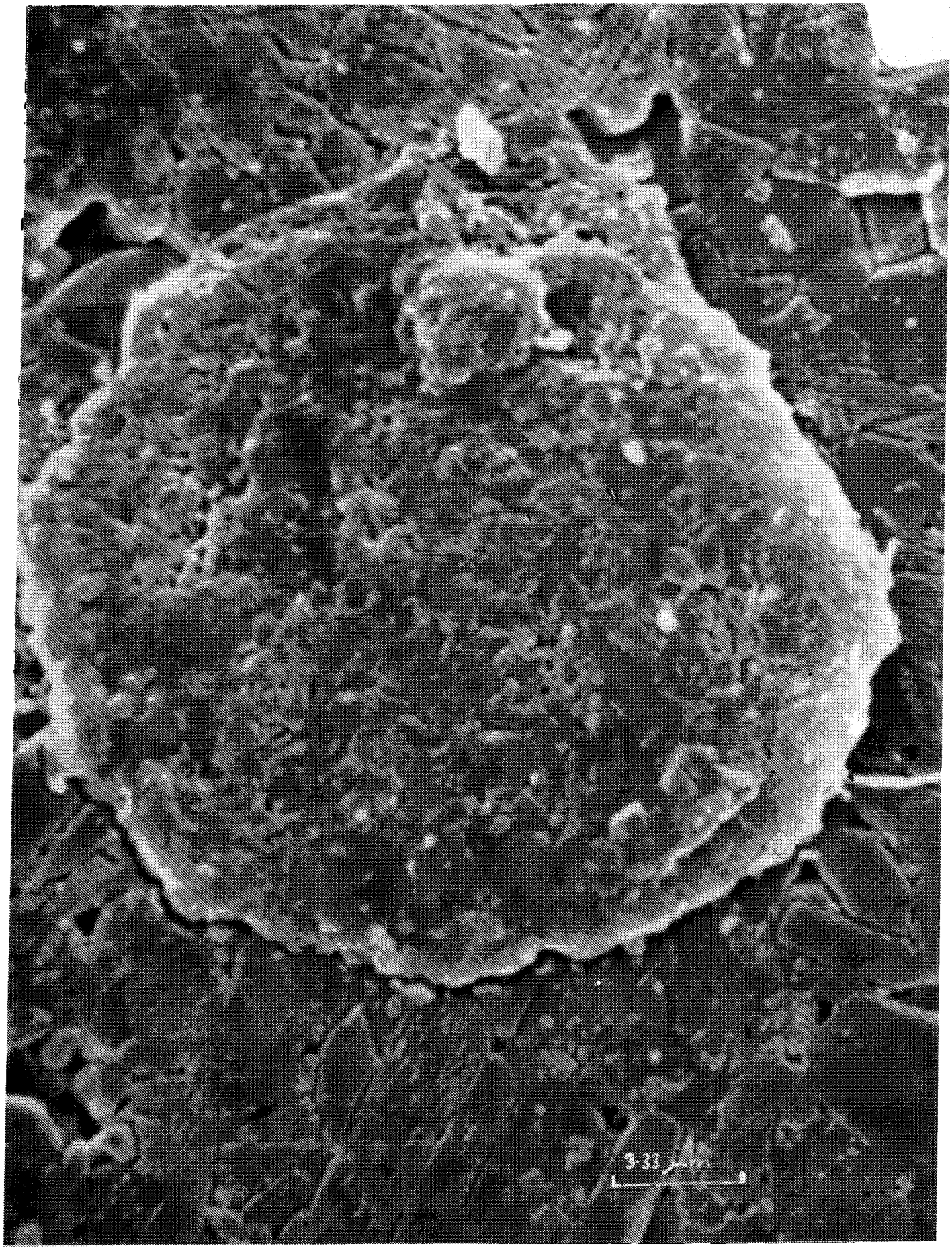

Fig. 4b SEM-photo of Al_2O_3 autoclaved in water at 195°C for 30 days. Close up of surface deposit

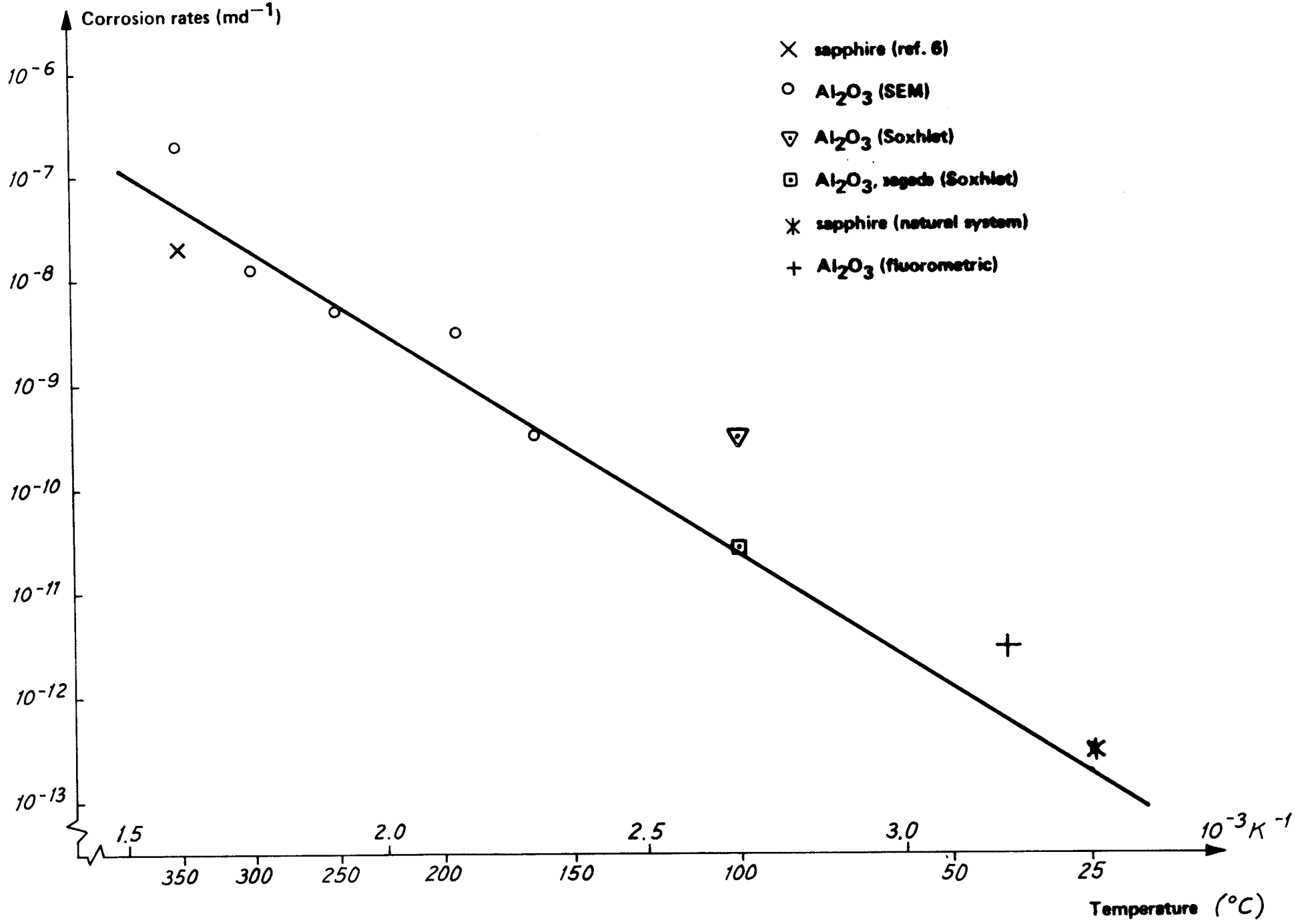

Figure 5. Arrhenius reaction rate curve for Al_2O_3 and natural sapphire. Log corrosion rate vs 1/T.

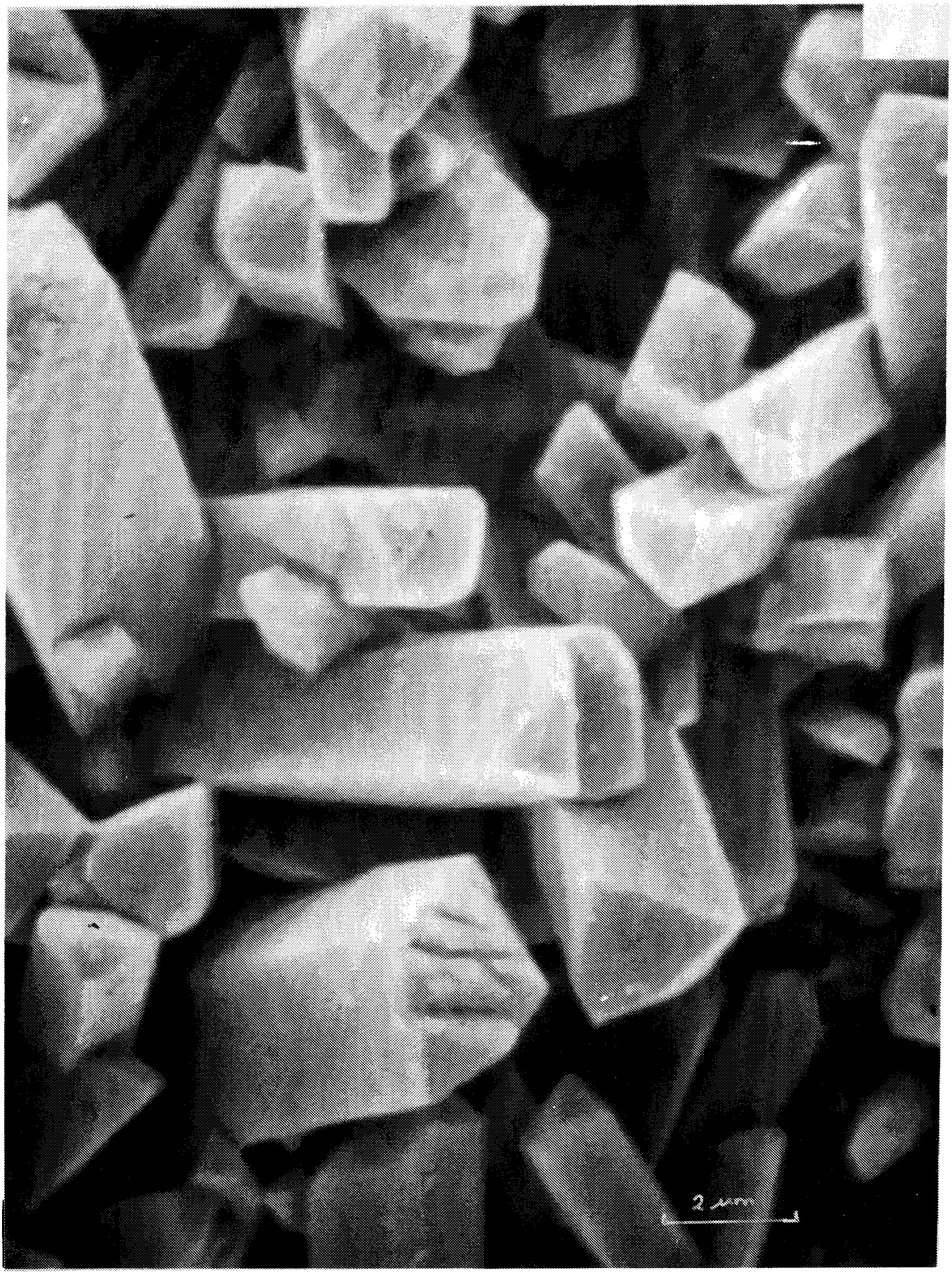

Fig. 6 SEM-photo of Al_2O_3 autoclaved in 1%. Na_2CO_3-solution at 260°C för 14 days. Boehmite crystals X-ray identified.

Studies of the durability of alumina in water

L Hydén

This report is a compilation of some investigations of the durability in water of alumina, to be used as an incapsulation material for high active nuclear waste. Within the KBS project this has also been studied by W.S. Fyfe, Canada, and his work is reported separately (Appendix C).

It is shown in a litterature-survey, carried out at Svenska Silikatforskningsinstitutet (Appendix B), that the solubility of Al_2O_3 in pure water at 20^oC is about 1 mg/l solution. The survey estimastes the solubility to increase by a factor 10 when pH increases one unit, and thus should be about 100 mg/l at pH 9.

Water with a composition similar to that of ground water, e.g. with dissolved SiO_2 and with multi-valent metal-ions, e.g. Mg^{2+}, can dissolve even less Al_2O_3, as sparingly soluble compounds (hydroxides, silicates) precipitate on the ceramic surface. This is mentioned in (Appendix B) and in two references therein. ESCA-studies of Al_2O_3 samples which have been exposed to synthetic ground water pH 8.5 at 90^oC, showed formation of $Mg(OH)_2$ with minor amounts of Si in the corrosion product layer (Appendix D1).

Similarly, the measurements at Studsvik, where Al_2O_3 samples were exposed to synthetic ground water at 90^oC, reveal that a first stage with preferably weight losses is followed by a second stage with weight gains; deposition of minerals (Appendix D2).

Likewise, one of the conclusions from the studies done by prof. Fyfe is that the corrosion rate is higher in pure water than in water in equilibrium with crushed quartz or granite.

For measurements of hydrogenprofiles in metals of hydration of glass, one can use the nuclear reaction

$$^{15}N + {}^{1}H = {}^{12}C^{*} + \alpha$$

where the excited ^{12}C decays emitting monoenergetic gamma-rays. The reaction has a very sharp resonance at 6385 keV and is unique in its capacity to produce gamma-rays. The method has been used by Tandemacceleratorlaboratoriet at Uppsala in order to measure the depth of hydration of alumina. The energy of the accelerated nitrogen ions is retarded in a known way and this makes possible a depth profiling of hydrogen. For various reasons it is necessary to relate the measurements to a reference plane and in this case a layer of arsenic was inplanted before the expose to water began. This inplantation was done by Asea Hafo and the depth should be about 500 Å.

The samples were exposed at Studsvik for various times (21, 54, 76, and 184 days) in 90°C water at pH 9.3 and pH 7. There has been some problems to measure how the hydrogen content varies with the depth. If, however, the depth of penetration is defined as the depth where the content of hydrogen has decreased to 50%, this can be measured with relatively good accuracy (± 30 Å).

For polycrystalline materials from Asea-Robertsfors a diagram of depth vs time has a least-square-adjusted line with a slope of 220 ± 90 Å/year and of 340 ± 90 Å/year for pH 9.3 and 7 respectively. Extrapolated linerarly this corresponds to a rate of penetration of 2.2 and 3.4 cm in a million years (Appendix D3). See above for definition of depth of penetration!

Monocrystalline alumina (sapphire) has been exposed the same way and did not show any hydration at all.

As the alumina samples were exposed at Studsvik for the ^{15}N-measurements the content of Al in the water was measured with atomic absorption. After

180 days at 90°C the results give a rate of 10-12 · 10^{-6} mm/year both at pH 7 and pH 9.3 (Appendix D4 and D5).

In good accordance with all the abovementioned measurements are those by N Ingri and L-O Öhman, who exposed alumina to 80°C dynamic water with pH 8.5. They measured the corrosion rate gravimetrically and analytically (spectrofluorometri) to be 68 · 10^{-6} resp 16 · 10^{-6} mm/year (Appendix D6).

For polycrystalline alumina the rate of attack (in nm/year) for the various measuring techniques has been compiled in the table below:

Method	Temp.	Corrosion rate nm/year at pH-7	pH 8.5	pH 9.3
Al in the water, atomic absorpt.	90°	10-12	-	10-12
Gravimetri	80°	-	68	-
Spectrofluoro-metri	80°	-	16	-
^{15}N-hydrogen profile*	90°	34	-	22

* See text for definition of depth of penetration!

Appendix D1

ESCA STUDY OF Al_2O_3 EXPOSED TO SIMULATED GROUNDWATER

I. Olefjord and U. Rilby, Dept. of Engineering Metals, Chalmers University of Technology, Fack, S-402 20 Gothenburg, Sweden

Summary

Al_2O_3 specimens exposed to simulated groundwater for 30, 100 and 268 days at 90°C and pH= 8.5 have been studied by means of ESCA (Electron Spectroscopy for Chemical Analysis). The ESCA technique has been chosen as a study method owing to its surface sensitivity and the fact that the method provides information on the chemical state and thickness of the surface layer. In order to permit verification of the surface composition, it has been necessary to study synthetic oxides and hydroxides as well as their naturally formed counterparts on metals.

Upon exposure of Al_2O_3 in synthetic groundwater, Mg is precipitated as a hydroxide on the surface. The layer also contains small amounts of Si. The composition and thickness of the layer has been determined by means of successive ion-beam etching and ESCA analysis. No clear-cut correlation between layer thickness and exposure time could be obtained. The measured maximum thickness is about 7500 Å and was obtained for the specimen exposed for 268 days. Layer thickness for the other specimens varied between 500Å and 1500 Å. The surface products do not form a smooth layer on the surface, but instead take the form of more or less interconnected nodules. There was relatively little Mg on one of the specimens, which was exposed for 100 days. The analysis of Al and the position of the oxygen signal show that no hydroxide binding of the Al-oxide took place after this exposure time.

Experiments

The specimens were prepared at ASEA in Robertsfors. Al_2O_3 was exposed in simulated groundwater (Appendix 1) at Studsvik Energiteknik AB (1). Exposure times, temperatures and pH are shown in Table 1. It was found that Mg and Si ions precipitate on the surface when Al_2O_3 is exposed in synthetic groundwater. It was therefore necessary to carry out calibration trials with these elements with respect to relative electron yield and their respective energy levels. This was done by studying not only the synthetic compunds Al_2O_3 and $Al(OH)_3$ plus MgO and $Mg(OH)_2$, but also oxide and hydroxide products formed on of Al, Mg and Si. In the calculations of the electron yield factors, oxygen has constituted the internal standard in the compounds Al_2O_3, MgO and SiO_2. For Al_2O_3, 17 measurements were carried out on synthetic Al_2O_3 and 3 measurements on an Al plate oxidized at 25°C in pure oxygen gas (p = 1 atm). For MgO, electron yield was calculated by measurement on an Mg sample (2 specimens) oxidized in the same manner as the above-mentioned Al plate. In addition, oxidation in oxygen of Al and Mg at 250° C was carried out. The obtained yield

Table 1. Materials exposured to simulated groundwater (Appendix 1)

Materials	Exposure times (days)	No. of samples	Environments	pH	Temperature (°C)	Remarks
Al_2O_3	0	17*	---	---	---	as received sintered Al_2O_3
$Al(OH)_3$	0	2	---	---	---	densificated powder
MgO	0	1	---	---	---	- " -
$Mg(OH)_2$	0	1	---	---	---	- " -
Al_2O_3	30	3	sim.gr.w.	8.5	90	
	100	3	-"-	-"-	-"-	
	268	1	-"-	-"-	-"-	

* Number of analyses of two different samples

ratio between Al and Mg was checked by analysis of $MgAl_2O_4$. The electron yield for SiO_2 was obtained by measurement on an oxidized Si plate (2 specimens). The obtained ratio between the yield factors for Mg and Al agrees very poorly with the values given in the literature (2,3). Our repeated measurements on synthetic and naturally formed oxides have given good agreement, so we have chosen our own values for the evaluation.

The thickness of the layer was determined by means of successive ion-beam etchings and ESCA analyses down to the level where only Al_2O_3 exists. The material removal rate was determined by means of calibration trials on oxidized Si plates with known oxide thickness. According to information in the literature (4), the material removal rate for Al_2O_3 is about 3 times lower than for SiO_2. The material removal rate obtained experimentally by us was used in determining the thickness of the surface layer, since the layer also contains Si and Mg compounds. Etching with Ar^+ ions leads to the implantation of these ions in the material. In the case of non-conductive materials such as Al_2O_3, this means that the surface becomes positively charged, whereby the ions are retarded, resulting in a reduced material removal rate. In order to avoid this effect, the charging was compensated with thermal electrons.

In ESCA analysis, electrons are emitted, whereby a non-conductive specimen assumes a surface charge. This broadens and shifts the signal. The charge was neutralized by continuously irradiating the specimen surface with electrons during the course of the experiment.

Results and discussion

Figure 1 shows the spectra from $Al(OH)_3$ and Al_2O_3, which were formed on an Al plate through exposure in water (solid line) and in pure oxygen gas (dashed line) at room temperature. In the former case, the specimen was polished under water, while in the

latter case it was ion-beam-etched to a nearly clean surface (dotted line) prior to oxidation. The double signal for Al shows that the layer thickness is of the same order of magnitude as the free mean path of the photoelectrons in the metal. The right-hand signal represents Al in the metallic state (117.8 eV) while the left-hand signal (higher binding energy) represents a contribution from Al in the oxidized state. The figure shows that the position of the oxygen signal is dependent upon the crystal type. For hydroxide, the O 1s signal is located at 1.3 eV higher bond energy than in Al_2O_3. This difference can be exploited in order to determine whether the surface layer is an oxide or a hydroxide. In the analysis of synthetic unexposed Al_2O_3 (17 trials) and $Al(OH)_3$ (2 trials), 411.9 $\pm$ 0.3 eV and 412.8 $\pm$ 0.3 eV, respectively, were obtained as the differences between the energy levels O 1s and Al 2s for the two different compounds. The corresponding literature values (5) are 412.1 for Al_2O_3 and 412.8 for $Al(OH)_3$. Thus, the agreement with our results is very good. Moreover, the author of the cited reference states that the difference for AlOOH is 412.4 eV.

The ESCA measurement on MgO formed on an Mg plate by means of oxidation at 250°C in oxygen gives 441.1 $\pm$ 0.3 eV as the difference in binding energy between the O 1s and Mg 2s levels. The corresponding difference in bond energy for $Mg(OH)_2$ prepared by means of water polishing of Mg is 443.1 $\pm$ 0.4 eV. 443.3 eV was obtained for compacted $Mg(OH)_2$ powder.

The advantage of carrying out calibration measurements on a thin oxide layer formed on a metal is that the correct signal positions are obtained, since the charging effect is negligible. Figures 2a and 2b show ESCA recordings on synthetic unexposed Al_2O_3. The dotted curves were obtained by direct measurement on the specimen surface. Due to charging, the signals are shifted about 7eV towards a higher binding energy compared with those obtained in figure 1. This charging effect was compensated for by irradiation of the specimen surface with lowenergy electrons. In the reported experiment, the Al 2s signal was shifted to the same position as was obtained in analysis of a thin oxide layer (solid line). The figure shows that the oxygen signal also assumes the correct position. This shows that the correction is linear and that the corrected differences can be used in order to determine oxide-hydroxide states.

Analysis of corrosion products on exposed Al_2O_3

Surface analyses of exposed specimens show that not only Al and oxygen, but also Mg and Si are present in the surface zone. The latter elements were precipitated from the solution. Appendix 1 shows that the water contains 166.9 mg/l $MgCl_2$ and 30 mg/l SiO_2. Table 2 shows the composition of the surface layer in atom percent for reference specimens and prior to ionbeam etching for the exposed specimens. Specimens A,B and C represent parallel trials carried out on the same exposure occasion.

Table 2. The composition in atom percent of surface layer on unexposed and exposed Al_2O_3.

Specimens		a/o Mg	a/o Si	a/o Al	a/o O
Unexposed (2 specimens)		C	0	40	60
Al_2O_3 30 days (3 specimens)	A	42	4	6	48
	B	51	5	3	40
	C	27	3	2	68
Al_2O_3 100 days (3 specimens)	A	11	1	25	63
	B	19	2	16	63
	C	27	1	9	63
Al_2O_3 100 days unpolished side		30	1	10	59
Al_2O_3 268 days (1 specimen)		49	2	0	49

As is evident from the table, the dominant element is Mg. Except for one trial, the Mg content varies between 20 and 50 percent, while the Si and Al contents only represent a few percent in the surface layer. The accuracy of the determination is relatively low, owing to the fact that the electron yield for Mg is considerably lower than for the other elements. A small error in determination of the intensity is therefore greatly magnified due to the high weighting factor.

The distribution of the cations in depth is shown by Figures 3 to 8. The thickness of the layer has been assumed to be equal to the etching depth where only Al (of the cations) is detectable. All specimens, where measurements were carried out after several etchings, are characterized by the fact that the Mg content is relatively constant for the first etching points, after which it declines continuously. This can be due to either the fact that the thickness of the layer varies over the surface, whereby point "break-throughs" take place, or to the fact that material is removed from certain surface regions at a faster rate than others, owing to the fact that the surface is not microscopically flat. In both cases, the underlying aluminium oxide is exposed at the same time as islands of magnesium and silicon compounds are present on the surface. An indication that the chemical composition of the surface products is nearly homogeneous and that their thickness varies is given by the fact that aluminium was not detectable in the surface zone on the specimen that was exposed for 268 days (Figure 8). Only after etching to a depth greater than 1 500 Ångström did the Al signal grow.

Table 3 shows the difference in bond energies between O 1s and Al 2s and between O 1s and Mg 2s before and after the first etching. It has been shown above that these differences are greater for the hydroxides than for the oxides. The table shows that the differences for the exposed specimens are greater before ionbeam etching than after etching. An exception is specimen A, which was exposed for 100 days (Figure 5). For this specimen, the difference

Table 3. Difference in binding energy between the O 1s and Al 2s and between the O 1s and Mg 2s levels before and after etching.

Specimen	Before etching		After etching		
	$(BE)_{O1s}-(BE)_{Al2s}$ (eV)	$(BE)_{O1s}-(BE)_{Mg2s}$ (eV)	$(BE)_{O1s}-(BE)_{Al2s}$ (eV)	$(BE)_{O1s}-(BE)_{Mg2s}$ (eV)	Layer thickness (Å)
Exp. Al_2O_3 A	412.5	442.8	412.0	441.9	500
30 d B	412.8	442.5	412.2	---	---xxx)
(3 specimens) C	412.6	443.0	412.0	439.4	1200
Exp. Al_2O_3 A	412.1	442.5	412.1	---	<250
100 d B	412.6	443.2	412.2	442.3	1500
(3 specimens) C	412.5	443.1	411.2	438.3	1300
Exp. Al_2O_3 100 d unpolished side	412.5	442.7	---x)	---	---xxx)
Exp. Al_2O_3 268 d (1 specimen)	---xx)	442.7	412.0	441.5	7500

x) Not etched
xx) No signal from the Al 2s areas
xxx) The layer thickness has not been determined

in binding energy between oxygen and aluminium is equal to the value obtained on unexposed Al_2O_3. As is evident from table 2 and Figure 5, there is relatively little Mg on this specimen and Mg could not be detected after etching of the specimen down to 250 Ångström.

The measured differences in binding energies as a function of the etching depths for all specimens are presented in Figures 9a and 10. As is evident from the figures, no noticeable change of the binding energy differences can be detected after the first etching. The statistical distribution from 17 analyses of unexposed Al_2O_3 is given in Figure 9b. The median value for the measured binding energy difference for these recordings is only a few tenths of an electron volt below the values obtained for the exposed specimens. This difference can be explained by the presence of $Mg(OH)_2$, whose position for the oxygen signal is located several tenths of an electron volt above the position for oxygen in the other oxygen compounds.

Conclusion

The difference in binding energy between oxygen and magnesium shows that the surface product consists for the most part of $Mg(OH)_2$. Silicon is present in its tetravalent state. It is not, however, possible to determine in which compound Si is incorporated. Owing to the fact that most of the surface is covered by $Mg(OH)_2$ after exposure, it is not possible to determine whether aluminium also occurs as a hydroxide. The result from the specimen that was exposed for 100 days, and on whose surface very little $Mg(OH)_2$ was precipitated, indicates that no change takes place in the surface state of the aluminium oxide. Hydroxide formation can not be demonstrated for this specimen because the positions of the oxygen signal before and after ionbeam etching agree with those obtained from the analysis of unexposed aluminium oxide.

References

1. Svensson, B-M, Dahl, L., Lakning av Al_2O_3 under simulerade deponeringsbetingelser ("Leaching of Al_2O_3 under simulated repository conditions"), Work report MS-78/213, AB Atomenergi (1978).

2. Nefedov, V.I. et al., Journal of Electron Spectroscopic and Related Phenomena, 7 (1985) 175.

3. Jörgensen, C. and Berthon, H., Faradays Discussions of the Chemical Society, No. 54, The Photoelectron Spectroscopy of Molecules, 1972.

4. Davidse, P.D. and Maissel, J.I., The Journal of Vacuum Science and Technology, 4 (1967) 33.

5. Pitton, O., Jörgensen, C.K. and Berthon, H., Chimia, 12 (1976) 540.

Simulated groundwater pH 8.5

All ion species are given in mg/l

Recipe ↓ Salts (equiv.)	mg/l	HCO_3^-	Ca^{2+}	Mg^{2+}	Na^+	K^+	Fe^{2+}	Mn^{2+}	SiO_2	NH_4^+	NO_3^-	Cl^-	F^-	NO_2^-	SO_4^{2-}
$NaHCO_3$	165.2	120			45.23										
K_2SO_4	31.2					14.0									17.19
$MnSO_4$	2.8							1.02							1.78
$(H_4N)_2SO_4$	0.37									0.1					0.27
NaF	3.3				1.81								1.49		
$NaNO_3$	0.4				0.108						0.292				
$NaNO_2$	0.3				0.1									0.2	
SiO_2	30								30						
$CaCl_2$	185.3		66.89									118.41			
$MgCl_2$	166.9			30.0								136.93			
Na_2SO_4	109.3				35.4										73.9
NaCl	568.1				223.5							344.66			
$FeSO_4$	10.9						4.0								6.9
		120	66.9	30.0	306.1	14.0	4.0	1.0	30	0.1	0.3	600	1.5	0.2	100.0

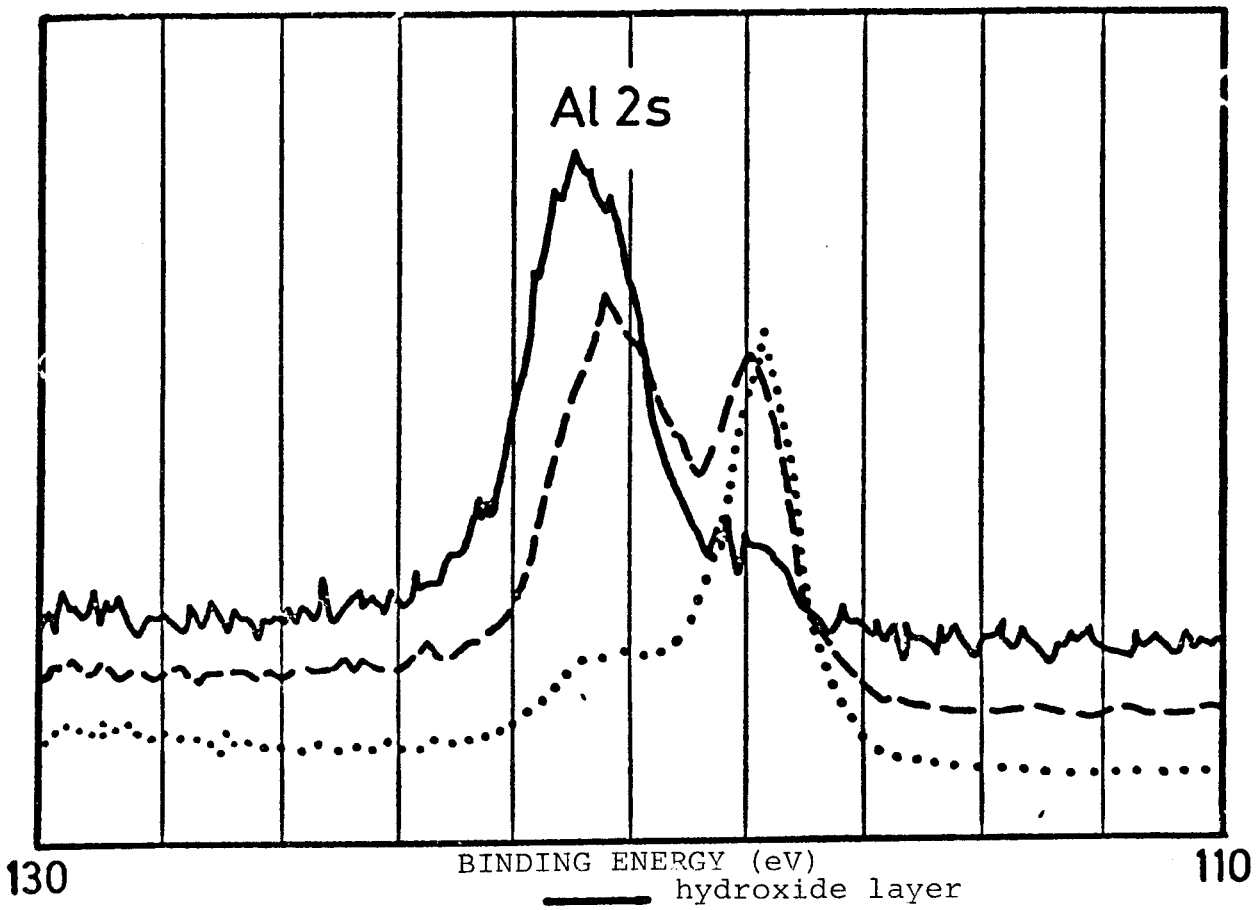

Fig. 1 Al plate

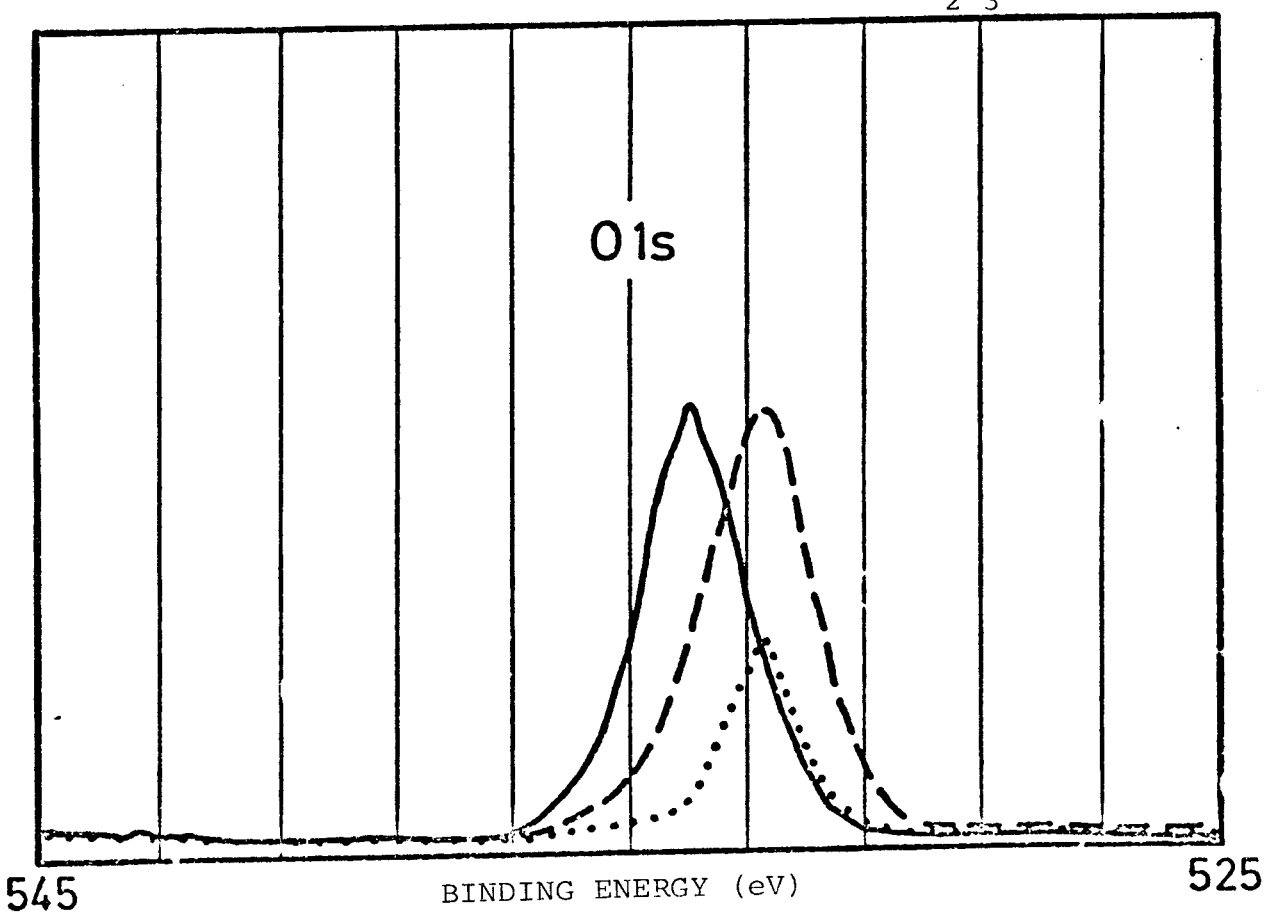

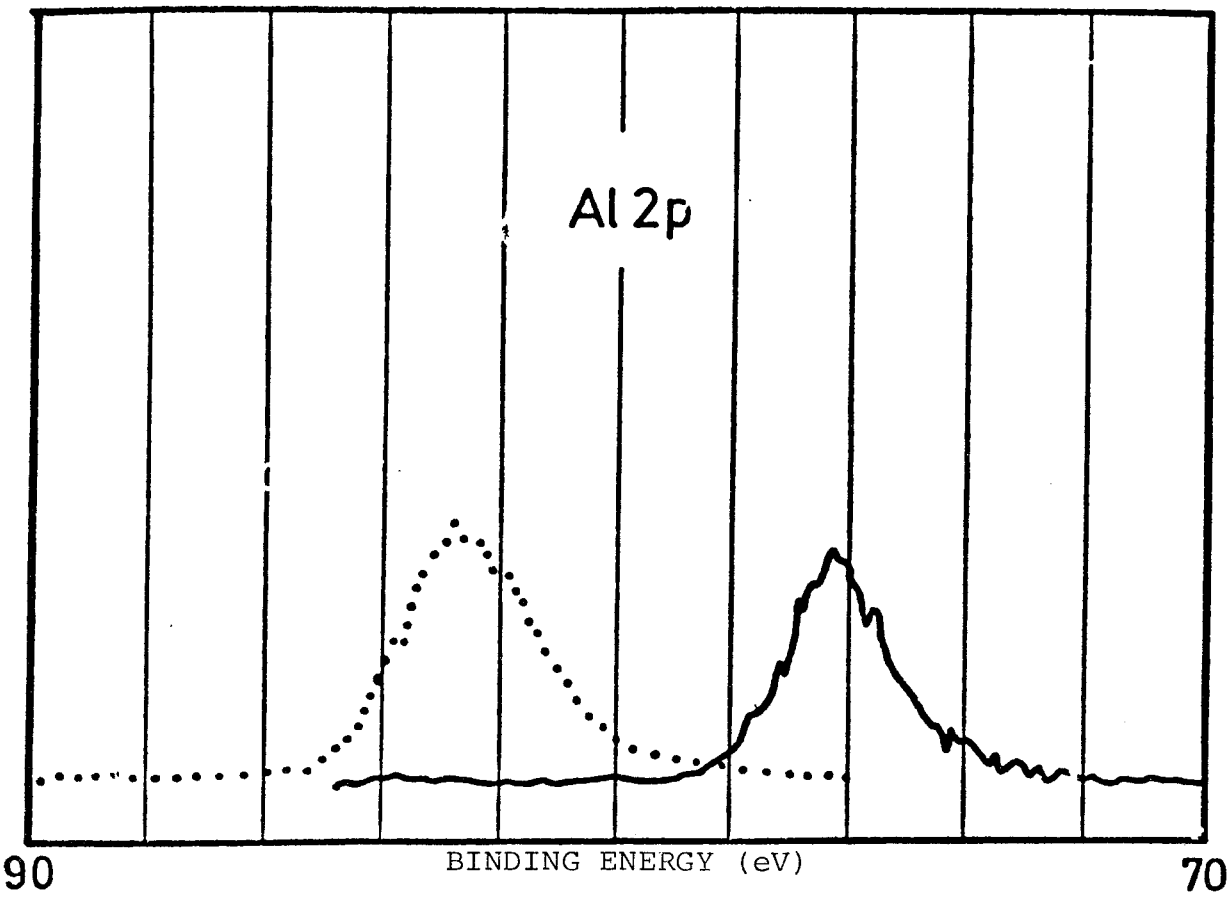

Fig. 2 a Unexp. Al_2O_3

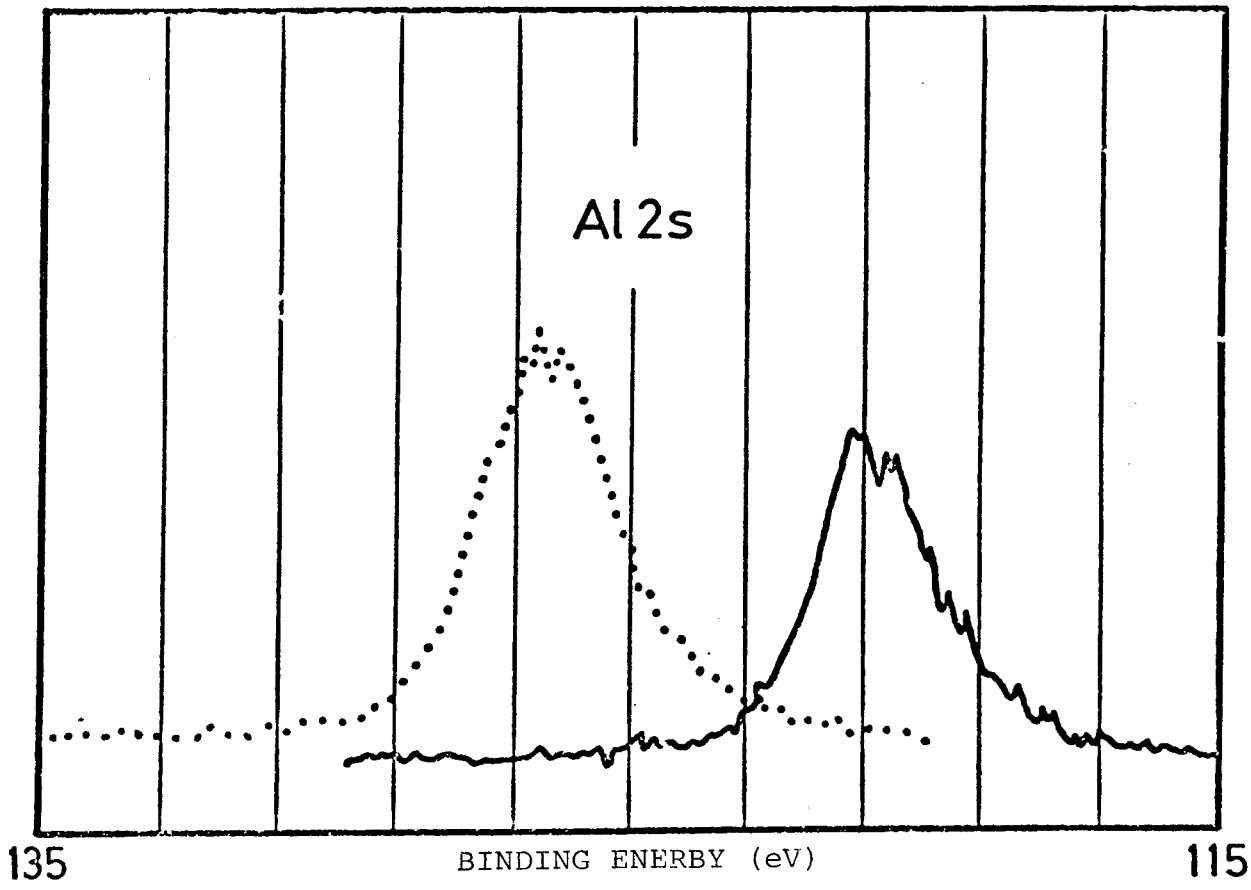

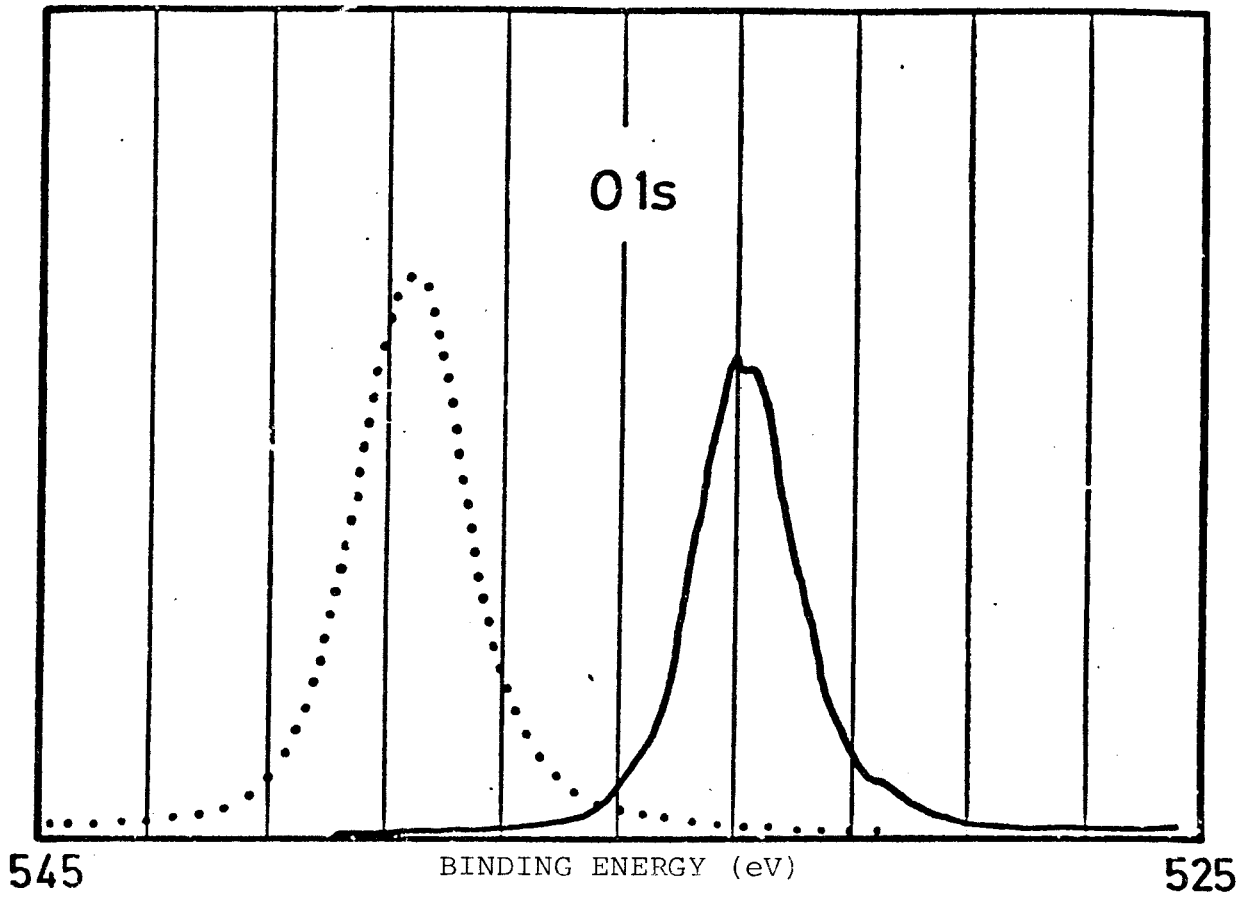

Fig. 2b Unexp. Al_2O_3

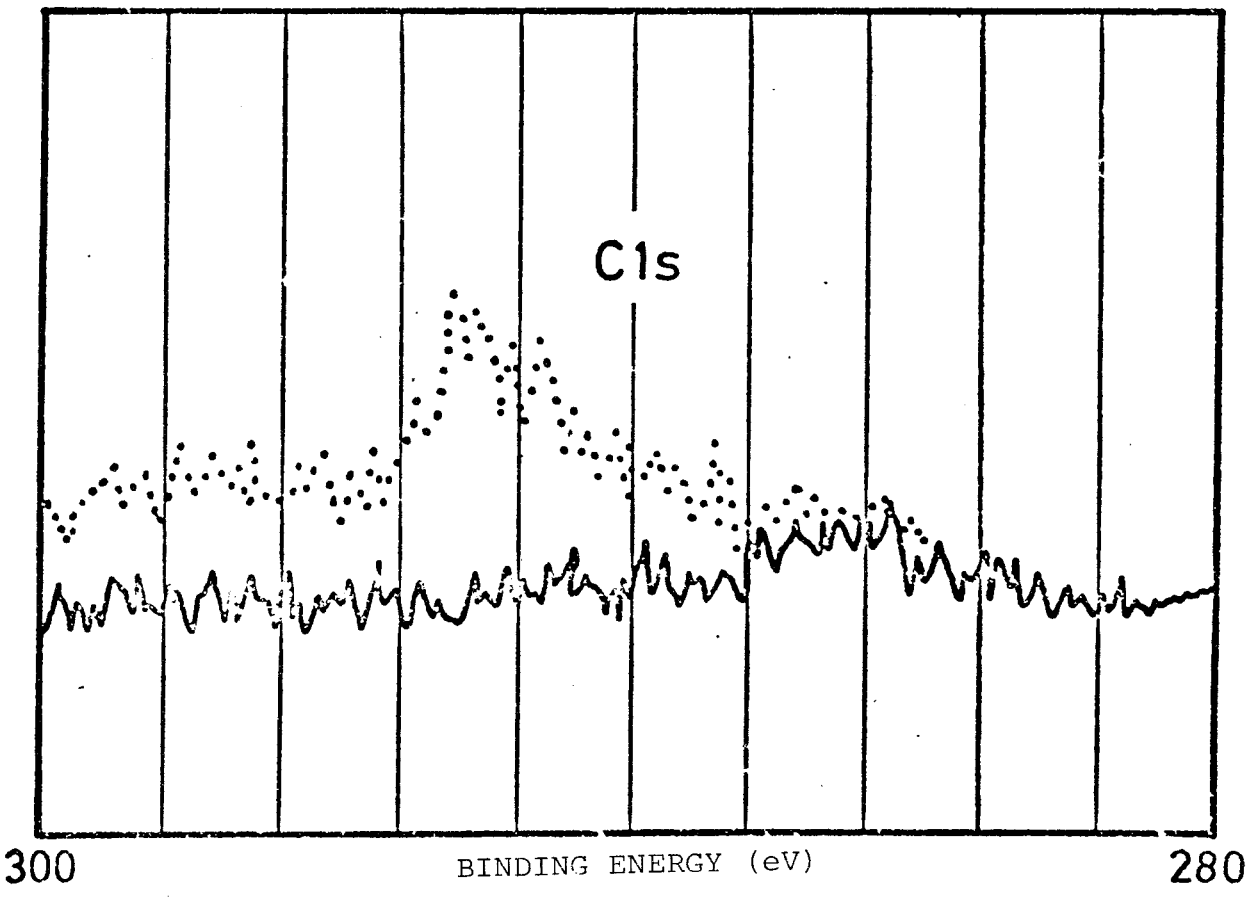

Fig 3

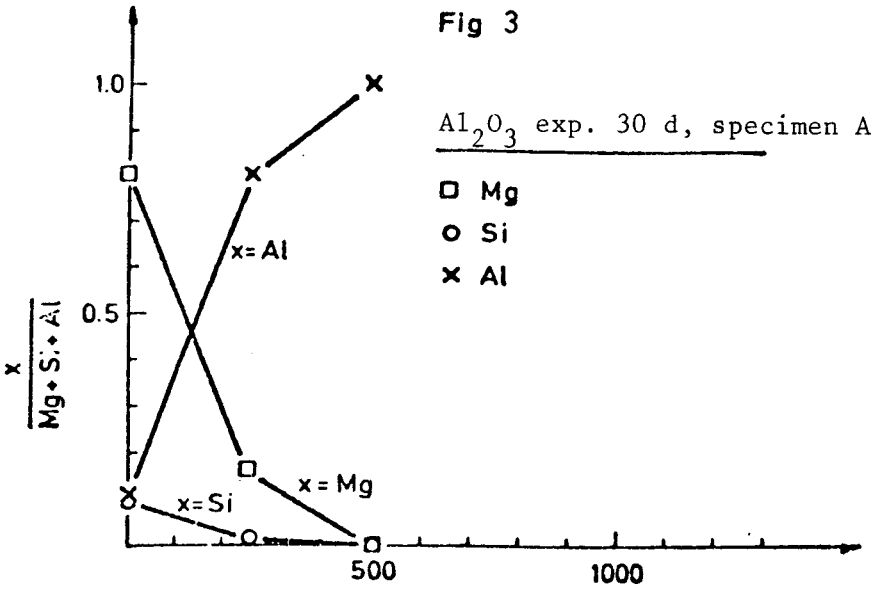
Al_2O_3 exp. 30 d, specimen A
Mg
Si
Al
1.0
0.5
x= Al
x = Mg
x=Si
500
1000
$\frac{x}{Mg+Si+Al}$
Etching depth (Å)

Fig. 4

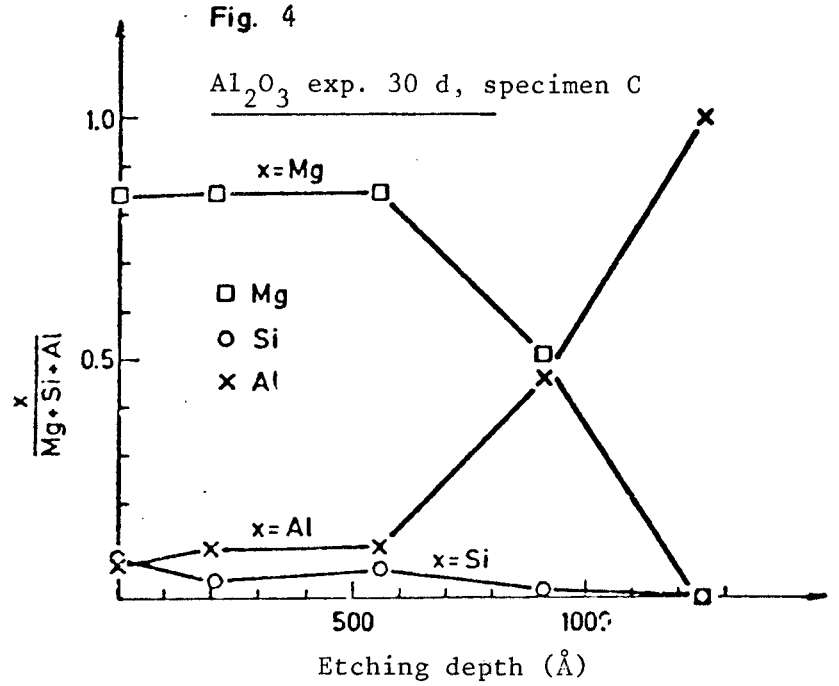
Al_2O_3 exp. 30 d, specimen C
1.0
0.5
x=Mg
Mg
Si
Al
x=Al
x=Si
500
$\frac{x}{Mg+Si+Al}$
Etching depth (Å)

Fig. 5

Al_2O_3 exp. 100 d, specimen A

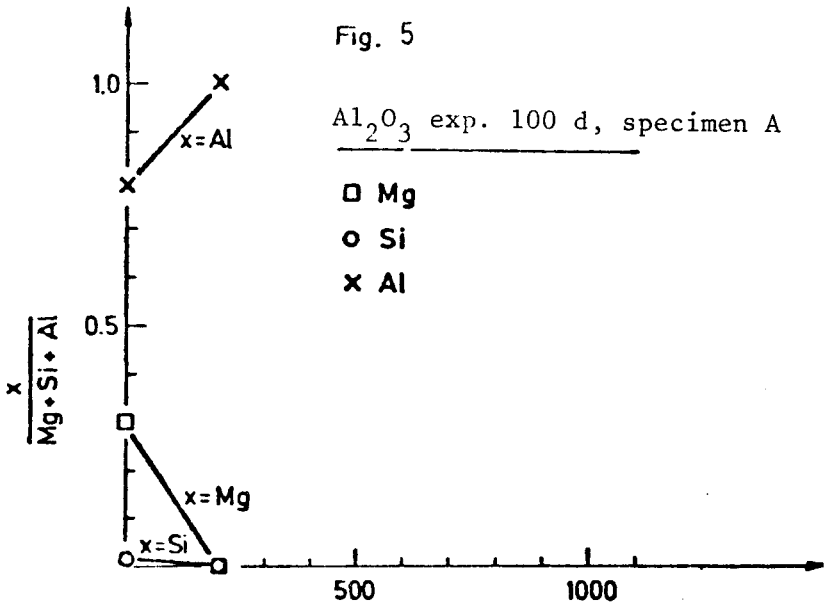

Fig. 6

Al_2O_3 exp. 100 d, specimen B

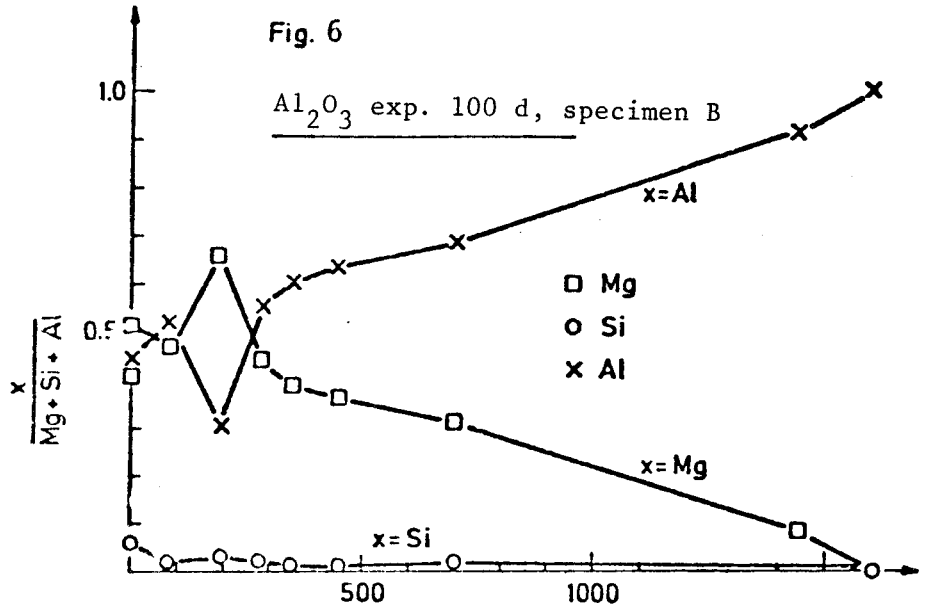

Fig. 7

Al_2O_3 exp. 100 d, specimen C

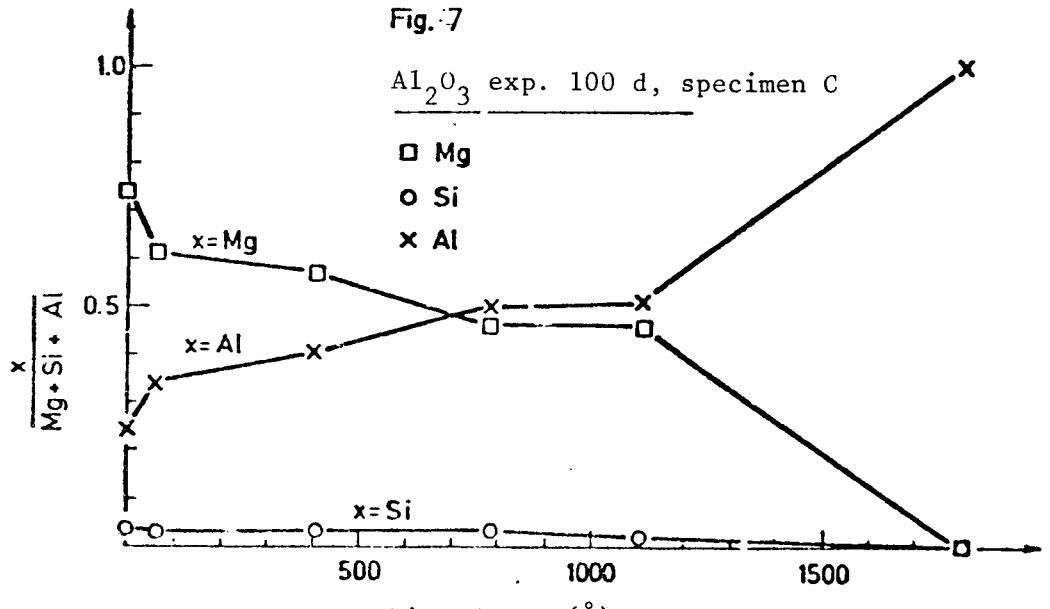

Fig. 8 Exp. Al_2O_3 268 d

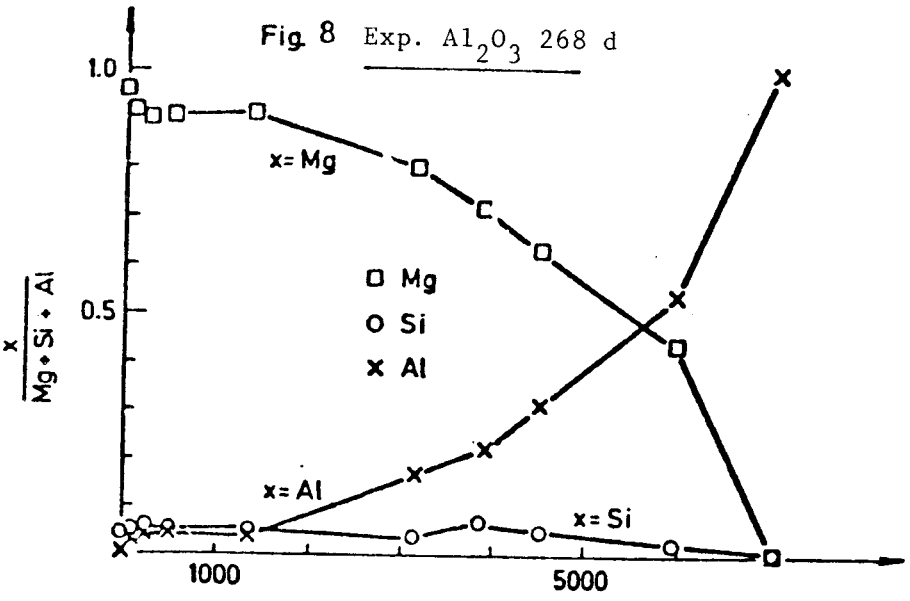

Fig. 9a. Difference in binding energy between the Os and Al 2s levels at different etching depths for all exposed specimens.

Fig. 9b. Distribution of 17 analyses of unexposed specimen.

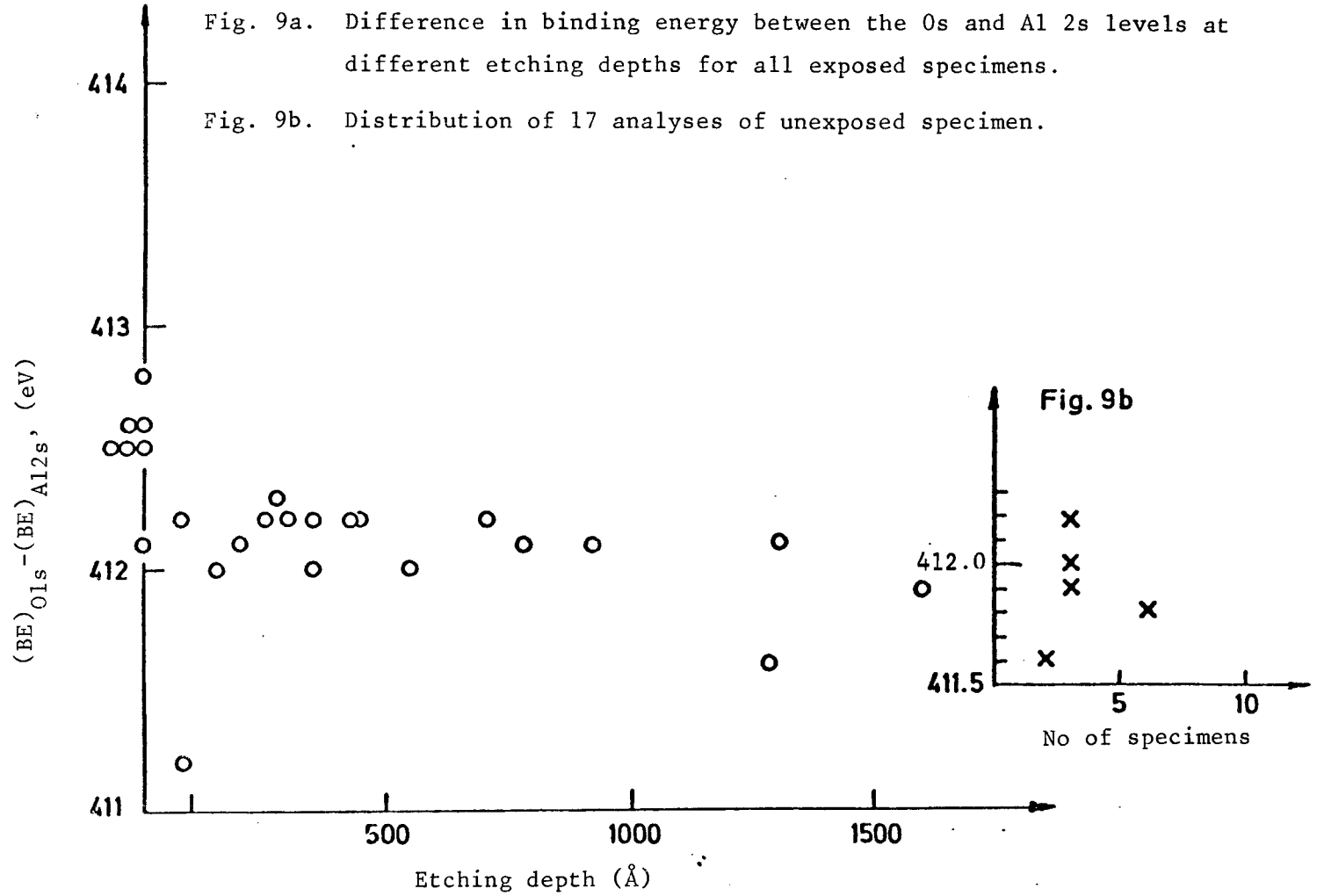

Fig 10. Difference in binding energy between the O 1s and Mg 2s levels at different etching depths for all exposed specimens.

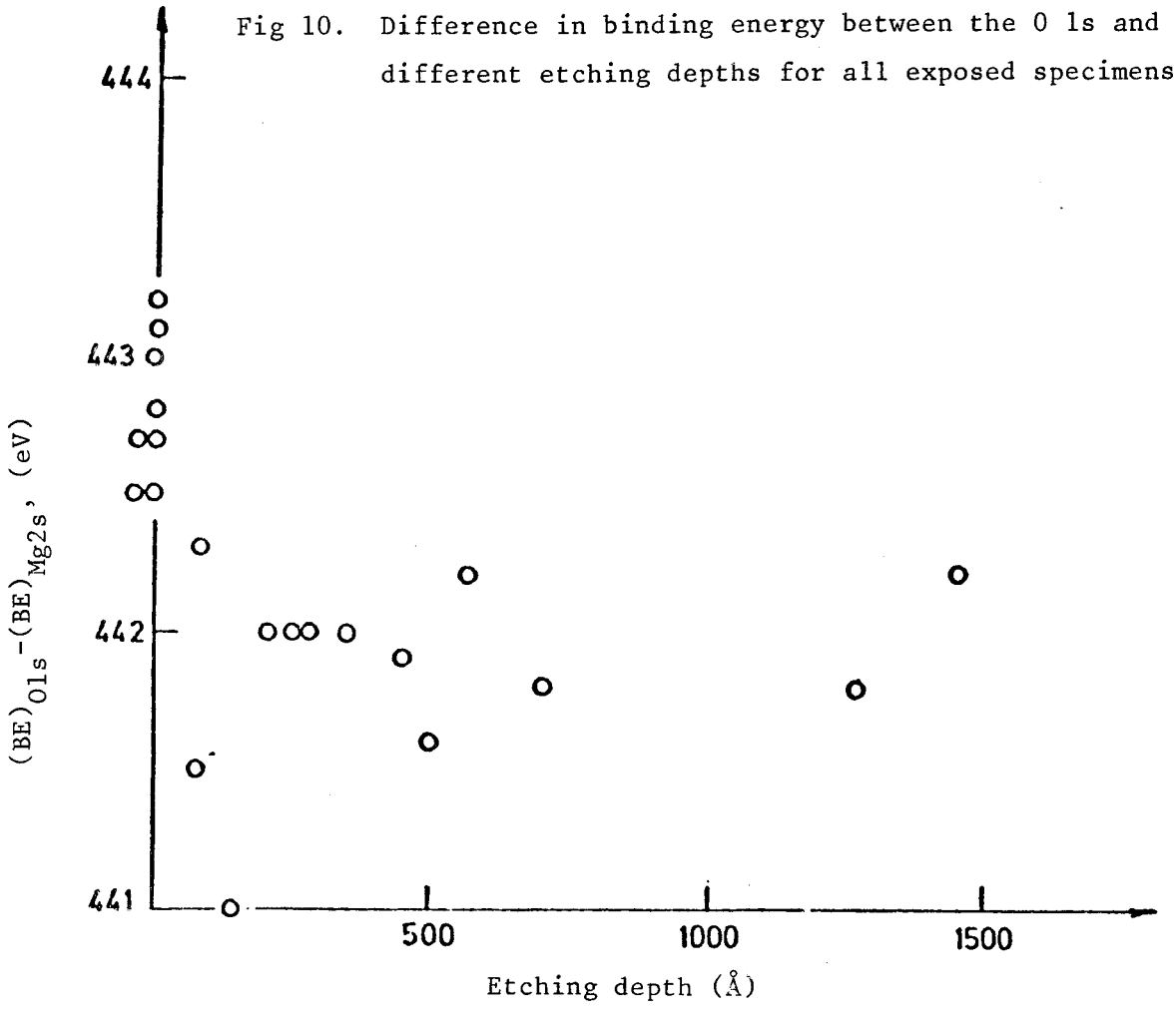

Appendix D2

Studsvik Report MS - 78/213 1978-06-02

LEACHING OF Al_2O_3 UNDER SIMULATED REPOSITORY CONDITIONS

Britt-Marie Svensson
Lennart Dahl

ABSTRACT In a study commissioned by KBS, Al_2O_3 has been leached in simulated groundwater at pH 8.5, and in a clay bed saturated with the same water, as well as in simulated groundwater at pH 6 and pH 10, all at 90°C.

Weight increases caused by deposits from the leachant water were obtained. These deposits mask the dissolution of Al_2O_3.

TABLE OF CONTENTS

1. INTRODUCTION

The leaching resistance of the following materials has been investigated, commissioned by KBS within the project "Leaching of ceramic encapsulation for nuclear waste" at the Department of Materials in Studsvik:

Cordierite, LD compound, Corning and Al_2O_3.

This report covers the tests with Al_2O_3. The tests with the other materials have been reported in AEMSI94.

The Al_2O_3 material was leached at 90°C in simulated groundwater at pH 6, pH 8.5 and pH 10, and in a clay bed saturated with simulated groundwater of pH 8.5. The leaching time was varied from 30 to 300 days. At pH 8.5 involved discs for determination of weight changes and plates for microscopic examinations were exposed. At pH 6 and pH 10 only discs for the determination of weight changes were leached.

2. EXPERIMENTAL

2.1 Equipment

2.1.1 Apparatus

Leaching vessel	Polypropylene or TPX vessel with polyethylene lid. Specimen holder of SIS 2343 (type 316) stainless steel.
Heating	Thermostatically controlled water baths, with stirring.
Balance	Mettler analysis balance, accuracy 0.0001 g.

2.1.2 Testing environment

Leachant solution	Simulated groundwater, see AP-MS-177, Appendix C.1. Stationary water.
Clay bed	90% silica sand + 10% bentonite is mixed with 25% simulated groundwater, pH 8.5, see Appendix C.1.
Temperature	90 $\pm$ 2°C
Leachant solution volume/test surface	2 ml·cm^2
Water change	Twice a week

2.1.3 Test material

Material	Al_2O_3	See Table A.1.
Dimensions		Disc dia. 70 mm, t=5 mm Rectangles 5 x 10 x 2 mm
Surface finish		Ground/polished. The specimens are delivered by and are assumed to have been characterized by KBS.

2.1.4 Specimen treatment

Cleaning, before	The specimens are ultrasonically cleaned for 10 min in acetone and then 10 minutes in alcohol.
Drying	1 h at 150°C in a heating chamber, cooling in a desiccator for 16 - 24 h.
Weighing	Mettler analysis balance, accuracy 0.0001 g.
Cleaning, after	Leached specimens are rinsed in de-ionized water during simultaneously lightly rubbed with rubber-gloved hands, followed by rubbing with a thinner-moistened paper napkin. Then ultrasonic cleaning for 10 min in de-ionized water and rinsing with alcohol.
Drying and weighing	As above.

2.2 Execution

24 discs and 30 rectangles were leached in water.
9 discs were leached in clay. See leaching scheme, Table A.2.

Seed crystals of $Al_2O_3.H_2O$ and $Al_2O_3.3H_2O$ were added during the leaching tests in order to achieve maximum leach rate (as recommended by professor W S Fyfe, University of Western Ontario, London, Canada).

2.2.1 Discs for gravimetric analysis

2.2.1.1 Leaching in water

The cleaned, dried and weighed specimens were placed horizontally on specimen holders of stainless steel in the leaching vessels. Seed crystals were then added and hot leachant solution was added to the vessel after filtration through a Munktell 100 filter paper. (See APMS177, Appendix C.1.) The leaching vessels were then placed in a thermostatically controlled water bath at 90 $\pm$ 2°C.

When the water was changed (twice a week), the leaching vessel was lifted out of the water bath, the leachant solution was removed by suction and warm, filtered leachant solution was added. Seed crystals and any material which had been deposited on the test discs and on the walls of the leaching vessels, were disturbed as little as possible, while any precipitate in the solution was removed.

2.2.1.2 Leaching in a clay bed

Bentonite, silica sand and water were mixed to a homogeneous, plastic paste, a centimetre-thick layer of which was packed in the bottom of a leaching vessel. A test disc was then placed horizontally on the clay surface with seed crystals in the immediate vicinity of the disc. Clay was packed all around and over the test disc, after which the next disc was packed in the same manner. Great care was taken to ensure good contact between the clay and the test disc over the entire surface of the disc.

After leaching, the specimens were cleaned, dried and weighed as described previously. Total weight changes and weight changes per unit time were calculated (see Table A.3). The discs were then stored in a desiccator.

2.2.2 Rectangles for microscopic examination

2 specimens in each leaching series were delivered with Au coated on 1/4 of the surface, in order to obtain a reference surface. The specimens were placed in wire baskets of stainless steel and leached in water. Leaching was carried out in the same manner as for discs, as described above.

After leaching, the specimens were rinsed with deionized water and dried in air. They were then sent to different laboratories for microscopic examination, according to agreement with KBS.

3. RESULTS

The results of the gravimetric determinations are presented in Table A.3 and Figure B.1.

During leaching in water at pH 6 and pH 10, weight reductions were obtained first, then, after about 100 days of leaching, weight increases were obtained. At pH 8.5 in water, weight increases were obtained throughout the entire exposure. These are about 10 times greater than at pH 6 and pH 10 for the same leaching times.

During leaching in a clay bed, a weight loss is obtained after 100 days, and a weight increase after 300 days.

The weight increases are caused by deposits from the leaching water and mask the actual dissolution of the Al_2O_3 material. It is difficult to draw conclusions regarding the leaching resistance of Al_2O_3 on the basis of this study.

Besides the authors, Eva Söderström, Nils Lagmyr and Maj Ljungberg participated in the studies. Walter Hübner, AE, and Lennart Hyden, KBS, participated in the planning of the project.

Table A.1

Al_2O_3 produced by ASEA's isostatic high-temperature pressing technique. Chemical composition, % by weight.

Al_2O_3	99.5
SiO_2	0.03
CaO	0.02
Na_2O	0.08
Fe_2O_3	0.01
Density	4.0 g · cm^{-3}

Table A.2

Al_2O_3. Leaching scheme, number of specimens

Type / Medium	Discs						Rectangles		
	Water			Clay			Water		
Leaching time d / pH	30	100	300	30	100	300	30	100	300
6	-	3	3	-	-	-	-	-	-
8.5	-	3	6	-	3	6	10	10	10
10	3	3	3	-	-	-	-	-	-

AB ATOMENERGI

TABELLBLAD A4

		Al_2O_3 leaching Gravimetric results				Table A.3	
Leaching environment		Leaching time d	Test surface cm^2	Weight change			
Medium	pH			mg total	Mean	$\mu g\ cm^{-2} d^{-1}$	Mean
Water	6	105	87	-1.4	-2 ± 2	-0.15	-0.24±0.15
			84	-4.1		-0.46	
			83	-1.5		-0.17	
			78	-1.3		-0.16	
Water	6	188	86	3.2	2 ± 1	0.20	-0.12±0.07
			82	1.3		0.08	
			86	1.5		0.09	
Water	8.5	97	86	13.9	14 ± 2	1.7	1.7±0.2
			87	12.3		1.5	
			89	16.8		1.9	
Clay	8.5	97	89	(8.4)	-	-	-
			89	-0.8	-1 ± 1	-0.09	-0.14±0.07
			88	-1.6		-0.19	
Water	8.5	300	94	28.3	33 ± 4	1.0	1.2±0.2
			91	33.1		1.2	
			91	32.4		1.2	
			95	32.2		1.1	
			94	34.9		1.2	
			90	38.0		1.4	
Clay	8.5	285	90	5.2	2 ± 3	0.20	0.06±0.10
			88	0.8		0.03	
			87	1.7		0.07	
			92	3.5		0.13	
			90	0		0	
			87	-1.6		-0.07	

BL 0142

TABELLBLAD A4

		Al_2O_3 leaching Gravimetric results				Table A.3 (cont.)	
Leaching environment		Leaching time d	Test surface cm^2	Weight change			
Medium	pH			mg total	Mean	$\mu g\ cm^{-2} d^{-1}$	Mean
Water	10	30	87	-2.3	-3 ± 1	-0.9	-1 ± 0.3
			87	-3.8		-1.4	
			82	-2.2		-0.9	
Water	10	107	86	-0.7	0 ± 1	-0.08	0 ± 0.1
			82	0.2		0.02	
			85	-0.2		-0.02	
Water	10	211	91	9.6	4 ± 5	0.50	0.2±0.3
			86	2.0		0.11	
			86	1.1		0.06	

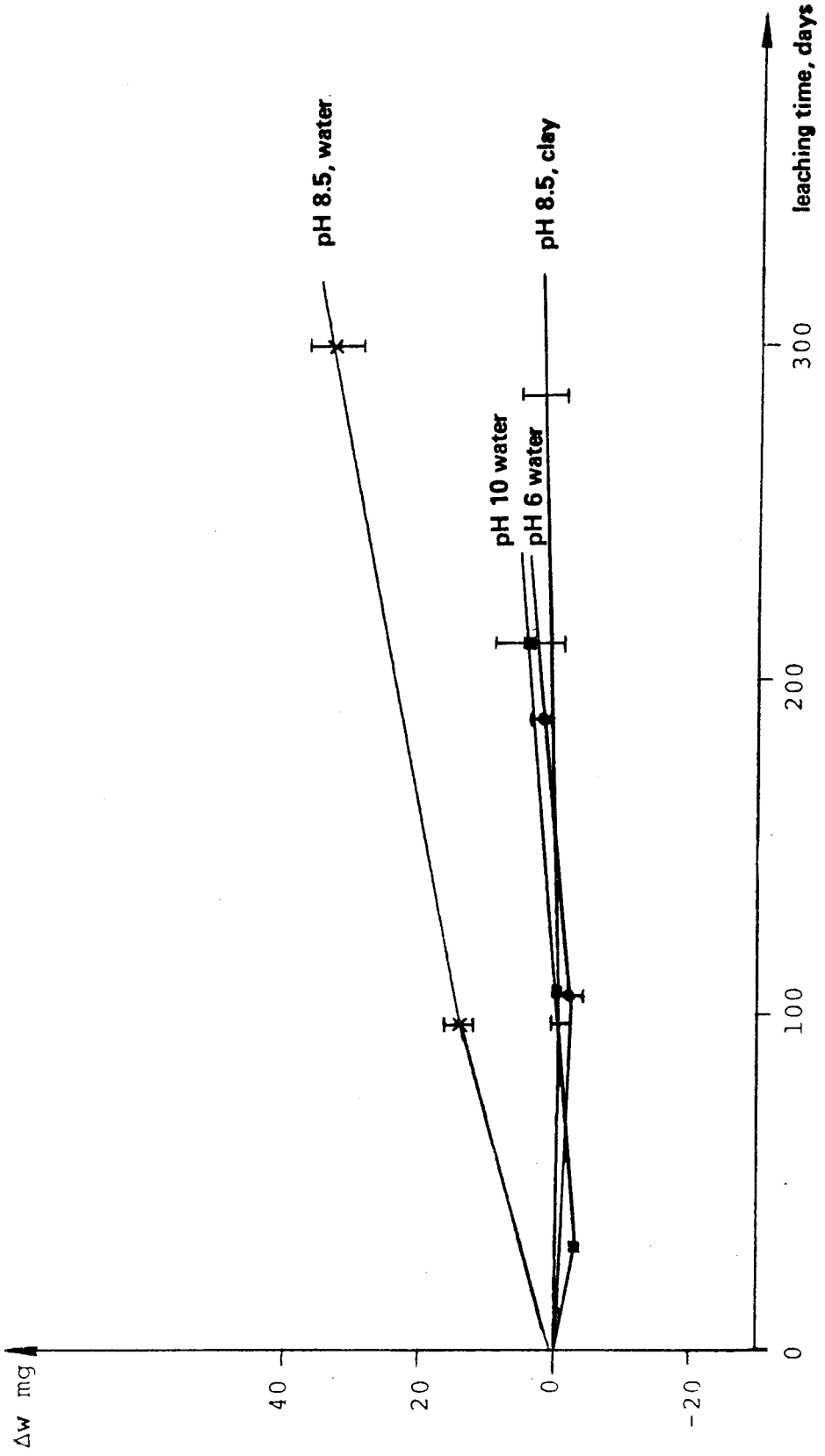

Figure B.1 Al_2O_3 leaching. Total weight changes

Preparation of simulated groundwater leachings for ceramic leachings, KBS project (AE AP MS 177, 1977-10-04)
BM Svensson

The composition of the leaching water is shown by Appendices 13. Stock solutions of each constituent compound were prepared with concentrations 200 or 1 000 times the desired leachant solution concentrations. The required amount of stock solution is taken out and diluted with deionized water in a stainless steel vessel, volume 50 l. The solution is mixed by bubbling air throughout, the pH is checked and adjusted. The solution is heated to 90°C and kept at this temperature until used, 1 - 2 weeks. The pH is checked again after 24 hours. Immediately prior to use, the leachant water is filtered through a Munktell 100 filter paper.

Simulated groundwater, pH 6

All ionic species are given in mg/l

Recipe ↓ Salts (equiv.)	mg/l	HCO_3^-	Ca^{2+}	Mg^{2+}	Na^+	K^+	Fe^{2+}	Mn^{2+}	SiO_2	NH_4^+	NO_3^-	Cl^-	F^-	NO_2^-	SO_4^{2-}
$NaHCO_3$	165.2	120			45.23										
K_2SO_4	31.2					14.0									17.19
$MnSO_4$	2.8							1.02							1.78
$(H_4N)_2SO_4$	0.37									0.1					0.27
NaF	3.3				1.81								1.49		
$NaNO_3$	0.4				0.108						0.292				
$NaNO_2$	0.3				0.1									0.2	
SiO_2	30								30						
$CaCl_2$	185.3		66.89									118.41			
$MgCl_2$	166.9			30.0								136.93			
Na_2SO_4	109.3				35.4										73.9
NaCl	568.1				223.5							344.66			
$FeSO_4$	10.9						4.0								6.9
HCl	~70											~70			
		120	66.9	30.0	306.1	14.0	4.0	1.0	30	0.1	0.3	~670	1.5	0.2	100.0

Simulated groundwater, pH 8.5

All ionic species are given in mg/l

Recipe ↓ Salts (equiv.)	mg/l	HCO_3^-	Ca^{2+}	Mg^{2+}	Na^+	K^+	Fe^{2+}	Mn^{2+}	SiO_2	NH_4^+	NO_3^-	Cl^-	F^-	NO_2^-	SO_4^{2-}
$NaHCO_3$	165.2	120			45.23										
K_2SO_4	31.2					14.0									17.19
$MnSO_4$	2.8							1.02							1.78
$(H_4N)_2SO_4$	0.37									0.1					0.27
NaF	3.3				1.81								1.49		
$NaNO_3$	0.4				0.108						0.292				
$NaNO_2$	0.3				0.1									0.2	
SiO_2	30								30						
$CaCl_2$	185.3		66.89									118.41			
$MgCl_2$	166.9			30.0								136.93			
Na_2SO_4	109.3				35.4										73.9
NaCl	568.1				223.5							344.66			
$FeSO_4$	10.9						4.0								6.9
		120	66.9	30.0	306.1	14.0	4.0	1.0	30	0.1	0.3	600	1.5	0.2	100.0

Simulated groundwater, pH 10

All ionic species are given in mg/l

Recipe ↓ Salts (equiv.)	mg/l	HCO_3^-	Ca^{2+}	Mg^{2+}	Na^+	K^+	Fe^{2+}	Mn^{2+}	SiO_2	NH_4^+	NO_3^-	Cl^-	F^-	NO_2^-	SO_4^{2-}
$NaHCO_3$	165.2	120			45.23										
K_2SO_4	31.2					14.0									17.19
$MnSO_4$	2.8							1.02							1.78
$(H_4N)_2SO_4$	0.37									0.1					0.27
NaF	3.3				1.81								1.49		
$NaNO_3$	0.4				0.108						0.292				
$NaNO_2$	0.3				0.1									0.2	
SiO_2	30								30						
$CaCl_2$	1.4		0.48									0.9			
$MgCl_2$	166.9			30.0								136.93			
Na_2SO_4	109.3				35.4										73.9
NaCl	763				300							463			
$FeSO_4$	10.9						4.0								6.9
NaOH	~40				~23										
		120	0.48	30.0	383	14.0	4.0	1.0	30	0.1	0.3	600	1.5	0.2	100.0

Appendix D3

TANDEM ACCELERATOR LABORATORY
Uppsala REPORT
1978-09-14

Determination of hydrogen profiles in aluminium oxide by means of nuclear physics methods

The work was carried out at the Tandem Accelerator Laboratory in Uppsala with the assistance of Anders Bäcklin, Arne Johansson, Bo Sundqvist and Lars Westerberg.

Goal

The purpose of the work is to determine with the aid of nuclear physical methods how hydrogen penetrates into aluminium oxide by measuring the depth distribution of hydrogen in specimens that have been leached for various periods of time in water. Special emphasis has been placed on the possibility of relating the depth scale to a "marker" implanted in advance in order to make the measurement results independent of various changes in the surface layer of the specimens, such as deposits or loss of material.

Description of methods

Two different methods were combined in order to try to realize this goal and obtain high precision in the depth scale:

a) The presence of hydrogen was determined by means of the nuclear reaction

$$^{15}N + {}^{1}H \rightarrow \alpha + {}^{12}C^{*} \rightarrow \alpha + {}^{12}C + \gamma\,(4{,}43\ \text{MeV})$$

b) The position of the marker was simultaneously determined by means of the back-scattering of the nitrogen ions.

We made use of the ^{15}N ions from the tandem accelerator in Uppsala, which are allowed to strike the specimen in the form of a narrow beam. The ions have a welldetermined energy ($\pm$ 3 keV) , which can be varied between 6 and 9 MeV. The nuclear reaction given above is unique in being able to produce gamma radiation of high energy for nitrogen ions in this energy range, and the reaction is therefore relatively easy to observe without disturbances in the form of background effects. The reaction has a very sharp resonance at 6385 keV , with a width of only 6 keV laboratory energy for the nitrogen ions. The probability that the reaction will take place at the resonance energy is also high, at least three orders of magnitude greater than at surrounding energies. Since the energy of the nitrogen ions decreases in a wellknown manner with depth of penetration into the specimen, a very thin range (i.e. the range where the ion energy passes 6385 keV) can be analyzed with regard to its hydrogen content. The resonance width 6 keV corresponds to an Al203 layer of 19 Å at a density of 4 gcm^{3} .

Upon elastic back-scattering, the scattered ion assumes an energy which is a wellknown fraction (K) of the energy of the impinging

ion. In the case in question with ^{15}N ions colliding with the marker's ^{75}As nuclei, after which nitrogen ions in the 165° direction are detected, this reaction is kept K=0.45016. The energy of the nitrogen ions can be measured with relatively high precision, better than 10 keV, permitting the amount of material in front of the marker to be measured and the position in the specimen where the ion energy passes 6385 keV to be determined. The situation is illustrated in Figure 1, where a surface coating of carbon has been assumed. The energy of the impinging ion, E_{in}, is wellknown , and the energy of the outgoing ion, E_{out}, is measured. With energies in keV and thicknesses in μgcm^{-2}, the following relations are obtained:

$$E_{out} = E_{in} \; K - 13.58 \; X_C - 10.09 \; X_{Al_2O_3}$$

$$E_{res} = E_{in} - 9.90 \; X_C - 7.77 \; (X_{Al_2O_3} - t)$$

where t is the distance in μgcm^{-2} between the position of the marker and the area where the ions pass the resonance energy E_{res}. The interesting parameter t can be calculated if X_C is assumed to be negligible at some phase of the experiment or if the near proportionality between the coefficients in front of X_C and Al_2O_3 is utilized. In practice, the impinging energy is regulated by means of proton resonance equipment, whereby the relation for $^{15}N^{2+}$ is

$$E_{in} = \frac{f^2}{0.1371} \quad (f \text{ in MHz}, \; E_{in} \text{ in keV})$$

For practical use, the following scale relations , which apply for ^{15}N ions in the energy range in question in Al_2O_3 with a density of 4 gcm^{-3}, can be used:

$$25 \text{ Å} = 1 \; gcm^{-2} = 7.77 \text{ keV} = 17.8 \text{ kHz}$$

$$\delta t \qquad \delta t \qquad \delta E \qquad \delta f$$

The apparatus that has been used is illustrated schmatically in Figure 2. The figure is naturally not to scale, the accelerator is greatly reduced in relation to the other equipment. It is possible to switch between four specimens without breaking the vacuum. The gamma detector is ringshaped and has high efficiency for 4.43 MeV gamma radiation. A ^{241}Am alpha source is mounted to permit continuous surveillance of the energy calibration of the particle detection system.

Studies performed

The specimens that have been studied were supplied by AseaAtom and were implanted with 5×10^{15} atoms/cm^2 of arsenic at 130 kV. The arsenic was chosen because the implanting was easily accessible and because the As atoms are sufficiently heavy to provide a relatively high energy for backward-scattered nitrogen ions. Specimens with 4 different leaching times (21, 54, 76 and 184 d) were tested with leaching in twice destilled water at pH 7 and 9.3 and 90°C. In addition, unleached specimens (so-called "normals") as well as leached and unleached sapphire were tested.

A number of measurement series were carried out with these

specimens. One measurement series on a specimen generally involves recording particle and gamma spectra for approximately 15 different energies chosen so that the resonance energy sweeps over the range with hydrogen once or twice. Each measurement carried out with around 30 nanoamperes $^{15}N^{2+}$ takes 23 min accelerator time, which means around 1 000 nitrogen ions can be recorded from the As marker. The following substudies have been performed:

1. Comparison of hydrogen distribution in an As-implanted specimen with the distribution for an untreated Al_2O_3 specimen. 2. Series with one unleached and two 21-day specimens leached in water at pH 7 and 9.3.

3. Same as 2, but with 54-day specimens.

4. Same as 2, but with 76-day specimens and including sapphire specimens.

5. Same as 2, but with 184-day specimens and sapphire specimen.

6. Test with gold vapourization on leached specimens (76-day specimens).

7. Test with electron spraying of the test surface during measurement in order to neutralize the effect of the positive charge of the nitrogen beam.

8. Study of carbon coating of specimens with backward scattering of oxygen ions.

1. The purpose of comparing the hydrogen distribution of an As-implanted specimen with an untreated specimen was, naturally, to ascertain whether the implantation itself or the presence of As atoms would affect the hydrogen distribution. The results, illustrated in Figure 3, were confirmed by several independent measurements and show that the very narrow surface distribution of hydrogen in an untreated specimen with a total width of half the height of 50 Å was around three times wider after implantation. This could be due to radiation damages in the Al_2O_3 specimen. The problem must be studied more closely, and the implantation of heavier atoms might be considered. Due to the higher atomic number and larger crosssection for backward scattering of such atoms, a smaller number of implanted atoms would be sufficient.

2, 3, 4 and 5. These measurements are illustrated in Figure 4 with the results from the 21-day specimen. A larger spread than expected is found between different measurement points. Similarly, the differences between the pH 7 and pH 9 specimens are not reproduced in detail in the later measurements. This can largely be explained by uncertainty in the correction for the carbon layer that is built up on the surface, but a structure in the material distribution of the specimens or an unstable hydrogen distribution may be other explanations. Despite these problems in definitely establishing what the hydrogen distribution looks like in its

entirety, the depth of penetration, defined e.g. as the point at which the hydrogen concentration drops to half its value in the direction into the specimen, can be determined with relatively good accuracy. The uncertainty in this value is estimated at around 30 Å, since it is related to the position of the As marker. With this definition of the depth of penetration, the results can be presented in a table that shows the distance between the depth of penetration and the marker position (Table 1). It can be noted that the (unleached) normal specimen, which was used as a reference specimen during the test with the 76day specimens, shows an abnormally short distance between the marker and the depth of penetration. This can be attributed to the fact that the same specimen also has an unusually shallow As layer. Moreover, for some reason the specimen has twice as many implanted As atoms as other examined specimens. It can also be noted that the marker lies relatively close to the surface in the sapphire specimens as well.

Table 1. Distance between depth of penetration and marker position in Å in Al_2O_3. Uncertainty about 30 Å.

Leaching time	Normal	pH 9	pH 7	Sapphire
0				210
21 d	480	390	460	
54 d	480	365	435	
76 d	280	380	225	195
184 d		295	295	260

6. It is conceivable that certain measuring problems could arise in connection with charging of the aluminium oxide specimen, which is a good insulator, or due to the retarding radiation that can arise when the nitrogen ions strike the relatively transparent specimens. Among other things, normal current measurement of the ion current cannot be done directly by collecting the charge that builds up on the specimen. There are no problems with regard to gamma detection, but we have found it necessary to protect the particle detector by placing a thin carbon foil (8.9 gcm^{-2}) between the specimen and the detector. However, it is also conceivable that these charging effects influence the parameters which we intend to measure, namely the hydrogen distribution or the material distribution in the specimen. In order to investigate this more closely, a thin layer of gold (50 Å) was vapourized on

one set of specimens leached for 76 days and one unleached set of specimens. The result shows clearly that in all of the specimens, the hydrogen distribution after the gold vapourization become strongly concentrated to a surface peak, most of which is located in the gold. No difference can be detected between leached and unleached specimens, nor does the sapphire specimen differ from the others in this respect, provided that the hydrogen distribution is related to the surface. The total thickness of Al_2O_3 down to the marker varies, however, depending on the specimen and the leaching.

7. An alternative way to solve charging problems would be to spray electrons on the surface of the specimen simultaneously with the ion bombardment. A preliminary test in this direction was carried out, but the improvement of the reproducibility of the details of the hydrogen distribution that could be noted is relatively moderate. In this provisional setup , it was unfortunately not possible to avoid a certain disturbing effect of the electron spraying on the particle detector as well.

8. Through both direct observation of irradiated specimens after a completed $^{N}15$ measurement series and analysis of material thickness in accordance with previously specified formulae, it is found that the vacuum in the test chamber is insufficient to prevent a carbon coating. A coating of about 5 μgcm^{-2} is deposited on a specimen during a measurement series. This can actually be taken care of directly, provided that the coating is stable and homogeneous over the surface. However, neither of these two conditions seems to be met (the coating exists largely only where the nitrogen beam strikes the specimen and presumably in proportion to the density of the beam), and strong reasons speak for the desirability of switching over to a system with 10^{7} Torr or better. Table 2 presents the results of the measurements of the thickness of the aluminium oxide layer up to the arsenic marker.

Table 2. Distance from surface to As marker in μgcm^{-2} Al_2O_3

Trial series	Normal (non-leached)	pH 9	pH 7	Sapphire
21-day leaching	x	x-2.38	x-0.75	
54-day leaching	20.4	16.1	19.7	16.1
76-day leaching Au-vapourized	20.5	18.3	19.2	18.1
Same, not Au--vapourized	14.7	17.6	16.0	15.1
184-day leaching		15.0	15.0	15.5
54-day e-spray	19.2	13.4	16.0	
^{16}O-backscattering new specimens	19.8	16.0	21.1	
Same, but after ^{15}N measurement series	20.7[x]	16.2[x]	20.0[x]	

[x] A carbon layer of 5.1 μgcm^{-2} has been discounted

Results and comments

The distance between the depth of penetration and the marker position t, (table 1) is illustrated in figure 5. The points for the sapphire specimen do not deviate significantly from a horizontal line. With this method, we can therefore not detect any attack on the sapphire. For both of the polycrystalline specimens, pH 9.3 and 7, straight lines have been obtained by means of the least squares method with slopes of 220 $\pm$ 90 Å/year and 340 $\pm$ 90 Å/year, respectively. Extrapolated linearly this corresponds to penetration rates of 2.2 cm and 3.4 cm, respectively, in one million years. At pH 7, the points are scattered more than expected ($^{+}$30 Å, owing to the low value for the 74-day point. However, the hydrogen distribution of this specimen deviates widely from that of the others. The fact that the attack takes place more rapidly in the polycrystalline material indicates that the attack takes place along the grain boundaries.

With improved vacuum equipment (ion pump 10^{-8} - 10^{-9} Torr), the uncertainty stemming from carbon build-up on the specimen could be eliminated. Measurements of the stability of the hydrogen distribution as a function of the beam current and a prolongation of the leaching time are necessary in order for more definite conclusions to be drawn concerning the corrosion rate.

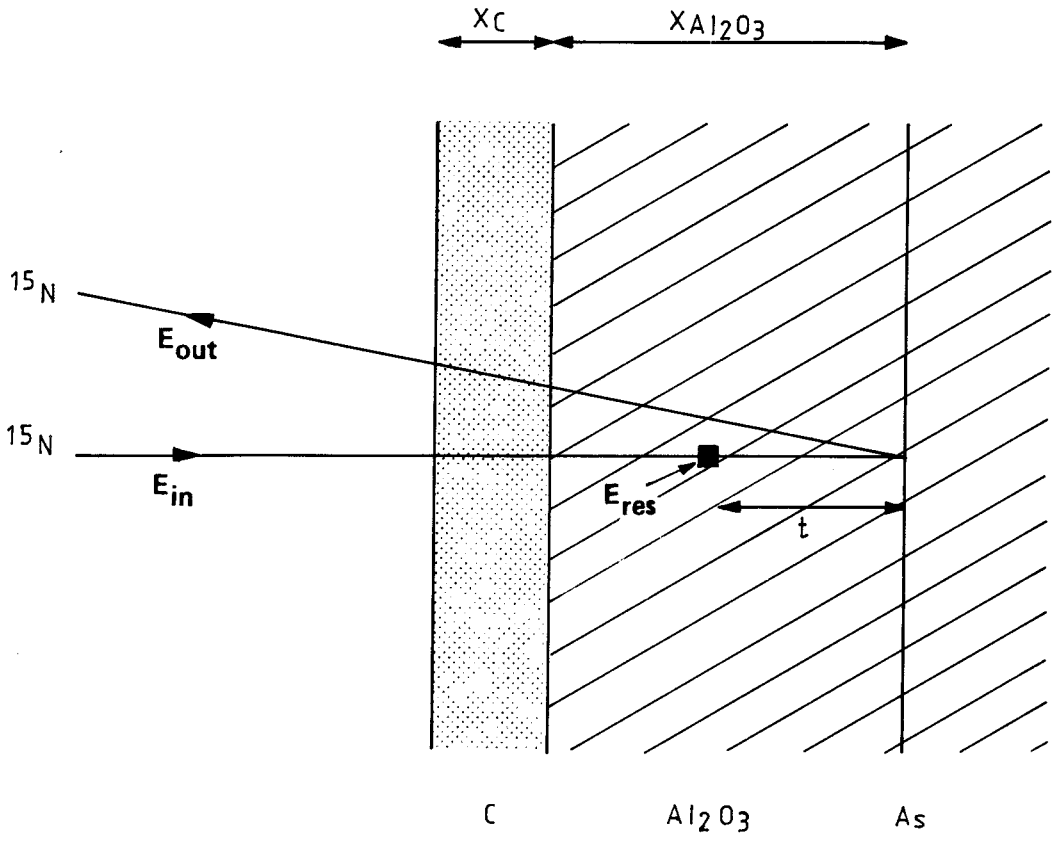

Figure 1

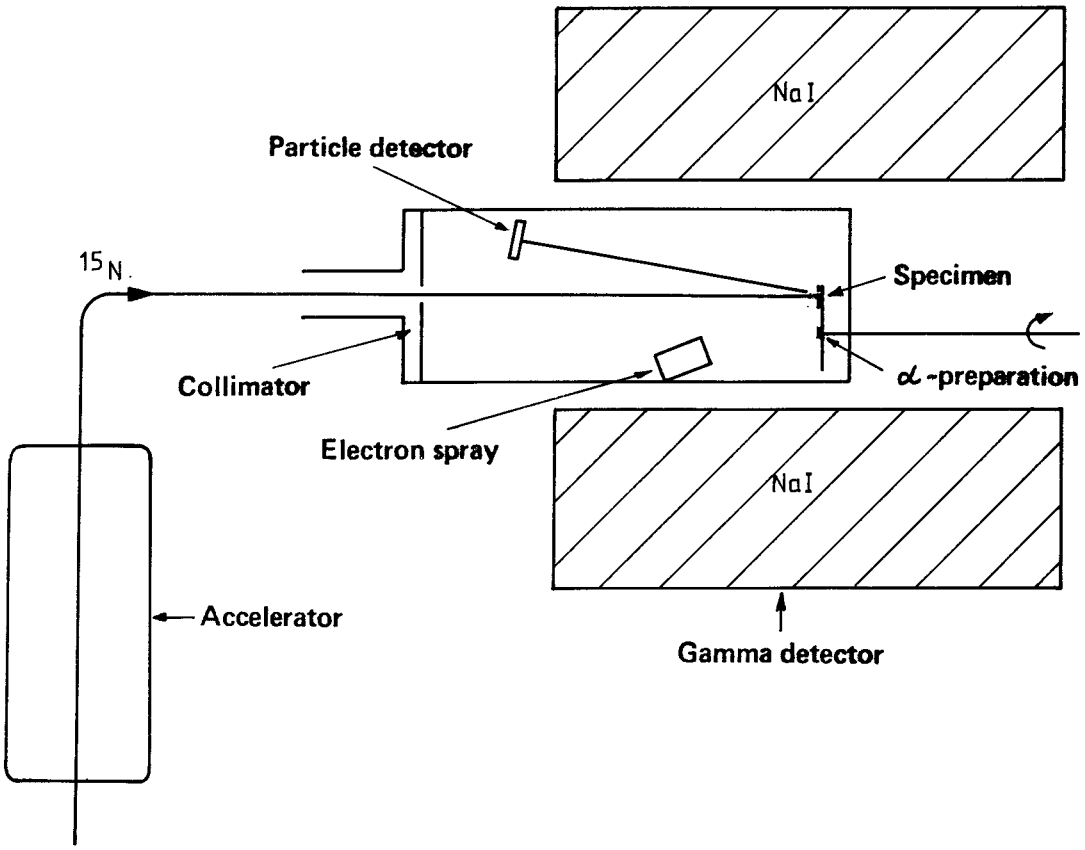
NaI
Particle detector
15N
Specimen
Collimator
α-preparation
Electron spray
NaI
Accelerator
Gamma detector

Figure 2

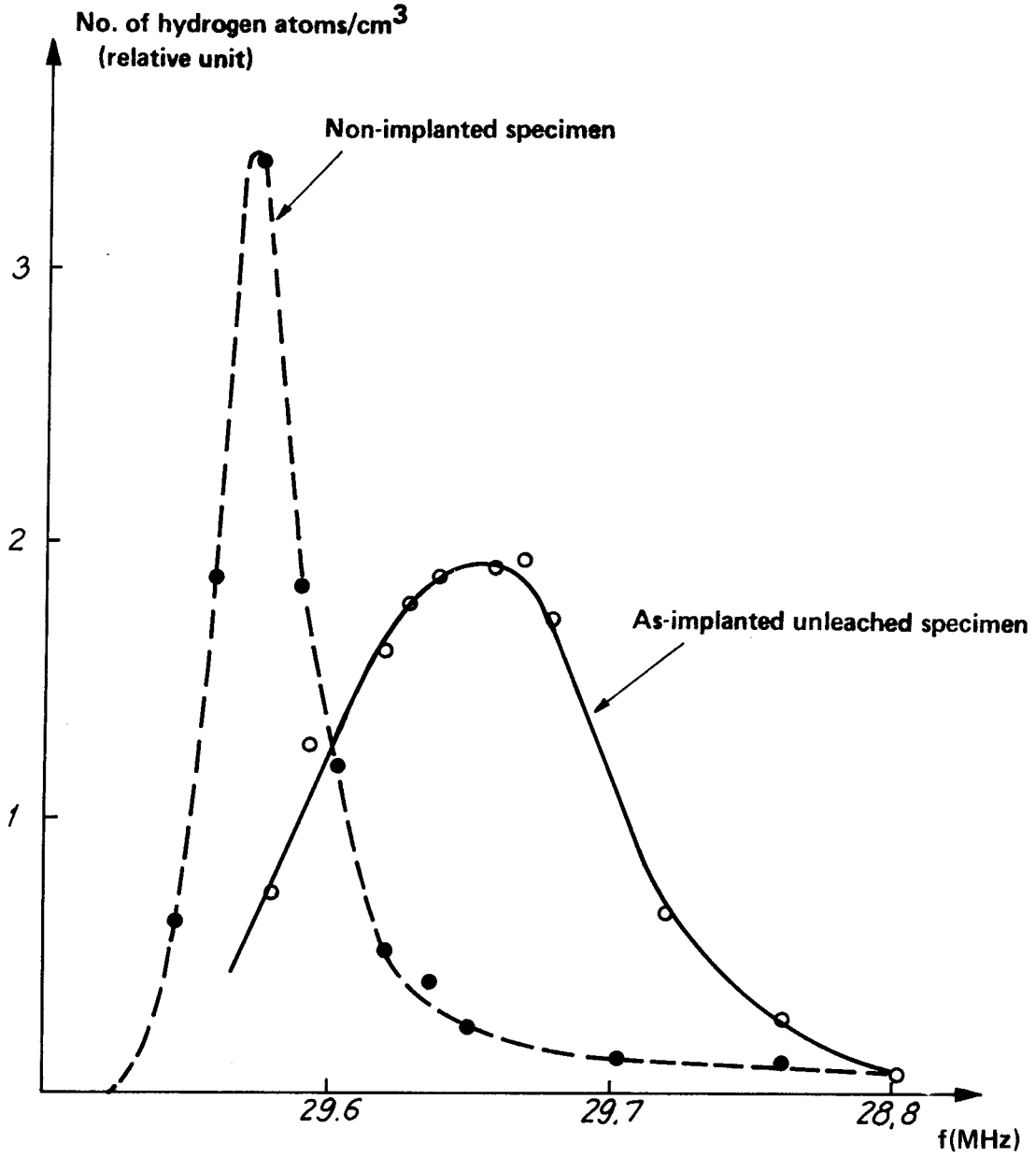
No. of hydrogen atoms/cm3
(relative unit)
Non-implanted specimen
As-implanted unleached specimen
3
2
1
29.6
29.7
28,8
f(MHz)

Figure 3

Figure 4

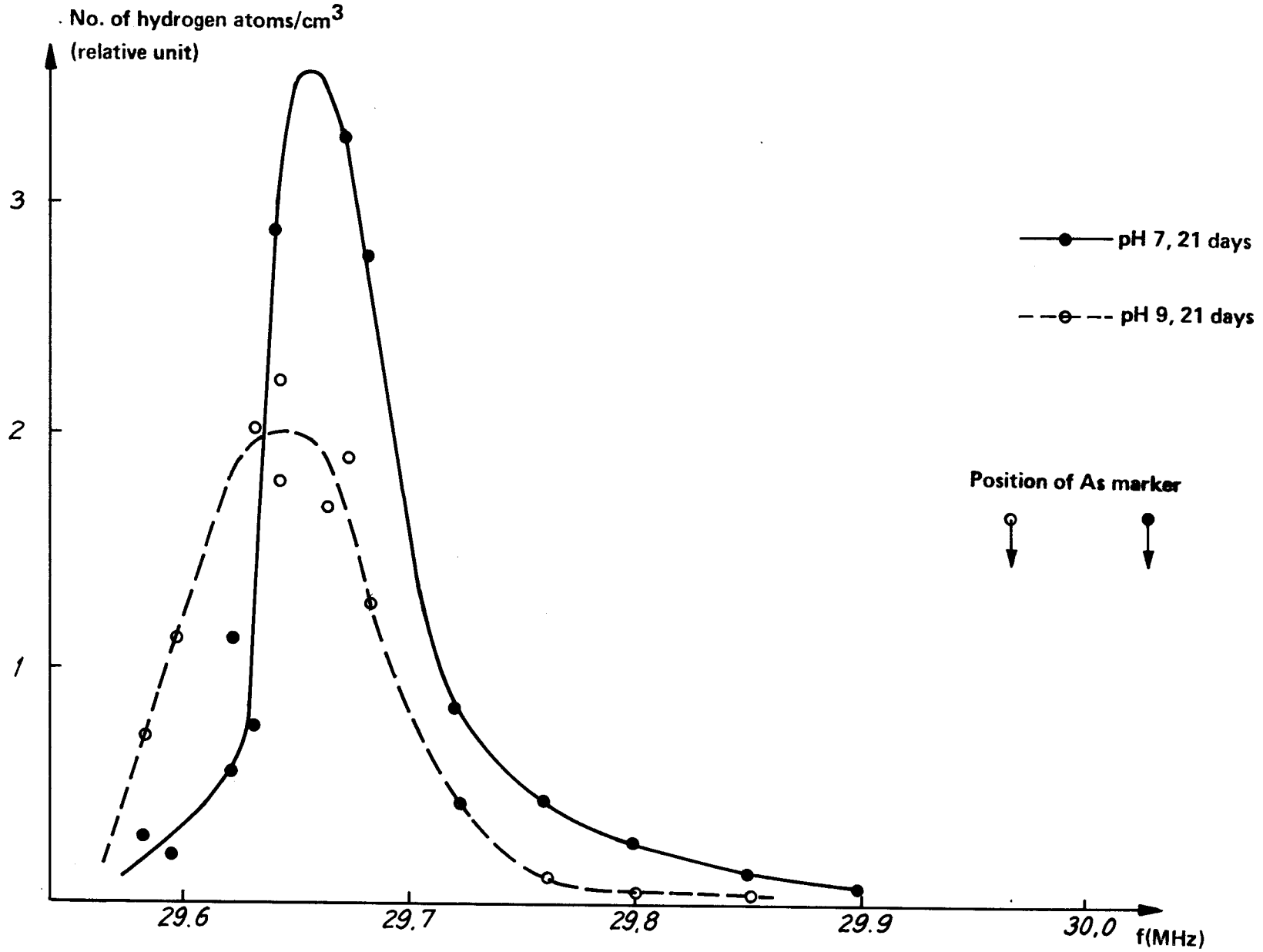
No. of hydrogen atoms/cm3
(relative unit)
3
2
1
29.6
29.7
29.8
29.9
30.0
f(MHz)
pH 7, 21 days
pH 9, 21 days
Position of As marker

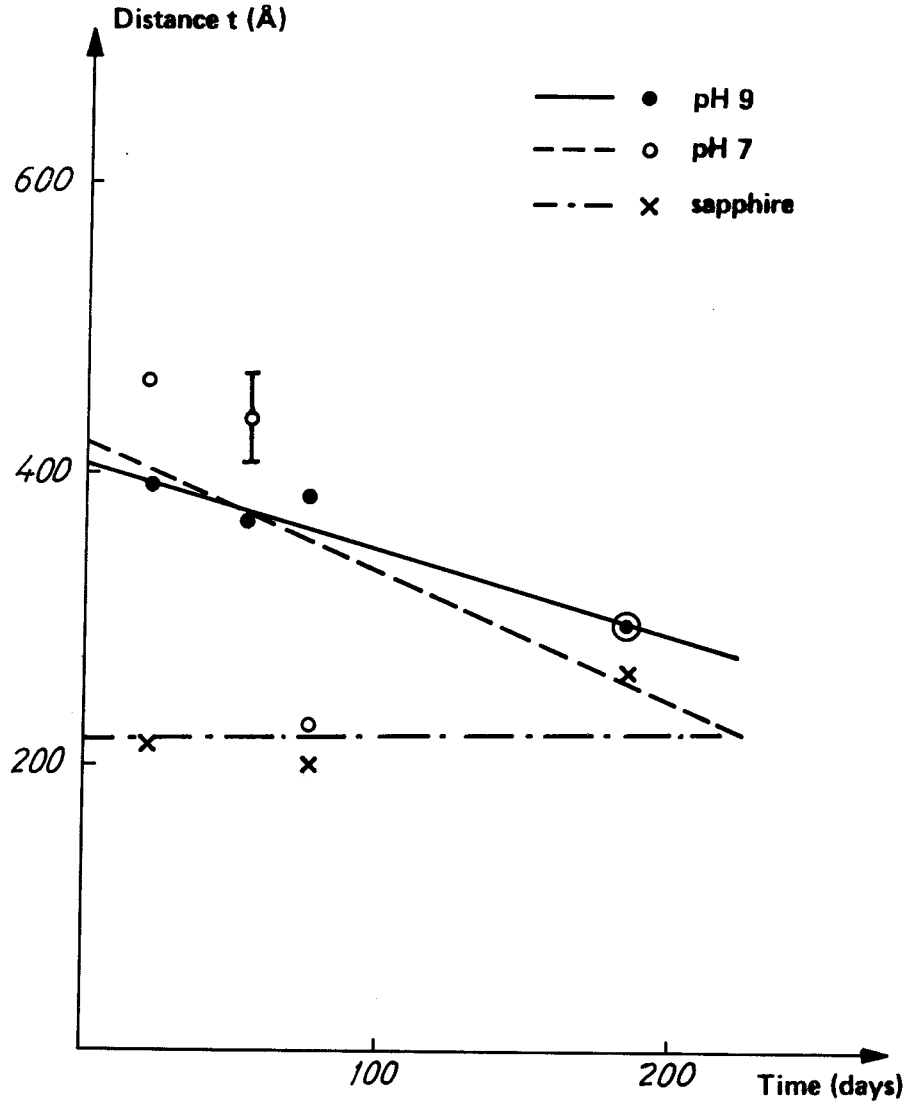

Figure 5

Appendix D4

Studsvik Report MS-78/214 1978-05-29

LEACHING OF Al_2O_3 IN DOUBLE-DISTILLED WATER

Britt-Marie Svensson
Göran Blomqvist

ABSTRACT

In a study commissioned by KBS, Al_2O_3 material was leached at 90° in double-distilled water, both pure and carbonate-buffered to pH 9.3.

The corrosion rate for Al_2O_3 was determined by means of Al analysis of the leachant solutions.

The corrosion rate after 60 days of leaching was:

in double-distilled water	$10 \cdot 10^{-6}$ mm . year^{-1}
the same pH 9.3	$11 \cdot 10^{-6}$ mm . year^{-1}
the same pH 9.3 sapphires	$47 \cdot 10^{-6}$ mm . year^{-1}

1. INTRODUCTION

On commission from KBS within the subproject "Encapsulation", Al_2O_3 material was leached in double-destilled water at two different pHs , in stationary water at 90°C. Rectangular plates and sapphires were leached. (All specimens were ionimplanted with As-75 prior to leaching. Five rectangular specimens were partially masked during the ion implantation.)

The leachant solutions were analyzed for Al in order to determine the corrosion rate for Al_2O_3 under the various experimental conditions.

2. EXPERIMENTAL

2.1 Equipment

2.1.1 Apparatus

Leaching vessels	Teflon with tightly-fitting lid 2 x 200 ml 1 x 100 ml
Storage vessel for leachant solution	Teflon beaker with lid of teflon foil
Vessels for test solutions	10 ml polyethylene bottles
Distillation apparatus	2-stage distillator, made completely of quartz
pH measurement	Radiometer PHM 63 with combination electrode Radiometer GK 2311 C
Heating	Water bath with quartz immersion heater, contact thermometer and temperature regulator plus level regulator.

2.1.2 Test environment

Leachant solution	Double-distilled, deionized water pH 6 Double-distilled, deionized water, buffered to pH 9.3 $\pm$ 0.1 with sodium carbonate CO_3 = 120 mg . l^{-1}
Temperature	90 $\pm^{3}_{1}$ °C
Leachant solution volume/test surface	5 ml cm^{-2}
Water change	once a week
Al analysis in leachant solution	once a week

2.1.3 Test material

Material	Al_2O_3, ion-implanted with As-75
Dimensions	Tablets 10 x 10 mm, t = 0.1 - 1 mm Sapphires dia. 8 mm, t = 0.2 mm
Surface finish	Ground/polished. The specimens were delivered and were assumed to have been characterized by KBS

2.1.4 Specimen treatment

Cleaning, before	The specimens were cleaned ultrasonically. 10 min in acetone 10 min in alcohol Rinsing with double-distilled H_2O
Drying	Drying in air on teflon foil
Cleaning, after	Rinsing with double-distilled H_2O
Drying	Drying in air on filter paper

2.2 Execution

2.2.1 Preparatory measures

All material in contact with the specimens and leachant solution before, during and after leaching was made of teflon or polyethylene and washed in warm 30% HNO_3 (pro analysi), rinsed carefully in deionized water and finally rinsed several times with doubledistilled deonized water. Followed by drying in air on and under teflon foil in order to prevent airborne contamination with Al.

For leaching in double-distilled water, freshly distilled water from a storage vessel was used, from which samples for the determination of the background level of Al were taken at the same time as the water for leaching.

For leaching in double-distilled water at pH 9.3, freshly distilled water was buffered with sodium carbonate. A_1 stock solution containing (165 g $NaHCO_3$ + 0.60 g NaOH) . l^{-1} , pH 9.3, was diluted 1 to 1 000 l with freshly distilled water to the leachant solution. The pH was checked and samples for determination of the background level of Al were taken at the same time as the water for leaching.

Control leaching of the equipment was carried out prior to the start of the test leaching.

2.2.2 Leaching of specimens

A total of 25 rectangles and 7 sapphires were leached in accordance with the leaching scheme in Table 1. The leaching times were 21, 54 and 76 days. Leaching involved 3 parallel series, vessels I, II and IV. At the time of writing leaching of 9 rectangular specimens and 5 sapphires is still in progress.

The cleaned Al_2O_3 specimens were placed on the bottom of the leaching vessels, after which the leachant solution was added and measured by weight. The lids were put on and the leaching vessels were placed in a thermostatically controlled water bath at 90 $\pm$ 1°C.

When the water was changed, the leaching vessels were lifted out of the water bath and allowed to cool to about 40°C, after which the vessels were opened, samples taken for Al analysis, the pH of the solution was measured and the remaining solution was removed using suction. New leachant solution was weighed in.

After leaching, the specimens were rinsed with double-distilled H_2O, allowed to dry in air, packed in soft paper and sent to different laboratories for further tests as agreed with KBS.

Leaching in vessel I (double-distilled deionized water) and vessel II (buffered double-distilled deionized water, pH 9.3) was started

simultaneously and both experienced a temperature interruption after 5 days. Nothing was done to the leachant solutions and the specimens stood at room temperature for 5 days, after which leaching continued at 90°C. Samples for Al analysis were taken after 12 and 19 days, the first water change was carried out after 21 days of leaching, after which water changes and Al analysis were performed weekly (all as requested by Lennart Hydén of KBS). Leaching in vessel IV (pH 9.3) was done with a weekly water change from the start of leaching.

2.2.3 Al analysis of leachant solution

The Al analyses were performed using flameless atomic absorption, Perkin Elmer 403. Al metal, Merck 99.99% Al, dissolved in HCl was used as an Al standard.

The leachant solutions were analyzed both directly and after evaporation with acid followed by dilution to the original volume with doubledistilled H_2O.

Estimated analysis error:
$\pm$ 10 % at concentrations $\geq$ 10 µg Al . l^{-1}
$\pm$ 1 µg Al . l^{-1} at concentrations < 10 µg Al.l^{-1}

Detection limit:
1 µg Al . l^{-1}

It should be observed that, due to the analysis error of the background, the uncertainty in the calculations of the leached quantities within the low concentration range may be slightly greater than the errors given above.

3. RESULTS

The analysis results from the leaching of rectangular plates in doubledistilled H_2O (leaching vessel I) are presented in Table A.2. Accumulated leached quantity of Al_2O_3 . cm^{-2} as a function of leaching time is shown in Figure B.1.

The analysis results from the leaching of rectangles + sapphires at pH 9.3 (leaching vessel II) are presented in a similar manner in Table A.3 and Figure B.2.

The analysis results from the leaching of sapphires at pH 9.3 (leaching vessel IV) are presented in Table A.4 and Figure B.3.

The corrosion rate has been obtained from the curves in Figures B.1 B.3 and has been plotted in Figure B.4.

The corrosion rate in the leaching of rectangles at pH 9.3 decreases with time, first rapidly then more slowly, from 230 . 10^{-6} mm . $year^{-1}$ at the start to 11 . 10^{-6} mm . $year^{-1}$ after 60 days. The curve indicates that the corrosion rate continues to decrease.

The corrosion rate in the leaching of sapphires at pH 9.3 decreases from 170 . 10^{-6} mm . $year^{-1}$ at the beginning to 47 . 10^{-6} mm . $year^{-1}$ after 60 days. Here as well, the corrosion rate appears to continue to decrease.

In the leaching of rectangles in double-distilled H_2O, the leached quantities of Al are considerably smaller than in the tests at pH 9.3, at least during the first part of the leaching period. At these lower concentrations the uncertainty of the analysis increases. The results obtained thus far indicate an increase of the corrosion rate from 6 . 10^{-6} mm . $year^{-1}$ at the beginning to 10 . 10^{-6} mm . $year^{-1}$ after 60 days. The increase appears to continue, but additional experiments for a longer period of time are necessary in order to establish whether the increase is statistically significant.

Table A.1

Leaching scheme Al_2O_3. Double-distilled H_2O

Environment	pH 9.3					H_2O						
Specimen type \ Leaching time d	21	54	76			21	54	76			No of specimens	Leaching vessel No.
Rectangle	-	-	-	-	-	2	2	2			10	I
Rectangle	2	2	2			-	-	-	-	-	10	II
Rectangle, masked	1	2	1			-	-	-	-	-	5	II
Sapphire		1	1			-	-	-	-	-	4	II
Sapphire						-	-	-	-	-	3	IV

TABELLBLAD A4

Leaching vessel I	Al_2O_3 leaching. Double-distilled H_2O Rectangles					Table A.2	
Test No.	Total leaching time d	Leaching period d	µg $Al \cdot l^{-1}$	Test volume ml	Test surface cm^2	Leached Al_2O_3 $g \cdot cm^{-2} \cdot 10^8$	
							Total
Al:1	Background	-	3	-	-	-	-
Al:2	12	12	12	100	20	8.6	8.6
Al:5	19	19	12	100	20	8.6	8.6
Al:9	21	21	16	100	20	12.4	12.4
Al:12	29	8	8	80	16	4.8	17.2
Al:15	35	6	11	80	16	7.7	24.9
Al:18	42	7	7	80	16	3.8	28.7
Al:21	49	7	8	80	16	4.8	33.5
Al:26	54	5	16	80	16	12.4	45.9
Al:30	62	8	7	60	12	3.8	49.7
Al:33	Background	-	3	-	-	-	-
Al:36	68	6	11	60	12	7.7	57.4
Al:40	76	8	11	-	-	-	-
Al:43	76 Acid evaporation		15	60	12	11.5	68.9

BL 0142

AB ATOMENERGI

TABELLBLAD A4

Leaching vessel II	Al_2O_3 leaching. Double-distilled H_2O, pH 9.3. Rectangles + sapphires					Table A.3	
Test No.	Total leaching time d	Leaching period d	µg $Al \cdot l^{-1}$	Test volume ml	Test surface cm^2	Leached Al_2O_3 $g \cdot cm^{-2} \cdot 10^{82}$	
							Total
Al:3	Background	-	3	-	-	-	-
Al:4	12	12	250	170	34	240	240
Al:7	19	19	300	170	34	288	288
Al:10	21	21	222 ?	170	34	-	-
Al:13	29	8	76	140	28	70	358
Al:16	35	6	38	140	28	33	391
Al:19	42	7	36	140	28	32	423
Al:22	49	7	14	140	28	11	434
Al:24	49 Acid evaporation		12	-	-	-	-
Al:27	54	5	8	140	28	5	439
Al:29	54 Acid evaporation		8	-	-	-	-
Al:31	62	8	11	100	20	8	447
Al:35	62 Acid evaporation		11	-	-	-	-
Al:[illegible]	Background	-	3	-	-	-	-
Al:37	68	6	22	100	20	18	465
Al:39	68 Acid evaporation		25	-	-	-	-
Al:41	76	8	11	100	20	8	473
Al:44	76 Acid evaporation		10	-	-	-	-

BL 0142

Leaching vessel IV		Al_2O_3 leaching. Double-distilled H_2O pH 9.3. Sapphires.				Table A.4	
Test No.	Total leaching time d	Leaching period d	mg $Al \cdot l^{-1}$	Test volume ml	Test surface cm^2	Leached Al_2O_3 $g \cdot cm^{-2} \cdot 10^8$	
							Total
Al:3	Background	-	3	-	-	-	-
Al:8	4	4	65	15	2.4	60	60
Al:11	6	6	100	14	2.4	93	93
Al:14	14	8	100	15	2.4	93	186
Al:17	20	6	79	15	2.4	73	259
Al:20	27	7	88	15	2.4	82	341
Al:23	34	7	66	15	2.4	60	401
Al:28	39	5	35	15	2.4	31	432
Al:32	47	8	46	15	2.4	41	473
Al:34	Background	-	3	-	-	-	-
Al:38	53	6	55	15	2.4	50	523
Al:42	61	8	38	15	2.4	34	557
Al:45	61 Acid evaporation		29	-	-	-	-

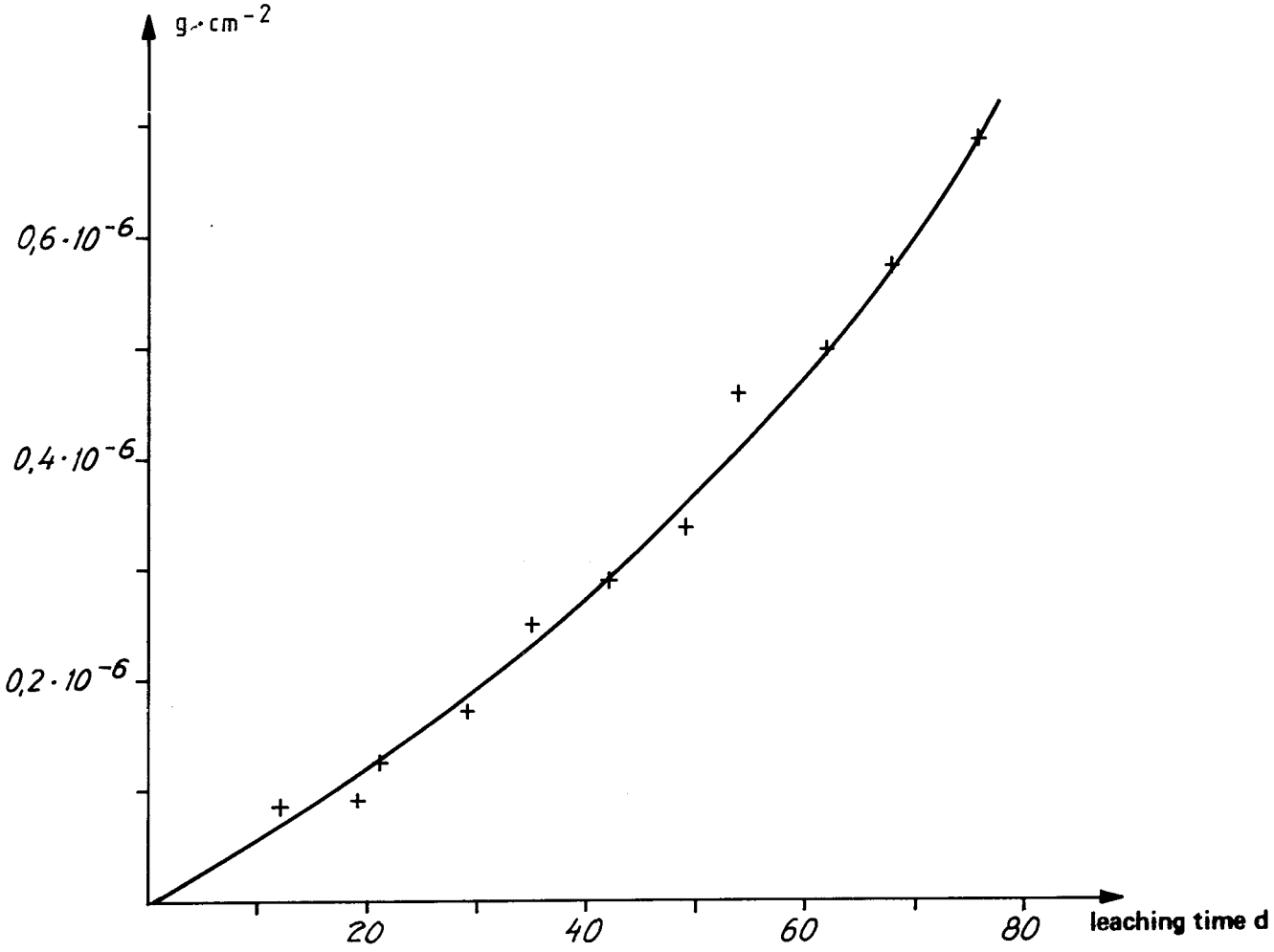

Figure B.1. Leached Al_2O_3. Double-distilled H_2O. Rectangles.

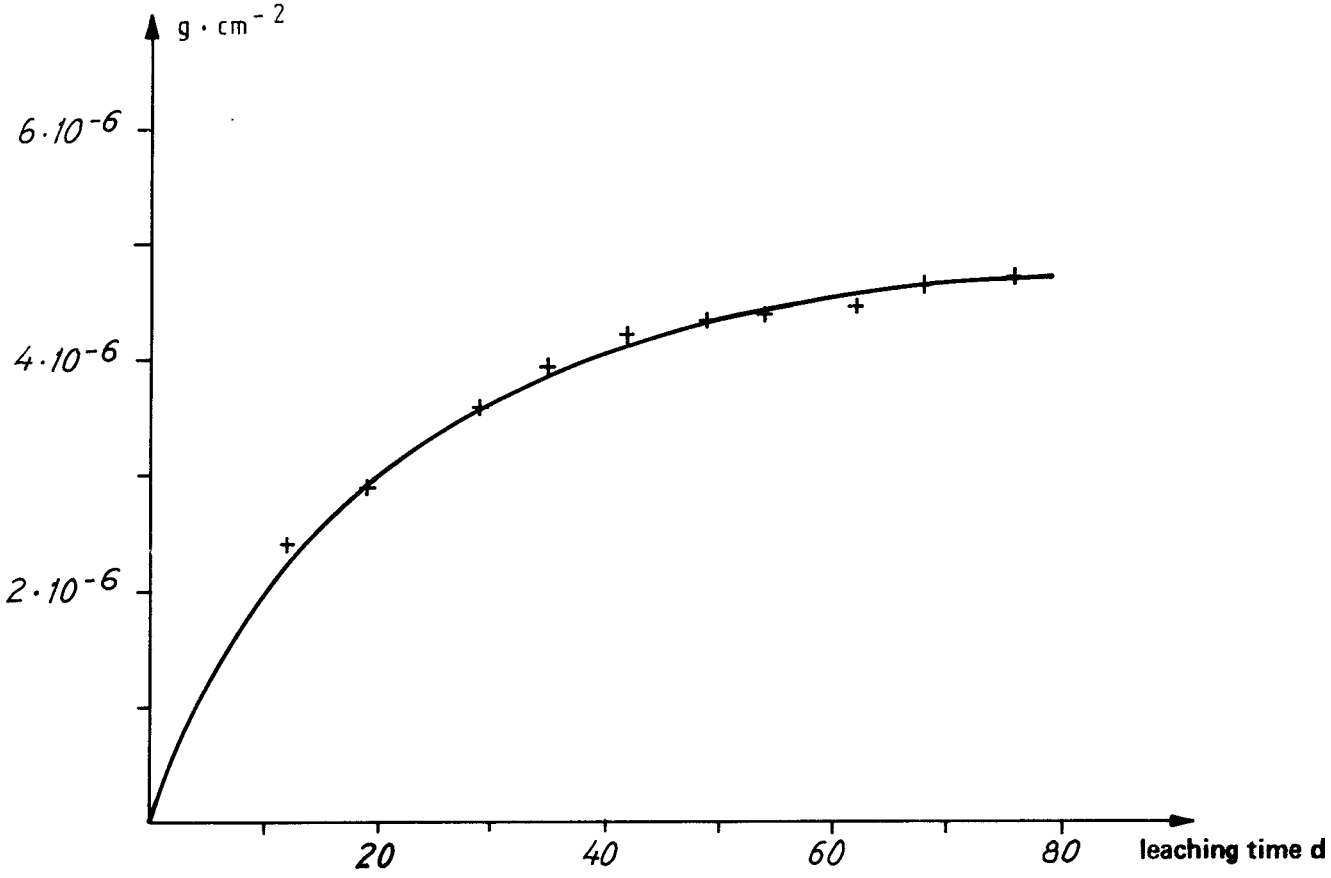

Figure B.2. Leached Al_2O_3. Souble-distilled H_2O, pH 9.3.
Rectangles + sapphires.

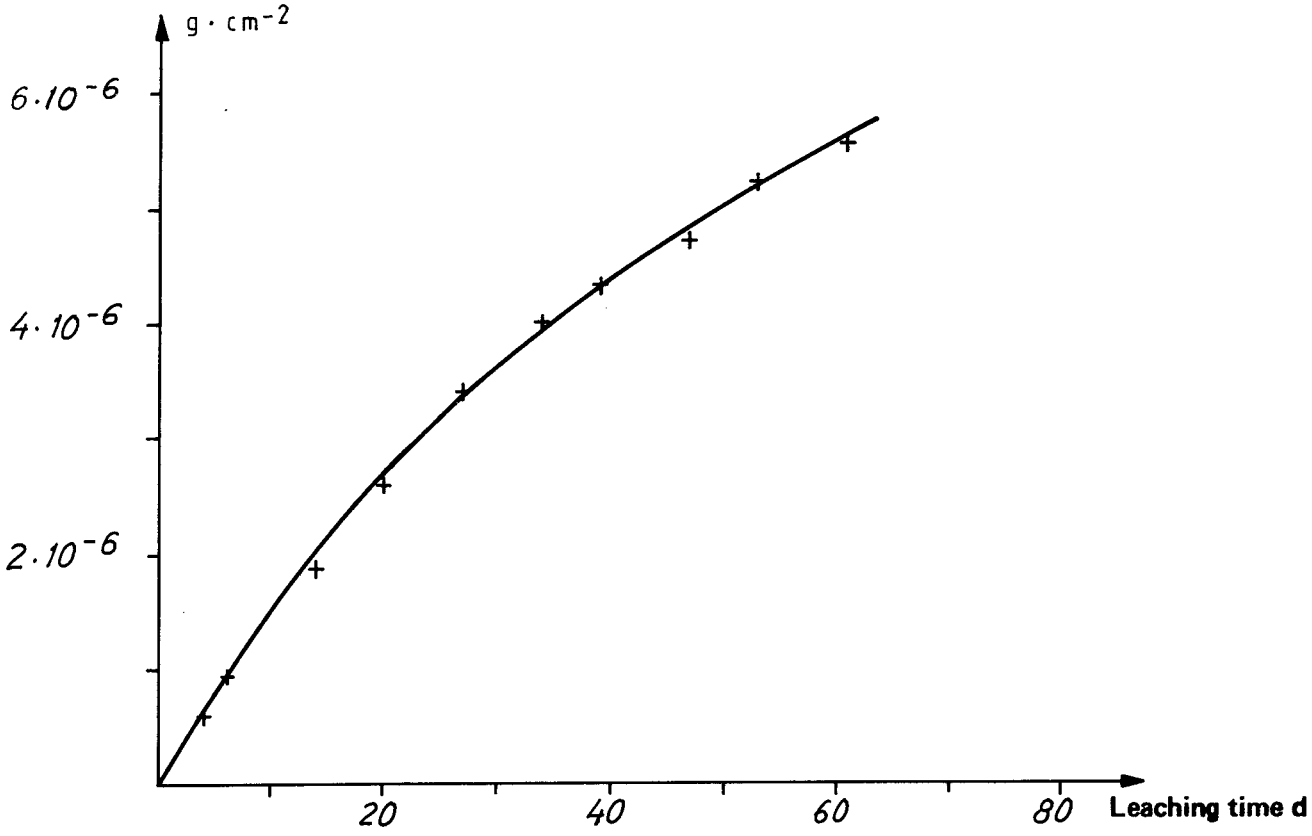

Figure B.3 Leached Al_2O_3. Double-distilled H_2O, pH 9.3. Sapphires.

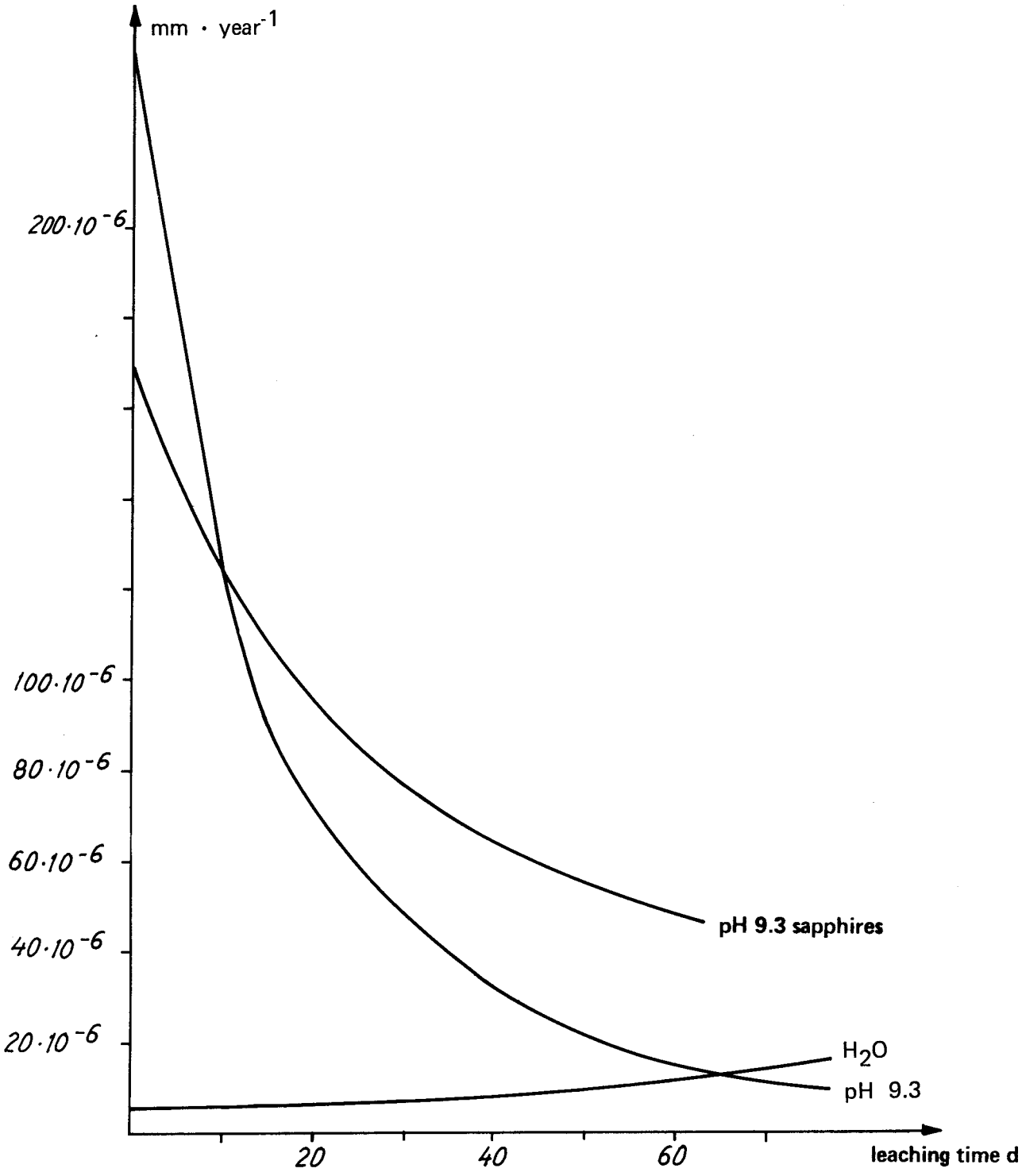

Figure B.4. Corrosion rate Al_2O_3

Appendix 5

Studsvik Technical Report MS-78/250 · 1978-09-12

Leaching of Al_2O_3 in double-distilled water.
Interim report, continuation of report STUDSVIK/MS-78/214

Britt-Marie Svensson

ABSTRACT

In a study commissioned by KBS, Al_2O_3 material was leached at 90° in double-distilled water, both pure and carbonate-buffered to pH 9.3.

The corrosion rate for Al_2O_3 was determined by means of Al analysis of the leachant solutions.

The corrosion rate after 180 days of leaching was 10-12. 10^{-6} mm.year^{-1} in both of the leaching environments and remained stable at this level after 120 days of leaching time.

TABLE OF CONTENTS

1 INTRODUCTION

Within the subproject "Encapsulation" commissioned by KBS, Al_2O_3 material was leached in double-distilled water at two different pHs, in stationary water at 90°C. Rectangular plates and sapphires were leached. (All specimens were ion-implanted with As75 prior to leaching. Five rectangular specimens were partially masked during the ion implantation.) The leachant solutions were analyzed for Al in order to determine the corrosion rate for Al_2O_3 under the different experimental conditions. The test period has thus far extended over 184 days.

2. EXPERIMENTAL

2.1 Equipment

Described in report Studsvik/MS-78/214.

2.2 Execution

Described in report Studsvik/MS-78/214.

2.2.1 Leaching of specimens

A total of 25 rectangles and 7 sapphires were leached in accordance with the leaching scheme in Table A.1. The leaching times were 21, 54, 76, 107 and 184 days. Leaching is still in progress on four rectangular specimens and four sapphires. Water was changed every week.

Al analysis of the leaching solution was performed every week during the first 80 days, and then every other week.

The following additonal leachings were performed at pH 9.3.

- 1 rectangular specimen, 45 days leaching, change of water every week, no Al analysis
- 2 rectangular specimens, 1 day leaching
- 2 rectangular specimens, 3 days leaching, water changed after one day. These last 4 specimens were not ion-implanted with As75 prior to leaching.

3. RESULTS

The analysis results from the leaching of rectangles in double-distilled H_2O (leaching vessel I) are presented in Table A.2. Accumulated leached quantity of $Al_2O_3 \cdot cm^{-2}$ is shown as a function of leaching time in Fig. B.1.

The analysis results from the leaching of rectangles + sapphires at pH 9.3 (leaching vessel II) are presented in a similar manner in Table A.3 and Figure B.2.

The analysis results from the leaching of sapphires at pH 9.3 (leaching vessel IV) are presented in Table A.4 and Figure B.3.

The corrosion rate was calculated from the curves in Figures B.1 - B.3 and plotted in Figure B.4.

The dashed parts of the curves B3 and B4 (sapphire leaching at pH 9.3) represent a period in the testing where abnormal evaporation of 60% occurred in test A158 (see Table A4). The test solution was diluted to its original volume prior to analysis.

As is evident from Figure B4, the corrosion rate stabilized during the period between 120 and 180 days at a level of $10\text{-}12.10^{-6}$ mm . year^{-1} in both of the leaching environments.

Estimated analysis error: $\pm$ 20% in this concentration range.

Table A.1

Leaching scheme Al_2O_3. Double-distilled H_2O

Environment	pH 9.3					H_2O						
Leaching time d / Specimen type	21	54	76	107	184	21	54	76	107	184	No of specimens	Leaching vessel No.
Rectangle	-	-	-	-	-	2	2	2	-	2	10	I
Rectangle	2	2	2	-	2	-	-	-	-	-	10	II
Rectangle, masked	1	2	1	1	-	-	-	-	-	-	5	II
Sapphire		1	1		1	-	-	-	-	-	4	II
Sapphire						-	-	-	-	-	3	IV

TABELLBLAD A4

Leaching vessel I		Al_2O_3 leaching. Double-distilled H_2O Rectangles				Table A.2	
Test No.	Total leaching time d	Leaching period d	µg Al·l^{-1}	Test volume ml	Test surface cm^2	Leached Al_2O_3 g·cm^{-2}·10^{82}	
							Total
Al:1	Background	–	3	–	–	–	–
Al:2	12	12	12	100	20	8.6	8.6
Al:5	19	19	12	100	20	8.6	8.6
Al:9	21	21	16	100	20	12.4	12.4
Al:12	29	8	8	80	16	4.8	17.2
Al:15	35	6	11	80	16	7.7	24.9
Al:18	42	7	7	80	16	3.8	28.7
Al:21	49	7	8	80	16	4.8	33.5
Al:26	54	5	16	80	16	12.4	45.9
Al:30	62	8	7	60	12	3.8	49.7
Al:33	Background	–	3	–	–	–	–
Al:36	68	6	11	60	12	7.7	57.4
Al:40	76	8	11	–	–	–	–
Al:43	76 Acid evaporation		15	60	12	11.5	68.9
Water change	83	7	11*	40	8	7.7	76.6
Al:47	89	6	7	40	8	3.8	80.4
Al:50	103	14	12	40	8	8.6	89.0
Al:53	107	4	4	40	8	1	90.0
Water change	112	5	7*	40	8	3.8	93.8
Al:56	138	26	13	40	8	10.6	104.4
Water change	145	7	11*	40	8	8.6	113.0
Al:59	152	7	12	40	8	9.6	122.6
Al:61	159	7	11	40	8	8.6	131.2
Al:64	Background	–	1	–	–	–	–
Water change	166	7	11*	40	8	8.6	139.8
Al:65	173	7	11	40	8	8.6	148.4
Al:68	Background	–	2	–	–	–	–
Water change	180	7	11*	40	8	8.6	157.0
Water change	183	3	5*	40	8	2.9	159.9
Al:69	187	4	10	20	4	7.7	167.6

* Calculated Al quantity

BL 0142

TABELLBLAD A4

Leaching vessel II		Al_2O_3 leaching. Double-distilled H_2O, pH 9.3. Rectangles + sapphires				Table A.3	
Test No.	Total leaching time d	Leaching period d	µg Al·l^{-1}	Test volume ml	Test surface cm^2	Leached Al_2O_3 g·cm^{-2}·10^{-8}	
							Total
Al:3	Background	–	3	–	–	–	–
Al:4	12	12	250	170	34	240	240
Al:7	19	19	300	170	34	288	288
Al:10	21	21	222 ?	170	34	–	–
Al:13	29	8	76	140	28	70	358
Al:16	35	6	38	140	28	33	391
Al:19	42	7	36	140	28	32	423
Al:22	49	7	14	140	28	11	434
Al:24	49 Acid evaporation		12	–	–	–	–
Al:27	54	5	8	140	28	5	439
Al:29	54 Acid evaporation		8	–	–	–	–
Al:31	62	8	11	100	20	8	447
Al:35	62 Acid evaporation		11	–	–	–	–
Al:34	Background	–	3	–	–	–	–
Al:37	68	6	22	100	20	18	465
Al:39	68 Acid evaporation		25	–	–	–	–
Al:41	76	8	11	100	20	8	473
Al:44	76 Acid evaporation		10	–	–	–	–
Water change	83	7	17*	60	12	13	486
Al:48	89	6	20	60	12	16	502
Al:51	103	14	20	60	12	16	518
Al:54	107	4	9	60	12	6	524
Water change	112	5	7*	50	10	5	529
Al:57	138	26	20	50	10	17	546
Water change	145	7	12*	50	10	10	556
Al:60	152	7	11	50	10	9	565
Al:62	159	7	17	50	10	14	579
Al:64	Background	–	1	–	–	–	–
Water change	166	7	12*	50	10	10	589
Al:66	173	7	6	50	10	4	593
Water change	180	7	11*	50	10	9	602
Water change	183	3	5*	50	10	3	605
Al:70	187	4	10	25	5	8	613

* Calculated Al quantity

BL 0142

TABELLBLAD A4

Leaching vessel IV		Al_2O_3 leaching. Double-distilled H_2O pH 9.3, Sapphires				Table A.4	
Test No.	Total leaching time d	Leaching period d	µg $Al \cdot l^{-1}$	Test volume ml	Test surface cm^2	Leached Al_2O_3 $g \cdot cm^{-2} \cdot 10^8$	
							Total
Al:3	Background	-	3	-	-	-	-
Al:8	4	4	65	15	2.4	60	60
Al:11	6	6	100	14	2.4	93	93
Al:14	14	8	100	15	2.4	93	186
Al:17	20	6	79	15	2.4	73	259
Al:20	27	7	88	15	2.4	82	341
Al:23	34	7	66	15	2.4	60	401
Al:28	39	5	35	15	2.4	31	432
Al:32	47	8	46	15	2.4	41	473
Al:34	Background	-	3	-	-	-	-
Al:38	53	6	55	15	2.4	50	523
Al:42	61	8	38	15	2.4	34	557
Al:45	61	Acid evaporation	29	-	-	-	-
Water change	68	7	47*	15	2.4	42	599
Al:49	74	6	39	15	2.4	34	633
Al:52	88	14	97	15	2.4	90	723
Al:55	92	4	26	15	2.4	22	745
Water change	97	5	33*	15	2.4	29	774
Al:58	123	26	36?	15	2.4	33	807
Water change	130	7	12*	15	2.4	10	817
Water change	137	7	12*	15	2.4	10	827
Al:63	144	7	12	15	2.4	10	837
Al:64	Background	-	1	-	-	-	-
Water change	151	7	10*	15	2.4	8	845
Al:67	158	7	10	15	2.4	8	853
Water change	165	7	10*	15	2.4	8	861
Al:71	172	7	9	15	2.4	7	868

* Calculated Al quantity

BL 0142

Figure B1. Leached Al_2O_3. Double-distilled H_2O. Rectangles.

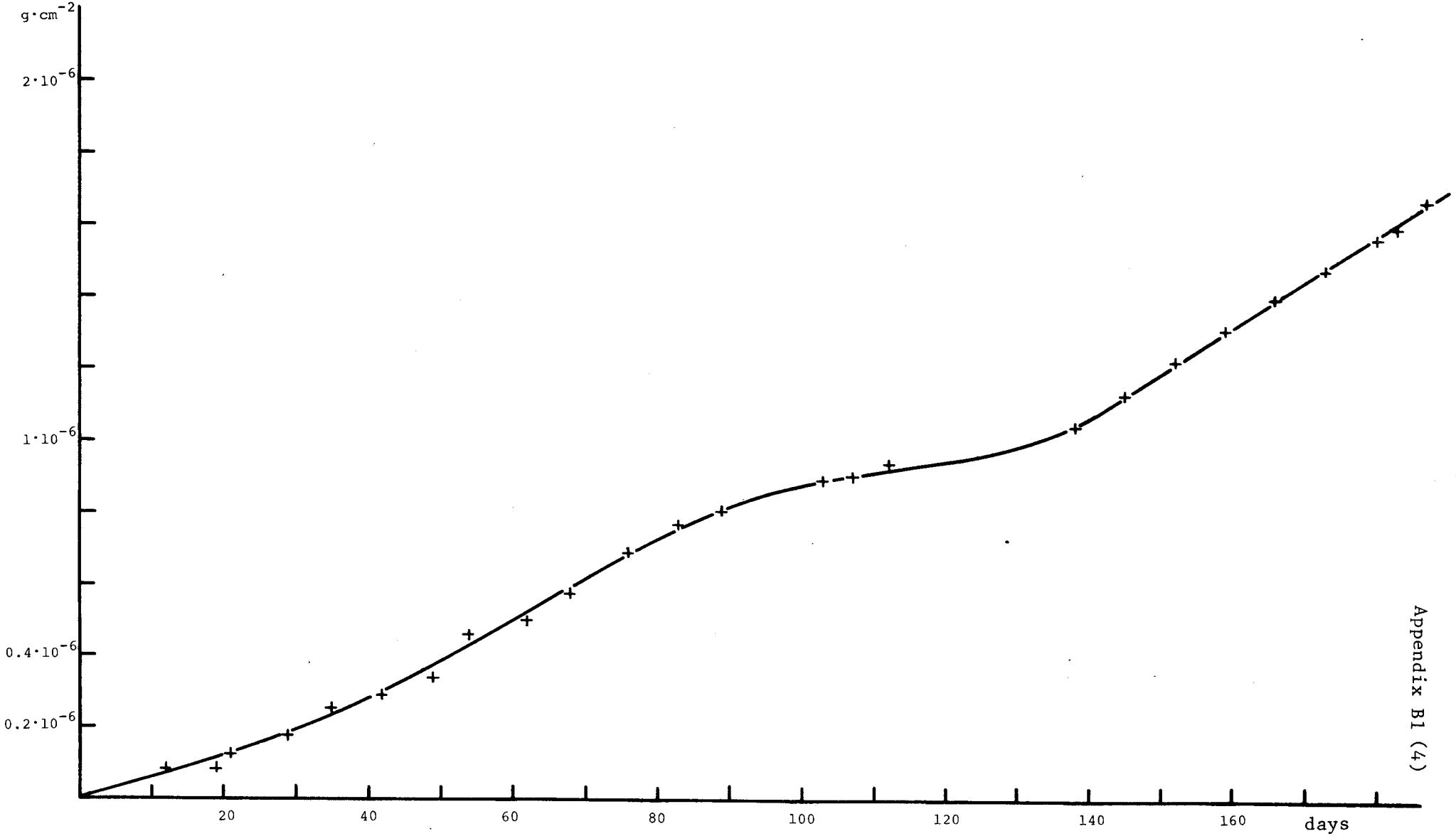

Figure B2. Leached Al_2O_3. Double-distilled H_2O, pH 9.3. Rectangles + sapphires.

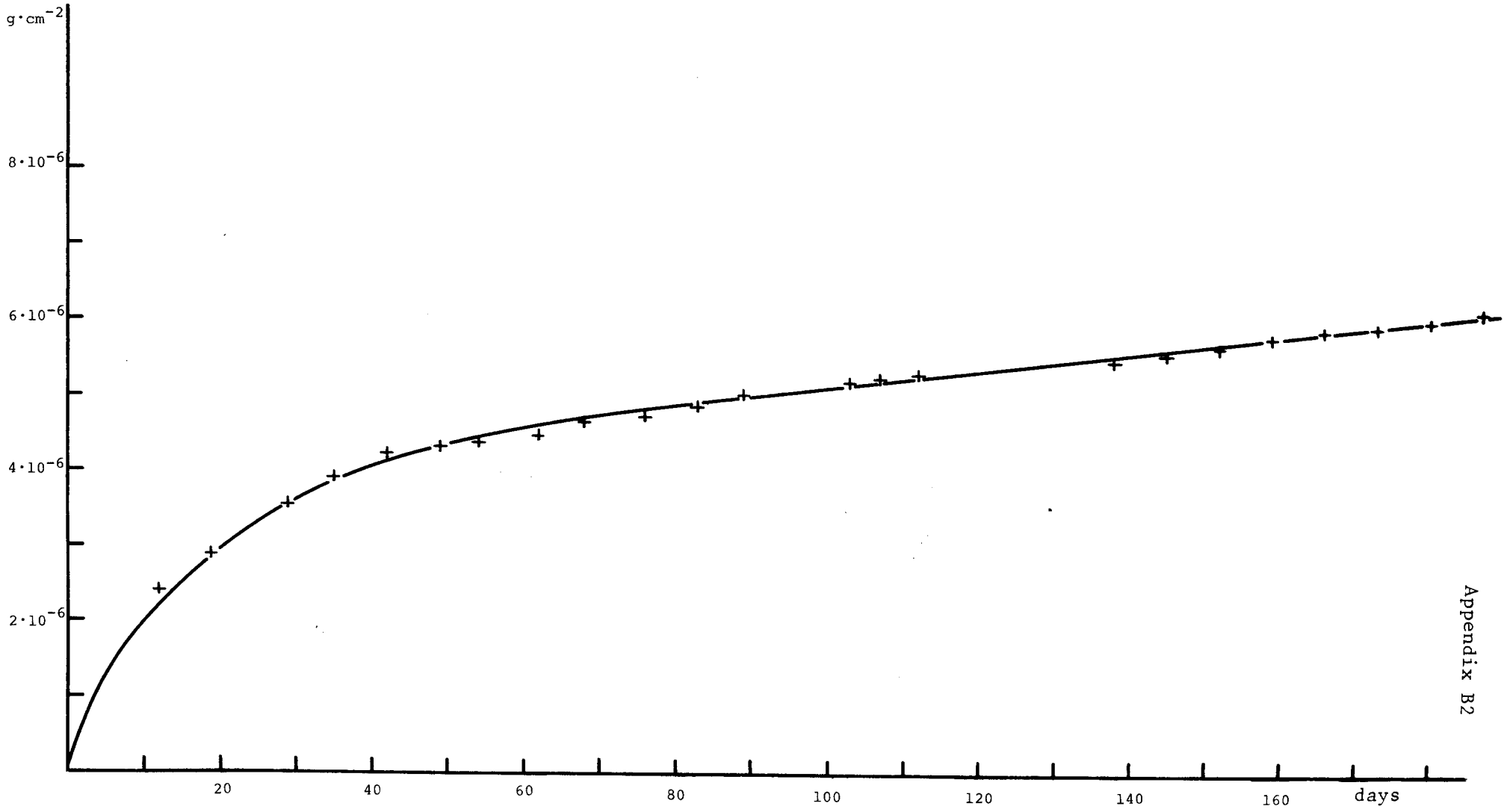

Figure B3. Leached Al_2O_3. Double-distilled H_2O, pH 9.3. Sapphires.

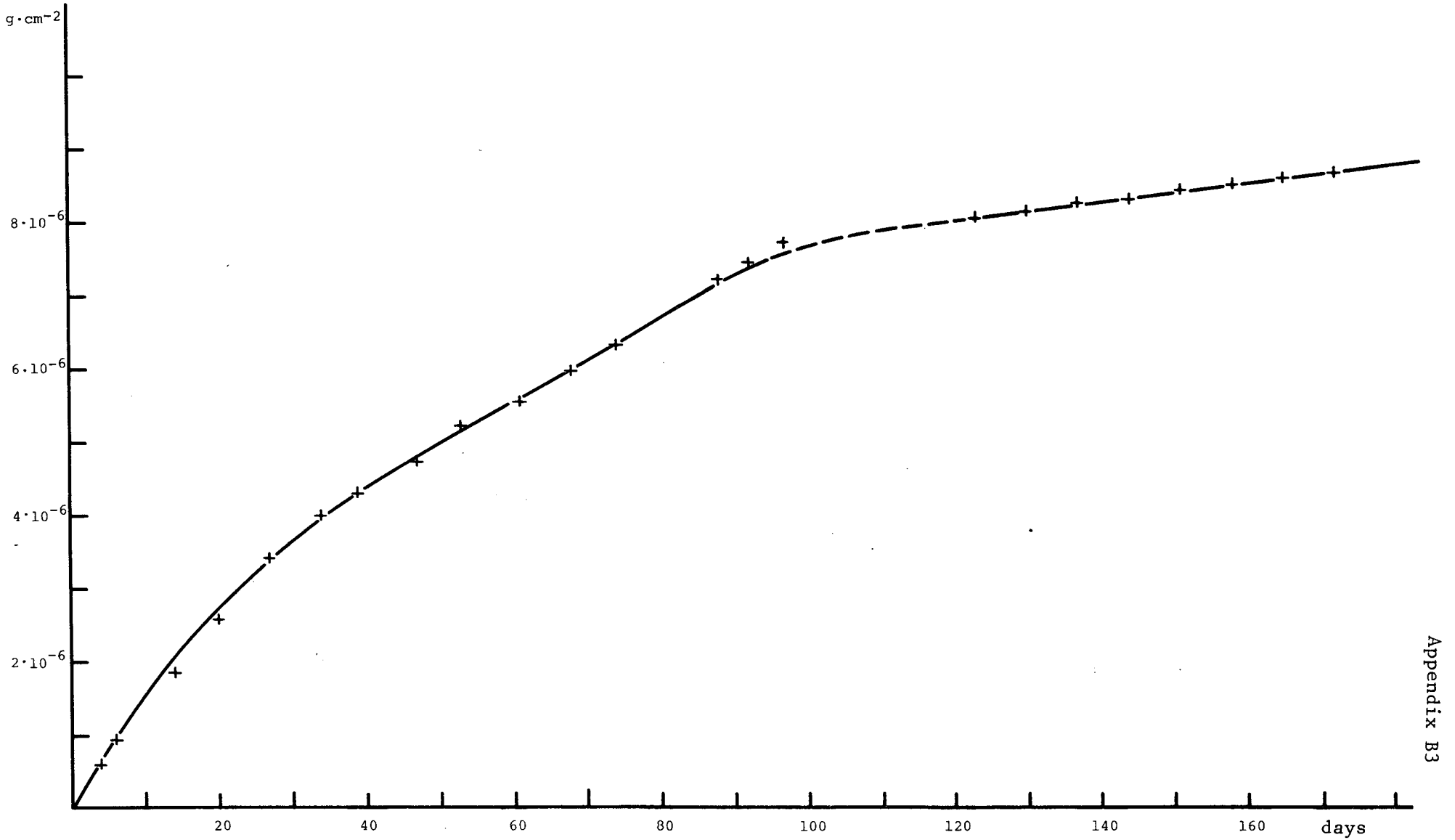

Appendix B3

Figure B4. Corrosion rate Al_2O_3

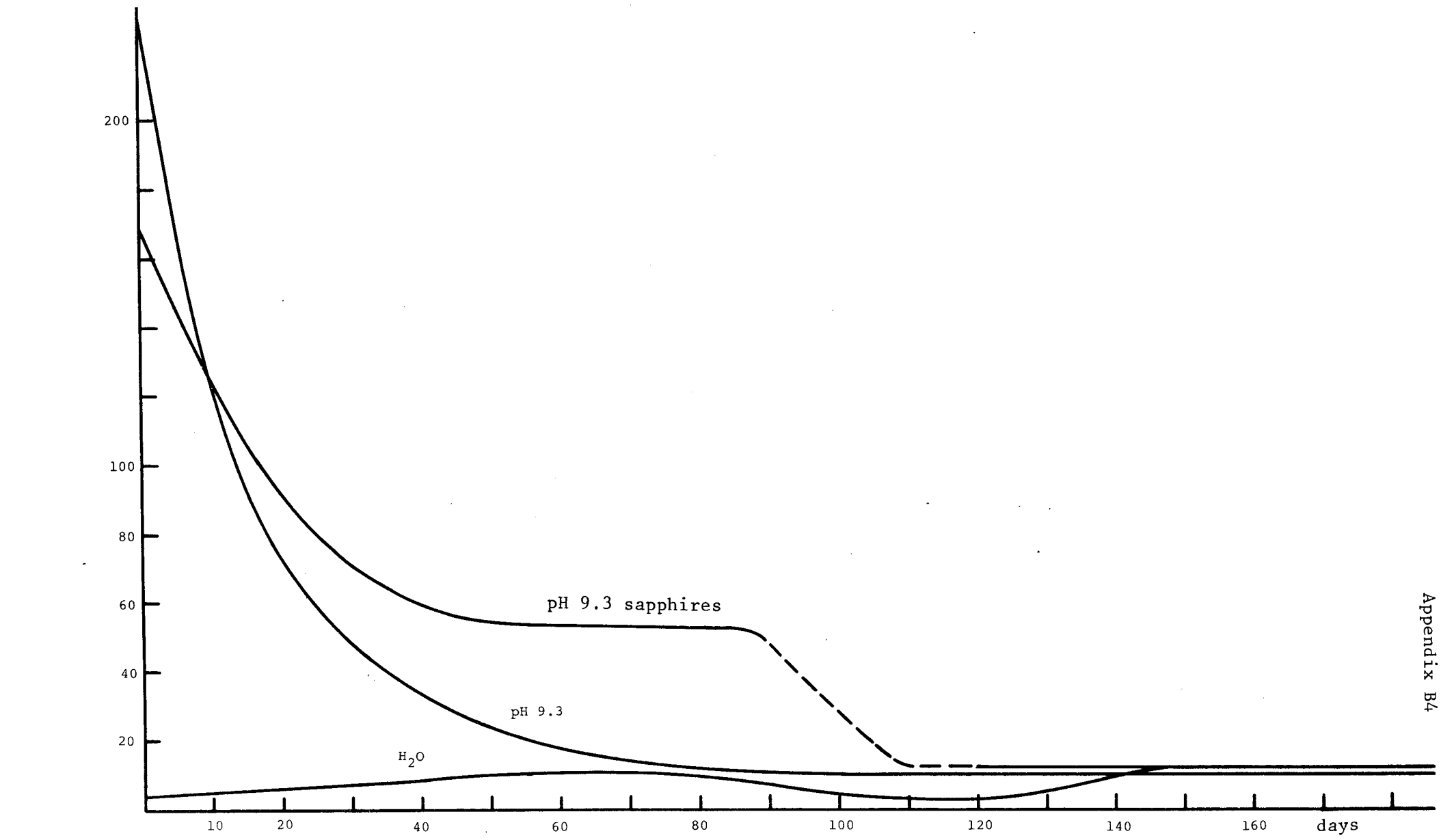

Appendix B4

Determination of corrosion rates for α Al_2O_3 in sodium-hydrogen-carbonate-buffered, chloridic water at 80°C and 40°C and pH = 8.5

Nils Ingri and Lars-Olof Öhman
Department of Inorganic Chemistry
University of Umeå, S-901 87 Umeå

Supersedes previously submitted report, 1978-08-31. (supplemented with data for 40°C)

SUMMARY
Polycrystalline α-Al_2O_3 was leached at 80°C and 40°C in flowing sodium-hydrogen-carbonate-buffered, chloridic water with pH = 8.5 for 75 and 60 days, respectively. By means of continuous addition of leachant solution, the solution was kept unsaturated with respect to Al(aq) in order to maximize corrosion.

The corrosion rate for Al_2O_3 was determined in two independent ways: first by regular weighing of the test body, second by spectrofluorometric Al analysis of the leachant solution. In the first test, which was carried out at 80°C, a constant corrosion rate was obtained according to both methods after about 10 days of leaching. The values that were obtained were:

$(68 \pm 6).10^{-9}$ m.year^{-1} according to the gravimetric analysis method
$(16 \pm 1).10^{-9}$ m.year^{-1} according to the fluorometric analysis method

The subsequent test, at 40°C, gave the following results:

$(5 \pm 14).10^{-9}$ m.year^{-1} according to the gravimetric analysis method
$(0.9 \pm 0.1).10^{-9}$ m.year^{-1} according to the fluorometric analysis method

The specified error limits correspond to a statistical significance level of 99%.

INTRODUCTION

This study was carried out on commission for ASEA AB's high-pressure laboratory.

The purpose of the study was to measure the corrosion rate in an environment corresponding to extreme groundwater conditions. The experimental objective was thereby:

i) to leach the test body in a flowing leachant solution and thereby keep the Al_2O_3 surface unsaturated with respect to Al(aq) throughout the entire leaching procedure in order to maximize corrosion.

ii) to use leachant solutions with a pH and a salinity that could correspond to an extreme groundwater composition without thereby causing precipitation of insoluble Al compounds on the test body. We chose a leachant medium containing 278 mg NaCl, 396 mg $NaHCO_3$ and 23 mg Na_2CO_3 per litre, which gives a pH of about 8.5.

iii) to carry out the tests at such high temperatures that the corrosion would be experimentally detectable.

iiii) to regularly measure the loss of weight of the test body and fluorometrically determine Al(aq) in the leachant solution. These two methods should be able to provide information on the division of the corrosion into a mechanical portion (particle loss) and a chemical portion (chemically dissolved aluminium).

The tests were planned and discussed in consultation with Ragnar Tegman, ASEA AB's high-pressure laboratory at Robertsfors.

EXPERIMENTAL

Fabrication and preparation of the test body

A body of Al_2O_3 with a weight of 50 kg was fabricated by means of hot isostatic pressing of fine-grained α-Al_2O_3 powder (Alcoa A15) at an isostatic pressure of a 150 MPa and a temperature of 1350°C for 20 hours. The resultant material has a mean grain size of 3 μm and a density of 3.975 $g.cm^{-3}$.

Test rods of dimensions 3.0x3.0x50 mm were cut with a diamond wheel from this body. Corners and edges were roundedoff lightly on a diamond wheel. At the same time, one end of the rods was given a slight taper. Metal filings and organic matter from the cutting procedure were then removed by washing in 70% HNO_3 for 15 minutes at 60°C. In order to get wellrounded edges and a uniform prehistory for the rods, they were used as grinding bodies in a rod mill for 16 hours. The rods were then rotated together with a water suspension of Al_2O_3 powder (Alcoa A15). The rods were then washed four times in distilled water. The base plate was fabricated and pretreated in a similar manner. The appearance of the finished test body is shown in figure 7. This part of the work was done at ASEA AB's highpressure laboratory at Robertsfors. When the test body was delivered to us, 28.50 mg of 0.1 mm platinum wire was attached to make it easier to lift the test body out of the test vessel. The test body was then cleaned once again in 70% HNO_3 for 10 minutes at 60°C.

Description of leaching equipment

Figure 6 shows the apparatus set-up that was used. The test vessel, with a tightly-fitting turned lid, was made of teflon. Thick-walled polyethylene cans were used as storage and collection vessels. Except for the hoses at the peristaltic pumps, which were made of silicone rubber, the hose material was polypropylene.

Heating took place in a heating cabinet, which was controlled by means of a proportional circuit. A rapidly rotating propeller in the lower part of the heating cabinet provided good air circulation. In this manner, the temperature was maintained constant throughout the heating cabinet. The temperature was measured and checked continuously during the tests with a Pt-Pt/10% Rh thermocouple inside the test vessel.

Cleaning of leaching equipment

Prior to the start of the study, the equipment was washed with 10% HCl (Merck, pro analysi) for 5 days, and then with distilled H_2O for one day and finally with leachant solution for 5 days. Flow and temperature were adjusted at the same time.

Chemicals, leachant solution and test runs

Great importance was attached during the tests to minimizing the amount of Al impurities from equipment and preparation. Since pilot tests showed that a leachant solution prepared with calibrated glass vessels contained 100.10^{-9} nM ($3\ \mu g\,l^{-1}$) Al(aq), it was decided to switch to the molal scale (moles per kilogram solvent). In converting to the unit $g.l^{-1}$, the density of pure water ($25^{o}C = 0.9971\ g.cm^{-3}$) was used.

In preparing the solution, weighed quantities of $NaHCO_3$ (Merck, pro analysi), NaCl (Merck, pro analysi) and the necessary volume of known NaOH solution were transferred to a polyethylene vessel, after which freshly distilled H_2O was added to the right mass (9 000 $\pm$ 1 g). In the prepared solution, $\Sigma CO_3 = 5.00$ mmolar (305 $mg.l^{-1}$), $m_{Cl} = 4.78$ mmolal (170 $mg\,l^{-1}$) and pH= 8.48 $\pm$ 0.02 at $25^{o}C$. The alkalinity of the solution is 5.22 mmolal. The reason why NaCl was added was to create a defined leaching environment for possible future tests. The amount of NaCl was chosen so that $m_{Na^+} = 10.0$ mmolal (230 $mg\,l^{-1}$) in the leachant solution (constant cation background).

During the first test, a sample was taken from the storage vessel and titrated against a coulometrically determined H^+ solution to H_2CO_3 composition. This determination agreed very well with the added quantities.

On the same occasion, the pH of the leachant solution was measured to be 8.48. This determination, at $25^{o}C$, was performed with a compensator bridge (Metrohm E 388), a combination electrode (Metrohm EA 120 ux) and four pH standard buffers (PH Tamm) in the pH range 69.

In an equivalent analysis of the leachant solution after leaching, i.e. from the collection vessel, pH = 8.61 was measured. This pH increase was probably caused by some CO_2 evolution at $80^{o}C$. Gas bubbles could be observed on the walls of the test vessel during the test.

Chemicals, distilled H_2O and reagents were tested with respect to Al impurities in accordance with the spectrofluorometric method described below. Al(aq) in the prepared leachant solution can be expected to amount to 4.10^{-9} molal ($0.1\ \mu g.l^{-1}$).

Prior to the tests, a control leaching of the equipment was performed. A total Al(aq) level of $7.7\ 10^{-9}$ molal was obtained at $80^{o}C$, i.e. the equipment gave an additional $3.7.10^{-9}$ molal ($0.1\ \mu g.l^{-1}$). At $40^{o}C$, it was not possible to detect any leaching from the equipment ($< 0.02\ \mu g.l^{-1}$).

Leaching procedure

The test body that was used has a geometric area of 148.5 cm^2 and its appearance is shown by Figure 7. The platinum wire attached to the test body has been assumed to be inert in the evaluation. During leaching, the test body was exposed to a continuous flow of leachant solution, both an external flow of fresh leachant solution of 1.10 $\pm$ 0.03 l . day^{-1} and an internal flow of 25 $ml.min^{-1}$ (see "apparatus set-up", Figure 6). The internal flow gives the solution a flow rate of 0.8 $mm.s^{-1}$ past the test body. The temperature in the test vessel was constant within $\pm$ 0.5°C. At the start of leaching, the collection vessel was emptied and the cleaned, dried and weighed test body was placed in the test vessel, after which the external pump was started. After leaching times shown by Tables 1 and 3, leaching was interrupted and the test body was rinsed in 3 x 1 l distilled water, dried for 1 h 45 min in vacuum over concentrated H_2SO_4 and weighed.On the same occasions, the contents of the collection vessel were weighed and samples were taken for fluorometric Al analysis. This procedure thus provides a value for the loss of weight of the test body and a value for the amount of Al(aq) in the leachant solution. At 40°C, samples were taken on several occasions for fluorometric analysis without interrupting leaching.

Gravimetric analysis of the test body

The balance that was used (Mettler H54) was tested before the study by means of repeated weighings of the test body. Reproducibility was found to be $\pm$ 0.00001 g.

When the test body was weighed during the experiments, the balance was read off continuously for 5 minutes. The read-off weight did not vary during this time. The total measuring error can be estimated to be $\pm$ 0.00003 g in a single measurement. The primary source of error is probably dust particles that have become stuck to, or have come loose from, the test body during the course of the experiment.

Fluorometric Al analysis of the leachant solution

A method described by Hydes and Liss (1) was used for the Al analyses. However, pilot studies show that the spectrofluorometer used (Perkin-Elmer 512) gave the highest resolution if the excitation and emission wave-lengths were changed to 467.5 nm and 585 nm, respectively. Otherwise, the described method was followed. The detectibility limit for the analysis is 1.10^{-9} molal ($0.025\ \mu g.l^{-1}$). The measuring error can be estimated to be $\pm$ 10% of the read-off value for concentrations above 10 nmolal and $\pm$ 1 nmolar for lower concentrations. The standard curves, which consisted of four points, thus exhibit very good linearity in the relevant concentration range (see Figure 8).

The standard solutions were prepared by adding known quantities of Al solution with a micropipette to a known quantity of leachant solution. The standard curve thereby gives the Al(aq) increment

from leaching, i.e. ~4 nmolal Al(aq) coming from chemicals and reagents has been subtracted. The Al concentration in the stock solution was determined by indirect titration of EDTA -$Pb(NO_3)_2$ with Pb^{2+} solution at pH = 5.5 using xylenol-orange as indicator.

RESULTS
$80^{\circ}C$

The weighing results from leaching are presented in table 1. Accumulated leached quantity of Al_2O_3 as a function of time is shown in Figure 1. The fluorometric analyses are reported in Table 2 and Figure 2. The corrosion rate was calculated from the slope of the plotted curves and plotted in Figure 5. As is evident from both of the methods, the test body exhibits higher corrosion at the start of the test. After about 10 days of leaching, a state has been reached where the corrosion rate is constant. According to the gravimetric analysis method, a corrosion rate of $(69 \pm 6) \cdot 10^{-9}$ m.year^{-1} is obtained, while the fluorometric analysis method gives a corrosion rate of $(16 \pm 1) \cdot 10^{-9}$ m.year^{-1}. The given error limits correspond to a significance level of 99%.

$40^{\circ}C$
A number of problems arose during this test. Immediately prior to the test, the platinum wire with which the test body is lifted out of the test vessel broke. A pair of crucible pliers was then modified so that it could be used to get down between the test body and the walls of the leaching vessel, grasp the outermost rods and lift the test body. In order to protect the test body during this procedure, the jaws of the pliers were covered with silicone rubber. After a leaching time of 975 h, the silicone rubber hose for internal circulation (see Figure 6) ruptured. It was then replaced with a similar hose, washed for 15 minutes in concentrated HCl and then in H_2O. Despite this washing, the subsequent 24-hour quantity of leachant solution exhibited a clearly elevated Al(aq) level. The hose appears to have released a total quantity corresponding to about ~0.5 - 0.8 µg Al_2O_3. In the evaluation of the corrosion rate, however, this amount has been counted as stemming from the test body as well.

After a leaching time of 1 422 h, the test had to be interrupted because one of the test rods broke at the level of the upper edge of the test plate. The break occurred when the test body was being lifted out of the test vessel and was caused by the large breaking force exerted by the pliers described above.

The results are reported in the same manner as at $80^{\circ}C$ in Tables 3-4 and Figures 3-4.

The corrosion rate is found to be $(5 \pm 14) \cdot 10^{-9}$ m.year^{-1} with the gravimetric method and $(0.9 \pm 0.1) \cdot 10^{-9}$ m.year^{-1} with the fluorometric method. The given error limits correspond to a significance level of 99%.

COMMENTS AND CONCLUSIONS

The elevated corrosion rate during the first 200 h of the test is undoubtedly attributable to the fact that the test body had not previously been leached and that the surface consisted of small grains and edges where the leachant solution caused an intense dissolution. After 200 h, these grain and edge effects had disappeared. This explanation is supported by the test at 40°C. Here, the specimen had previously been leached and an elevated corrosion rate was not obtained at the beginning of the test (see Fig. 5).

The difference in the corrosion rate at 80°C cannot be explained by reference to statistical or technique-related factors. However, a probable explanation is that the gravimetric method measures a combined chemical and mechanical effect, while the fluorometric method only measures the chemical portion, i.e. the Al_2O_3 quantity that has been dissolved and has come out into the leachant solution. The mechanical portion can be imagined to take place in one of the following manners:

When the test body is lowered into the leachant solution, a hydrated layer gradually grows on the Al_2O_3 surface. This layer can be between 50 and 100 Å thick. Aluminium is continuously dissolved on the outermost parts of the layer. The dissolved aluminium may consist partly of aluminium ions, which can easily be measured by the fluorometric method, and partly of large colloidal aluminium aggregates, which could possibly escape fluorometric measurement. This could be part of the reason for the differences in corrosion rate between the gravimetric and the fluorometric determination. Another reason could be that when the test body is taken out, dried and weighed, some of the hydrated layer dries, resulting in a "chapped" and crumbly surface where the particles sit more or less loosely and can easily fall off. When the test body is once again lowered into the leachant solution after the weighing procedure, some of this loose material will probably fall off and follow the leachant solution out into the collection vessel. This "weighing effect" is a very possible explanation and is described in the literature in connection with, among other things, leaching tests on glass.

It should perhaps be mentioned that at 40°C, only the fluorometric method is sufficiently accurate to give a significant result. The effects are much too small to be weighed. This is also clearly evident from the error limits for the gravimetric analysis method.

REFERENCE

1. D.J. Hydes and P.S. Liss, Fluorometric Method for the Determination of Low Concentrations of Dissolved Aluminium in Natural Waters, Analyst 101 (1976) 922-931.

Table 1.

Results from gravimetric analysis at $80^{o}C$

Test quantity: 42.90035 g
Volume/area: 0.727 mm
Test surface: 148.5 cm^2
Platinum wire: 0.02850 g
Density: 3.975 g cm^{-3}

Date	Time (h)	Weight (g)	Total weight loss		Total corrosion	
			(mg)	(Share of total mass)$\cdot 10^6$	($\mu g cm^{-2}$)	(nm)
780613	0	42.92885	0	0	0	0
780614	24	42.92849	0.36	8.39	2.42	6.10
780616	72	42.92825	0.60	14.0	4.04	10.2
780620	168	42.92831	0.54	12.6	3.64	9.15
780628	352	42.92818	0.67	15.6	4.51	11.4
780705	516	42.92816	0.69	16.1	4.65	11.7
780712	686	42.92809	0.76	17.7	5.12	12.9
780719	857	42.92799	0.86	20.0	5.79	14.6
780727	1038	42.92791	0.94	21.9	6.33	15.9
780807	1289	42.92779	1.06	24.7	7.14	18.0
780814	1470	42.92774	1.11	25.9	7.48	18.8
780822	1655	42.92761	1.24	28.9	8.35	21.0
780828	1800	42.92754	1.31	30.5	8.82	22.2

The corrosion rate in the linear range 168h-1800h is found, after least squares adjustment, to be, $(68 \pm 2).10^{-9} m.year^{-1}$

Table 2

Results from fluorometric Al analysis at 80°C

Test quantity: 42.90035 g Volume/area: 0.727 mm

Test surface: 148.5 cm^2 Platinum wire: 0.02850 g

Density: 3.975 $g.cm_{-3}$

Date	Time (h)	^{m}Al (nmolal)	Leachant solution (g)	Weight loss Al_2O_3			Total corrosion	
				(µg)	Σ(µg)	Σ(share of total mass).10^6	(µgcm^{-2})	(nm)
780613	0	-	-	0	0	0	0	0
780614	24	370	1065	20.1	20.1	0.469	0.135	0.340
780616	72	100	2135	10.9	31.0	0.723	0.209	0.526
780620	168	61	4328	13.5	44.5	1.04	0.300	0.755
780628	352	41	8341	34.9	79.4	1.85	0.535	1.35
780705	516	53	7486	20.2	99.6	2.32	0.671	1.69
780712	686	44	7781	17.5	117.1	2.73	0.789	1.98
780719	857	54	7872	21.7	138.8	3.24	0.935	2.35
780727	1038	41	8382	17.5	156.3	3.64	1.05	2.65
780730	1110	46	3270	7.7	164.0	3.82	1.10	2.78
780807	1289	43	8115	17.8	181.8	4.24	1.22	3.08
780814	1470	43	8159	17.9	199.7	4.66	1.34	3.38
780822	1655	47	8362	20.0	219.7	5.12	1.48	3.72
780828	1800	45	6536	15.0	234.7	5.47	1.58	3.98

The corrosion rate in the linear range 352h-1800h is found, after least squares adjustment, to be $(15.7 \pm 0.2) \cdot 10^{-9}$ m·$year^{-1}$.

Table 3

Results from gravimetric analysis at $40^{o}C$

Test quantity: 42.89905 g Volume/area: 0.727 mm

Test surface: 148.5 cm^{2} Platinum wire: 0.01410 g

Density: 3.975 g cm^{-3}

Date	Time (h)	Weight (g)	Total weight loss		Total corrosion	
			(mg)	(Share of total mass)·10^{6}	($\mu g cm^{-2}$)	(nm)
780921	0	42.91315	0	0	0	0
780928	165	42.91320	-0.05	-1.2	-0.34	-0.85
781005	330	42.91316	-0.01	-0.2	-0.07	-0.17
781013	518	42.91318	-0.03	-0.7	-0.20	-0.51
781019	660	42.91313	0.02	0.5	0.13	0.34
781102	993	42.91314	0.01	0.2	0.07	0.17

The corrosion rate in the "linear" range 0h-993h is found, after least squares adjustment, to be, $(5.3 \pm 4.7) \cdot 10^{-9}$ m·year^{-1}.

Table 4

Results from fluorometric Al analysis at 40°C

Test quantity: 42.89905 g Volume/area: 0.727 mm

Test surface: 148.5 cm^2 Platinum wire: 0.01410 g

Density: 3.975 $g.cm^{-3}$

Date	Time (h)	^{m}Al (nmolal)	Leachant solution (g)	Weight loss Al_2O_3			Total corrosion	
				(µg)	Σ(µg)	Σ(Share of total mass)·10^6	(µgcm^{-2})	(nm)
780921	0	-	-	0	0	0	0	0
780928	165	2.4	6567	0.81	0.81	0.02	0.0055	0.0137
781005	330	2.0	7745	0.81	1.62	0.04	0.0109	0.0274
781013	518	2.2	8532	0.98	2.60	0.06	0.0175	0.0441
781019	660	3.9	6425	1.30	3.90	0.09	0.0263	0.0661
781026	830	1.3	7513	0.51	4.41	0.10	0.0297	0.0747
781101	975	1.6	6400	0.53	4.94	0.12	0.0333	0.0837
781102	993	13.2	717	0.49	5.43	0.13	0.0366	0.0920
781104	1040	7.2	1994	0.75	6.18	0.14	0.0416	0.105
781106	1089	3.7	2081	0.40	6.58	0.15	0.0443	0.111
781109	1164	2.1	3181	0.35	6.93	0.16	0.0467	0.117
781114	1283	1.7	5730	0.51	7.44	0.17	0.0501	0.126
781120	1422	1.2	6169	0.39	7.83	0.18	0.0527	0.133

The corrosion rate in the linear range 0h-1422h is found, after the squares adjustment, to be $(0.86 \pm 0.03)\cdot 10^{-9}$ $m\cdot year^{-1}$.

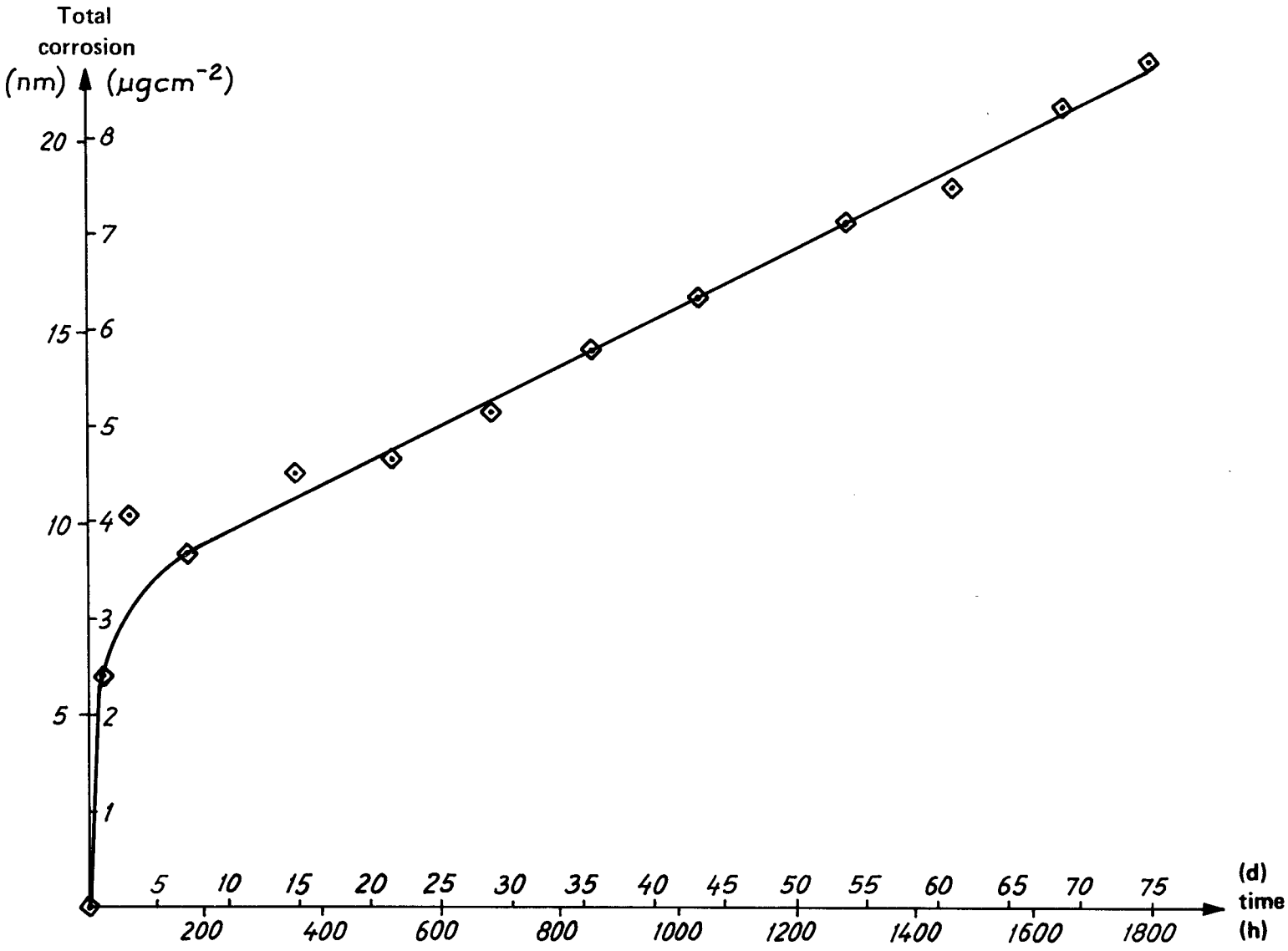

Figure 1

Accumulated corrosion as a function of leaching time according to the gravimetric determination method at 80°C.

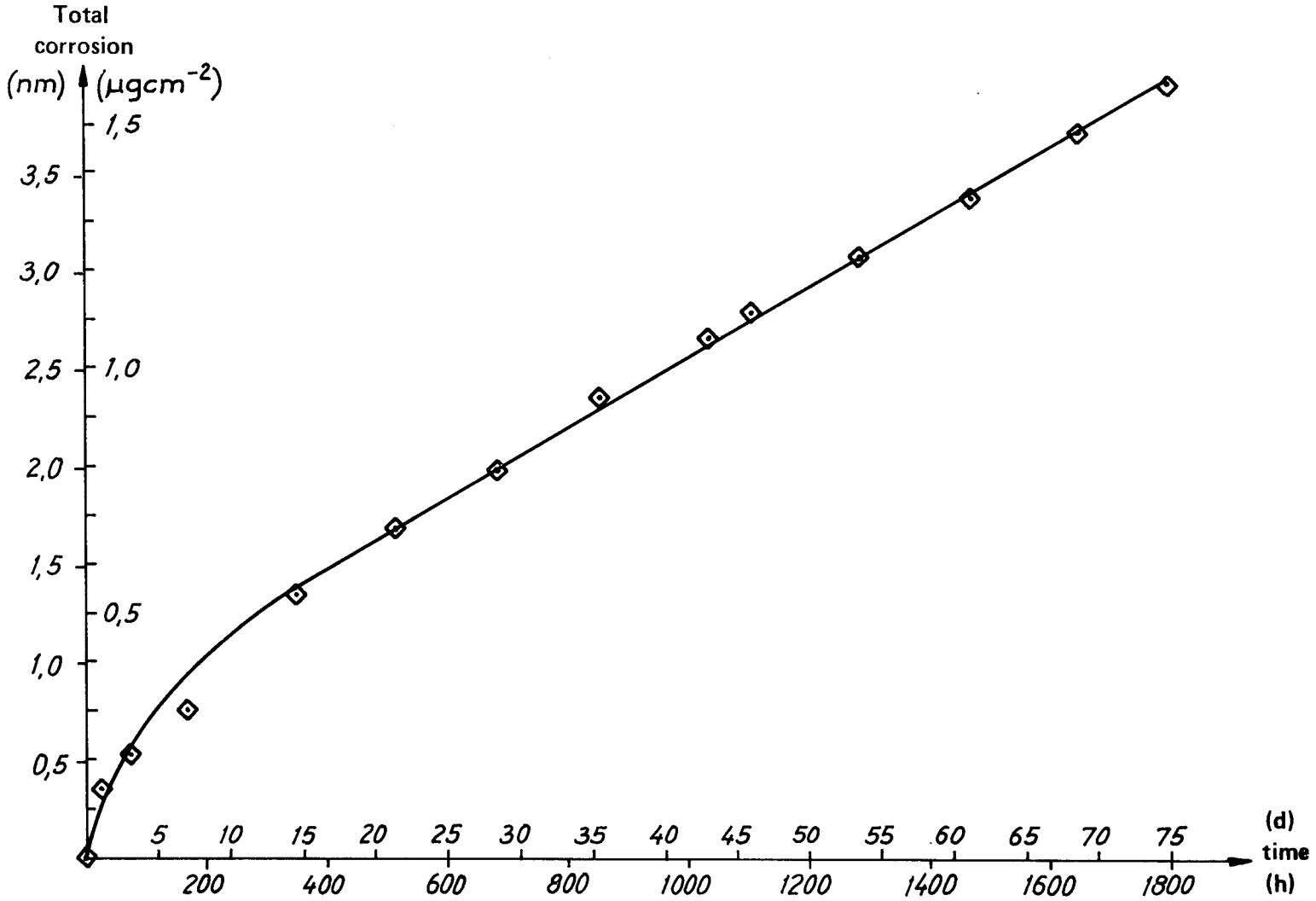

Figure 2

Accumulated corrosion as a function of leaching time according to the fluorometric determination method at 80°C.

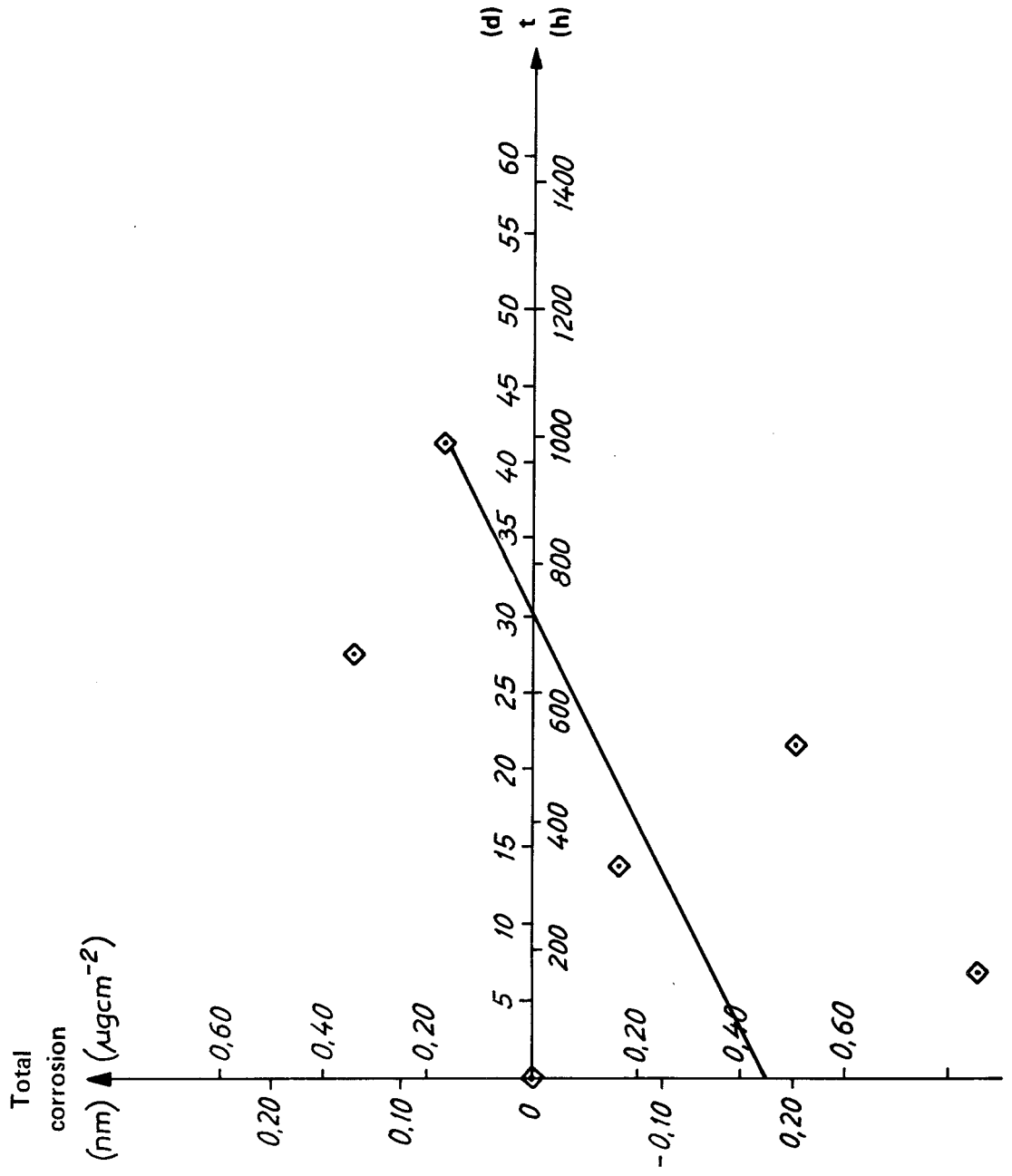

Figure 3

Accumulated corrosion as a function of leaching time according to the gravimetric determination method at 40°C.

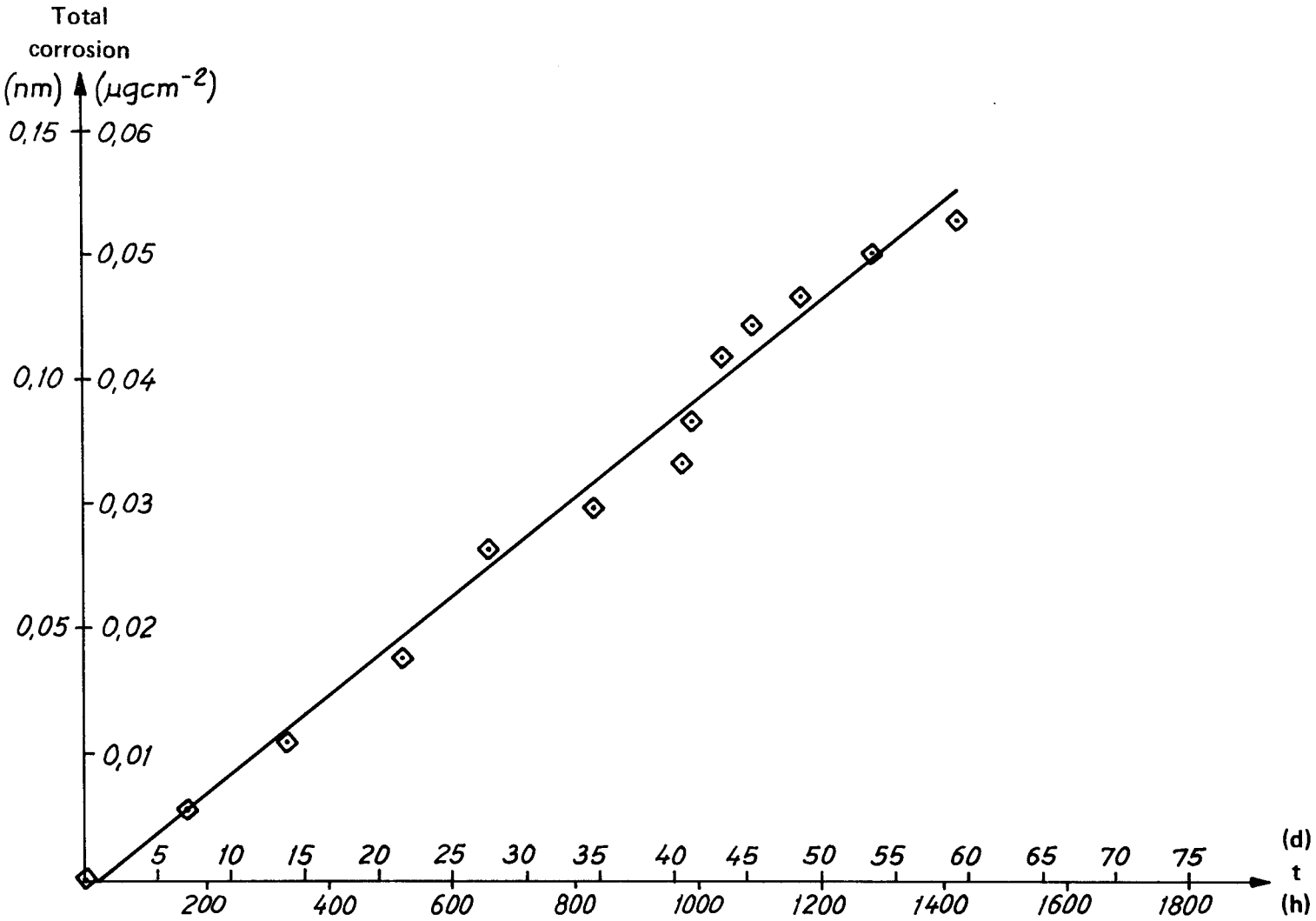

Figure 4
Accumulated corrosion as a function of leaching time according to the fluorometric determination method at 40°C.

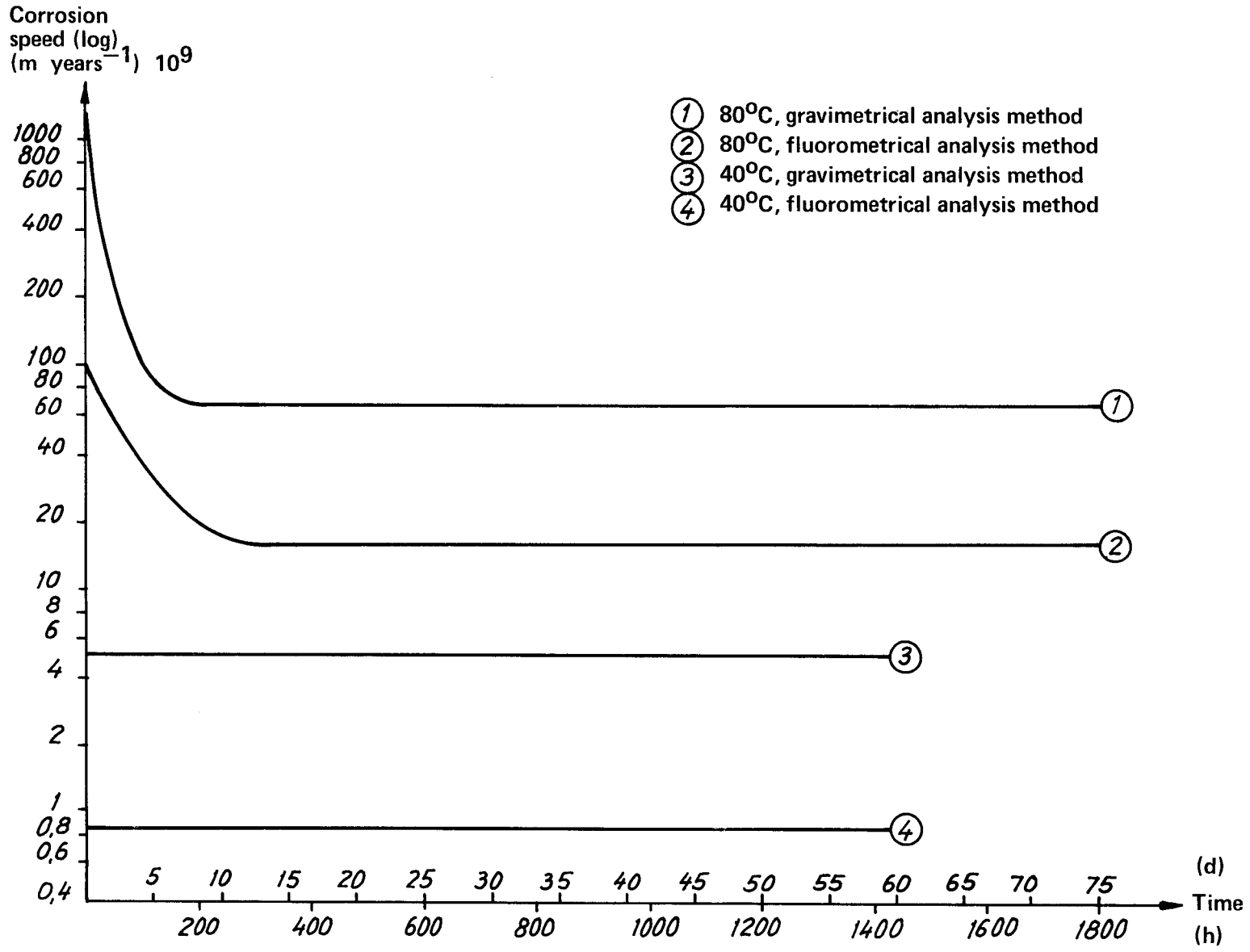

Figure 5.

Corrosion speed as a function of leaching time, calculated from figures 1 – 4.

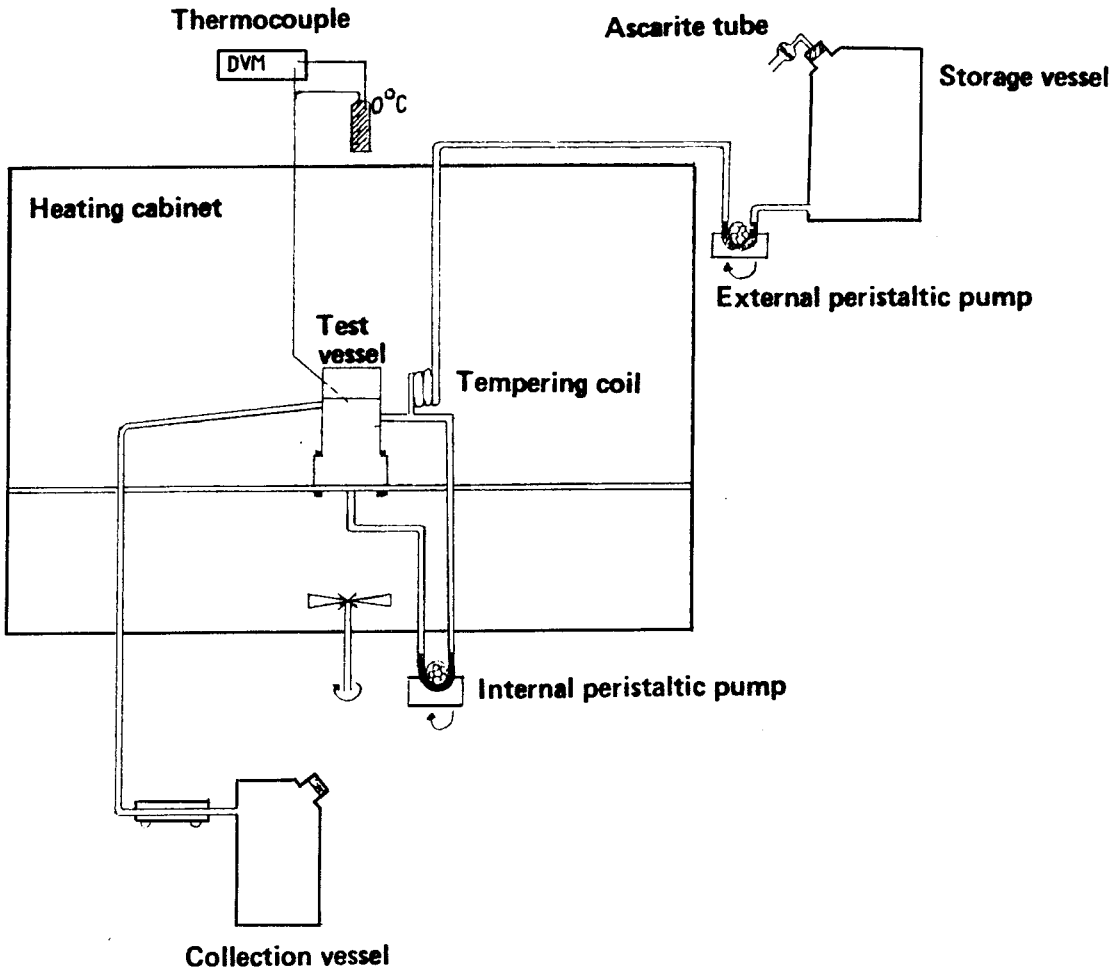

Figure 6
Apparatus set-up, not to scale

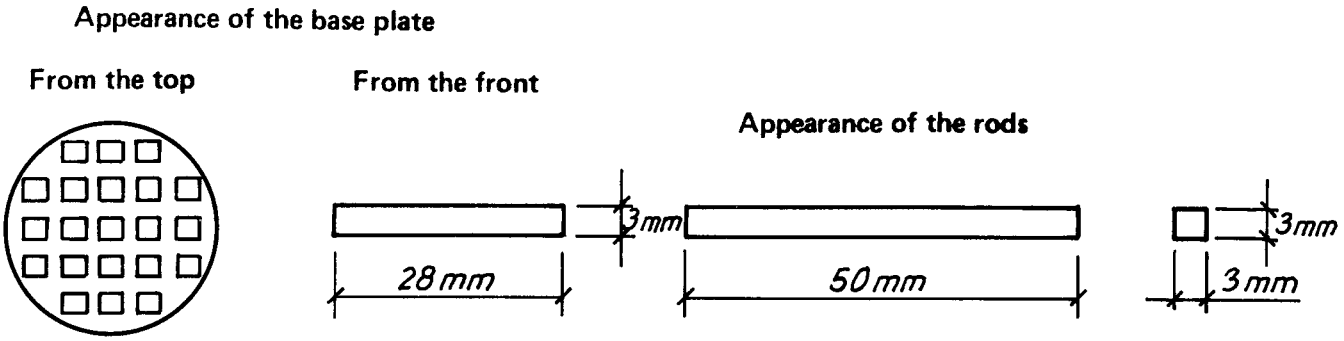

The test body consisted of 21 Al_2O_3 rods, slightly tapered at one end, inserted into the base plate. The holes in the base plate were not exactly square, so the contact surfaces between the rods and the base plate were points. In calculating the geometric area, these surfaces were not subtracted.

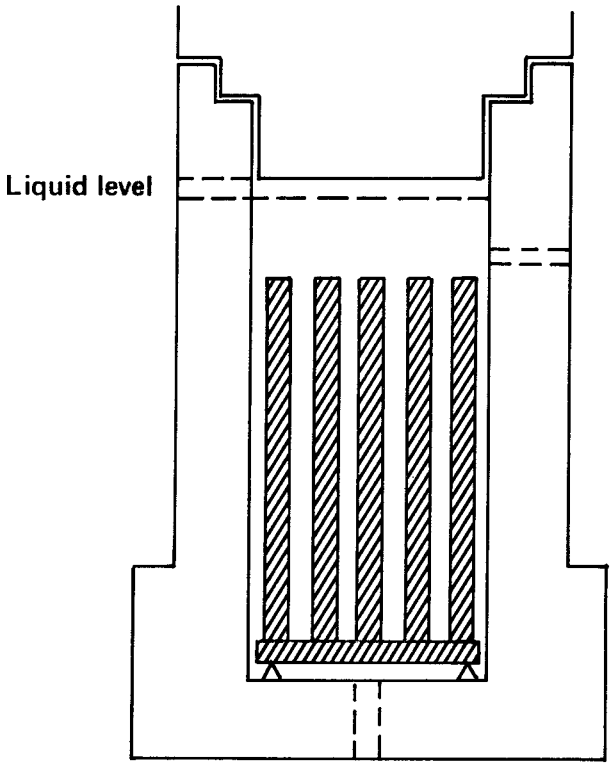

The test body rests in the vessel on a pin of Al_2O_3. Leaching from this pin was neglected in the fluorometric calculations.

Figure 7

Appearance of the test body and its location in the test vessel.

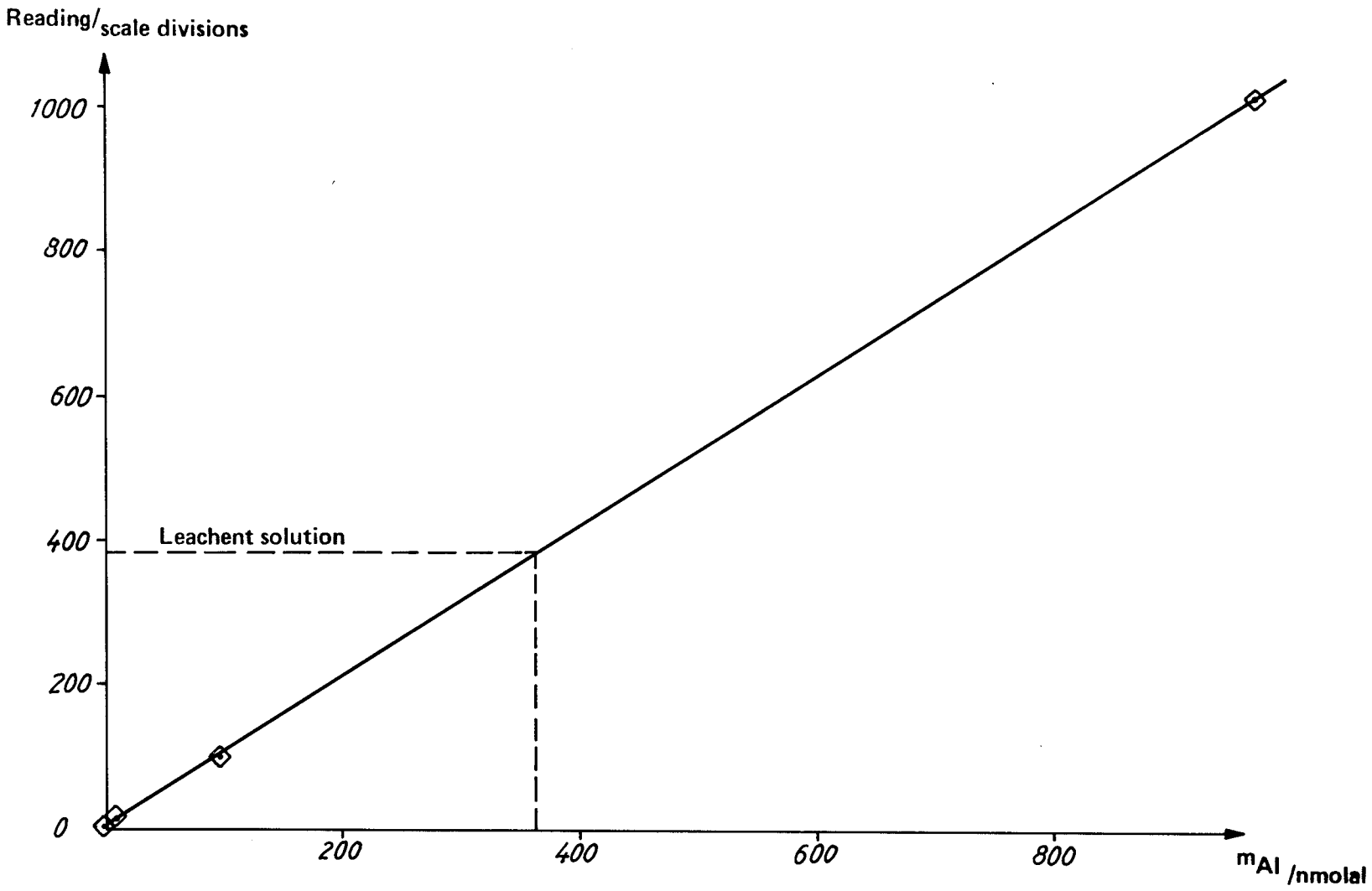

Figure 8
Example of standard curve obtained in the spectrofluorometric determination.

A THERMODYNAMIC STUDY OF THE EQUILIBRIUM BETWEEN ALUMINIUM OXIDE AND KAOLINITE

Sten-Åke Lindqvist
Nils-Gösta Vannerberg

According to a proposal by KBS, a canister of aluminium oxide (corundum) is to be used for the final storage of radioactive material. The canister is to be placed in a buffer mass consisting of silicon dioxide and bentonite. Bentonite contains, among other things, the mineral kaolinite.

In the tests carried out thus far to determine the corrosion rate of aluminium oxide, distilled water, in some cases pH-corrected to 8.5 with sodium bicarbonate, has been used. A small but detectable corrosion rate has been consistently found. However, all of these tests suffer from a defect that they have not taken into consideration the aluminium concentration provided by the bentonite. If this concentration should exceed the equilibrium concentration of the aluminium oxide, it is even possible that the aluminium oxide canister will grow in thickness. It must therefore be determined in which direction the transport of aluminium ions at pH 8.0 occurs. Is $Al_2Si_2O_5(OH)_4(s)$, kaolinite, or $Al(OH)_3(s)$, gippsite, the stable phase?

The following data were used in the study:

Table 1.

Species	Gypsum-free energy at 25°C	Reference
Al^{3+}	-114.8	1
α-Al_2O_3	-376.8	1
$Al_2Si_2O_5(OH)_4$	-977.0	4
	-857.0	4.1
$Si(OH)_4$	-197.8	1.3
SiO_2	-192.4	1
OH-	-37.6	2
H_2O	-56.7	2

The ΔG^o value for the reaction is obtained from these data

$$Al_2O_3 + 3H_2O \rightleftarrows 2Al^{3+} + 6OH^-$$

$$\Delta G^o = -152 \text{ kcal/mole}$$

which, at pH=8, gives an equilibrium activity of aluminium ion of 10^{-15}M. The total concentration of aluminium ion will naturally be much higher due to complex formation. In the same manner, ΔG^o is calculated for the reaction

$$Al_2Si_2O_5(OH)_4 + H_2O \rightleftarrows 2Al^{3+} + 2SiO_2(s) + 6OH^-$$

the ΔG^o value is 75 kcal/mole.

It should be observed that references 1 and 4 use different reference states, so the value for kaolinite must be converted to the reference 1 state. The hydrolysis of quartz is not taken into consideration. The activity of aluminium ion is then 10^{-13}M. A calculation of the equilibrium constant for the reaction

$$Al_2Si_2O_5(OH)_4(s) + 5H_2O \rightleftarrows 2Al(OH)_3(s) + Si(OH)_4(aq)$$

has been carried out by R.M. Garrels, 1957. He obtained the value $10^{-7.5}$ (3). Since the level of $Si(OH)_4$ is determined by the equilibrium $SiO_2(s) + 2H_2O \rightleftarrows Si(OH)_4$ and the equilibrium constant is 10^{-4}, this means that $Al(OH)_3(s)$, the hydrated aluminium oxide, is more stable than kaolinite (3).

Conclusion

Calculations show that hydrated aluminium oxide, gippsite, $Al(OH)_3$, is more stable than kaolinite. The thickness of the canister will therefore grow with time. This has also been shown experimentally by Ingemar Olefjord (5)

References

1. Rossini et al. Circular of the National Bureau Standards 500, Selected values of chemical thermodynamic properties, Feb. 1952.

2. Lattimer and Hildebrand, Reference book of Inorganic Chemistry, MacMillan, New York 1951.

3. Sillén, L.G. and Martell, A., Stability constants, Special publication, No. 17, London, the Chemical Society 1964

4. Baring and Knacke, Thermochemical properties of Inorganic Substances.

5. Olefjord and Rilby, ESCA-undersökning av Al_2O_3 exponerad för simulerat grundvatten ("ESCA-study of Al_2O_3 exposed to simulated groundwater"). The Corrosion Institute's Final report Aluminium oxide as an encapsulation material, appendix D1.

Residual stresses, defects and calculated life of synthetic corundum canisters

Bertil Larsson, Central Research and Development Department, ASEA AB, Västerås

Abstract

When synthetic corundum (α-Al_2O_3) canisters for the storage of spent nuclear fuel are sealed, residual stresses are introduced as a consequence of the temperature difference, which of necessity must be maintained during the process. A slow growth of defects exceeding a certain size may occur under the influence of primarily water on that part of the canister where these residual stresses are positive. This report outlines which initial defects that can be permitted with regard to this crack growth and how inadmissible defects can be detected.

Comprehensive computer calculations show that the tensile residual stress in the outer surface of the canister amounts to max. 38 MN/m^2. Results of these calculations, which apply to full-scale canisters, have been confirmed by measurements of residual stresses in a 1/3-scale canister.

By applying a generally accepted relationship between crack velocity and load, it is possible to determine the size of initial defects for a given life. This has been done and the results show that a permissible initial crack depth of 1.6 mm is obtained with the stress of 38 MN/m^2 and a stipulated life requirement of 10^6 years. This value is determined mainly by the residual stress level, while varying the life requirement results in only a marginal change in the permissible initial defect. Conversely, this can be expressed in such a way that with a suitable safety margin for the permissible initial defect a very large reduction in the crack velocity is obtained, i.e., practically speaking no growth at all.

Defects that are considerably smaller than the above-mentioned permissible initial crack depth can be detected using ultrasonic examination.

As an alternative to ultrasonic examination it is possible to apply proof testing. From a proof test diagram it is possible to determine in a generally accepted manner the minimum time to failure as a function of the applied stress σ_a and the proof stress ratio σ_p/σ_a (σ_p = proof stress). Such a diagram has been plotted on the basis of experimentally determined data for the material in question. From this diagram it can be seen that proof testing to σ_p = 81 MN/m^2 with a maximum residual stress of 38 MN/m^2 gives a minimum life of 10^6 years. The proof stress ratio σ_p/σ_a varies only insignificantly with σ_a.

Introduction

During the sintering together of the cover and container of synthetic corundum (α-Al_2O_3) for the storage of spent nuclear fuel, residual stresses develop in the material owing to the temperature differences, which must be maintained during the sealing process. These residual stresses may give rise to a slow growth of defects exceeding a certain size under the influence of primarily water. This report outlines which intial defects that can be permitted with respect to the slow crack growth and how inadmissible defects can be detected.

Residual stresses

The residual stresses after the sealing have been calculated and are reported in Appendix EI. Since a slow crack growth necessitates tensile stresses and the presence of water, it is only the zones with tensile stress on the outside of the canister that are of interest. The calculations have shown that tensile residual stresses occur with $Z > 350$ mm, where Z denotes the distance from the joint along a generatrix towards the bottom. The largest tensile stress occurs with $Z = 500$ to 600 mm and amounts to 30 to 38 MN/m^2, depending on the size of the gap between the container and the internal support used during the sealing operation.

The calculated distribution of residual stresses is supported by measurements made on a sealed 1/3-scale canister. These measurements are reported in Appendix EII.

Slow crack growth

The phenomenon of slow crack growth is described in Appendix EIII together with the testing methods used to determine the material data. From this it is apparent that the crack velocity depends primarily on the stress intensity factor K_I. The relationship between the crack velocity V and the stress intensity factor K_I is described by means of the generally accepted manner in the interval determining the life by

$$V = A \cdot K_I^{\,n} \qquad (1)$$

where A and n are material constants. Results of tests performed to determine these constants are reported in Appendix EIV.

Deviations from the relationship according to Eq. (1) occur with high crack velocities and, in certain cases, also with very low velocities, as is apparent from Fig. 5 in Appendix EIII, where the appearance of the K, V diagram is shown schematically. The deviation for high crack velocity has been observed during tests according to Appendix EIV and this has also been reported in the literature according to Appendix EIII, Fig. 4. This deviation gives a lower crack velocity and thus a longer life compared with the relationship according to Eq. (1), but the deviation is of very little significance to the total life.

The deviation for low crack velocity, on the other hand, may be of great importance to the life. The schematic appearance of the K, V diagram (Fig. 5 in Appendix EIII) indicates a lower limit for the stress intensity factor K_I below which no crack growth occurs. It has not been possible to find in the case of synthetic corundum any tendency to deviation from the relationship according to Eq. (1) within the range where measurements have been made. However, such a lower limit has been found during experiments on many other materials (e.g., certain types of glass). In general it can be stated that in those cases where it has been possible to prove experimentally that deviations from the relationship according to Eq. (1) occur for low crack velocities, the actual crack velocity has been lower than that obtained according to Eq. (1).

To be able to calculate permissible initial defects with the life of interest in this connection, i.e., 10^6 years, the relationship between the stress intensity factor and the crack velocity must be extrapolated to a crack velocity which is considerably lower than that measured during the experiments. With regard to what has been mentioned above about the deviations observed for low crack velocities, such an extrapolation gives conservative results.

Permissible initial defects

Applying the relationship between the crack velocity, $V = da/dt$, and the stress intensity factor, K_I, according to Eq. (1), it is possible to determine the time to failure if the initial size of the crack and the critical crack size are known. Conversely, the permissible initial defect can be determined with a given time to failure and critical size.

The following equation

$$K_I = \sigma_a \, Y \sqrt{\pi a} \qquad (2)$$

applies in general to a crack, where σ_a is a nominal stress acting perpendicular to the crack plane, Y is a geometry constant of the order of unity and a is the crack depth. Eqs. (1) and (2) give

$$V = \frac{da}{dt} = A \left(\sigma_a \, Y \cdot \sqrt{\pi} \cdot \sqrt{a} \right)^n$$

Integration gives

$$t = \frac{2}{A\left(\sigma_a \cdot Y \cdot \sqrt{\pi} \right)^n (n-2)} \left[a_o^{-(\frac{n}{2} - 1)} - a_c^{-(\frac{n}{2} - 1)} \right] \qquad (3)$$

where a_o and a_c are the initial size and the critical size, respectively, of the crack.

According to Eq. (2) the failure condition $K_I = K_{IC}$ gives

$$a_c = K_{IC}^2/(\sigma_a \ Y \sqrt{\pi})^2 \qquad (4)$$

where K_{IC} is the fracture toughness of the material. It is possible to calculate from Eqs. (3) and (4) the permissible initial defect for a given time to failure. Such calculations have been made and the results are reported in Appendix 1. Data from Appendix EIV have been used for the calculations.

Experimental controls

Inadmissible defects can be detected by means of ultrasonic examination. Appendix EV[1] describes the testing method and possible resolution.

As an alternative to ultrasonic examination it is possible to apply proof testing. This method is described in Appendix EIII. Proof testing means that any inadmissible defect leads to an instantaneous failure when the proof load is applied.

If the proof testing is done in such a way that the stress in the material amounts to σ_p, this means that all defects larger than a_1 result in failure. a_1 is determined from the condition

$$\sigma_p \cdot Y \sqrt{\pi a_1} = K_{IC}$$

No defects larger than a_1 therefore occur after the proof testing in the canisters which have successfully coped with the proof testing. A minimum time to failure, t_{min}, can then be determined from Eq. (3) with $a_o = a_1$ and with a_c according to Eq. (4). This gives

$$t_{min} = \frac{2}{A \cdot Y^2 \pi (n-2) K_{IC}^{(n-2)} \sigma_a^2} \left(\frac{\sigma_p}{\sigma_a}\right)^{(n-2)}$$

A proof test diagram can be plotted with this relationship. This gives t_{min} versus σ_a with (σ_p/σ_a) as parameter. From this diagram it is possible to determine the necessary proof stress with a given applied stress σ_a and with a given required value of t_{min}. Since the canister is fully enclosed in a steel jacket, which prevents the synthetic corundum from coming into contact with water, it has been assumed here that no slow crack growth takes place during the proof testing.

1) Appendix EV not enclosed here.

A proof test diagram has been plotted in Appendix 2. In this case the largest measured value of K_{IC} is a conservative calculation of σ_p. A value of K_{IC} = 6.5 $MN/m^{3/2}$ has therefore been used. From the diagram it is apparent that with a maximum residual stress of 38 MN/m^2 and with a required minimum life of 10^6 years, the material must undergo proof testing to σ_p = 2.13 × σ_a = 81 MN/m^2.

In reality the probable life after the proof testing is greater than t_{min}. The calculation of the mean life after proof testing is described in Appendix EIII. However, only t_{min} has been used in this investigation.

The proof stress required in compacted containers without cover can be achieved by bringing about a temperature difference between the inside and the outside. The fact that this gives a satisfactory stress distribution, with regard to the residual stresses occurring after the sealing, has been confirmed by means of comprehensive calculations on both full-scale and 1/3-scale containers. Appendix EVI reports examples of these calculations. Data from the literature have been used here to determine the necessary proof stress. With the data from Appendix EIV the requirements on proof stress and temperature difference will be less severe.

Equipment for the proof testing of 1/3-scale containers has been built and tried out with satisfactory results.

$\log A = -120$ (with K_I in $MN/m^{3/2}$ and V in m/s)

$n = 210$

$K_{IC} = 6.0\ MN/m^{3/2}$

$K_I = 1.12\ \sigma_a \sqrt{\pi a}$

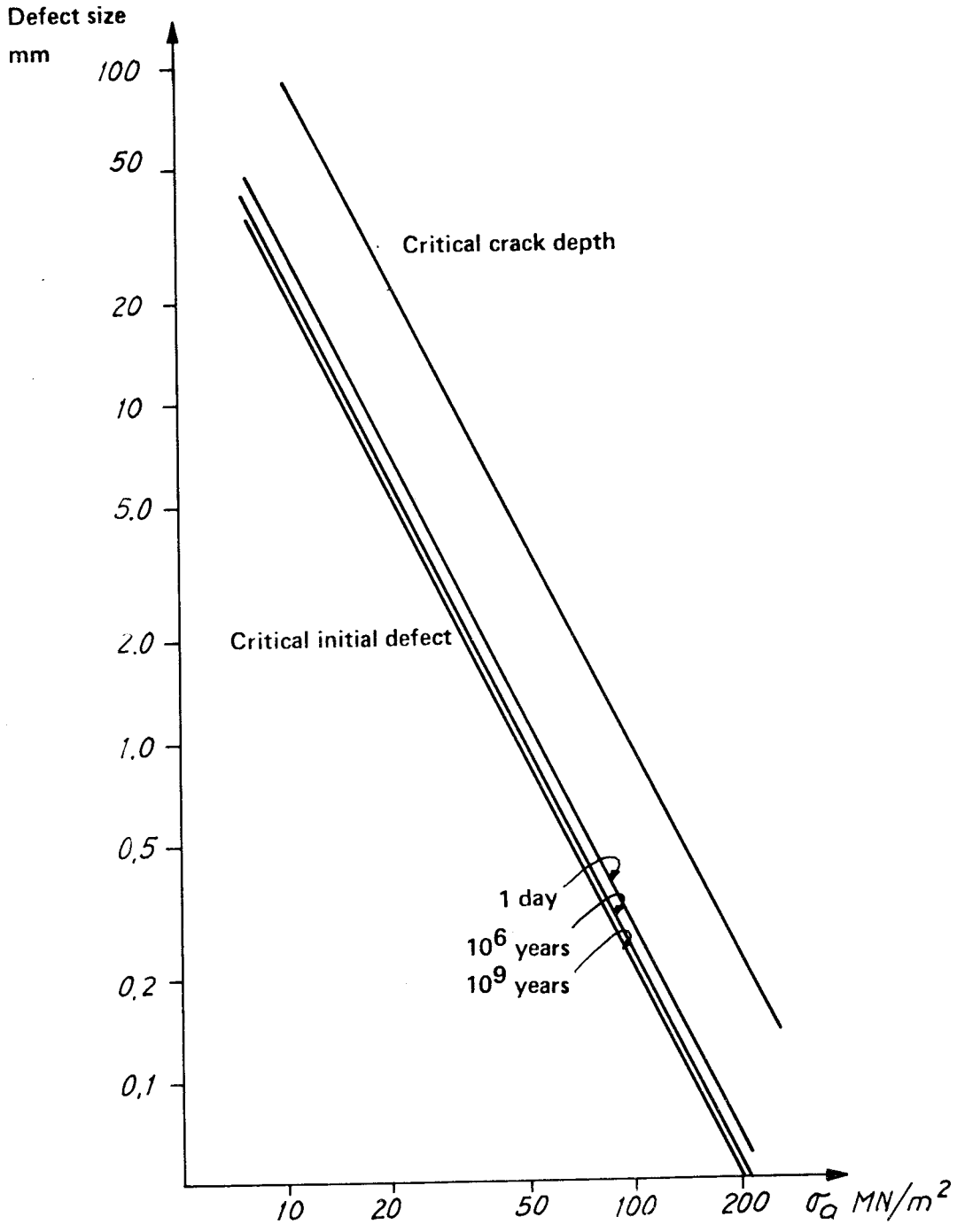

Permitted initial defect

Material data according to appendix E IV

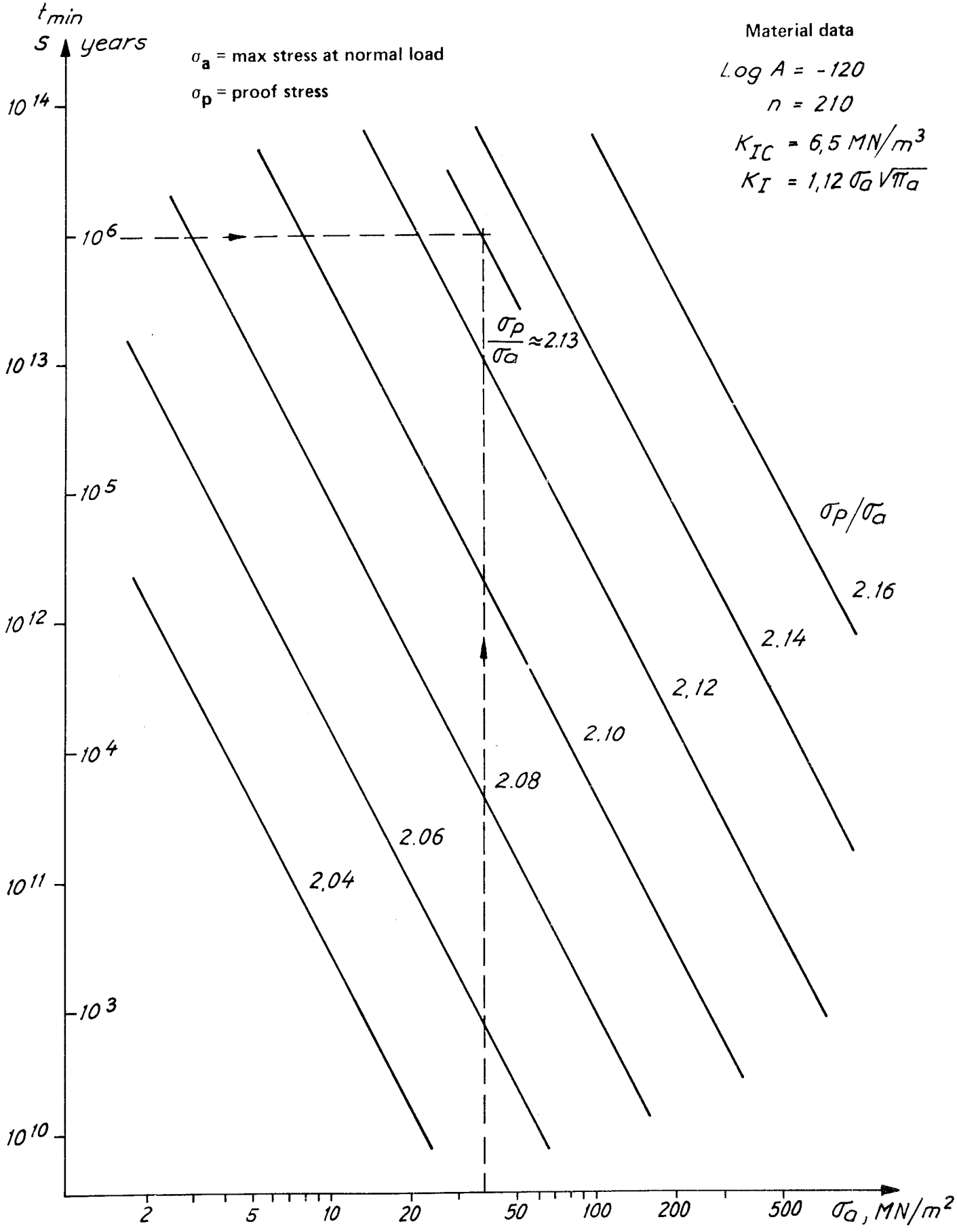

Test loading diagram Minimum time to fracture t_{min} (σ_a, σ_p/σ_a)

Calculation of stresses during the sealing of ceramic canisters for WCP

Bertil Larsson

Summary

The stresses occurring during the sealing process have been calculated. A thermoelastic model has been used for the heating and cooling stages. Creep calculations have been performed for that stage of the process where the temperature reaches its maximum value.

During the sealing process tensile stresses occur axially in the outer surface after pressure relief. With an inner support and a radial gap of 1 mm $\sigma_{z\ max} \approx 50$ MN/m^2 is obtained about 530 mm from the joint (T = 1050°C). This maximum value is dependent on the size of the gap. With a gap of 5 mm $\sigma_{z\ max} \approx 100$ mN/m^2 is obtained about 450 mm from the joint (T = 1100°C). 5.5 h after the pressure relief $\sigma_{z\ max}$ on the outside has decreased to 30 MN/m^2 about 600 mm from the joint with a gap of 1 mm. The corresponding values for 5 mm the gap is $\sigma_{z\ max}$ = 38 MN/m^2, 550 mm from the joint 5.8 h after the pressure relief.

During the cooling down tensile stresses occur on the inside of the canister by the joint. These tensile stresses will be less than 50 MN/m^2.

Introduction

Sintering together of the cover and container requires a high temperature and a high pressure in the sintering surface for a certain length of time. Parameters necessary for synthetic corundum ($\alpha - Al_2O_3$) are p = 100 MPa at 1350°C for about 2 hours. The normal pressure of 100 MPa in the sintering surface is obtained by means of an external pressure of 64 MPa. Another condition for the sealing process is that the fuel rods must not be subjected to a temperature exceeding 900°C. An axial temperature gradient must therefore be maintained in the zone between the joint and the space for the fuel rods.

The thermal stresses and the stresses caused by the external pressure bring about a non-elastic creep deformation in those parts of the canister subjected to the highest temperature. Residual stresses therefore also occur in these parts. The size of the residual stresses is of great importance to the risk of failure after a long time owing to the slow crack growth in the material.

Computing model

Fig. 1 shows the geometry of the canister. An internal support is included to prevent excessive creep deformation during the sealing. Fig. 2 shows the pressure and temperature loading during the process.

The presence of residual stresses can be briefly described as follows:

The heating produces rotational symmetric bending stresses in the zones where the temperature is not a linear function of the length coordinate, i.e., in the zone by the joint between cover and container and close to the bottom. In the zone near the bottom, where the temperature is low and no creep occurs, these bending stresses disappear when the temperature has returned to the ambient temperature. In the hot part creep deformation occurs under the simultaneous influence of the above-mentioned thermoelastic bending stresses and external pressure. After a short time the canister wall comes into contact with the internal support and the bending stresses decrease as a result of creep relaxation. A conservative assumption is that the relaxation takes place for such a long time that all bending stresses in this zone disappear. During the cooling down thermoelastic bending stresses then develop, these being of the same magnitude as, but acting in the opposite direction to, those that occurred during the heating. These residual stresses by the joint are positive on the inside of the canister and negative on the outside.

The stress distribution during the heating up has been calculated for a two-dimensional model of thermoelastic material using the ALEXANDER-LUCAS FEM-programs. The influence of different temperature distributions has been investigated with a thin shell model and the TEXAS program. These calculations show that the bending

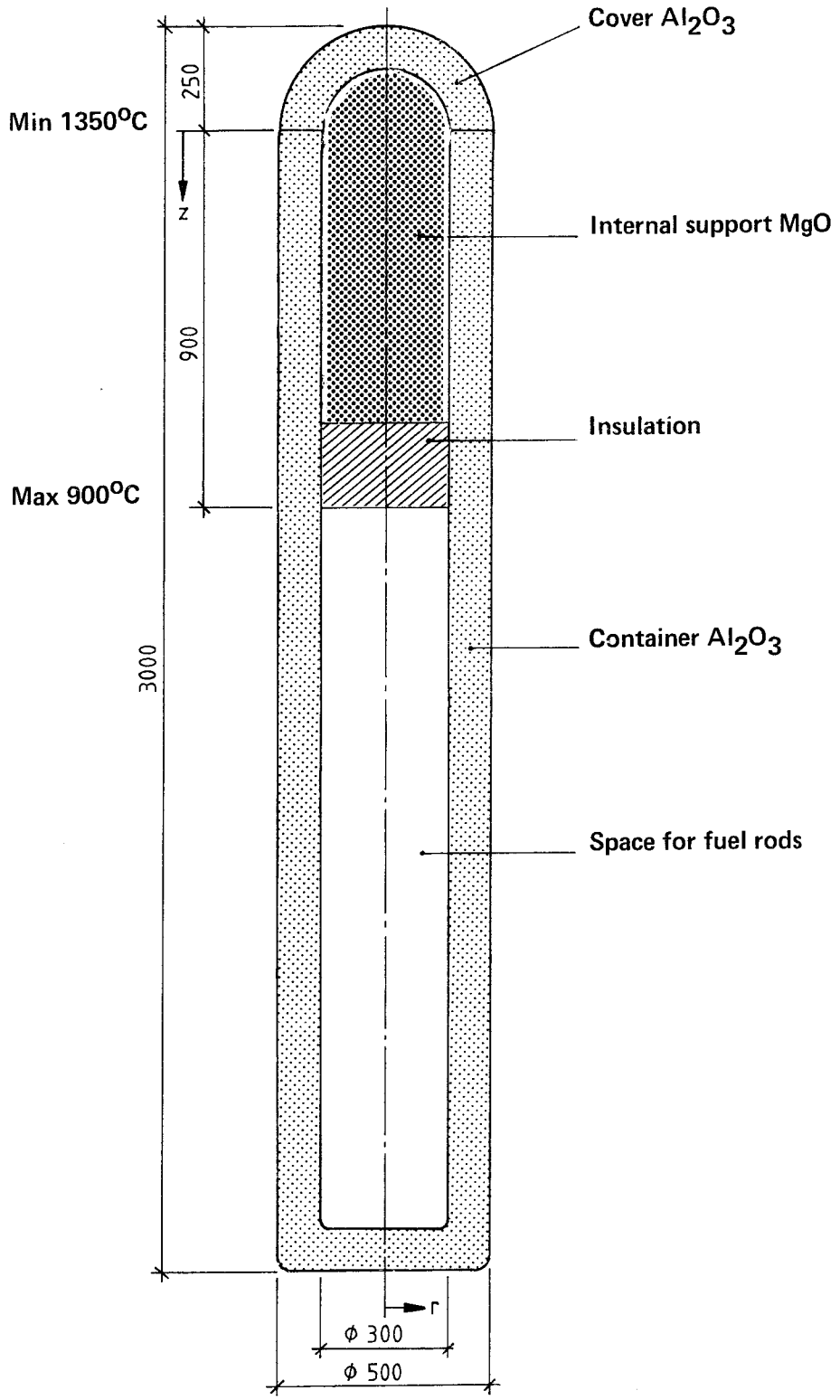

Figure 1. Aluminium oxide canister

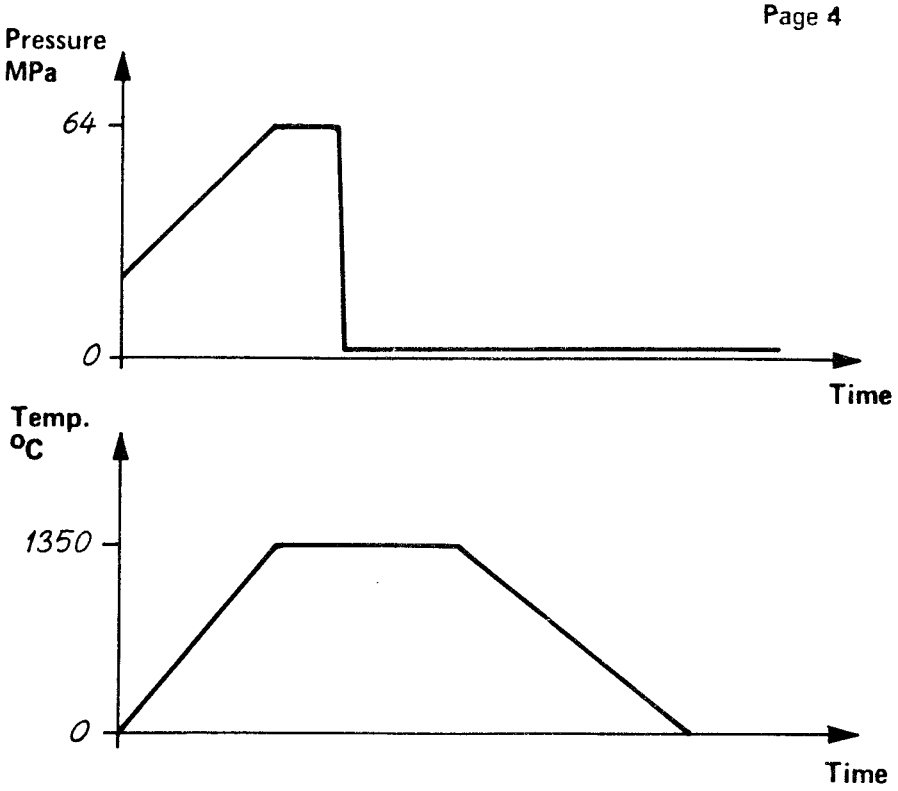

Figure 2

residual stresses will remain after the cooling down in the zone around the joint. The maximum stress in the z-axis will be less than 50 MN/m^2 and negative on the outside of the canister.

In the zone with linear temperature distribution creep deformation occurs under the influence of the external pressure. The creep rate is greatly temperature-dependent and in a transition zone, where the temperature is about 1000-1200°C, rotational symmetric bending stresses occur. These stresses develop relatively quickly after the application of pressure. The stress peak moves towards the cooler part of the canister, as the canister wall comes into contact with the internal support. The stress relaxes if the pressure is reduced and the temperature maintained. The stress distribution remaining after the relaxation will be largely speaking unaffected on the return to ambient temperature if the temperature distribution is linear with respect to the length coordinate.

Stress calculations with due regard being paid to creep deformation in the material have been made with the ADINA program. Only that part of the canister where the above-mentioned creep-induced stresses occur has been included in the computing model. In other words, the model consists of a thickwalled tube, where the temperature varies linearly from 1350°C to about 900°C. The internal support is present in the form of special gap-elements. The importance of the support and the influence of varying gap sizes between the inside of the canister and the support have been investigated with experimentally obtained material data.

Pressing and relaxation

Creep calculations have been made on a computing model in the form of a thick-walled tube according to Appendix 1 with a time independent temperature distribution. This model corresponds to the zone from the joint between the cover and the container to a cross-section, where the temperature is about 900°C and no creep deformation occurs. The load consists of external pressure (including axial pressure). The creep properties of the material have been determined by means of tests. Appendix 2 gives the creep data. Other data have been obtained from "Engineering properties of selected ceramic materials", (The American Ceramic Society, Ohio, 1966).

Calculations have been performed without an internal support, with an internal support and a radial gap of 5 mm and with a support and a radial gap of 1 mm.

Appendix 3 shows the results of the calculations without internal support. The bending stress peak develops rapidly, about 250 mm from the joint and gives $\sigma_{z\ max} = 50\ MN/m^2$, 320 mm from the joint after 0.51 h. The pressure relief was made after 0.54 h owing to large deformations. Radial displacements in the hot end amounted already then to 16 mm. The maximum axial tensile stress 5 mm below the outer surface amounted to $\sigma_{z\ max} \approx 150\ MN/m^2$ immediately after the pressure relief and at the time 1.55 h (1.0 h after pressure relief) had decreased to $\sigma_{z\ max} = 42\ MN/m^2$, about 450 mm from the joint.

Appendices 4 to 6 show the results of the calculations with internal support and a gap of 5 mm. The bending stress peak decreases as soon as the canister wall touches the support. The pressure relief was made at t = 1.71 h. Immediately after the pressure relief a value of $\sigma_{z\ max} \approx 100\ MN/m^2$ was obtained and at the time 7.54 h (5.8 h after the pressure relief) $\sigma_{z\ max} = 34\ MN/m^2$ was obtained about 550 mm from the joint.

Appendix 7 shows the stresses obtained with a gap of 1 mm between the internal support and the canister wall. In this case the pressure relief was made after 1.43 h. After the pressure relief $\sigma_{z\ max} \approx 50\ MN/m^2$ was obtained and at the time t = 6.90 h (5.5 h after the pressure relief) $\sigma_{z\ max} = 27\ MN/m^2$ was obtained about 600 mm from the joint.

Total residual stresses

Appendix 8 shows the total remaining axial stress in the outer surface of the canister in the zone below the joint. $\sigma_{z\ max}$ is not influenced by the cooling down. σ_z on the outer surface is less than 0 from the joint to a section 440 and 370 mm towards the cold end with a gap of 1 and 5 mm, respectively.

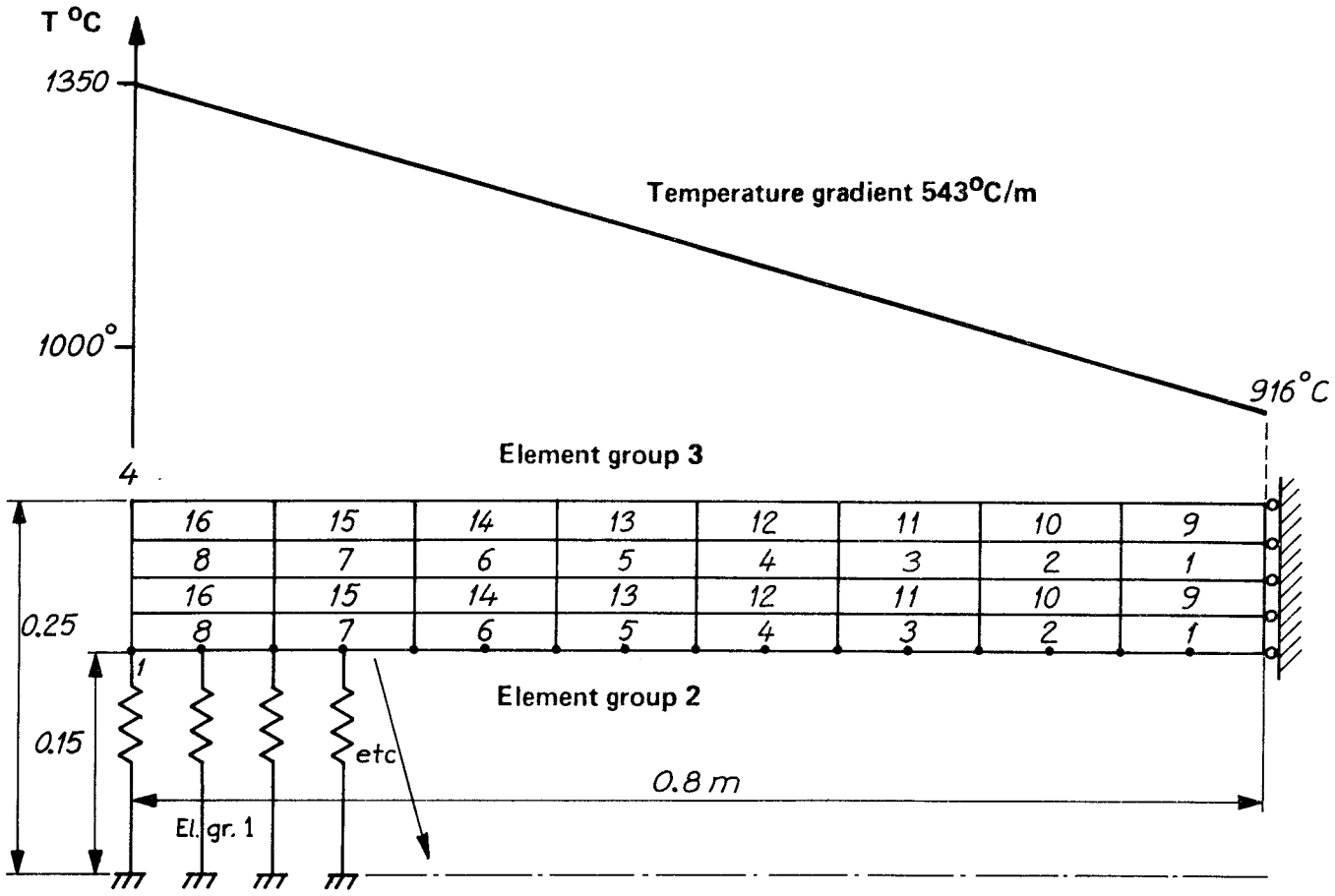

Gauss points

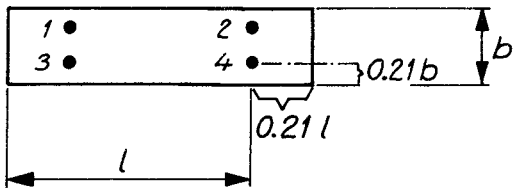

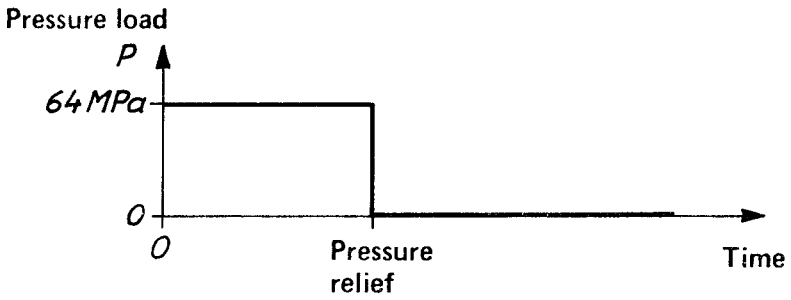

Material data for Al_2O_3, creep

The creep constants were determined from four test specimens of material 1719-6. This material has a high bending strength at room temperature. The creep laws in ADINA have the form

$$\varepsilon^c = F\,(1 - e^{-Rt}) + G \cdot t$$

where $F = a0\ \sigma^{a1}$

$R = a2$

$G = a5\ \sigma^{a6}$ a0-a6 = temperature dependent

Test results and evaluation

A "converse reference stress method" was used to evaluate the creep tests, i.e., stresses and strains were calculated in the fibre in the bending test specimen where the stresses are largely speaking constant during the test (see Penny and Mariott, Design for creep). This applies to the distance of about 0.16 h from the outer fibre. The stress here will be

$$\sigma_{ref} = \frac{\frac{H}{2} - 0{,}16\ H}{\frac{H}{2}} \cdot \sigma_{max,el} = 0{,}68 \cdot \sigma_{max,el}$$

$$\dot{\varepsilon}_{ref} = 0{,}68 \cdot \dot{\varepsilon}_{max}$$

Test No.	Temp. °C	Temp. °K	$\sigma_{max,el}$ N/m²	σ_{ref} N/m²	F	R h⁻¹	G h⁻¹
A28	1200	1473	50×10^6	34×10^6	1.64×10^{-3}	0.091	141×10^{-6}
A30	1300	1573	24.1×10^6	16.4×10^6	(8×10^{-3})	(0.6)	918×10^{-6}
A32	1100	1373	50×10^6	34×10^6	0.12×10^{-3}	0.15	19×10^{-6}
A33	1100	1373	100×10^6	68×10^6	0.33×10^3	0.33	56.10^{-6}

Table 1 (F, R and G calculated with ε_{ref}.)

The constants a0 and a5 are assumed to vary with the temperature as

$$a0 = k0\ e^{-\frac{C0}{T}}$$

and $$a5 = k5\ e^{-\frac{C5}{T}}$$

where T = the absolute temperature.

I addition, CO = C5 = C . This assumption for a temperature variation of a0 and a5 differs somewhat from the rest results. C will have a higher value if the tests at 1200°C and 1300°C are used than if data from the tests at 1100°C and 1200°C are used for the calculations. The constants k0, k5 and C are thefore determined for both $T < 1200°C$ and $T \geqslant 1200°C$. a1 and a6 are supposed to be equal and independent of the temperature.

Finally, a2 does not show any definite tendency in the experiments. a2 is therefore made independent of the temperature.

Results

$a1 = a6 = 1.56$

$a2 = 0.33$

$T < 1200°C$

$$a0 = 3.581 \times 10^{-3} \, e^{-(41000/T)}$$

$$a5 = 3.079 \times 10^{-4} \, e^{-(41000/T)}$$

$T \geqslant 1200°C$

$$a0 = 6.449 \times 10^{+5} \, e^{-(69000/T)}$$

$$a5 = 5.544 \times 10^{+4} \, e^{-(69000/T)}$$

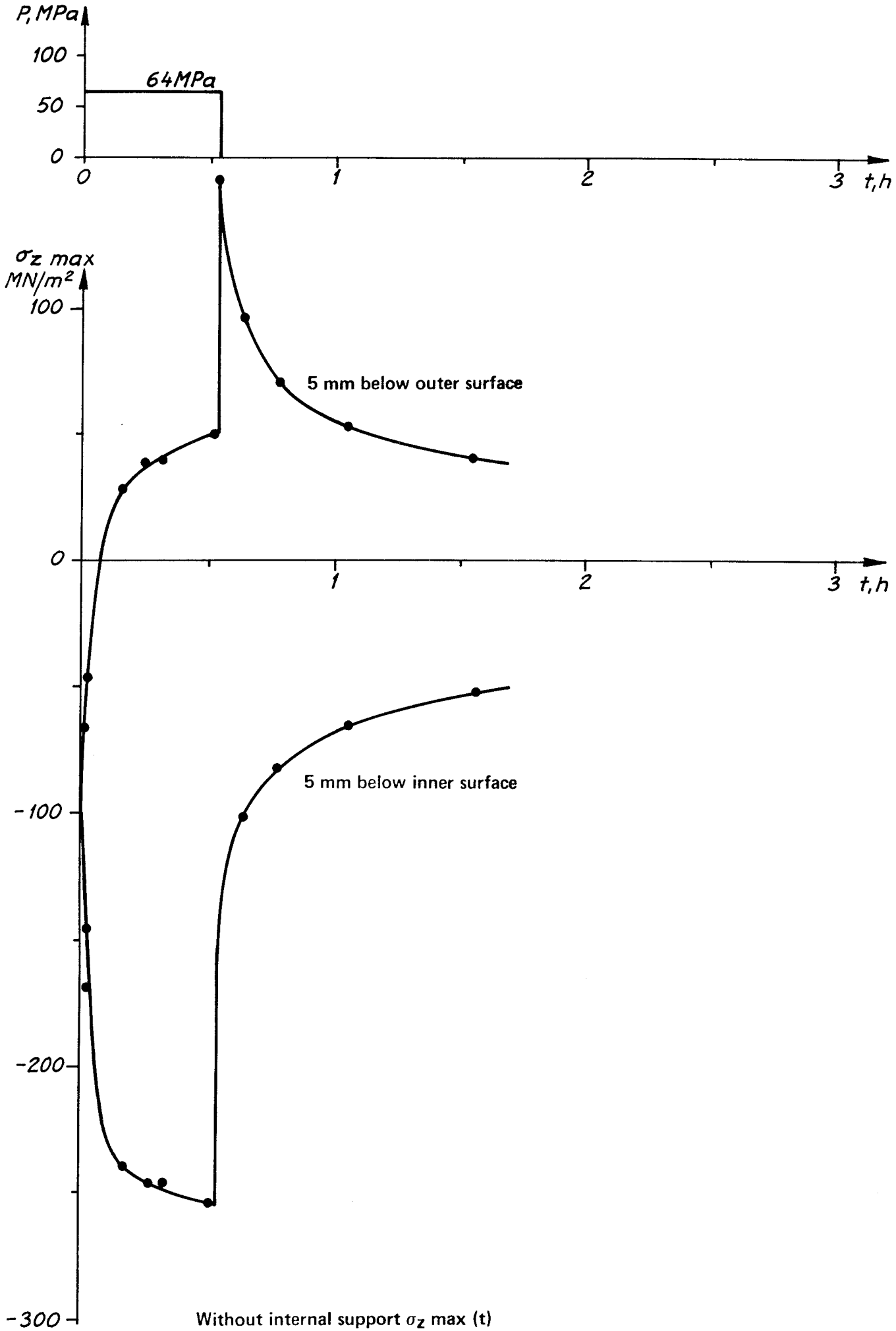

Without internal support σ_z max (t)

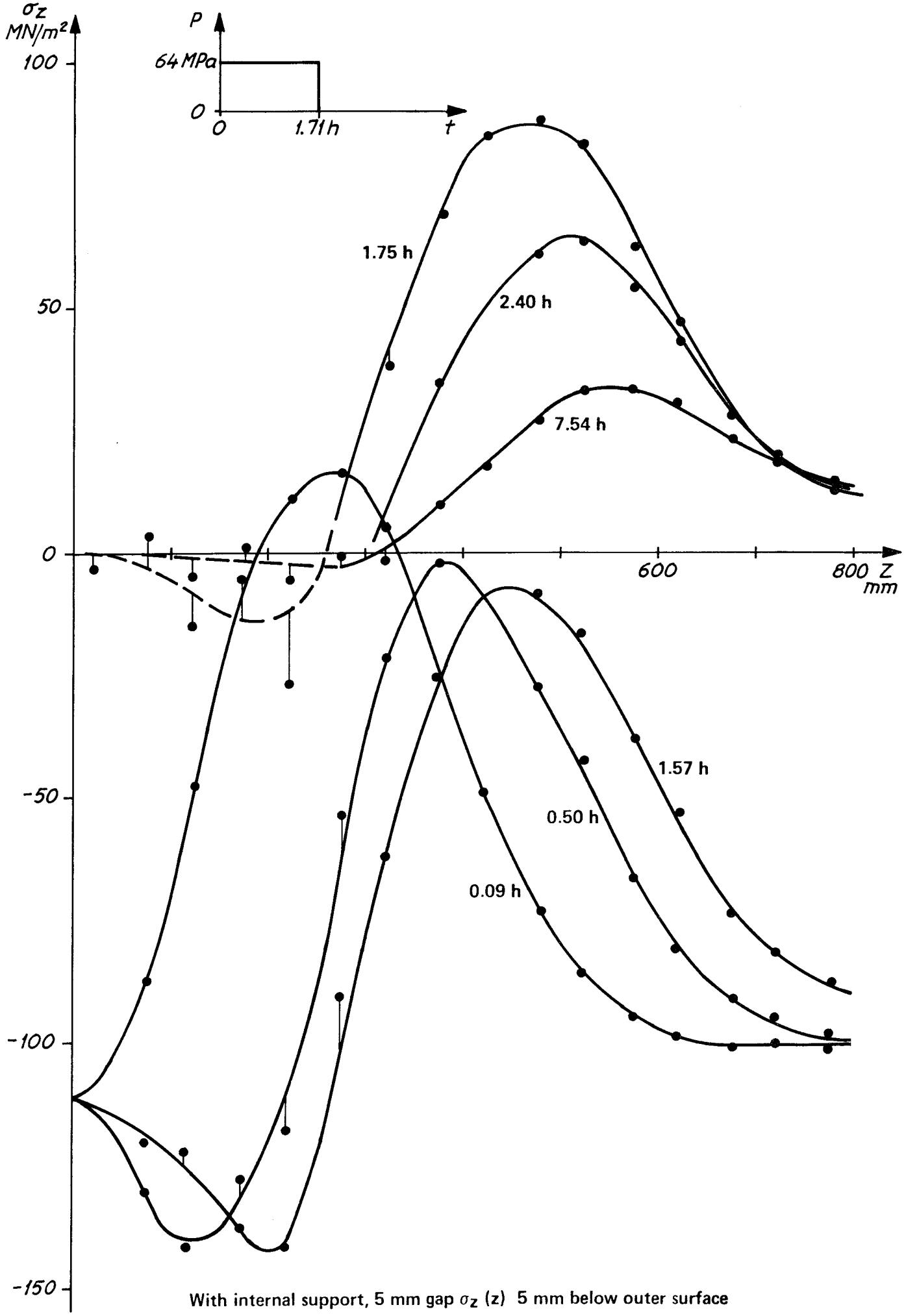

With internal support, 5 mm gap σ_z (z) 5 mm below outer surface

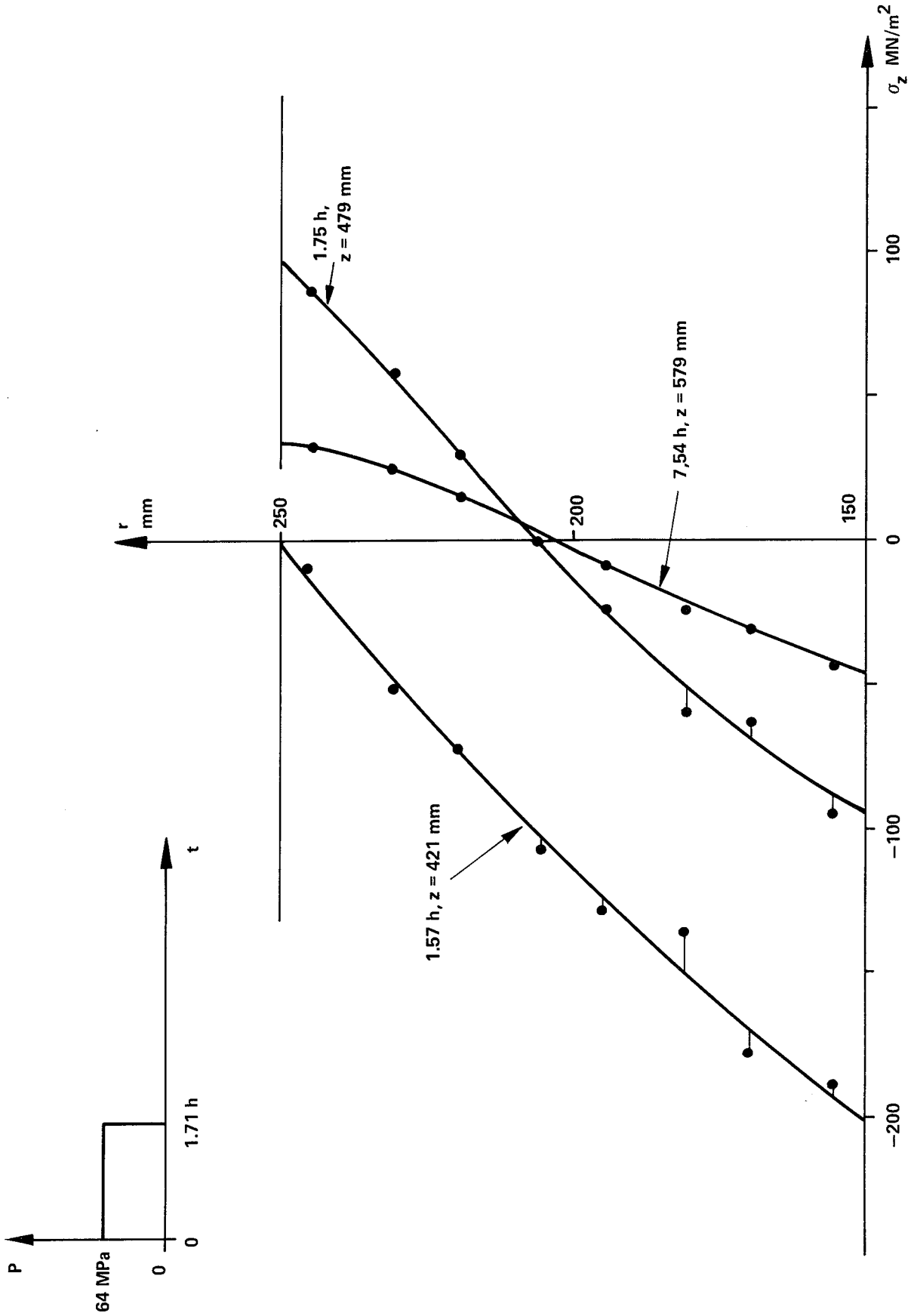

With internal support, 5 mm gap σ_z (r)

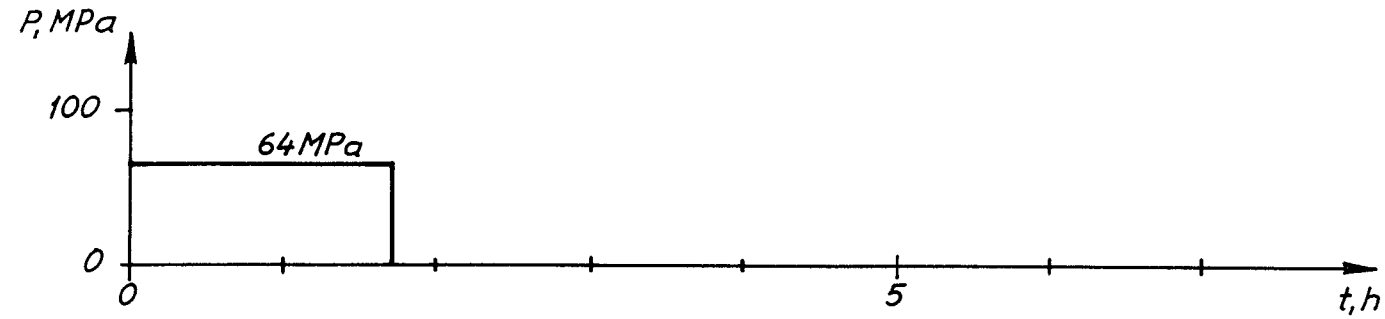

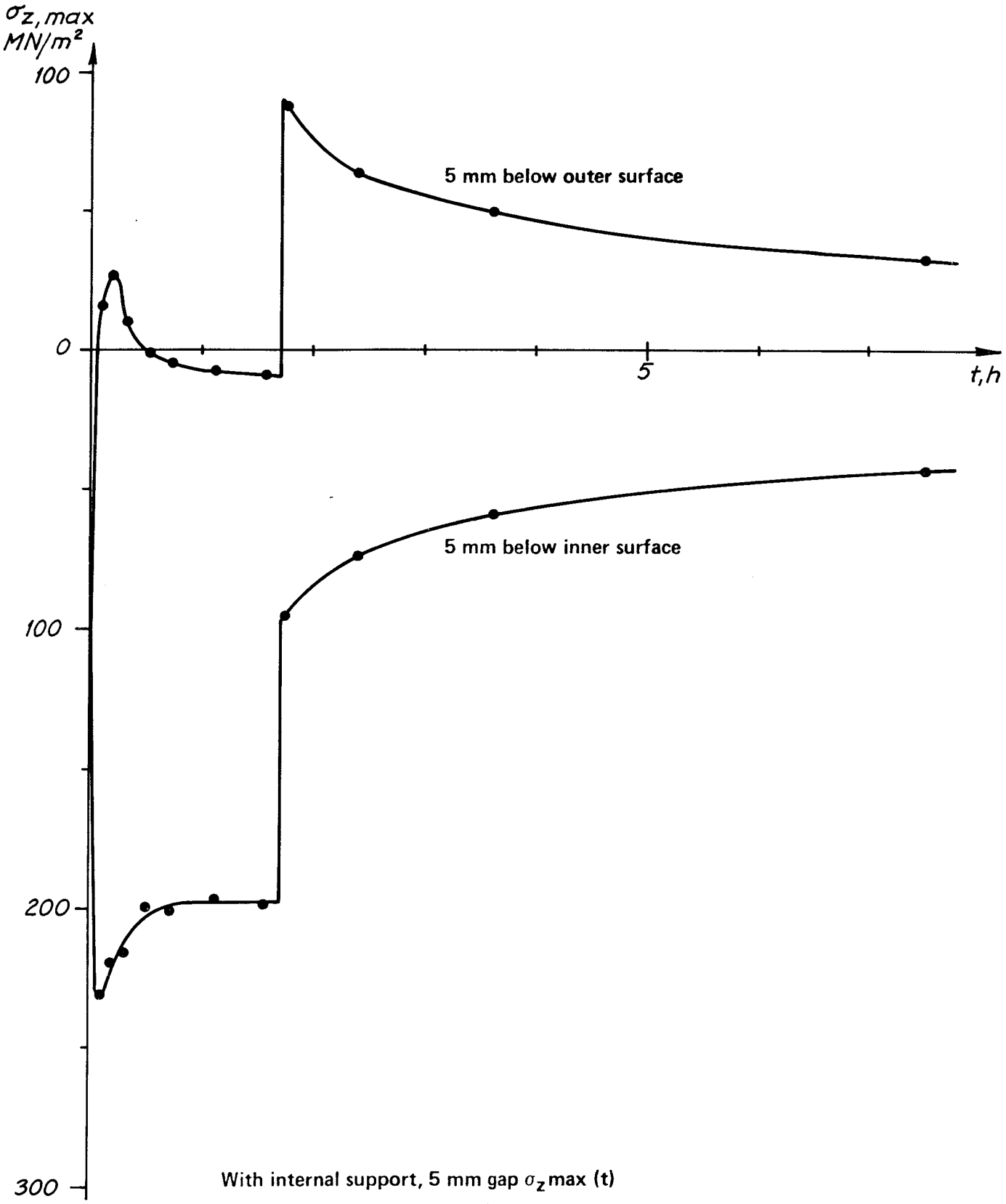

With internal support, 5 mm gap σ_z max (t)

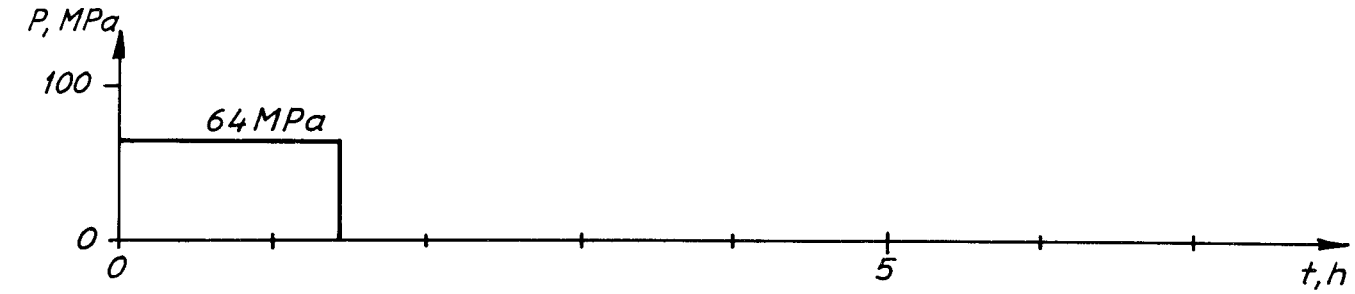

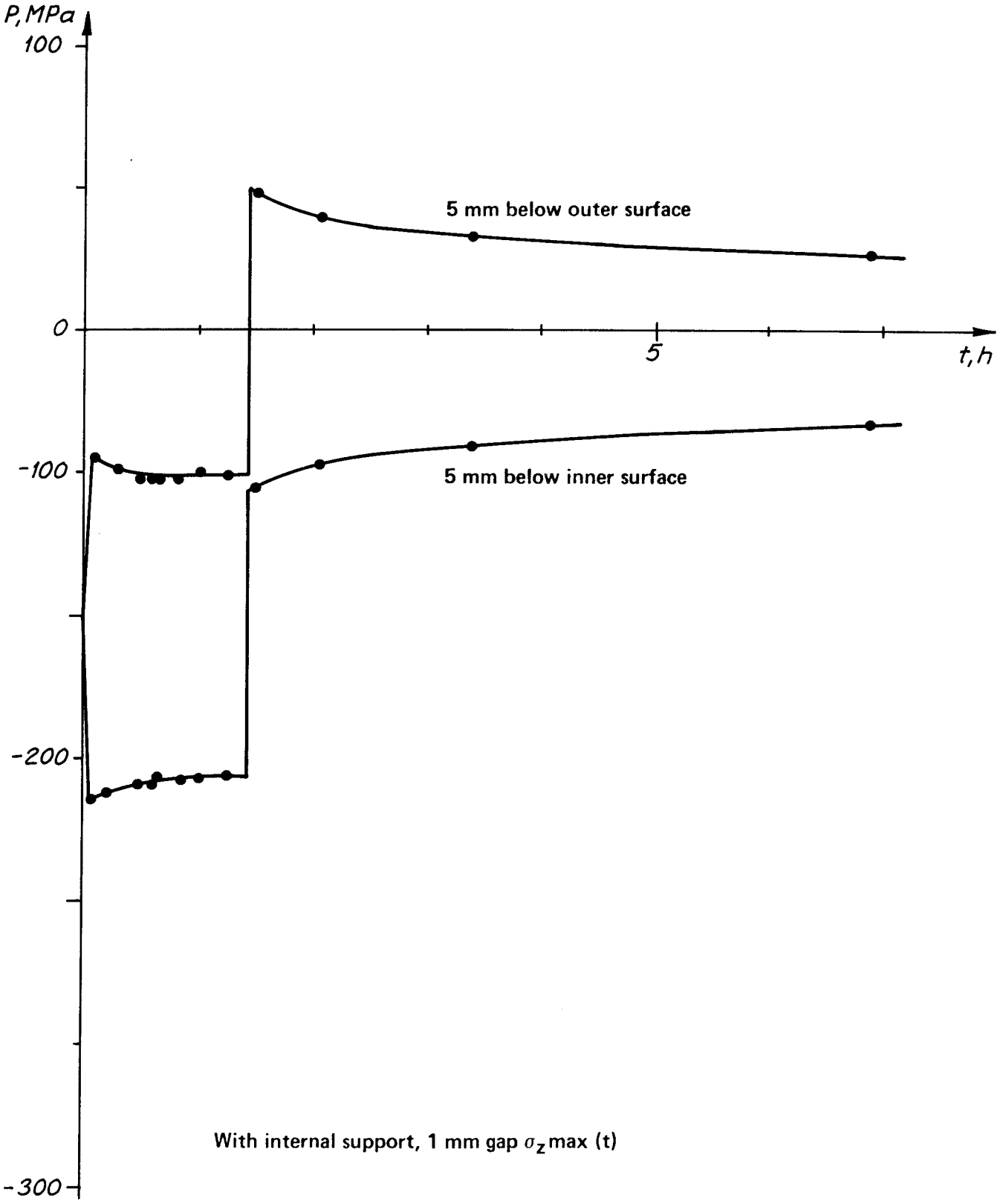

With internal support, 1 mm gap σ_z max (t)

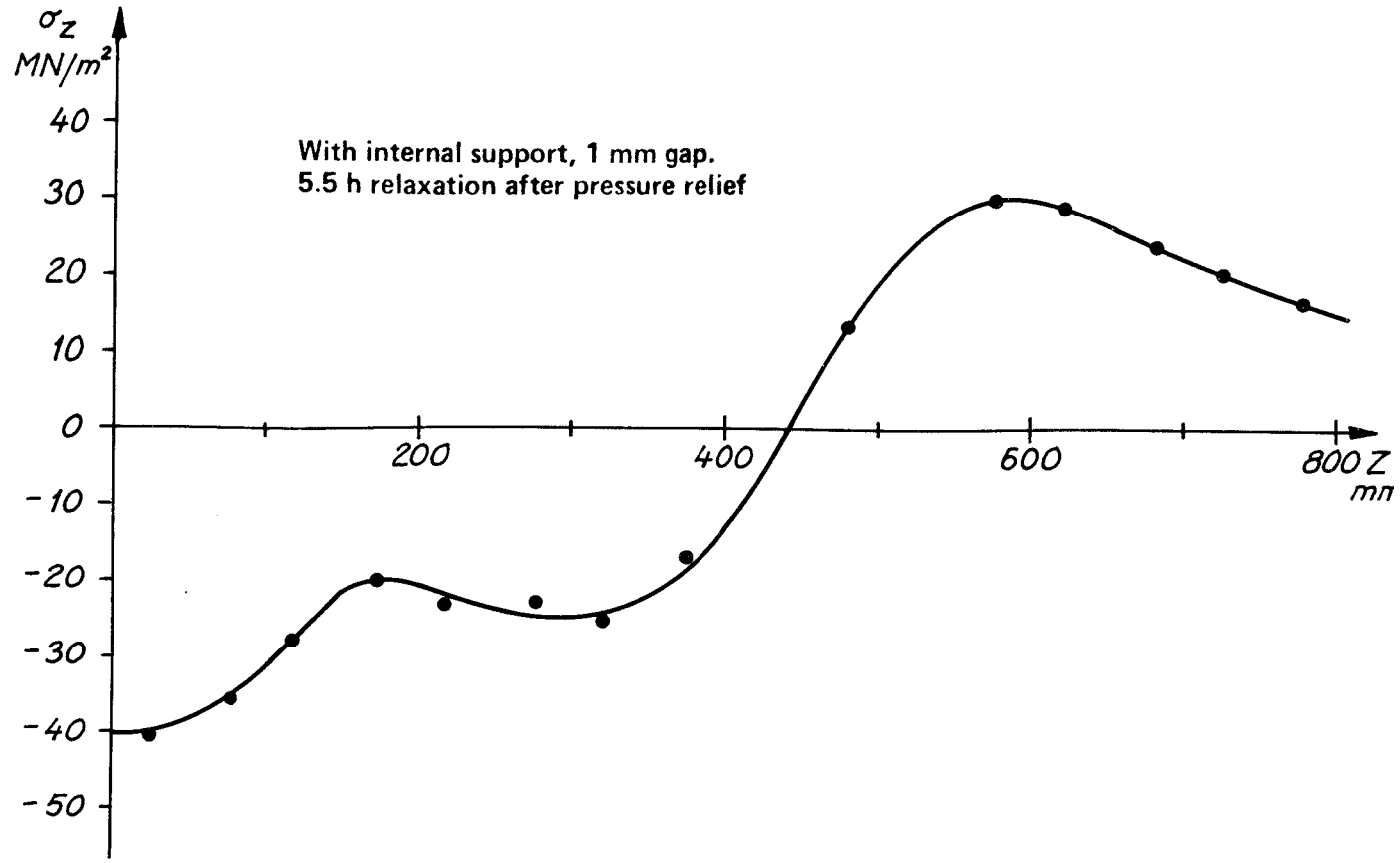

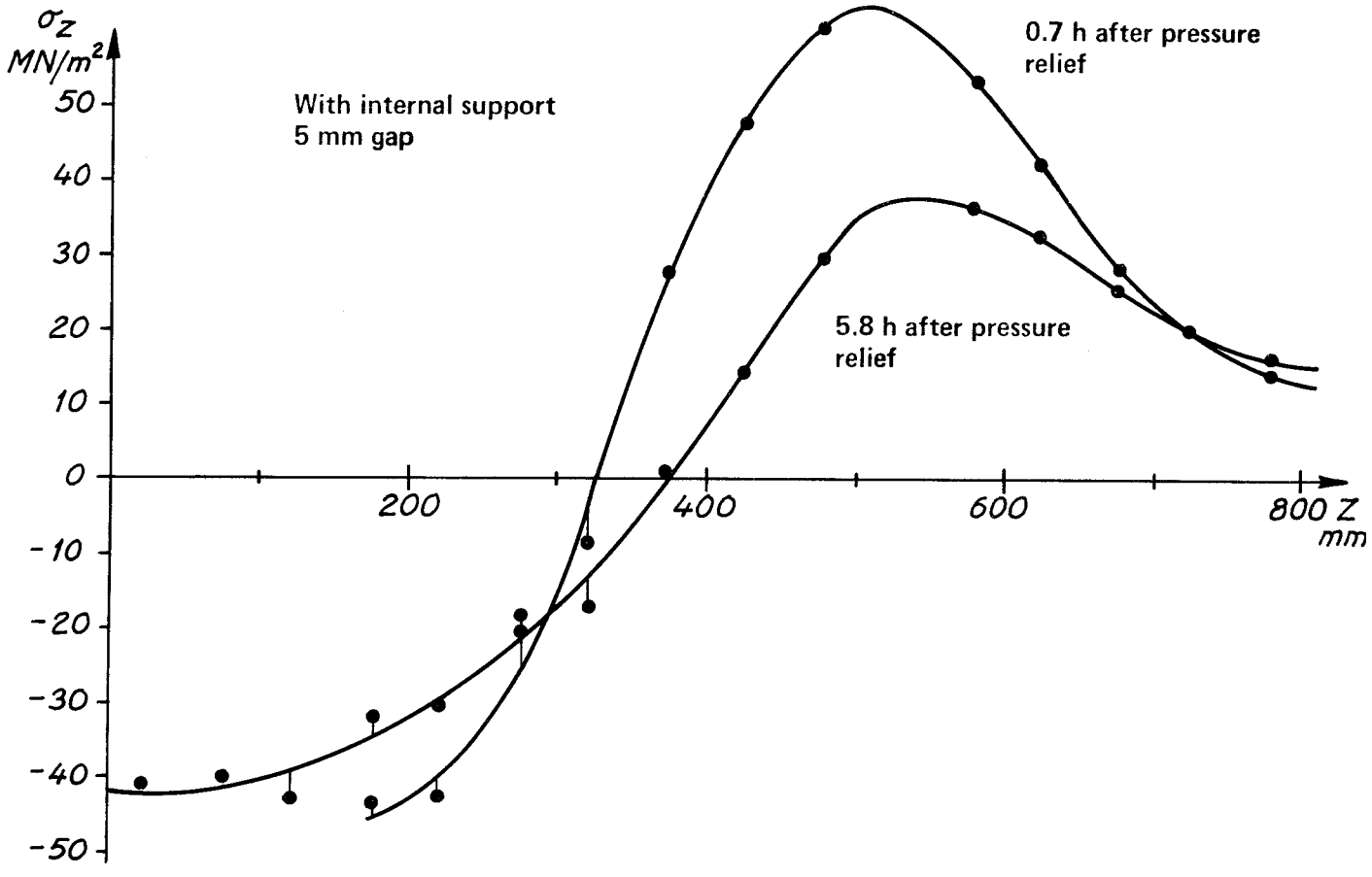

Total axial stress remaining in outer surface

Measurement of residual stresses in synthetic corundum canisters for WCP using the trepanning method

Bertil Larsson

Summary

The residual stresses present in a synthetic corundum (α-Al_2O_3) canister with sealed cover have been measured. The trepanning method has been used for these measurements. This method means that a circular cylindrical plug with a diameter of 13 mm is exposed to a depth that is sufficiently large for all stresses in the surface to be relaxed. Changes in the strain in the surface are measured with strain gauges and the residual stress state is calculated from the strain values. Appendix 1 shows a diagram of the trepanning arrangement. Boring has been carried out to a depth of 7 to 8 mm. The total change in the strain was read off after about 30 min after the completion of the boring to avoid the influence of local temperature increases.

The measurements have been performed on a 1/3-scale canister. An internal support of M_gO was used during the sintering together of the cover and container. After the sealing process had been completed, the canister was cut both by means of a longitudinal section into two halves and of a section at right angles to the longitudinal axis about 100 mm from the joint. The calculated residual stresses have been corrected for this.

The trepanning measurements have been performed at the High-Pressure laboratory with the assistance of Department KYYM.

Appendix 2 shows the measured changes in the strain, while Appendices 3 and 4 give the corresponding calculated residual stresses. A comparison is made in Appendix 4 between the measured values and the calculated residual stresses. The trend in the distribution of residual stresses is the same according to the measurements and calculations. The largest measured tensile stress was 29 N/mm^2, 192 mm from the joint. According to the calculations the corresponding value is 70 N/mm^2 about 220 mm from the joint with 0.7 h relaxation after the pressure relief and 38 N/mm^2 about 230 mm from the joint with 5.8 h relaxation after pressure relief.

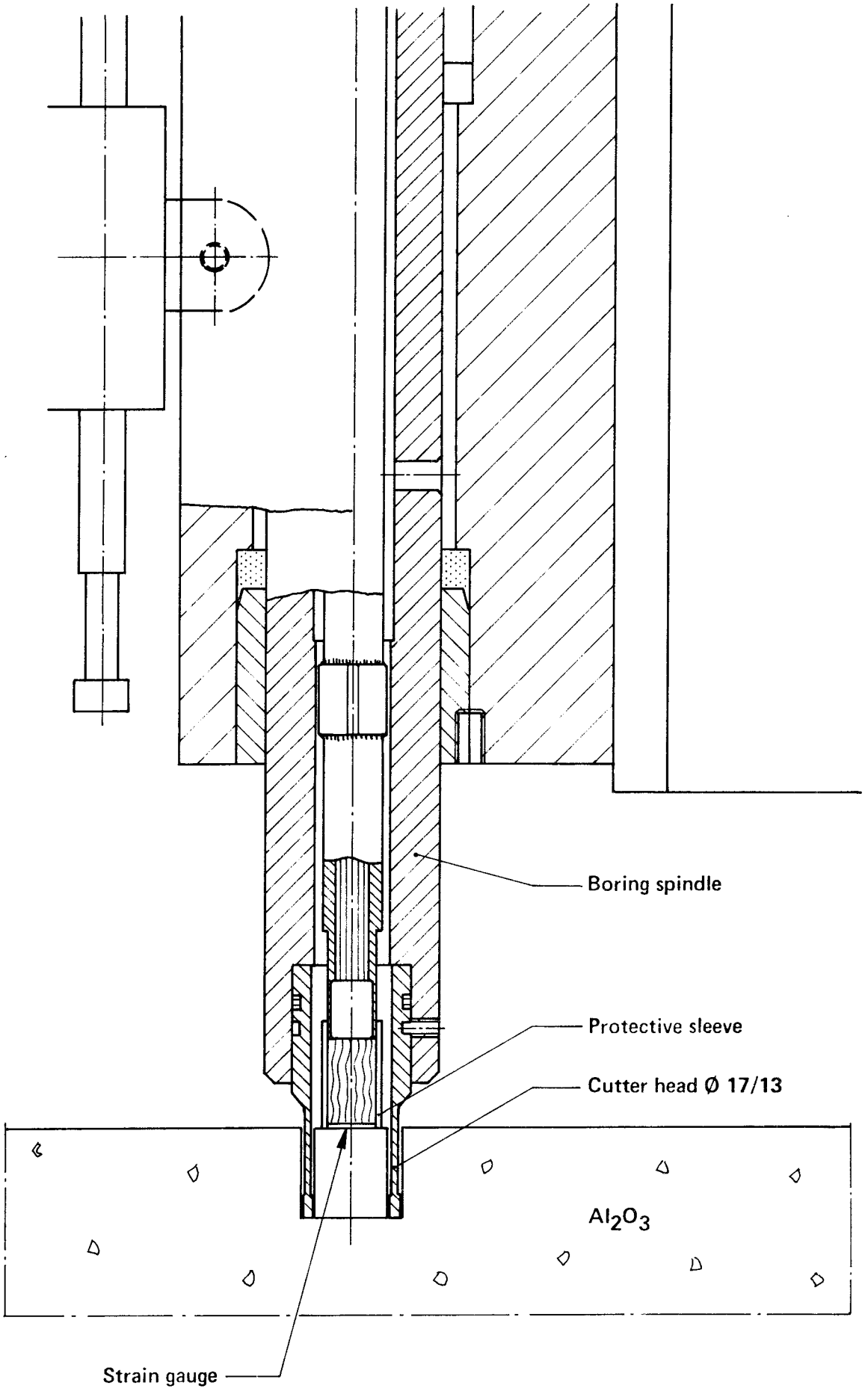

Trepanning arrangement

Measured strain changes

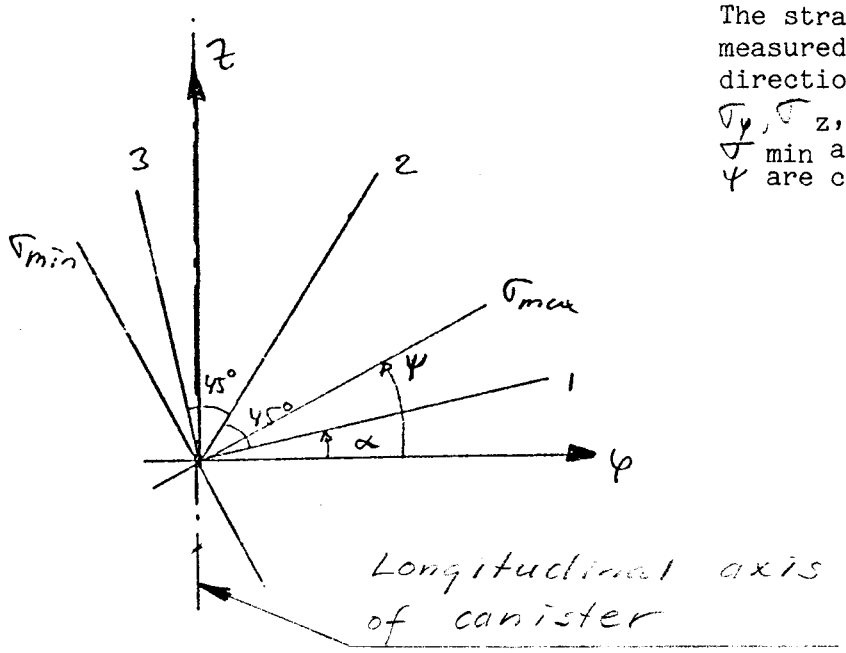

The strains were measured in the directions 1, 2 and 3. σ_φ, σ_z, σ_{max}, σ_{min} and the angle ψ are calculated.

Measurement No.	Distance from joint mm	α °	Measured strain change during trepanning after temperature equalisation		
			$\Delta\varepsilon_{1}\times10^{6}$	$\Delta\varepsilon_{2}\times10^{6}$	$\Delta\varepsilon_{3}\times10^{6}$
1A	121	0	+10	+5	0
1B	122	5	+10	-5	+8
2A	153	0	-5	+25	+20
2B	165	0	+25	+24	+27
3A	192	0	-45	-50	-30
3B	205	0	-34	-25	-32
4A	209	0	+10	-10	-15
4B	234	5	+30	-11	+16

Calculation of residual stresses

The strain state $\varepsilon_\varphi, \varepsilon_z, \gamma_{\varphi z}$ before the trepanning is calculated from the measured strain values from the following system of equations:

$$-\Delta\varepsilon_1 = \varepsilon_\varphi \cos^2\alpha + \varepsilon_z \sin^2\alpha + \gamma_{\varphi z} \sin\alpha\cos\alpha$$

$$-\Delta\varepsilon_2 = \varepsilon_\varphi \cos^2(\alpha+45) + \varepsilon_z \sin^2(\alpha+45) + \gamma_{\varphi z} \sin(\alpha+45)\cos(\alpha+45)$$

$$-\Delta\varepsilon_3 = \varepsilon_\varphi \cos^2(\alpha+90) + \varepsilon_z \sin^2(\alpha+90) + \gamma_{\varphi z} \sin(\alpha+90)\cos(\alpha+90)$$

The stress state is then calculated using Hooke's law.

$$\sigma_\varphi = \frac{E}{1-\nu^2}(\varepsilon_\varphi + \nu\,\varepsilon_z)$$

$$\sigma_z = \frac{E}{1-\nu^2}(\varepsilon_z + \nu\,\varepsilon_\varphi)$$

$$\tau_{\varphi z} = \frac{E}{2(1+\nu)}\gamma_{\varphi z}$$

where $E = 390{,}000\ MN/m^2$ and $\nu = 0.27$. The principal stresses will be

$$\sigma_{max} = \frac{1}{2}(\sigma_\varphi + \sigma_z) + R$$

$$\sigma_{min} = \frac{1}{2}(\sigma_\varphi + \sigma_z) - R$$

$$R = \left[\left(\frac{\sigma_\varphi + \sigma_z}{2}\right)^2 + \tau_{\varphi z}^2\right]^{1/2}$$

$$\tan 2\Psi = 2\tau_{\varphi z}/(\sigma_\varphi - \sigma_z)$$

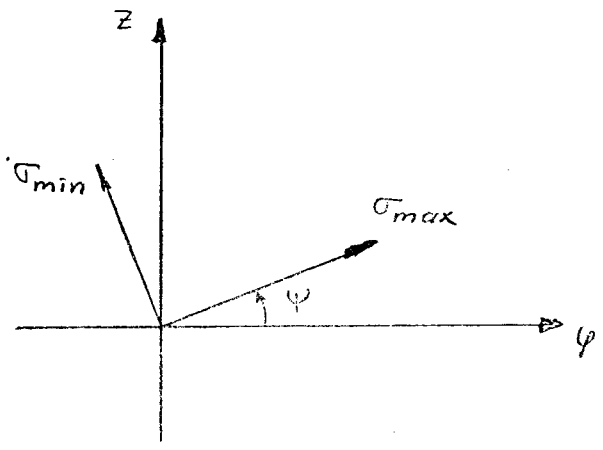

Correction for splitting of canister into halves

From the results from earlier calculations of the distribution fo residual stresses in the sealed canister it is apparent that σ_z is close to a linear function of r in those sections where the maximum residual stress in the Z-axis occurs. The following approximative σ_z-distribution has been used to calculate the change in the residual stress state in the split canister:

$$\sigma_z(r) = C_0 + C_1 \cdot r$$

The constants C_0 and C_1 are determined from the conditions that the total normal force $N_z = 0$ and that $\sigma_z = \sigma_{z\,max}$ on the outside of the canister ($r = b$). We obtain from the 1/3-scale canister ($a = 48$ mm, $b = 83$ mm)

$$\sigma_z(r) = \sigma_{z\,max} \cdot 4{,}207 \left(\frac{r}{67{,}06} - 1\right) \qquad (1)$$

After the splitting of the canister the section moment in each section must be still zero. The change in the residual stresses in the Z-axis is calculated by first determining the moment results, M_y, due to the original σ_z-distribution. The change is then obtained as the bending stress distribution on half the cross-section due to the moment $-M_y$.

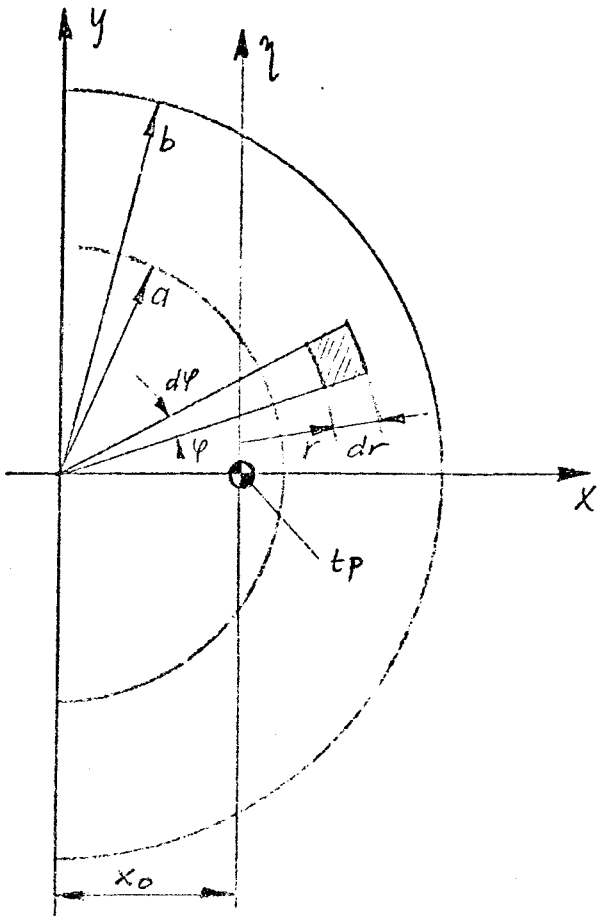

Equilibrium gives

$$M_y = 2 \int_0^{\pi/2} \int_a^b \sigma_Z (r)\, r\, dr\, d\varphi \cdot r \cos\varphi$$

$$= 2 \int_a^b r^2 \sigma_Z (r)\, dr \qquad (2)$$

with $\sigma_Z (r)$ according to Eq. (1) we obtain

$$M_y = 2{,}864 \cdot 10^4 \cdot \sigma_{Z\,max}$$

($\sigma_{Z\,max}$ in N/mm^2 , M_y in Nmm)

The change in the residual stresses will be

$$\Delta \sigma_Z = - \frac{M_y}{I_\eta} (x - x_0)$$

where I_η is the moment of inertia with respect to the η-axis and x_0 is the distance to tp according to the figure. I_η and x_0 for the 1/3-scale canister will be 3.426×10^6 mm^4 and 42.7 mm, respectively.

The largest decrease in σ_Z in the outer surface is obtained for a point half way between the section surfaces

$(\varphi = 0)$, $\Delta\sigma_Z = -0{,}34\ \sigma_{Z\,max}$

Half way between the section surfaces the residual stress in the Z-axis before the splitting would have been about 50 % larger than that measured after the splitting.

Results

The following table lists the calculated and corrected residual stresses.

Measure-ment No.	Distance from joint mm	Calculated residual stresses, MN/m^2				
		σ_φ	σ_Z	σ_{max}	σ_{min}	ψ °
1A	121	-4.2	-1.5	-1.5	-4.2	0
1B	122	-5.2	-6.8	-1.6	-10.4	39.7
2A	153	-0.2	-12.0	+1.9	-14.1	-21.2
2B	165	-13.6	-21.6	-13.6	-21.6	+4.3
3A	192	+22.3	+26.9	+29.0	+20.2	-29.4
3B	205	+17.9	+26.3	+27.0	+17.2	+15.4
4A	209	-2.5	+7.9	+8.4	-3.0	-11.9
4B	234	-14.4	-15.4	-4.5	-25.3	+43.6

Measured and calculated residual stresses

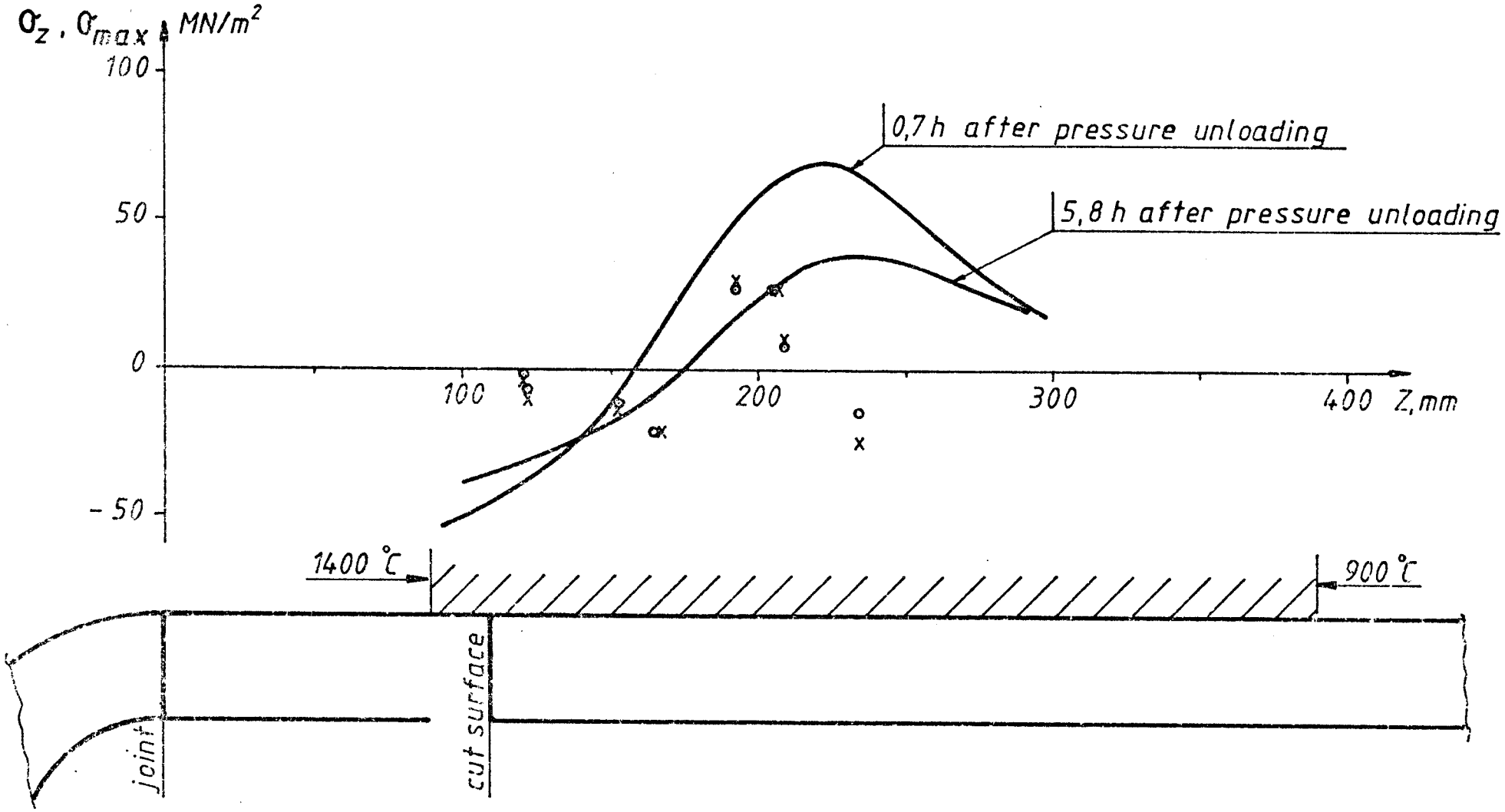

Measured residual stresses

○ σ_z , axial stress

× σ_{max} , maximum principal stress

—— Calculated residual axial stress. (With internal support, 5 mm clearance)

Appendix E III

Delayed failure in ceramic materials

Summary

This review of the literature was occasioned by WCP and the material testing that is being carried out to determine the strength properties and fracture mechanics data of aluminium oxide.

Ceramic materials normally contain small defects (pores, inclusions, cracks, intergranular phases 2100 μm), which, under the influence of a corrosive environment (mainly water) and mechanical stress, slowly grow to failure. This time-dependent process is called delayed failure.

The report contains a description of delayed failures and how they can be treated formally by means of fracture mechanics. Among other things, it is shown how the time to failure can be estimated by means of proof testing before the structure is put to use.

The principles of testing technique and references to how the proof testing technique has been used in a number of practical cases are also presented (insulators of porcelain, laser window glass, space shuttle glass, Si_3N_4 at 1400°C).

Contents Page

1. Theoretical background

Fracture mechanics is based on ideas from 1910-1920 originated by, among others, Griffith (1), who postulated that for a body containing a crack, the reduction in potential energy (related to stored elastic energy and work performed by the external loads) when the crack grows is equal to the increase in the surface energy associated with the new crack surfaces. The failure stress was formulated to be (for plane strain):

$$\sigma_f = \left(\frac{2 E \gamma}{\pi (1-\nu^2) a} \right)^{\frac{1}{2}} \qquad (1)$$

where E is the modulus of elasticity, γ is the surface energy, ν is Poisson's ratio and a is the length of the crack. This relationship applies for elastic materials containing an infinitely sharp crack.

Eventually, surface energy considerations were abandoned, and instead Irwin 1957 (2) formulated the fundamentals of modern fracture mechanics, which describes the stresses adjacent to the crack as:

$$\sigma = \frac{K_I}{(2 \pi r)^{\frac{1}{2}}} + \text{higher order terms} \qquad (2)$$

where the first term dominates near the crack. The effect of external loads, crack dimensions and the geometry of the body are described by K_I, the stress intensity factor, where failure occurs when K_I assumes a critical value, K_{IC}:

$K_I = K_{IC}$ (K_{IC} = material constant)

For a crack with a length of 2a in a body subjected to a stress of σ_a, the following holds true:

$$K_I = \sigma_a \sqrt{a} \cdot Y \qquad (3)$$

where Y is a dimensionless factor dependent upon the crack configuration and the geometry of the body. Y for the most common geometries can be found in the fracture mechanics literature, for example TA 0305101. The formulation of the condition for crack growth in practical situations, either in the form of rapid or delayed failures, can be dealt with quantitatively and is always based on equation 3.

2. Delayed failures in ceramic materials

2.1 General

According to Griffith's model, no crack growth is obtained below the critical stress, σ_f, the stress that is required for rapid crack growth to failure. Slow growth of cracks in glass has, however, long been known, especially in the presence of water (=delayed failure). Charles and Hillig (3) assumed that the crack growth velocity (as well as the stress corrosion rate) in glass is controlled by a chemical reaction between the glass and the water in the surrounding environment. Since chemical processes are

activated, crack growth should also be an activated process dependent upon an activation energy, which is in turn dependent upon the applied stress. This theory describes well many experimental results pertaining to environmentally determined crack growth. It is, however, probable that slow crack growth in glass and ceramics cannot always be blamed on stress corrosion. Wiederhorn (4) showed that in some glass types, crack growth occurs even in a vacuum. Several theories have been proposed to describe crack growth without the participation of corrosion.

2.2 Testing technique

The following description is limited to testing with a "double torsion specimen" (Fig. 1) which is usually used and has been recommended (5) for the determination of delayed failure in ceramics. This specimen, which will probably be used by KYDP for determining crack growth in Al_2O_3, WCP, has a number of advantages from the viewpoint of testing.

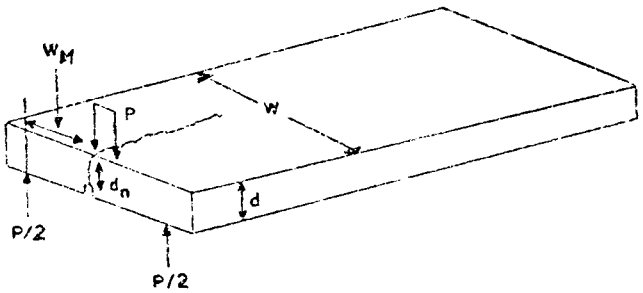

Fig. 1—A schematic of the double torsion configuration showing the specimen dimensions.

Fig. 1

With this specimen, crack growth is measured as a function of time under the influence of e.g. the water content of the environment. The specimen is called a "constant-K specimen", which means that the stress intensity factor, K_I, is independent of crack length, which is also evident from the expression:

$$K_I = PW_m \left[\frac{3(1+\nu)}{Wt^3 t_n}\right]^{\frac{1}{2}} \qquad (4)$$

where P is the applied load, ν is Poisson's ratio and the other parameters are the dimensions of the specimen.

As is evident from Fig. 2, the specimen is a simple rectangular plate supported by two parallel rollers or four hemispheres, one at each corner. The load can be applied by two parallel plates via two points on the upper plate (6). The crack grows along the length of the specimen, emanating from the edge where the load is applied. Normally, a longitudinal groove is made in order to ensure that the crack grows as straight as possible.

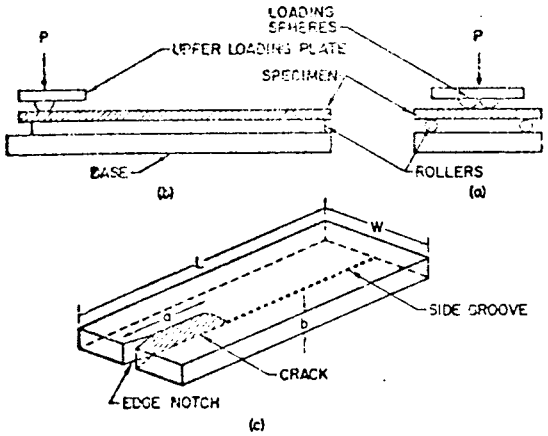

A schematic representation of the test device. (a) Side projection ; (b) end projection ; (c) the test specimen.

Fig. 2

In principle, the compliance function of the specimen is used to measure crack growth. Compliance is the inverse of the slope of the load/deflection curve (P Y), and it has been demonstrated experimentally that compliance is a linear function of crack growth a.

$$\frac{Y}{P} = Ba + C \tag{5}$$

where B and C are constants determined by the modulus of elasticity and the specimen dimensions. Experimentally, the variation of compliance with time can be measured either at constant load or constant deflection. At constant deflection, which is the most common, differentiation of equation 5 gives the following:

$$\frac{dy}{dt} = (Ba+C)\frac{dP}{dt} + BP\,\frac{da}{dt} \tag{6}$$

Thus, dy/dt = 0 at constant deflection and the crack velocity is:

$$\frac{da}{dt} = V = -\,\frac{Ba + C}{BP}\,\frac{dP}{dt} \tag{7}$$

At constant deflection, the following is also true:

$$P(Ba+C) = P_i(Ba_i+C) = P_s(Ba_s+C) \tag{8}$$

where a_i is crack length and P_i is load at the start of the load relaxation and a_s and P_s are the same quantities at the end of the relaxation. Insertion for (Ba + C)/P in equation 7 gives:

$$V = -\,\frac{P_i}{P^2}\left(a_i + \frac{C}{B}\right)\frac{dP}{dt} \tag{9}$$

In general, except for small initial cracks, $a_i >> C/B$ and V is reduced to

$$V = - \frac{a_i P_i}{p^2} \frac{dP}{dt} = - \frac{a_s P_s}{p^2} \frac{dP}{dt} \qquad (10)$$

Thus, the crack velocity is obtained by measurement of the load-time function at constant deflection (e.g. with a Servogord recorder) and the size of the initial crack (or skrivare? the final crack). At every load point, the associated stress intensity factor, K_I, can be calculated with the aid of equation 4. When the relaxation is completed, the specimen can be used for determining $K_I = K_{IC}$ (= fracture toughness).

In principle, the entire $K_I V$ diagram can be determined with only one specimen by means of measurements of the load/time relationship at constant deflection, the initial crack (or the final crack) and the load at rapid growth P_{IC}.

Observations of the crack during crack growth have shown that it grows more rapidly on the lower face of the specimen (with Δa, Fig. 3).

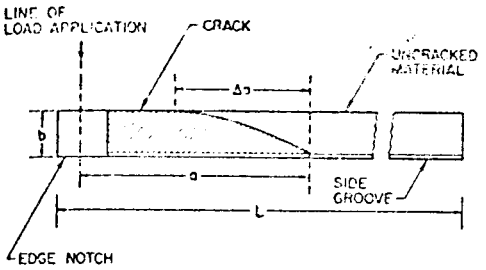

The crack front in the test specimen, showing that the crack extends further along the lower face.

Fig. 3

For more accurate measurements, equation 10 must be corrected by a factor of ϕ so that the crack velocity is

$$V^* = \phi V$$

where

$$\phi = b/(\Delta a + b^2)^{\frac{1}{2}}$$

Experimental calibration of the specimen's compliance function was within 10% in relation to equation 4. It may therefore be necessary to test more than one specimen in practical tests, and possibly use other types of specimens as well, for example "Double cantilever beam" specimens.

The method has been demonstrated to be successful in a number of cases, for example for Al_2O_3, Fig. 4.

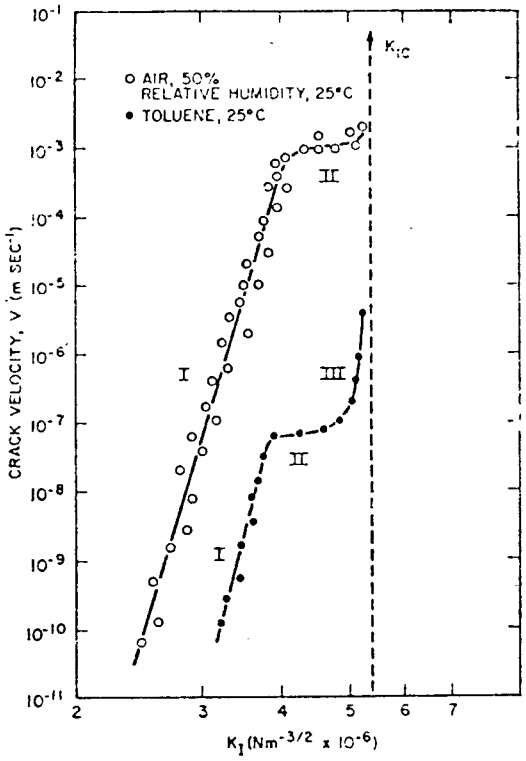

Crack velocity, stress-intensity factor data for polycrystalline alumina in moist air, 50% relative humidity and in toluene. Regions I, II and III are apparent.

Fig. 4

2.3 KV diagram

It has been shown that crack velocity in most materials under the influence of a corrosive environment is a unique function of the stress intensity factor, K_I (Fig. 5) (7). Three regions for crack growth have been observed I, II and III from K_O, below which no growth takes place, to K_{IC}, at which unstable failure occurs.

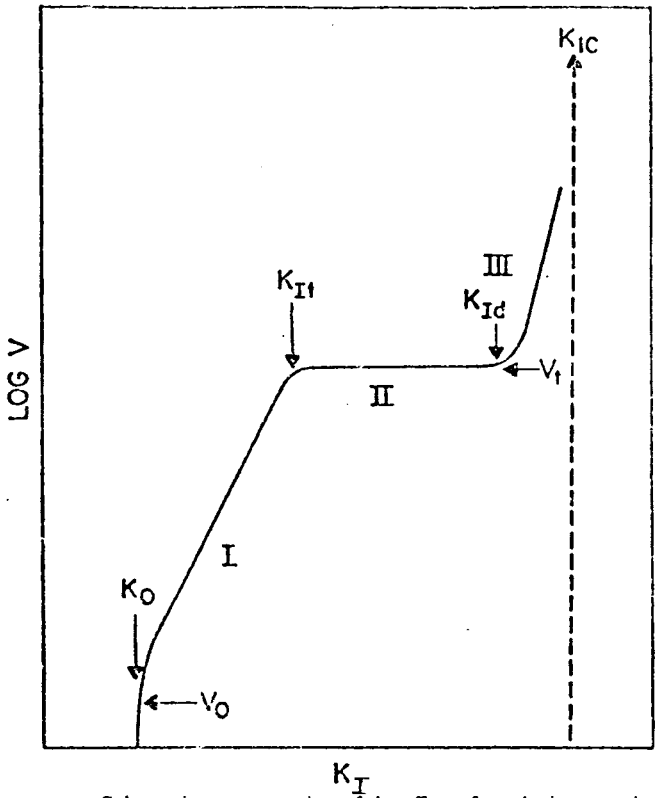

Schematic representation of the effect of crack tip stress intensity, K_I, on crack velocity, V, during slow crack growth.

Fig. 5

Region I is characterized by a crack growth that is determined by a tensile-stress-promoted chemical reaction between material and water in the environment in the vicinity of the crack tip. The crack velocity is reaction-rate-dependent, so that an increase of the water concentration leads to an increase in the crack velocity. An increase in temperature also leads to an increase in crack velocity. Region II is also dependent upon the water concentration, but V is independent of K_I. In region III, V becomes independent of the water concentration (when K_I approaches K_{IC}), but is instead determined by temperature and material composition. The crack growth phenomenon is often referred to in brief as stress corrosion, the diagram shown in Fig. 5 is called a KV diagram.

2.4 Estimation of life for delayed failures

In general, failure processes consist of three stages: Crack initiation, stable crack growth and, finally, unstable failure. One of the first two stages often dominates, and most ceramics that are used in practice already contain from the start so many sharp microcracks (260 μm) that crack growth is the dominant process (8). An estimation of life with the aid of crack growth analysis should therefore be possible and should also be conservative if there is also some crack initiation time.

For most ceramics, region II (Fig. 5) exists at such a high V level that the crack growth time is controlled only by crack growth in region I. The crack velocity in region I can, as a rule, be approximated by means of the relationship:

$$V = A \cdot K_I^n \tag{11}$$

where n and A are constants and n usually assumes high values, 9-50. In contrast to in metals, small changes in K_I thus lead to large changes in V. It should also be pointed out that the threshold value K_O probably first occurs at such low velocities, $< 10^{-10}$ m/s, that its existence has not generally been verified.

The crack growth kinetics described by the KV diagram in Fig. 5. can be used to estimate the time to failure under constant load. The time, t, required for a crack to grow from subcritical to critical size can easily be derived from the definition of crack velocity, da/dt = V (where a is crack length), and the relationship between the stress intensity factor, applied stress and crack length, equation 3.

The following is obtained from equation 3:

$$a = \frac{K_I^2}{\sigma_a^2 Y^2}$$

which, after differentiation becomes

$$\frac{da}{dt} = V = \frac{2\,K_I}{\sigma_a^2 Y^2}\,\frac{dK_I}{dt}$$

and

$$t = \frac{2}{\sigma_a^2 Y^2}\int_{K_{Ii}}^{K_{If}} \left(\frac{K_I}{V}\right)\, dK_I \tag{12}$$

where K_{Ii} and K_{If} are the crack intensity at the beginning and at the end, respectively.

After integration, the insertion of equation 11 gives

$$t = \frac{2}{(n-2)A\,\sigma_a^2\,Y^2}\left(K_{Ii}^{2-n} - K_{If}^{2-n}\right) \tag{13}$$

In connection with rapid, unstable failure, $K_{If} = K_{IC}$, and this gives the time to failure

$$\tau = \frac{2}{(n-2)A\,\sigma_a^2\,Y^2}\left(K_{Ii}^{2-n} - K_{IC}^{2-n}\right) \tag{14}$$

Since for ceramic materials $9 < n < 50$, i.e. $K_{IC}^{2n} \ll K_{Ii}^{2n}$ for ordinary load cases $K_{Ii} < 0.9\,K_{IC}$), the following expression holds true with good approximation:

$$\tau \approx \frac{2}{(n-2)A\,\sigma_a^2\,Y^2}\,K_{Ii}^{2-n} \tag{15}$$

Thus, the time to delayed failure can be calculated as long as K_{Ii}, the stress intensity factor in the initial phase at the largest existing crack, and the K-V diagram are known.

2.5 Proof testing

2.5.1 Time to failure after proof testing (PT)

In connection with the test pressurizing of a steel pressure vessel slightly above the operating pressure, it has been demonstrated that an upper limit for K_{Ii} and thereby a lower limit for time to failure can be estimated. If the structure survives this proof testing, it is guaranteed that the stress intensity factor for the most serious defect in the material does not exceed the material's fracture toughness, K_{IC}.

The condition for this can be written:

$$K_{Ii}/\sigma_a = \left(K_I\right)_{PT}/\sigma_p < K_{IC}/\sigma_p$$

(σ_p = proof stress)

Inserting $K_{Ii} < \sigma_a K_{IC}/\sigma_p$ in equation 15 gives the largest value of K_{Ii} and therefore the minimum time to failure:

$$\tau_{min} = \frac{2}{\sigma_a^2 Y^2} \frac{K_{Ic}^{2-n}}{A(n-2)} \left(\frac{\sigma_p}{\sigma_a}\right)^{n-2} \qquad (16)$$

It follows from equation 16 that τ_{min} is dependent upon the ratio between the proof stress and the applied stress (σ_p/σ_a) and the applied stress σ_a. It is then possible to present the minimum time to failure for a structure in graphic form with a series of parallel lines (slope 2) in a double logarithmic diagram with coordinates as in Fig. 6.

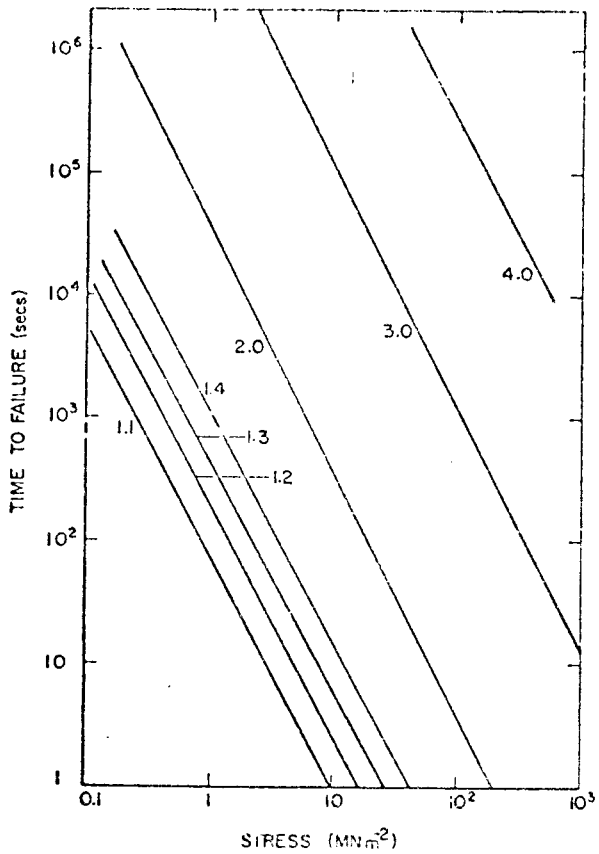

A proof test diagram for soda-lime glass in water. The numbers below each line refer to the proof stress/applied stress ratio (σ_p/σ_a) corresponding to that line.

Fig. 6

It can be immediately determined from Fig. 6 which level of proof testing is required to guarantee "no failures" within a given time at a given applied stress.

The minimum time to failure predicted in this manner can in reality be considerably less than the observed time to failure due to variation in material properties, and thereby also the time to failure, i.e. the life of the structure is dependent upon which failure probability is assumed. When a given life is required, it is therefore often possible to permit the structure to stay in operation a longer time than τ_{min}. If no crack growth is assumed during PT, the extended time to failure, t, can formally be obtained directly from equation 15 by inserting $K_{Ii} < \sigma_a K_{IC}/\sigma_f$, where σ_f is the failure stress ($\sigma_f > \sigma_p$) after PT.

$$\frac{\tau}{\tau_{min}} = \left(\frac{\sigma_f}{\sigma_p}\right)^{n-2} \equiv R^{n-2} \qquad (17)$$

Values of τ that are suitably larger than τ_{min} are obtained for $\sigma_f > = 1.5\ \sigma_p$ (i.e. $\tau/\tau_{min} \simeq 17$). Since σ_f is not generally known, τ can be calculated with the aid of the material's original strength distribution, which can, for example, be a Weibull distribution. Assume that we have such a distribution in Fig. 7.

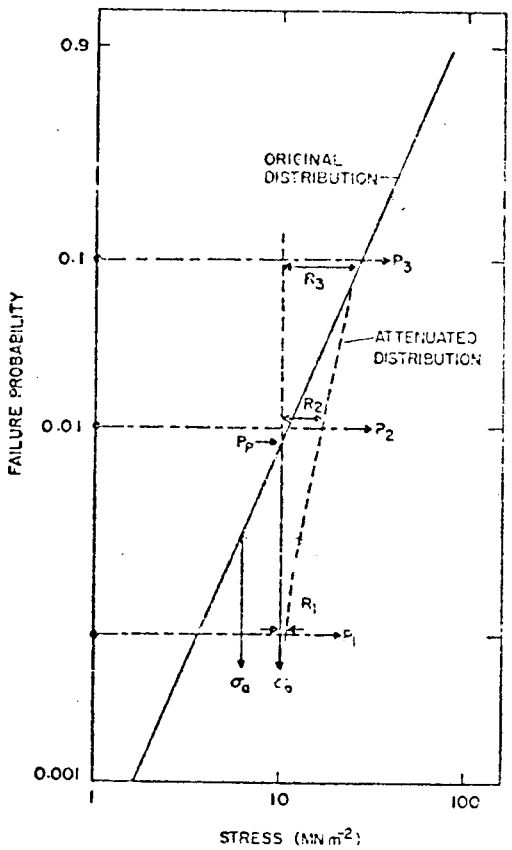

A typical strength distribution for a ceramic material plotted on Weibull axes. σ_p is the proof stress, σ_a is the applied stress and P_1, P_2, and P_3 are different levels of component failure probability. The quantities R_1, R_2, and R_3 are related to the time to failure ratio, τ/τ_{min}.

Fig. 7

PT to a stress, σ_p, eliminates, after survival of PT, all structures with lower strengths. In this manner, the distribution is "attenuated" to the "strengths that are left", which is shown by the dashed curve in Fig. 7. The failure probability P_a for the "attenuated" distribution can be derived to

$$Pa = \frac{P_i - P_p}{1 - P_p} \qquad (18)$$

where P_i is the probability for failure before PT and P_p is the failure probability during PT. As is evident from Fig. 7, τ / τ_{min} is dependent primarily on which failure risk is taken as a design requirement.

If the failure probability of a structure is set low so that $P < P_p$, is $\sigma_f \simeq \sigma_p$, $R \simeq 1$ (see R_1), then τ_{min} is the only usable time to figure. If a higher failure probability is chosen, $P \simeq P_p$, $R >> 1$ (see R_2) and τ is considerably larger than τ_{min} (several orders of magnitude). Finally, the use of τ_{min} is meaningless if $P > P_p$ and PT is no longer a useful method to determine the durability of the structure. The above line of reasoning can be expressed analytically as follows. If the strength of the material is Weibulldistributed, the parameter m can be taken as a measure of the strength variation, which can be written approximately, after taking the logarithm twice, as follows:

$$\ln \ln \left(\frac{1}{1-P}\right) = m \ln \sigma_{Ri} + J \qquad (19)$$

where σ_{Ri} are the original strength values and J is an empirical constant.

The time to failure that also incorporates the failure probability without PT can be obtained with the aid of equations 15 and 19.

It follows from equation 15:

$$\tau_0 = \frac{2 \sigma_{Ri}^{n-2}}{A \sigma_a^n Y^2 (n-2) K_{IC}^{n-2}} \qquad (20)$$

Insertion of σ_{Ri} from equation 19 and taking the logarithm gives

$$\ln \tau_0 = \frac{n-2}{m} \ln \ln \left(\frac{1}{1-P_i}\right) - n \ln \sigma_a - \frac{J}{m} + \ln \left[\frac{2}{A(n-2)Y^2 K_{IC}^{n-2}}\right] \qquad (21)$$

For small $P_i < 0.1$, this is reduced to

$$\ln \tau_0 = \frac{n-2}{m} \ln P_i - n \ln \sigma_a - \frac{J}{m} + \ln \left[\frac{2}{A(n-2)Y^2 K_{IC}^{n-2}}\right] \qquad (22)$$

The values of time to failure without PT can thus be plotted on the PT diagram (Fig. 6) for varying P_i as a series of parallel lines (slope -n), which are illustrated in Fig. 8 and which applies for sodalime glass. It can be determined directly which stress levels below which PT is a useful technique to establish the

durability of a structure. The above-specified strength values must naturally be corrected for possible size-dependence.

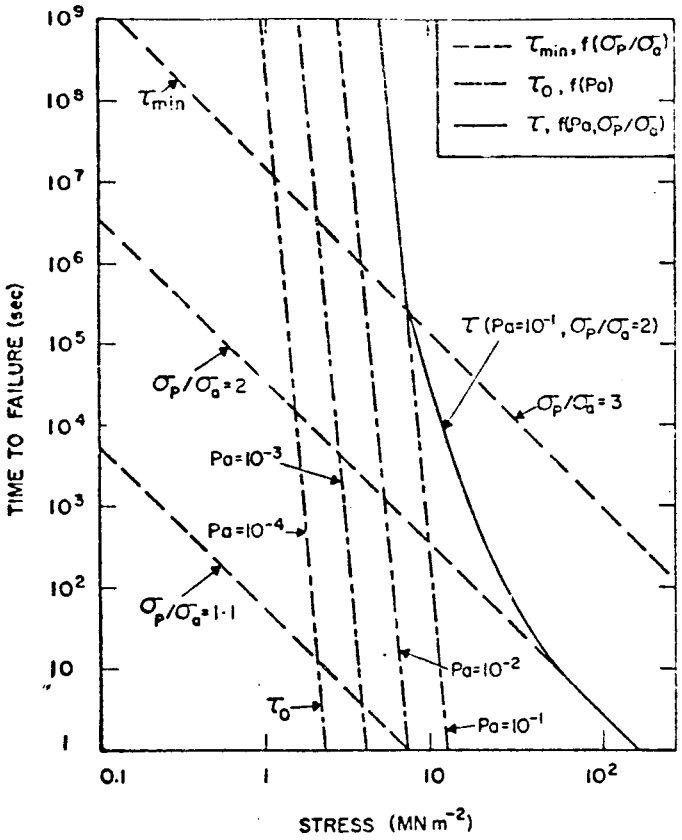

A complete time to failure diagram for ground soda-lime glass immersed in water, under a flexural load. The minimum time to failure after proof, τ_{min}, the time to failure without proof, τ_0, and the time to failure after proof, τ, are shown for various P_a and σ_p/σ_a.

Fig. 8

An analytical expression for complete time to failure (incl. failure probabilities) can be determined in a similar manner as above with the ratio τ/τ_{min} by combining equations 17 and 19. Inserting P_i in equation 18 gives the following:

$$\ln\left[\frac{-\ln(1-P_a) - \ln(1-P_p)}{-(1-P_p)}\right] = m \ln\left(\frac{\sigma_f}{\sigma_p}\right)$$

and inserting σ_f/σ_p from equation 17 gives, for small P_a and P_p (< 0.1):

$$\ln\left(\frac{\tau}{\tau_{min}}\right) = \frac{n-2}{m} \ln\left(\frac{1+P_a}{P_p}\right) \qquad (23)$$

As is evident, the time to failure is much greater than the minimum value only for $P_a > P_p$ and if (n2)/m is a relatively large ratio. For soda-lime glass, which is illustrated here (Fig. 7), (n-2)/m ≅ 5

and the effect is marked with $P_a = 10\text{-}1$ and $\sigma_p / \sigma_a = 2$. For $P_a >> P_p$, equation 23 is reduced to equation 22 so that $\tau \to \tau_0$; for $P_p >> P_a$, $\tau \to \tau_{min}$, as is evident from the figure.

2.5.2 Time to failure with crack growth during PT

Up to now, it has been assumed that no crack growth takes place during PT itself. This is true if PT is performed very rapidly or in an environment that does not give any crack growth. Normally, however, some crack growth is obtained, and an analysis of this effect on statistical strength and time to failure beyond τ_{min} must be carried out. Slow crack growth during PT does not, however, affect in any way the calculated minimum time to failure (equation 16). The weakening that is brought about can be obtained from equation 13.

We define K_A as

$$K_A^{2-n} \equiv \frac{n-2}{2} A \sigma_a^2 Y \cdot t$$

which gives equation 13 the following appearance

$$K_A^{2-n} = K_{Ii}^{2-n} - K_{If}^{2-n} \tag{24}$$

For $K_{If} = K_{IC}$, the failure condition is now

$$\left(K_{Ii}^*\right)^{2-n} = K_A^{2-n} + K_{Ic}^{2-n} \tag{25}$$

where K_{Ii}^* can be regarded as the critical (i.e. the minimum) value of the stress intensity factor that results in failure in connection with PT. Inserting equation 25 in equation 24 gives the relative change of the stress intensity factor during PT:

$$\left(\frac{K_{Ii}}{K_{If}}\right)^{n-2} = 1 - \left(\frac{K_{Ii}}{K_{Ii}^*}\right)^{n-2} \cdot \left[1 - \left(\frac{K_{Ii}^*}{K_{IC}}\right)^{n-2}\right] \tag{26}$$

The relative change in strength due to PT can now be determined using equation 26. When the stress during PT is σ_p = constant, it is also true that $K_{Ii} = K_{If} = (a_i/a_f)^{1/2}$, where a_i and a_f are crack lengths at the beginning and end of PT, respectively. Furthermore, since unstable failure is obtained when $K_I = K_{IC}$, the failure stress after PT is given due to the fact that $\sigma_f / \sigma_f^* = (a_f/a_i)^{1/2}$, where σ_f is the failure stress without slow crack growth during PT and σ_f^* is the actual failure stress after PT. In a similar manner, it can be shown that $K_{Ii}/K_{Ii}^* = \sigma_p / \sigma_f^*$ where σ_p^* is the equivalent failure stress during PT and $K_{Ii}^*/K_{IC} = \sigma_p / \sigma_p^*$. These different parameters are shown in an example in Fig. 9.

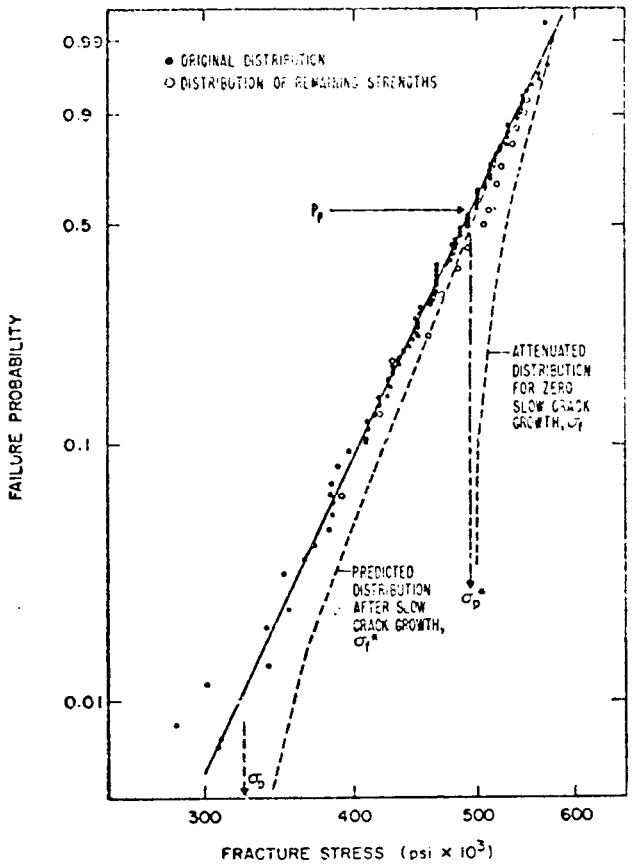

The strength of E-glass fibers before and after a constant stress proof test at σ_p. Also shown are the strengths after proof testing when no slow crack growth occurs, σ_f, and the predicted strengths due to slow crack growth, σ_f^*. Data obtained rom Ref. (7).

Fig. 9

Inserting stresses instead of stress intensity factors in equation 26 gives the following expression for the relative weakening of the material's failure stresses (e.g. measured as flexural strength).

$$\left(\frac{\sigma_f^*}{\sigma_f}\right)^{n-2} = 1-\left(\frac{\sigma_p}{\sigma_f}\right)^{n-2}\left[1-\left(\frac{\sigma_p}{\sigma_p^*}\right)^{n-2}\right] \qquad (27)$$

The attenuated strength distribution of the structures remaining after PT can also be derived. The values of σ_f^* calculated for t-glass that are shown in Fig. 9 (n = 12) exhibit good agreement with tests performed after PT.

The slow crack growth during PT has an influence on the time to failure, but not on the minimum time τ_{min} (equation 16), since the condition $K_{If} < K_{Ic}$ also applies after PT. The failure stress σ_f^* shall thus be used to calculate $\tau > \tau_{min}$ by replacing σ_f with σ_f^* in equation 17.

In order to verify the above analysis, Evans and Wiederhorn (8) carried out a series of experiments. They are illustrated in Fig. 10.

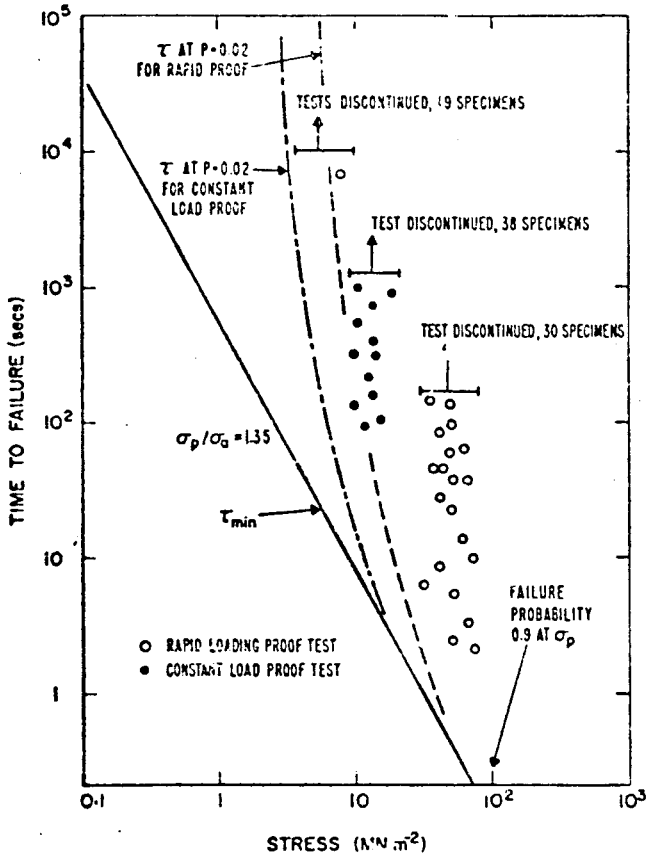

A comparison of failure times after proof testing for ground soda-lime glass in water, with the predicted minimum failure time for the soda-lime glass/water system (full line), and the times in excess of the minimum for a probability of 0.02.

Fig. 10

As is evident from the above diagram, all measured times to failure exceed the calculated τ_{min}. The PT technique was later also used in a number of practical cases in order to design against delayed failure, as for example in ref. 9 (porcelain insulators), ref. 10 (laser window glass), ref. 11 (space shuttle window glass) and in a presumptive use of Si_3N_4 at 1400°C, ref. 12.

2.5.3 Influence of measuring error on time to failure

In calculating the minimum time to failure (equation 16), the measuring errors associated with the determination of K_{IC}, n and A have not been taken into account. Relatively small errors in n and A can give large errors in t. Error theory has been used by Wiederhorn et al (13) to assess the influence of the measuring errors on t and has permitted the establishment of confidence limits for estimating the minimum time to failure.

The variance in t expressed as V (lnt) (= the natural logarithm of t) can be written as:

$$V(\ln t)= \left[\ln K_{Ii}+(n-2)^{-1}\right] V(n) +2\left[\ln K_{Ii}+(n-2)^{-1}\right] \mathrm{Cov}(n,\ln A)+V(\ln A) +(n-2)^{2} V(\ln K_{Ii}) \quad (28)$$

For a calculation of equation 28, the reader is referred to ref. 13, which describes in detail the procedure for calculating the uncertainty in t due to the measuring errors in n, A and K_{IC} as well as how to use the PT diagrams where confidence limits for the minimum time to failure are given.

In an alternative method described in ref. 14, the Monte Carlo technique is used to determine the distribution function for time to failure based on experimental measuring errors.

3 BIBLIOGRAPHY

1. A.A. Griffith: Phenomena of Rupture and Flow in Solids, Phil. Trans. Roy. Soc. London, Ser. A 221 (4) 163-98 (1920-21).

2. G.R. Irwin: Analysis of Stresses and Strains Near the End of a Crack Traversing a Plate, J. Appl. Mech, 24 (3), 361-64 (1957).

3. W.S. Hillig, R.J. Charles: pp 682-705 in High Strength Materials Edited by V.F. Zackay. John Wiley & Sons, New York, 1965.

4. S.M. Wiederhorn et. al: Fracture of Glass in Vacuum, J. Amer. Soc. Ceram. Soc. 53 (8), 336-41 (1974).

5. A.G. Evans: pp 17-48 in Fracture Mechanics of Ceramics Vol. 1 Plenum Press, New York, 1974.

6. A.G. Evans: A Simple Method for evaluating slow crack in brittle materials, Int. J. Fract. Mech., 9 (3), 267-275 (1973).

7. A.G. Evans: A method for evaluating the time-dependent failure characteristics of brittle materials - and its applications to polycrystalline alumina, J. Mater. Sci 7, pp 1137-1146 (1972).

8. A.G. Evans, S.M. Wiederhorn: Proof testing of ceramic materials, an analytical basis for failure prediction, Int. J Fracture 10 (3) pp 379-92 (1974).

9. A.G. Evans, S.M. Wiederhorn et al: Proof testing of porcelain insulators and application of acoustic emission, Ceram. Bull., 54 (6), pp 576-81 (1975).

10. A.G. Evans, H. Johnson. A fracture-mechanics study of ZnSe laser window applications, J, Am. Cer. Soc., 58 (5-6) pp 244-49 (1975).

11. S.M. Wiederhorn, A.G. Evans et al: Application of fracture mechanics to space-shuttle windows, J. Am. Cer. Soc., 57 (7) pp 319-23 (1974).

12. A.G. Evans et al: Slow crack growth in ceramic materials at elevated temperatures, Met. Trans, 6A (4) pp 707-16 (1975).

13. S.M. Wiederhorn et al: An error analysis of failure prediction techniques derived from fracture mechanics, J. Am. Cer. Soc. 59 (9-12), pp 403-411 (1976).

14. E.M. Lenoe, D.M. Neal: Assessment of strength-probability-time relationships in ceramics, Cracks and Fracture, ASTM STP 601, 1976, pp 63-85.

Other literature

General treatments of delayed failures, testing technique, fracture mechanics principles and much more:

A) Fracture mechanics of ceramic materials - Volume I and II, Plenum Press, New York, 1974.

B) J.B. Wachtman, Jr: Highlights of progress in the science of fracture of ceramics and glass, J. Am. Cer. Soc, 57 (12), pp 509-19 (1974).

Determination of slow crack growth in isostatically pressed Al_2O_3

Willy Hermansson

Summary

Experimental data on the crack growth in isostatically pressed Al_2O_3 have been obtained to be able to assess the life of WCP containers for the storage of spent nuclear fuel.

Small defects, which are always present in ceramic materials, grow under the influence of a humid environment and mechanical loading until failure occurs. This process is called delayed failure. The crack growth can be described with the crack growth law

$$V = A \cdot K_I^{\,n}$$

where V = crack velocity
K_I = stress intensity factor in the crack tip
A, n = material and environmental constants

The testing has been performed by means of the load relaxation method with double-torsion test specimens.

The report also discusses the influence of different sources of error on the results. Such error sources may be irreversible relaxations due to settlement in the test rig, errors in the test specimen geometry, inhomogeneities in the material and weakness (resilience) in the test rig.

The test invironment has been ground water I according to the KBS recipe and the testing temperature 21°C.

The experimental results give the following conservative values of the constants n and A:

$n = 210$

$\log A = -120$

The fracture toughness K_{IC} for the material has been found to be 6.2 ± 0.2 $MNm^{-3/2}$ in double-torsion test specimens.

The test method used has been checked with test specimens of glass. Results obtained show a good correlation with data published in the literature for glass of the corresponding composition.

CONTENTS

1 INTRODUCTION

Ceramic materials always contain small defects of the type pores, cracks, inclusions, etc. These defects need not be of critical size for unstable brittle fracture to occur instantaneously when the material is subjected to a load. However, under the influence of the environment (particularly the presence of water) and mechanical stresses these defects grow slowly until brittle fracture occurs.

It is therefore important to know how this crack growth takes place in structures of ceramic material subjected to mechanical loading, thermal stresses or containing residual stresses. Tests must therefore be performed to study how quickly a crack grows under different environmental conditions and loads. From the data obtained it is then possible to calculate a reasonable life for the structure. Alternatively, proceeding from the desired life it is possible to calculate a largest permissible initial size of defects from which cracks will propagate. The size of these initial cracks must then be compared with the size of the defects that can be detected by means of available testing methods such as radiographic examination, ultrasonic examination, etc.

With the aim of obtaining data to permit calculation of the life of canisters of isostatically pressed Al_2O_3 intended for the storage of spent nuclear fuel, experiments have been performed to determine the crack velocity in the material.

An earlier technical report KYDP 77-7101 (1) describes the theoretical background and presents different testing methods. This report also presents measured values of the fracture toughness K_{IC}.

To check the testing method used for determining the crack growth, measurements have been performed on glass test specimens to permit comparison with data published in the literature.

2 EXPERIMENTAL

2.1 Test method

The load relaxation method (1) has been used to determine the crack velocity. Double-torsion test specimens were used during this testing. Fig. 1 shows the geometry of the test specimen and the test device. During the testing the deflection at the point of load application was maintained constant. When the crack grows, the load P decreases, which is registered on a recorder. By applying this load relaxation it is then possible to calculate the crack velocity, see below. Fig. 2 shows the test set-up.

2.2 Test specimens

The test specimens used were of double-torsion type. Two different test specimen sizes have been tested. Different values of the notch width Wg were also tested in the case of the larger test specimen. The purpose of the notch Wg is to guide the crack along the centreline of the test specimen.

The test specimens used had the following dimensions (for the notation see Fig. 1):

I	W	= 50 mm
	d	= 4.0 mm
	d_n	= 3.0 mm
	L	= 150 mm
	Wg	= 2.0, 2.75 and 4.0 mm
II	W	= 25 mm
	d	= 2.0 mm
	d_n	= 1.0 mm
	L	= 75 mm
	Wg	= 3.0 mm

2.3
Test environment

The testing was performed with the test specimens immersed in ground water environment 1 according to the KBS recipe, see Appendices 3 and 4. The test rig was set up in an air-conditioned room with a temperature of 21°C. At the beginning of the test the H_2O_2 content was about 0.30 per cent by weight. During the test period of about 24 h for each test the H_2O_2 content as a rule decresed to about 0.24 w.p.

2.4
Evaluation

The crack growth is a function of the environment and stress intensity factor at the crack tip (1). If the environment is maintained constant, the following relationship can be written

$$V = A \cdot K_I^{\,n} \qquad (1)$$

where

V	= crack velocity [ms^{-1}]
A	= constant
K_I	= stress intensity factor in the crack tip [$MNm^{-3/2}$]
n	= constant

A and n are constants, which depend on the material and the test environment. By determining these values it is possible to obtain a K, V relationship for the material in question. This relationship can subsequently be used to estimate the life of a material. Fig 3 shows a schematic K, V diagram.

The stress intensity factor K_I for the double-torsion test specimen is independent of the crack length, a, and depends only on the applied load, P, and the test specimen geometry:

$$K_I = P\, W_m \left(\frac{3(1+\nu)}{W d^3 d_n \xi} \right)^{1/2} \qquad (2)$$

For the notations see Fig. 1. For Al_2O_3 Poisson's ratio, ν, is 0.27. ξ is a geometric correction factor for the test specimen thickness and is (2)

$$\xi = 1 - 1.25 \left(\frac{d}{W} \right) \qquad (3)$$

The independence of K_I from the crack length, a, applies only for the values (3)

$$0.55 < \frac{a}{W} < 2.34 \qquad (4)$$

and therefore the crack length during the test must not lie outside this range.

The deflection for the double-torsion test specimen is a linear function of the crack length (1)

$$Y = P\,(Ba + C) \qquad (5)$$

where

Y = deflection at the point of load application
P = applied load
a = crack length

B and C are constants, which are dependent on the modulus of elasticity and the test specimen geometry. Differentiation of Eq. (5) with respect to time gives

$$\frac{dY}{dt} = \frac{dP}{dt}(Ba + C) + PB\frac{da}{dt} \qquad (6)$$

where da/dt is consequently the crack velocity. With the load relaxation method the deflection is maintained constant with time, i.e., dY/dt = 0.

Eq. (6) then becomes

$$\frac{da}{dt} = V = -\frac{Ba + C}{PB}\frac{dP}{dt} \qquad (7)$$

With constant deflection, $Y = Y_i = Y_s$ also applies or

$$P\,(Ba + C) = P_i\,(BA_i + C) = P_s\,(Ba_s + C) \qquad (8)$$

where

Y_i, P_i, a_i = values at the start of the load relaxation

Y_s, P_s, a_s = values at the end of the load relaxation

Eqs. (7) and (8) give

$$V = \frac{da}{dt} = -\frac{P_i}{P^2}\left(a_i + \frac{C}{B}\right)\frac{dP}{dt} = -\frac{P_s}{P^2}\left(a_s + \frac{C}{B}\right)\frac{dP}{dt} \qquad (9)$$

Except for short cracks $a >> C/B$ and Eq. (9) becomes

$$V = -\frac{a_i P_i}{P^2}\frac{dP}{dt} = -\frac{a_s P_s}{P^2}\frac{dP}{dt} \qquad (10)$$

The crack velocity is therefore obtained by measuring the load as a function of time and the length of the initial crack (or final crack). In practice it is simplest to determine a_s and the associated value of P_s. For each value of P it is possible to calculate da/dt and K_I (see Eq. 2) to obtain a K, V relationship.

It has been observed that the crack during the crack growth propagates more rapidly along the bottom of the test specimen than along its top (1), see Fig. 4. The crack velocity according to Eq. (10) must therefore be corrected with a factor ϕ:

$$V^* = \phi V \tag{11}$$

where

$$\phi = \frac{d}{(\Delta a^2 + d^2)^{1/2}} \tag{12}$$

where

d = thickness of test specimen
Δ a = difference in crack length

3 RESULTS

3.1 Measured values

Appendices 6 to 8 show the measured values in the form of K, V diagrams.

As can be seen from the diagrams, the scatter between the same type of test specimen is large, cf., for example, DT 1751-2/5 and DT 1751-2/6 in Appendix 6. The reason is that the crack in the first test specimen propagated straight along the centreline, while the crack in the second test specimen propagated obliquely along the edge of the notch. In those cases where the crack propagated straight, along the centreline of the notch, considerably higher crack velocities were obtained for the same calculated value of K_I. Compare also Appendix 7 with Appendix 8.

Table 1 in Appendix 9 summarises the calculated values of A and n in Eq. (1). These values have been determined by means of the method of least squares from straight lines in the diagrams.

Table 1 gives for those cases where the crack propagated straight along the centreline of the notch the following intervals for n and A:

Test specimen I	W = 50 mm	n = 232 - 330
	L = 150 mm	log A = -148 - -236
Test specimen II	W = 25 mm	n = 208 - 349
	L = 75 mm	log A = -146 - -245

The values for the two test specimen types overlap one another and no significant difference can be observed.

3.2
Discussion of error sources

Many factors can bring about errors in the determination of the K, V relationship (4). Such sources of error may be inhomogeneities in the test specimens, errors in the test specimen geometry owing to manufacturing defects, propagation of the crack along the edge of the notch, branched crack, faults in test rig, irreversible load relaxations owing to temperature variations or settlement, weaknesses in the test rig, etc.

3.2.1
Irreversible relaxations

These may arise owing to temperature variations or settlement in the clamping arrangements and are added to the load relaxation occurring owing to the crack growth. Temperature variations are kept down to a minimum by maintaining the temperature constant during the testing by, for example, placing the test rig in an air-conditioned room. Settlements in the loading arrangement and fixture are added to the original load relaxation and this therefore gives a larger load relaxation than when no settlement occurs. Fig. 5 shows this schematically. Since the exponent n in Eq. (1) is calculated according to $n = \Delta \log V / \Delta \log K_I$, an increased relaxation caused by settlement will give a higher value of ΔK_I and thus a lower value of n, see Fig. 5. If such irreversible relaxations occur, a lower calculated value of the exponent n is obtained compared to cases where they are not present (4).

Calculated n-values containing contributions from settlement and the like therefore give conservative values for life estimates.

To reduce the contribution from settlement, a procedure described by Pletka (4) has been used during the tests. According to this method the load is applied in steps up to about 90 per cent of the load at which crack growth is expected to commence. A pause is made between each load step until no relaxation can be recorded.

3.2.2
Errors in test specimen geometry and inhomogeneities

Inhomogeneities in the material as well as errors in the test specimen geometry and the test set-up may have the consequence that the crack does not propagate straight along the centreline but is deflected towards the edge of the notch. The crack may also form branches. Such a crack will give a different stress field in the crack tip and the actual K_I-value differs from the theoretically calculated one. The curves in Appendices 6 to 8 show the effect on test specimens where the crack has propagated straight along the centre line and is deflected towards the edge of the notch, respectively. An oblique crack will give an estimated velocity which is lower for the corresponding K_I-value than for straight propagation of the crack. As can be seen from the diagrams, those cases where the crack has propagated straight along the centre line give conservative values for the life calculations.

App. 6 also shows that test specimens with a small Wg-value appear to display the same tendency as those where the crack is deflected towards the edge of the notch. In the case of too narrow a notch width, Wg, these edge effects are in fact obtained much earlier than for wide notchos, where the crack can be guided back to the centreline again by the stress field. The statistical data for assessing this effect, however, are too limited to enable reliable conclusions to be drawn.

To asses the magnitude of the error in the calculated K_I-values owing to errors in the test specimen geometry, it is possible to estimate the errors by means of logarithmic derivation. According to Eq. (2) we have

$$K_I = P W_m \left(\frac{3(1+\nu)}{W d^3 d_n \xi} \right)^{1/2} \qquad (2)$$

Logarithmic derivation gives for the maximum error (if ξ is assumed to be 1)

$$\frac{\Delta K_I}{K_I} = \frac{\Delta P}{P} + \frac{\Delta W_m}{W_m} + \frac{1}{2}\frac{\Delta W}{W} + \frac{3}{2}\frac{\Delta d}{d} + \frac{1}{2}\frac{\Delta d_n}{d_n} \qquad (13)$$

The following values of the errors are assumed

ΔP = 0.5 N

ΔW_m = 0.1 mm

ΔW = 0.05 mm

Δd = 0.05 mm

Δd_n = 0.05 mm

For the smaller test specimens (with P = 130 N, which is a realistic value) we then obtain

$$\frac{\Delta K_I}{K_I} = 0.08$$

For the larger test specimens (with P = 450 N) we obtain

$$\frac{\Delta K_I}{K_I} = 0.04$$

3.2.3
Influence of weakness in the test rig

Weakness in the test rig, or the spring stiffness of the test rig, has the effect that the deflection is not maintained absolutely constant throughout the duration of the test, since the load relaxes and the "spring deflection" is thus changed. Weakness occurs in the load cell, test frame and loading arrangement. Through

measurements the spring stiffness of the rest rig has been found to be about 10^4 Nmm^{-1}. The following applies for the displacement, Y, in relation to the final state, Y_S

$$Y-Y_S = -K_r\,(P-P_S) \tag{14}$$

where

K_r = spring stiffness

Derivation with respect to time gives

$$\frac{dY}{dt} = -K_r \frac{dP}{dt} \neq 0 \tag{15}$$

Inserting this in Eq. (6) we obtain

$$\frac{dY}{dt} = -K_r \frac{dP}{dt} = \frac{dP}{dt}(Ba+C) + PB\frac{da}{dt}$$

or

$$V = \frac{da}{dt} = -\frac{1}{PB}\frac{dP}{dt}\left(Ba+C+\frac{1}{K_r}\right) \tag{16}$$

From Eqs. (5) and (14) we obtain

$$P(Ba+C) = -\frac{P-P_S}{K_r} + Y_S = -\frac{P-P_S}{K_r} + P_S(Ba_S+C) \tag{17}$$

Eqs. (17) and (16) give with $a_S >> C/B$

$$\frac{da}{dt} = -\frac{P_S}{P^2}\left(a_S+\frac{1}{BK_r}\right)\frac{dP}{dt} = -\frac{a_S P_S}{P^2}\left(1+\frac{1}{a_S B K_r}\right)\frac{dP}{dt} \tag{18}$$

The constant B is (4)

$$B = \frac{6\,W_m^2\,(1+\nu)}{W d^3 E}$$

where E is the modulus of elasticity, ν Poisson's ratio and the other notation is according to Fig. 1.

If due regard is paid to the weakness of the rig, the crack velocity thus increases with a factor $\delta = (1+1/(a_S B K_r))$, which means a parallel displacement of the K, V line to the left. The exponent n does not therefore change.

The values for test specimen DT 1751-2/5 are inserted (see Appendix 6, where this test specimen in the K, V diagram lies furthest to the left). This gives

W_m = 19 mm
ν = 0.27
W = 50 mm
E = 350,000 N/mm2
d = 4.0 mm
a_s = 80 mm

whis give B $\approx$ 2.5 x 10^{-6} N^{-1}

and

$$\delta = 1 + \frac{1}{a_s B K_r} \approx 1.5$$

The error in the calculated crack velocities, if due regard is not paid to the weakness of the test rig, is therefore a factor $\approx$ 1.5.

3.2.4
Summary of error analysis

From Appendices 6 to 9 it is apparent that a total of eight tests were free from errors, i.e., the crack has propagated along the centreline.

In Appendix 11 the adapted K, V lines for these test specimens have been plotted with a correction for ΔK_I according to 3.2.2 and ΔV according to 3.2.3. This correction has been made here conservatively, i.e., the lines have been displaced to the left in the diagram.

A mean value and the scatter in the log K_I-axis have been calculated at a number of levels (in the V-axis). The mean value line determined in this way has the following values for the constants n and log A:

n = 252
log A = -164

From the standard deviation on each level a 99.9 per cent single confidence limit for conservative calculations can be determined, its constants being

n = 211
log A = -128

The following rounded-off values can be used for the calculations

n = 210
log A = -120

3.3
Checking of testing method with glass test specimens

To check the testing method, some experiments were carried out with glass test specimens for comparison with data published in the literature. Test specimens with the same dimensions as Test specimen II (see 2.2) were used.

3.3.1
Test material and test environment

Test specimens were made from glass having an analysis according to Table 2 in Appendix 12. As comparision the analysis for glass tested according to ref. (5) has been included. Analysis values are not available for the glass tested in reference (4).

The testing was performed with the test specimens immersed in deionised tap water in the laboratory. The test rig was placed in an air-conditioned room and a temperature of 21°C was used.

3.3.2
Results

Appendix 13 shows the crack velocity obtained versus the stress intensity factor for the three test specimens, tests Nos. 1 to 3. Table 3 in Appendix 12 summarises the results and a comparison is made with data published in the literature for glass tested in distilled water.

For test No. 1 the crack velocity increases at lower K_I-values. The reason for this is that the crack propagated so much that the test specimen broke and the crack velocity accelerated towards the end (with the load relaxation method the testing is started at high K_I-values and the crack growth causes K_I to decrease with a consequent reduction in V). The last two measuring points (denoted (.)) have therefore not been included in the fitting.

The conclusion that can be drawn from this test is that the values obtained correspond to the data published in the literature.

3.4
Fracture toughness, K_{IC}

The fracture toughness has been determined with double-torsion test specimens, which have been loaded until failure occurred. If the crack length fulfills the condition according to Eq. (4), K_I is independent of the crack length and K_{IC} can be determined from the value of the failure load P_c.

The following values were obtained for three test specimens:

K_{IC} = 6.1, 6.0 and 6.4 $MNm^{3/2}$

The mean value of K_{IC} was therefore 6.2 $MNm^{-3/2}$ and the standard deviation 0.2 $MNm^{-3/2}$

4
REFERENCES

1. Dahle, T.: Fördröjda brott i keramiska material (Delayed failure in ceramic materials). ASEA Technical Report KYDP 77-7101.

2. Evans, A.G., et al.: Acoustic emission and crack propagation in polycrystalline alumina. Mat. Sci. and Eng., 15(1974), pp. 253-261.

3. Trantina, G.G.: Stress analysis of the double-torsion specimen. Journ. of the Amer. Cer. Soc. 60(1977): 7-8, pp. 338-341.

4. Pletka, B.J.: An evaluation of double torsion testing-experimental. (To be published).

5. Wiederhorn, S.M., et al.: Stress corrosion and static fatigue of glass. Journ. of Amer. Cer. Soc., 53(1970):10, pp. 543-548.

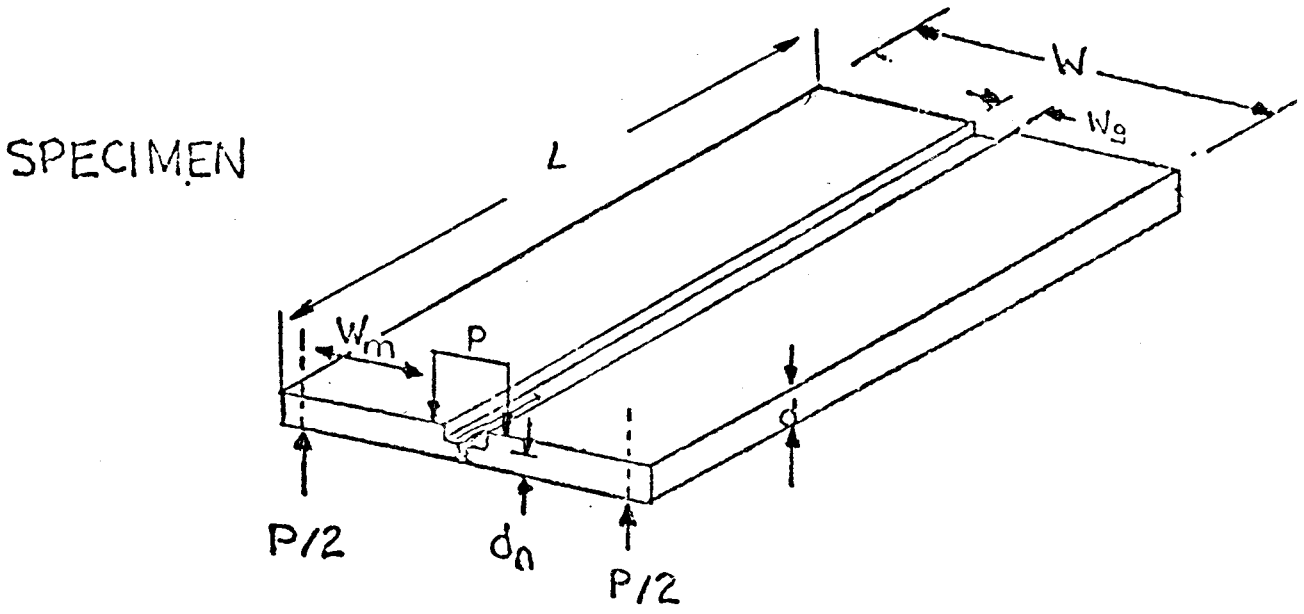

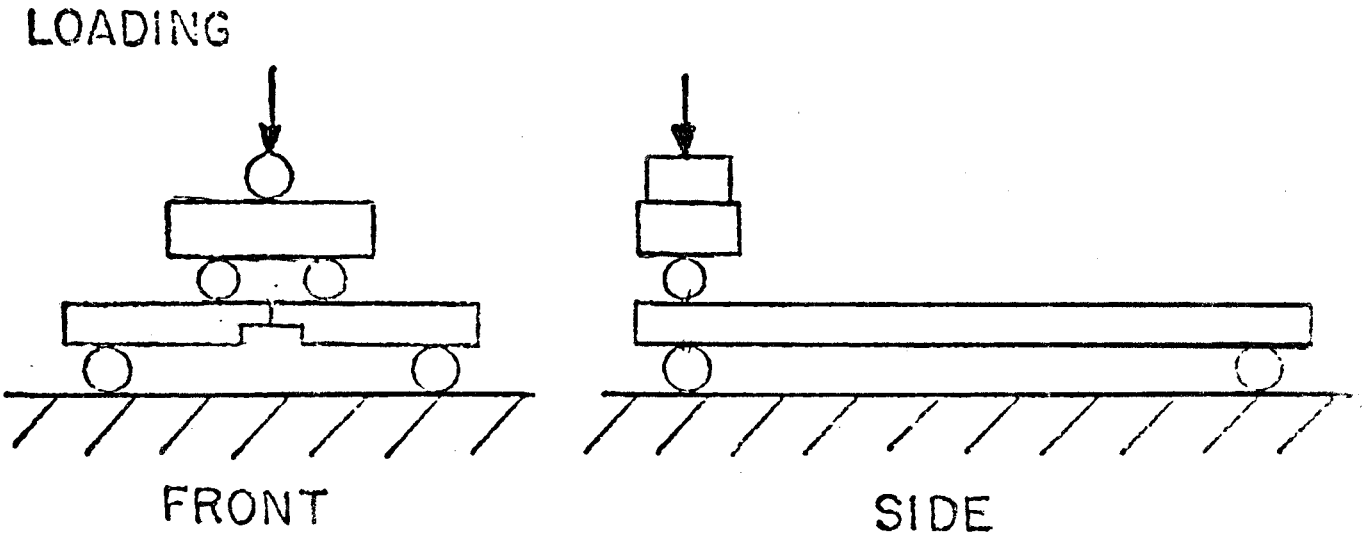

Fig 1

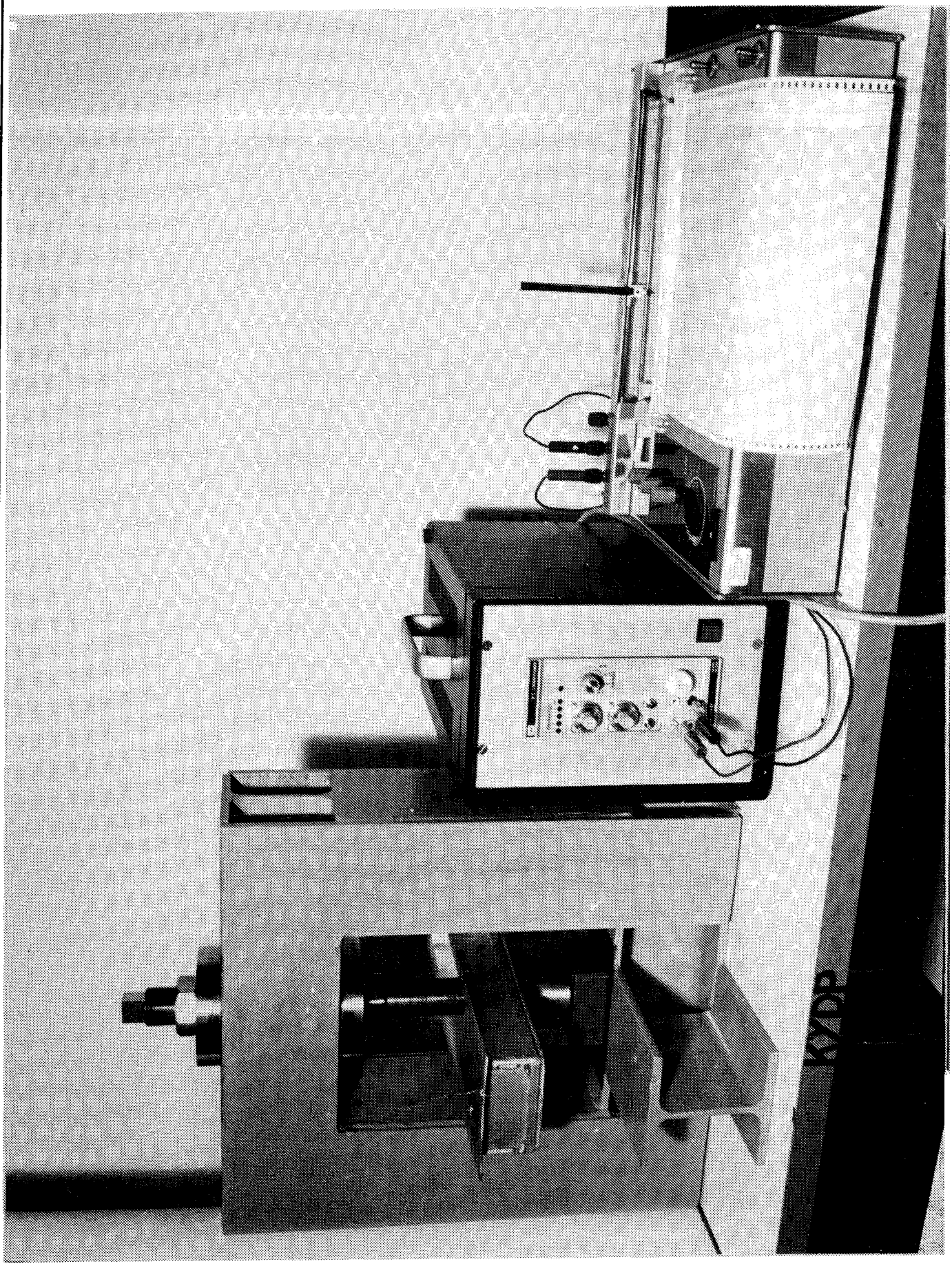

Fig 6

Environment for the testing and ageing

Ground water environment 1

In five parts by volume of "ground water" according to the KBS recipe (see Appendix 4) is mixed at the testing temperature (21°C and 90°C) one part by volume of a mixture of 90 per cent by weight quartz sand and 10 per cent by weight bentonite. The quartz sand and bentonite are separated by filtering. To the filtrate is added 0.5 per cent by weight H_2O_2 in the form of 10 per cent by weight agueous solution, 10 per cent by weight of the above-mentioned mixture of quartz sand and bentonite, 5 per cent by weight fine-grain powder of Al_2O_3-hydrate and 5 per cent by weight fine-grain powder of Fe_2O_3-hydrate. The content of H_2O_2 in the filtrate of the liquid according to the above must not be less than 0.1 per cent by weight during the testing and shall be regularly checked with the iodo thiosulphate method.

Ground water environment 2

To the ground water according to the KBS recipe (Appendix 4) is added 0.5 per cent by weight H_2O_2 in the form of 10 per cent aqueous solution and 10 per cent by weight finely crushed pure granite. The water is changed once a week without the test specimens being allowed to dry out. The content of H_2O_2 in the filtrate of the liquid must not be less than 0.1 per cent by weight during the testing and shall be regularly checked by means of the iodo-thiosulphate method.

Ageing procedure

To the ground water according to the KBS recipe (Appendix 4) is added 10 per cent by weight finely crushed granite. The liquid is used for autoclaving of the test specimens at 140°C. The autoclave is filled with oxygen prior to the testing. Venting of the air must not take place (the total pressure will be about 5 bar). The liquid is changed twice a week without the test specimens being allowed to dry out.

"Ground water" for leaching of ceramics

All types of ion are given in mg/l

Recipe

Salts (corresponding)	mg/l	HCO_3^-	Ca^{2+}	Mg^{2+}	Na^+	K^+	Fe^{2+}	Mn^{2+}	SiO_2	NH_4^+	NO_3^-	Cl^-	F^-	NO_2^-	SO_4^{2-}
$NaHCO_3$	165,2	120			45,23										
K_2SO_4	31,2					14,0									17,19
$MnSO_4$	2,8							1,02							1,78
$(H_4N)_2SO_4$	0,37									0,1					0,27
NaF	3,3				1,81								1,49		
$NaNO_3$	0,4				0,108						0,292				
$NaNO_2$	0,3				0,1									0,2	
SiO_2	30								30						
$CaCl_2$	185,3		66,89									118,41			
$MgCl_2$	166,9			30,0								136,93			
Na_2SO_4	109,3				35,4										73,9
NaCl	568,1				223,5							344,66			
$FeSO_4$	10,9						4,0								6,9
		120	66,9	30,0	306,1	14,0	4,0	1,0	30	0,1	0,3	600	1,5	0,2	100,0

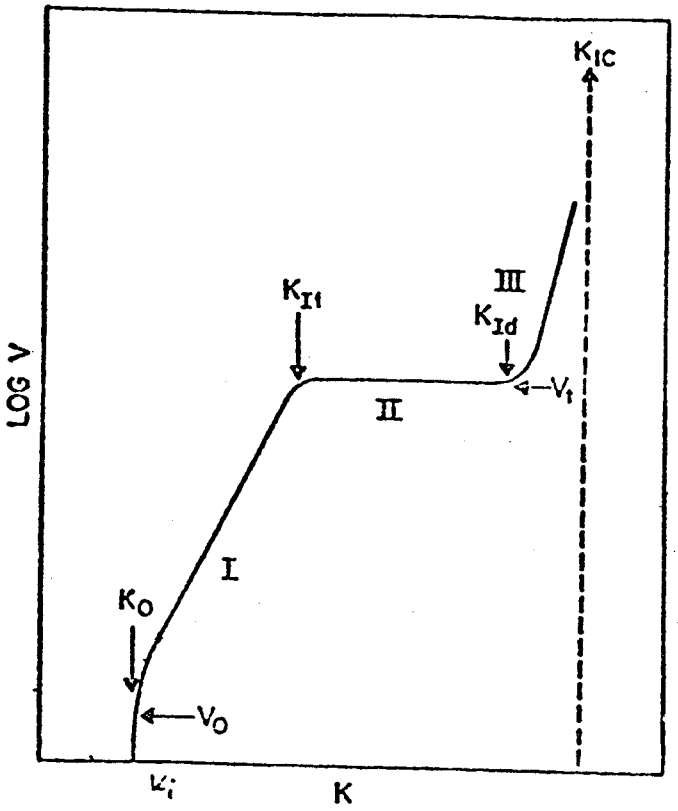

Fig. 3

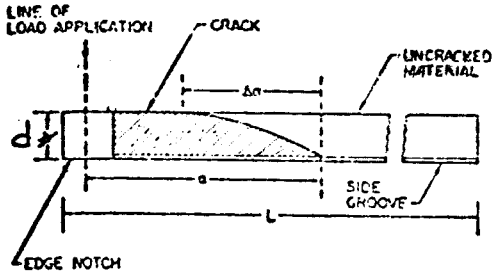

The crack front in the test specimen, showing that the crack extends further along the lower face.

Fig. 4

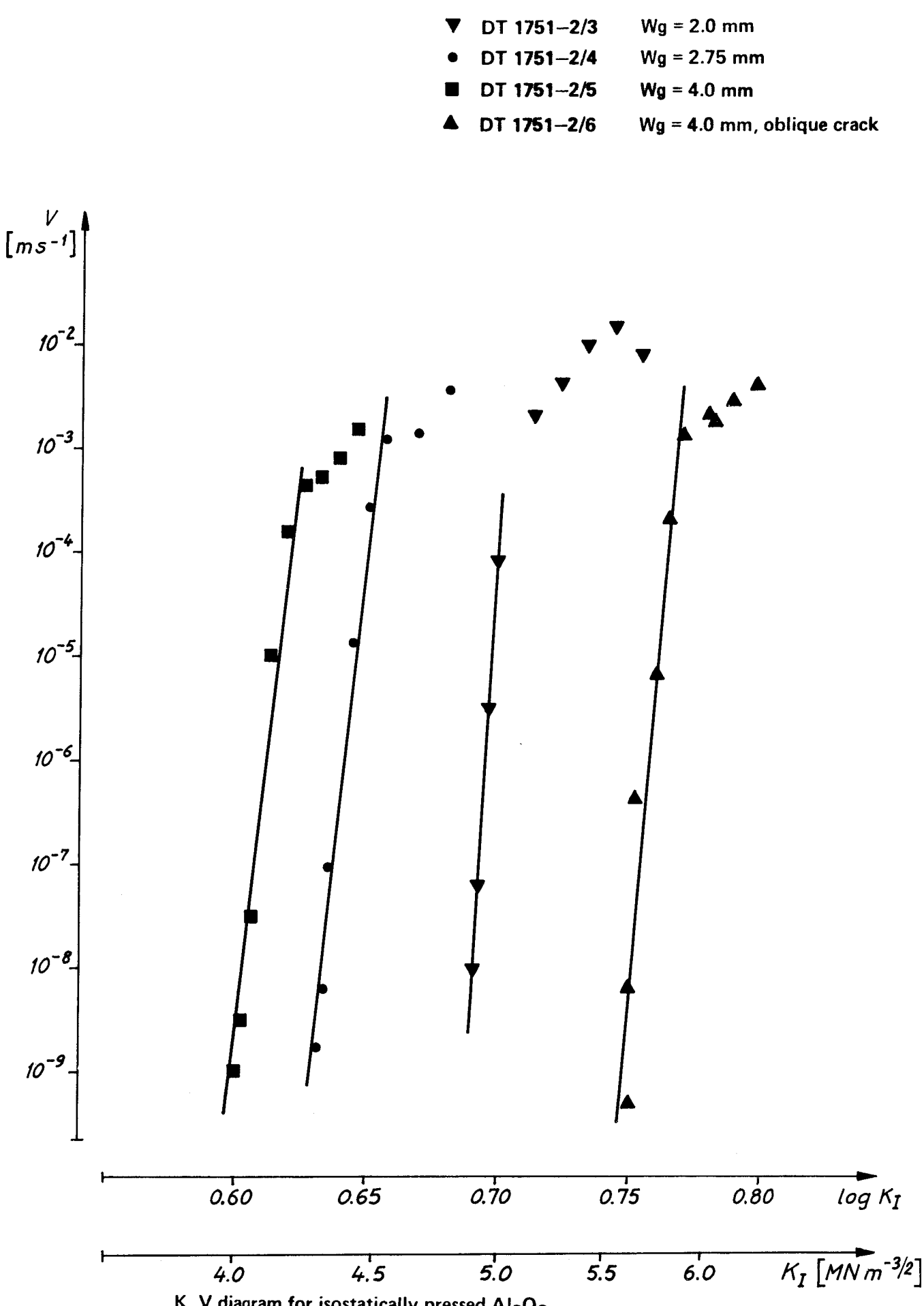

K, V diagram for isostatically pressed Al_2O_3

Test specimen I

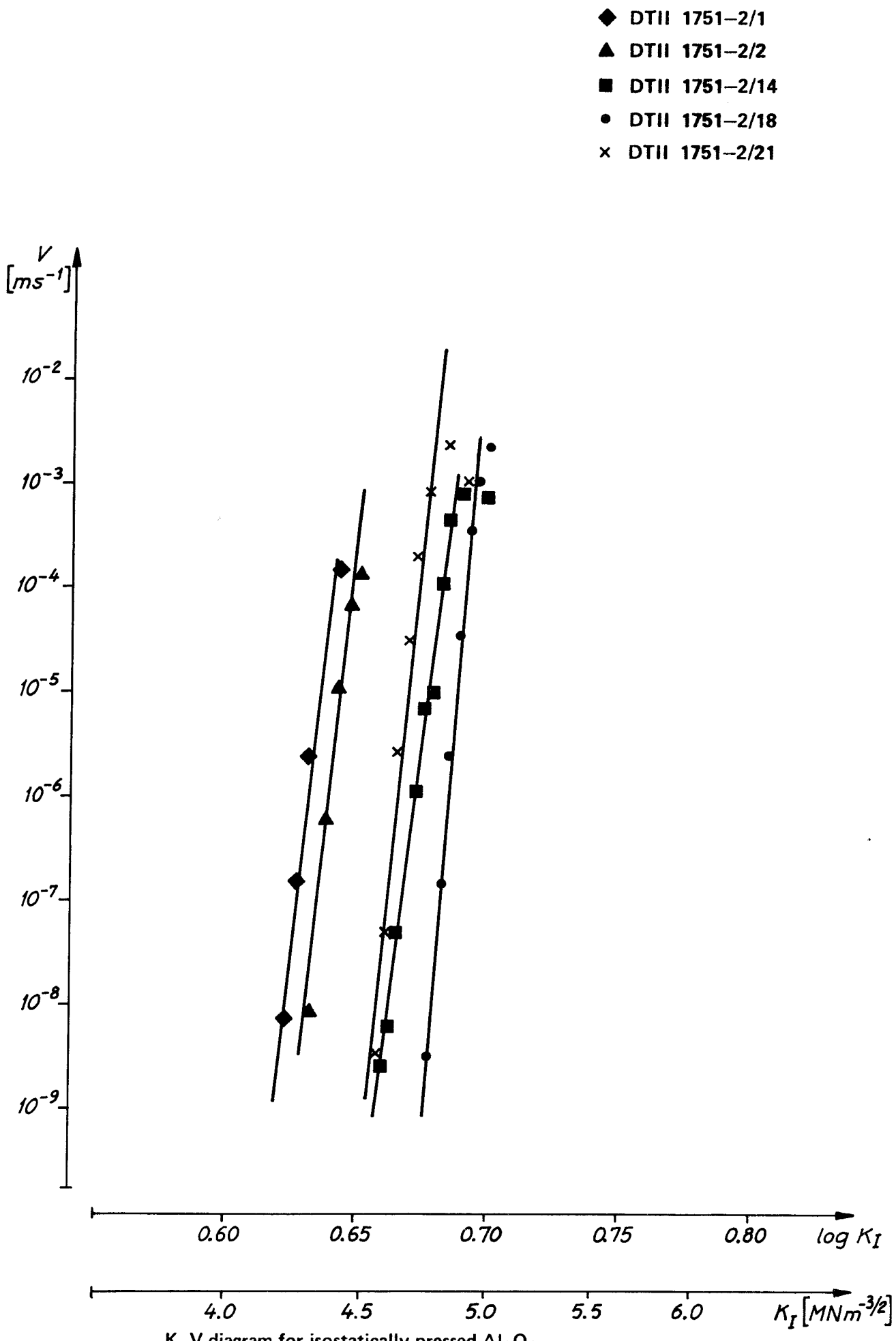

K, V diagram for isostatically pressed Al_2O_3
Test specimen II

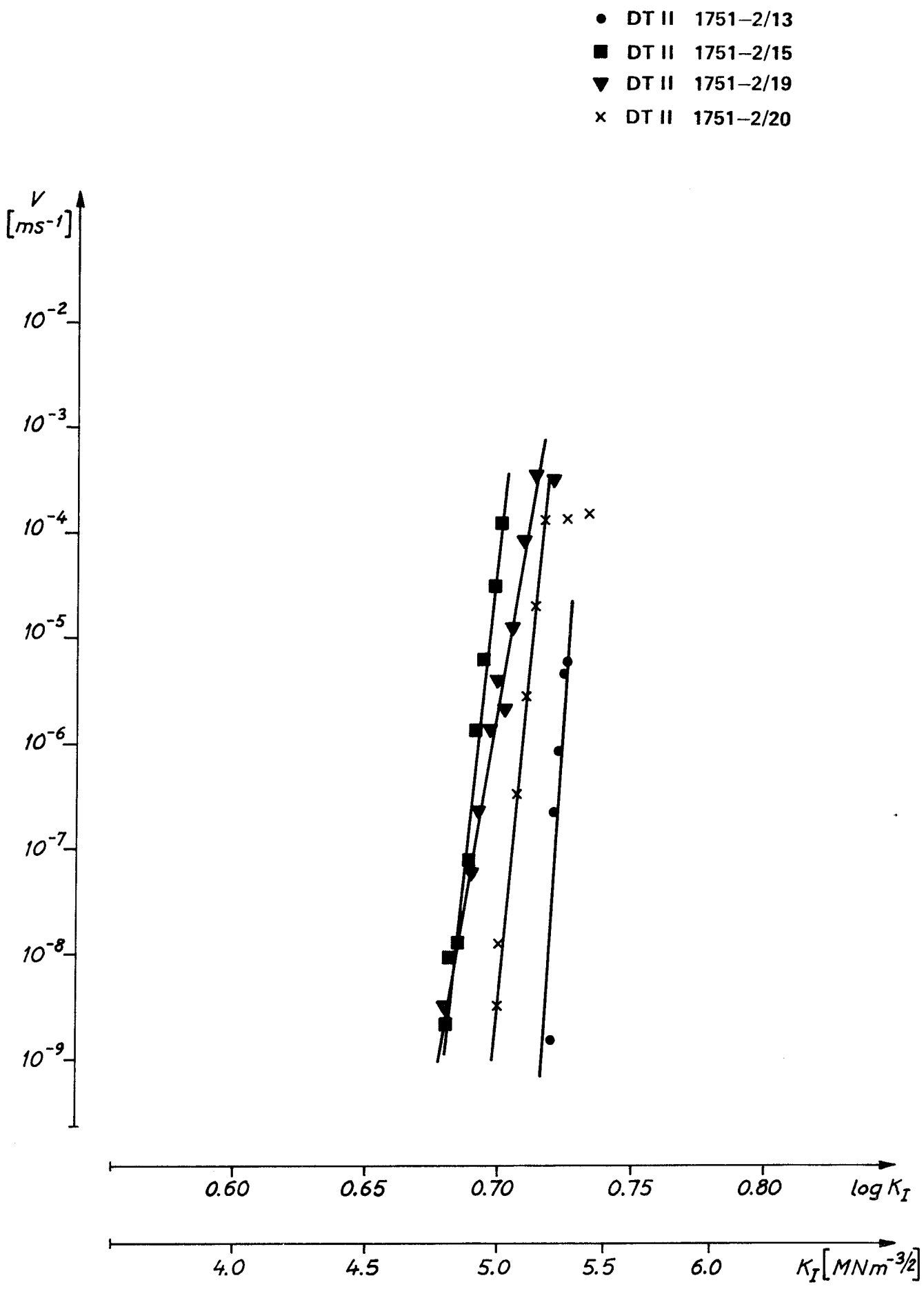

K, V diagram for isostatically pressed Al_2O3
Test specimen II, oblique crack

Table 1

A and n in Eq. (1) calculated from the K, V diagrams in Appendices 6-8.

$V = AK_I^n$; $\log V = \log A + n \log K_I$

Test specimen type	Wg	Test No.	Log A	n	Remains
W = 50 mm L = 150 mm	2.0 mm	DT 1751-2/3	-236	330	
"	2.75 mm	DT 1751-2/4	-159	238	
"	4.0 mm	DT 1751-2/5	-148	232	
"	4.0 mm	DT 1751-2/6	-232	298	Oblique crack
W = 25 mm L = 75 mm	3.0	DT II 1751-2/1	-150	227	
"	3.0 mm	DT II 1751-2/2	-161	243	
"	3.0 mm	DT II 1751-2/14	-146	208	
"	3.0 mm	DT II 1751-2/18	-245	349	
"	3.0 mm	DT II 1751-2/21	-173	251	
"	3.0 mm	DT II 1751-2/13	-300	407	Oblique crack
"	3.0 mm	DT II 1751-2/15	-171	239	"-
"	3.0 mm	DT II 1751-2/19	-110	150	"-
"	3.0 mm	DT II 1751-2/20	-232	319	"-

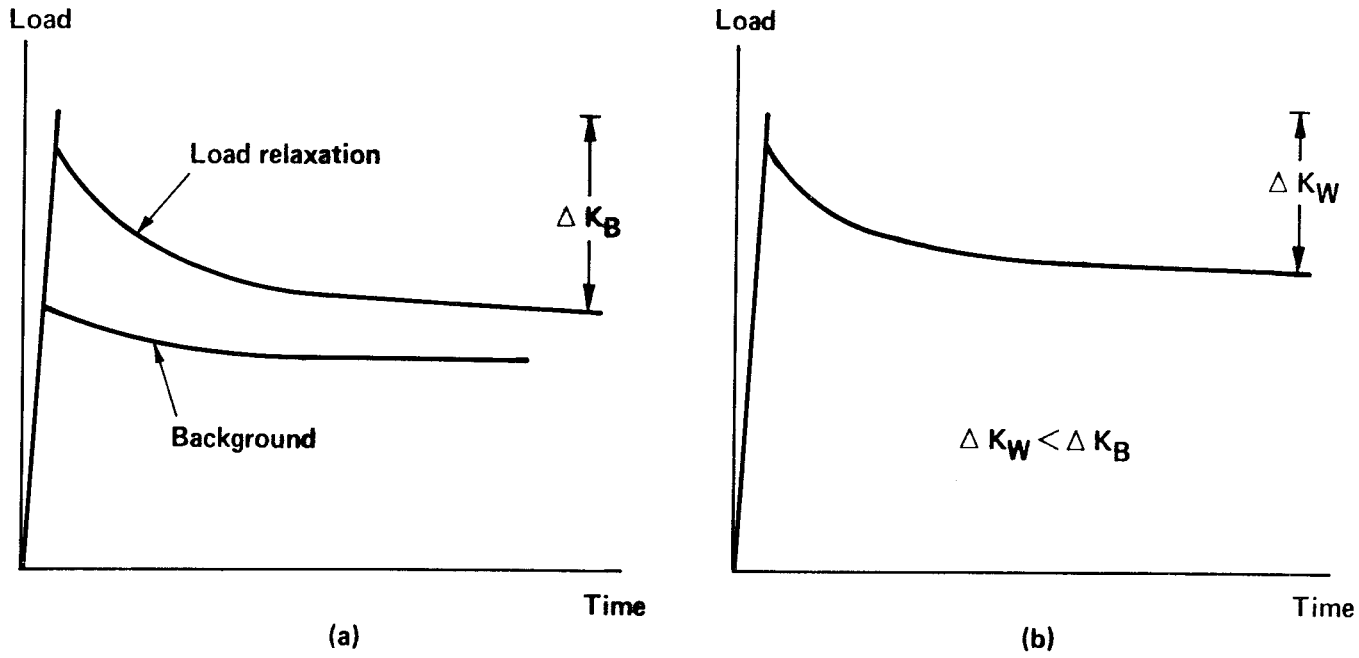

Figure 5.a. Typical load relaxation and background curves

Figure 5.b. After minimizing the background relaxation the total range of K_I measured in the test, ΔK_W, is smaller than when excessive background relaxation is present in Figure 4.a, ΔK_B. If uncorrected, the presence of the background relaxation results in the calculation of low values of n.

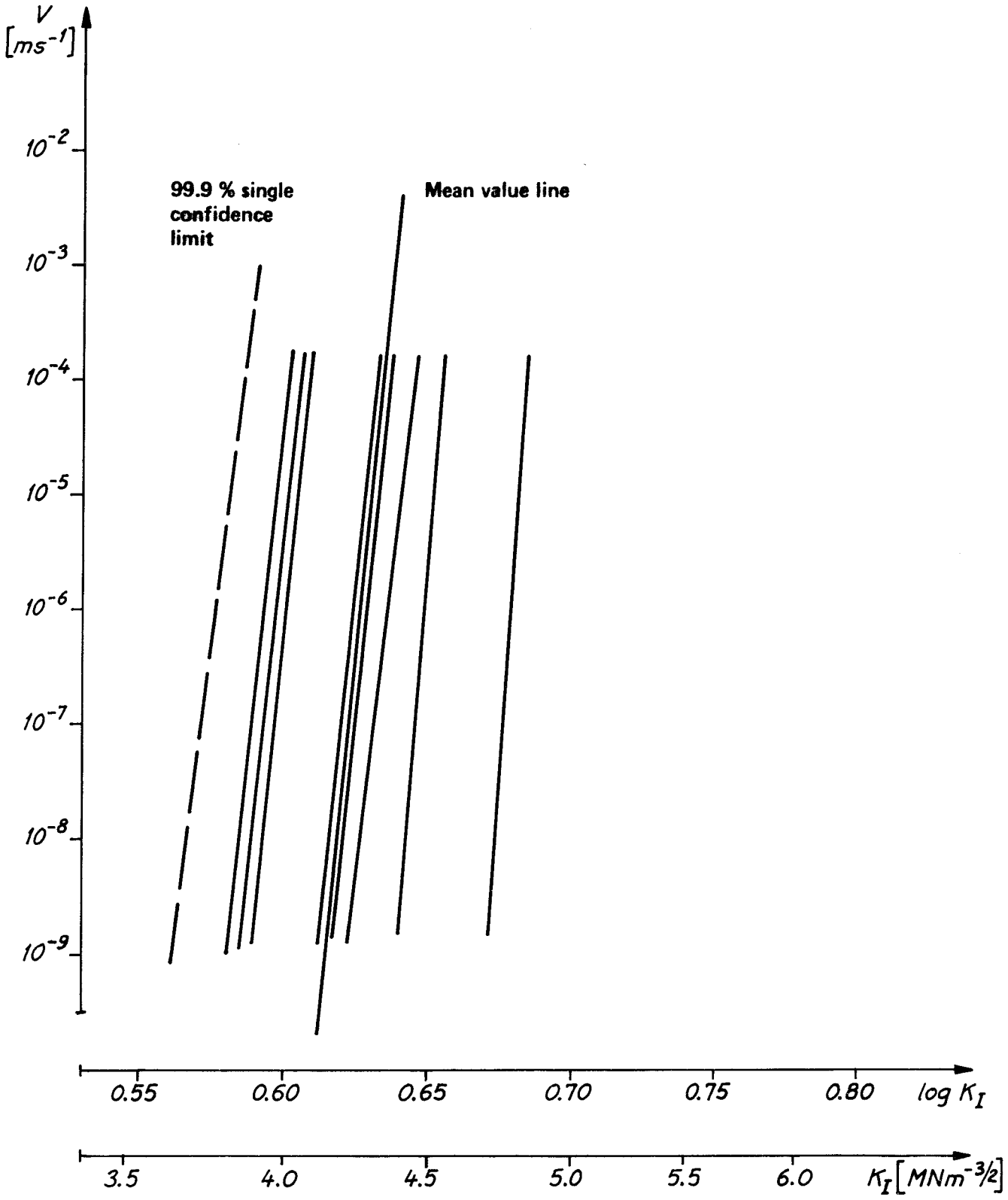

K, V lines for perfect test specimens corrected for error sources

Table 2 Analysis of tested glass (contents given in per cent by weight)

	SiO_2	Al_2O_3	Fe_2O_3	CaO	MgO	Na_2O	K_2O	B_2O_2
Tested glass	72.6	1.1	0.07	8.6	3.8	13.3	0.35	traces
Glass acc. to ref. (5) (soda-lime silicate)	72.0	2.0		7.0	4.0	14.0	1.0	

Tabel 3 Values of the constants A and n

Test No.	A	n
1	0.03	12
2	9.77	19
3	184	23
Acc. to ref. (5) (soda-lime silicate) Tested in distilled water	0.71	15
Acc. to ref. (4) (soda-lime silicate) Tested in distilled water	Not available	11-30

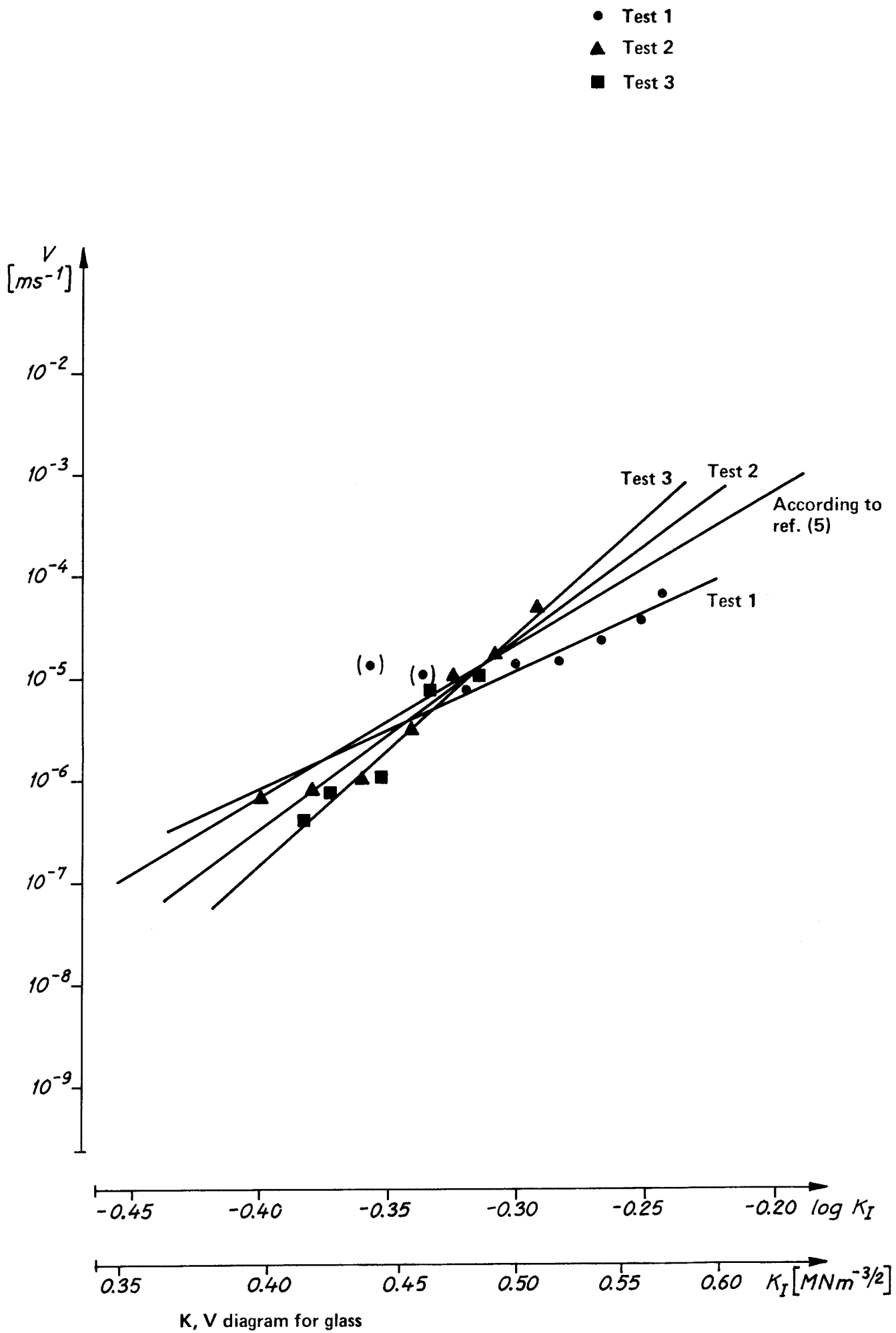

K, V diagram for glass

ULTRASONIC TESTING

Testing strategy

One method to check that the synthetic corundum canister does not contain unpermitted defects is ultrasonic testing. Containers and lids are tested directly after fabrication, with regard to both internal defects which could disqualify them for the sealing operation and surface defects that are determinant for the life of the canister in the final repository. An approved container is loaded with spent nuclear fuel and the container is joined together with an approved lid in a sealing pressing operation. After joining, the joint is checked ultrasonically in order to ensure a perfect bond. An additional scan of surface defects is also performed in order to make sure that dangerous surface cracks have not been created during the joining process. The residual tensile stresses in the surface of the canister which, under the influence of water, can cause any surface defects that might be present to grow slowly are only present in the upper part of the container. Scanning for small surface defects is therefore carried out from the joint to a point 1 m down on the canister.

Testing method

Ultrasonic testing is carried out in the form of immersion testing, whereby the ceramic canister is immersed in a tank of water. The material is scanned by moving the ultrasonic probe, also immersed in the water, along the canister at different angles of inclination. The canister can be rotated so that different generatrices can be scanned. A helical scanning track is obtained if the canister is rotated at the same time as the probe is moved axially.

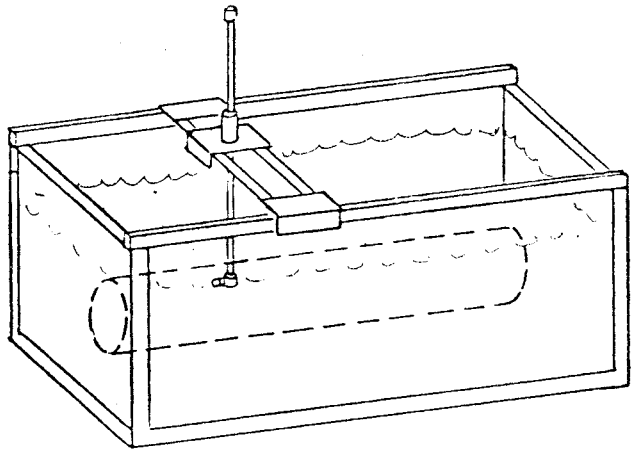

The Technical X-ray Centre (TRC) has carried out thorough tests of the testability of the aluminium oxide and the influence of the steel shell in connection with immersion testing. Appendix 1 contains a detailed description of the testing procedure for a ceramic canister and shows that the resolution is sufficient to detect critical defects.

In its rough outlines, the testing procedure involves the following:

- Scanning of internal defects is carried out both with a normal incident sound wave and with an angled incident sound wave and with a helical scanning path.

- Scanning of small external defects is carried out primarily in order to detect tangential cracks, since the largest positive residual stresses are axially directed. With a sound path as shown in the figure, cracks with a depth of about 1 mm and larger can be indicated in the ceramic surface of the canister.

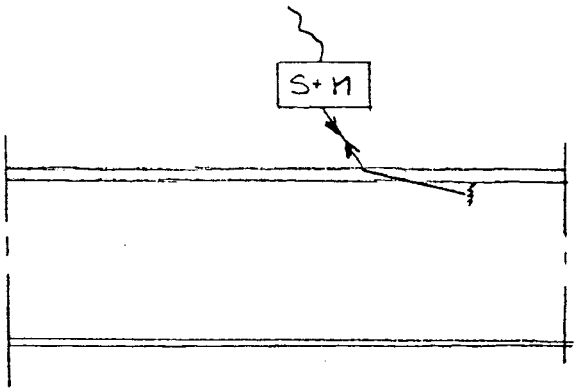

- The joint is also tested with an angled incident sound wave, where regions with poor bonding give a false echo.

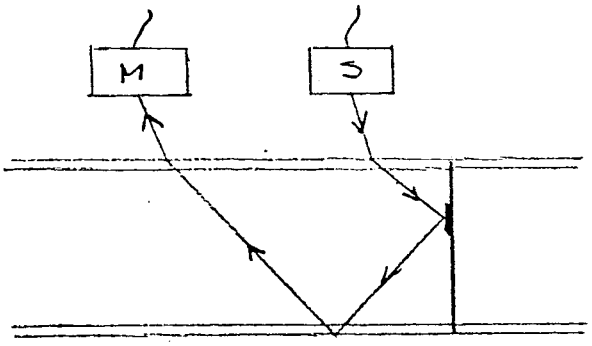

Appendix 1

METHOD FOR ULTRASONIC TESTING OF CERAMIC CONTAINER FOR ENCAPSULATION OF SPENT NUCLEAR FUEL

1. Test object

2. Test methodology

3. Testability

4. Testing procedure

5. Equipment

1. Test object

Container consisting of cylindrical portion and lid with a wall of aluminium oxide, externally and internally clad with a metal shell.

After the cylinder and the lid have been joined together, the container is enclosed by yet another metal shell 3 mm in thickness.

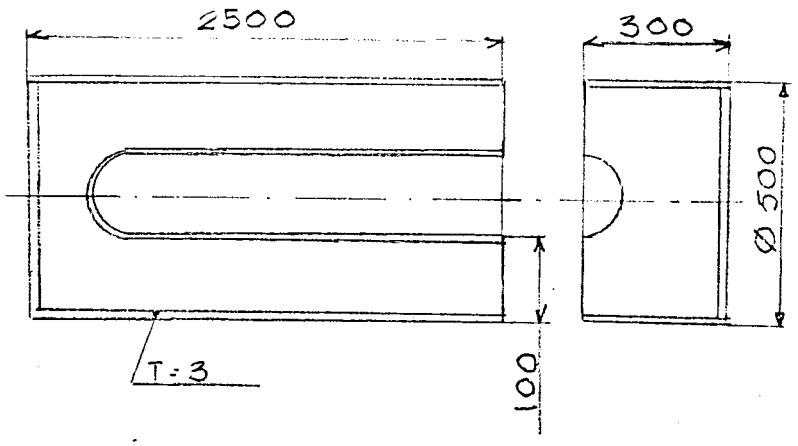

2. Test methodology

Conventional immersion technique with water as the coupling medium according to the pulseecho method.

The ultrasonic probes (transducers) work according to two principles:

1) The probe works both as a transmitter and a receiver, points a, b and d under the heading "Testing procedures".

2) The probe works only as a transmitter or a receiver, points c and d under the heading "Testing procedure" (tandem technique)

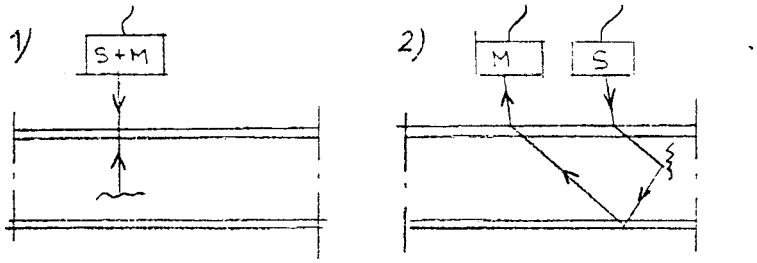

3. Testability

Aluminium oxide of the composition in question can, after the ultrasonic tests that have been conducted, be considered to be fully testable by means of ultrasonics. Sound transmission in the material is judged as good and with ordinary attenuation in the material.

The velocity of sound in ceramic has been measured at 11 000 m/s for longitudinal waves and 6 300 m/s for transverse waves.

The density of aluminium oxide = 3.97×10^3 kg/m^3.

Acoustic impedance for aluminium oxide is 42 kg/mm^2, second and for steel 45 kg/mm^2, second.

One of the reasons why the testability of the container can be considered to be good is that the acoustic impedance of aluminium oxide is very close to the acoustic impedance of steel.

On the basis of the acoustic impedances, it is found that only 3% of the impingent energy in the incident sound wave is reflected in the interface between the steel shell and the ceramic material.

This means that there are no problems with sound transmission between the two component materials.

Interferences in the form of structural indications or high noise level in relation to received signals have not occurred. The signal-to-noise ratio in all cases has been 4:1 or better.

4. Testing procedure

Testing is carried out by rotating the container or the lid at the same time as the ultrasonic probe(s) is (are) moved axially, producing a helical scan of the object.

All scans take place from the cylindrical part of the container.

The scans are divided into two phases, of which the first phase is testing of container and lid in the unsealed condition and phase 2 is testing in the sealed condition.

In the first phase, testing is carried out according to points a - d below, and in phase 2, testing is carried out according to points a, c, d and e.

A prerequisite for such scanning with acceptable results is that the bond between the steel shell and the aluminium oxide, and between the steel shells is perfect.

In the tests that have been carried out, the bond has been fully acceptable from the viewpoint of ultrasonics, and no problems have been caused by imperfect bonding.

The ultrasonic probes that are used may not be exposed to higher temperatures than about 50°C, and in order to ensure that the coupling medium does not exceed this temperature, the equipment is built so that water can circulate, guaranteeing that the temperature limit will not be exceeded.

The total scanning volume is divided into five different scans, depending on which type of defect is to be indicated:

a) Bond between steel and aluminium oxide and between steel shells.
The scan is performed with an incident sound wave 90° to the scanning surface. Bond flaws corresponding to min. Ø 5 mm are detected.

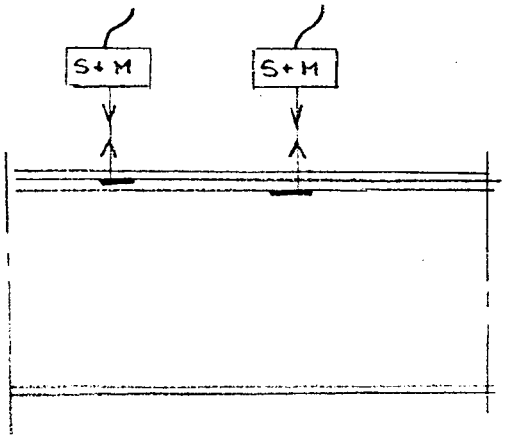

b) Volume defects such as inclusions of impurities are scanned with the indicent sound wave 90° to the scanning surface.

It is sufficient that internal defects with a reflecting surface of at least Ø 5 mm are detected. Any volume defects near the outer surface can be critical. These are detected by testing according to point d, where flaw detectability is increased so that flaws with a reflecting surface of Ø 3 mm can be detected within 10-20 mm of the scanning surface.

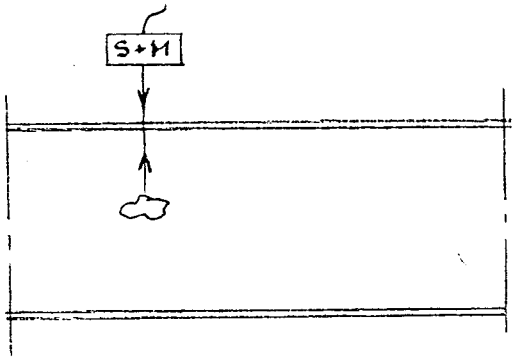

c) Large defects inside the volume, such as cracks, emanating from either surface with tangential/axial extension.

The scan shall detect cracks with a length of min. 50 mm and a depth of min. 25 mm.

Testing is carried out to make sure that the canister has not suffered damage due to e.g. a power failure during cooling after pressing or in connection with handling.

The angle of the incident sound wave in this scan is 45^{o}. The container is tested by means of the tandem technique. The lid is tested by means of conventional technique, where the probes operate as both transmitters and receivers.

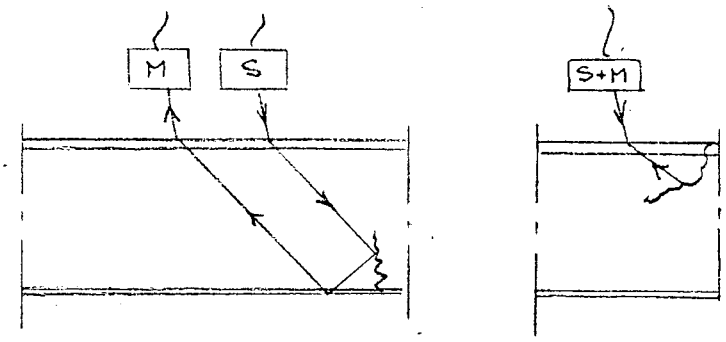

d) Small defects in the outer surface of the container and the lid, such as cracks oriented tangentially amd emanating from the interface between the aluminium oxide and the steel shell.

Defects with a depth of 1 mm and a length of 2 mm shall be detected. In previous studies of the testability of the material, surface defects in pure aluminium oxide with a depth of 0.6 mm have been detected.
The angle of the incident sound wave with the reflecting defect is 70^{o}.

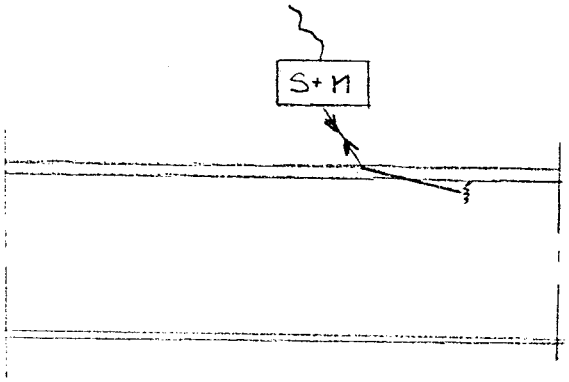

e) Scanning of the joint between the container and the lid, intended to detect defects (incomplete bonding) which follow the joint surface.

Defects with a reflecting surface of at least Ø 5 mm are considered to be large enough to detect. The scan is performed using tandem technique from the cylinder surface with a 45° angle of the indicident sound wave with the joint surface.

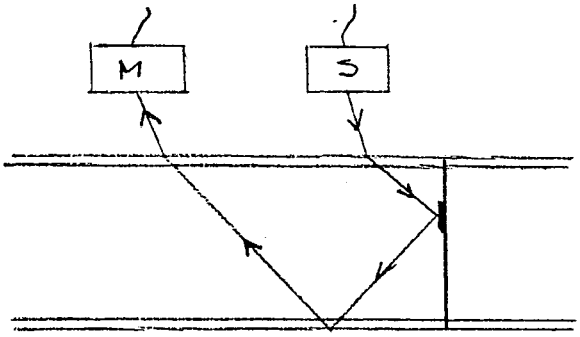

5. Testing equipment

The apparatus consists of the following components:

a) Immersion tank
b) Rail stand with rotary table and roller supports
c) Manipulator
d) Electronics for motor control, position and angle indication
e) Ultrasonic equipment
f) Ultrasonic probe
g) Recording equipment

For illustration of points a-c, see appended general drawing (No. 31634).

a) The tank consists of a framework lined with stainless steel. There is a system for cleaning and circulation of the water in the tank. The tank is of unit construction (self-supporting) and can be unloaded at both ends.

b) The stand rests on the tank framework and is sized according to the particular load in question. Devices for rotation of horizontal ceramic containers and a rotary table for testing lids are mounted in the stand.

c) The manipulator consists of the following units:
   a) Carriage for longitudinal movement (x)
   b) Carriage for transverse movement (y)
   c) Mast for vertical movement (z), rotatable 360° and anglable probe holder.

All movements can be controlled either manually or via remote control and are equipped with sensor systems for digital position and angle indication.

d) The above-described movements are controlled from an electronics unit, which can be controlled either manually or according to a program by a microprocessor.

e) The equipment consists of an ultrasonic unit of the system type, for example Krautkrämer KS 3000.

These systems include the following units:

a) Display unit
b) Time base unit
c) Amplifier unit
d) Amplitude monitor, running time monitor

f) In order to detect bond flaws between the external steel shell and the ceramic material as well as small cracks in the outer surface of the ceramic material with maximum sensitivy, focusing probes of the 2-crystal type, 2-6 MHz, and crystal size 10-20 mm are used. With this type of probe approximate resolution (i.e. the probe's ability to indicate and distinguish flaws immediately below the surface of the material) is very good.

For detection of large internal defects, volume defects, and scanning of the joint between the lid and the cylinder, non-focusing standard probes with crystal size about 20 mm are used.

Since production testing will take place in a radiological environment with a strong gamma field, it can be mentioned that the crystals in the ultrasonic probes are not affected by this, i.e. their testing sensitivity is not reduced and the test results are not affected in any other way.

This has been verified by placing scanners in the core region of a reactor at Studsvik and verifying sensitivity before and after.

Another consequence of the strong gamma field is that all ingoing movements in the equipment are remotecontrolled and adapted to the environment in question.

g) This equipment may contain the following alternatives as desired:

1) A-image presentation
shows the result in the form of a chart sheet with reflector.

2) B-image presentation
shows the result in a cross-section of the tested object.

3) C-image presentation
shows the result with the tested object viewed from above, i.e. from the surface from which testing takes place.

Test data can be recorded on magnetic tape for later evaluation with the aid of a computer.

The items of equipment described above are currently available on the market, so no extensive development work is necessary before a production unit can be put into operation.

TEKNISKA RÖNTGENCENTRALEN AB
(TECHNICAL X-RAY CENTRE LTD)
Technology
Special Testing

Glenn Sparw

Tol. för icke direkt toleranssatta mått enl. SMS. 715

Ytjämnhet där ej annat angives Ra √

Nr	Ant.	Ändring och eller medd -nr	Datum	Inf.	Gno

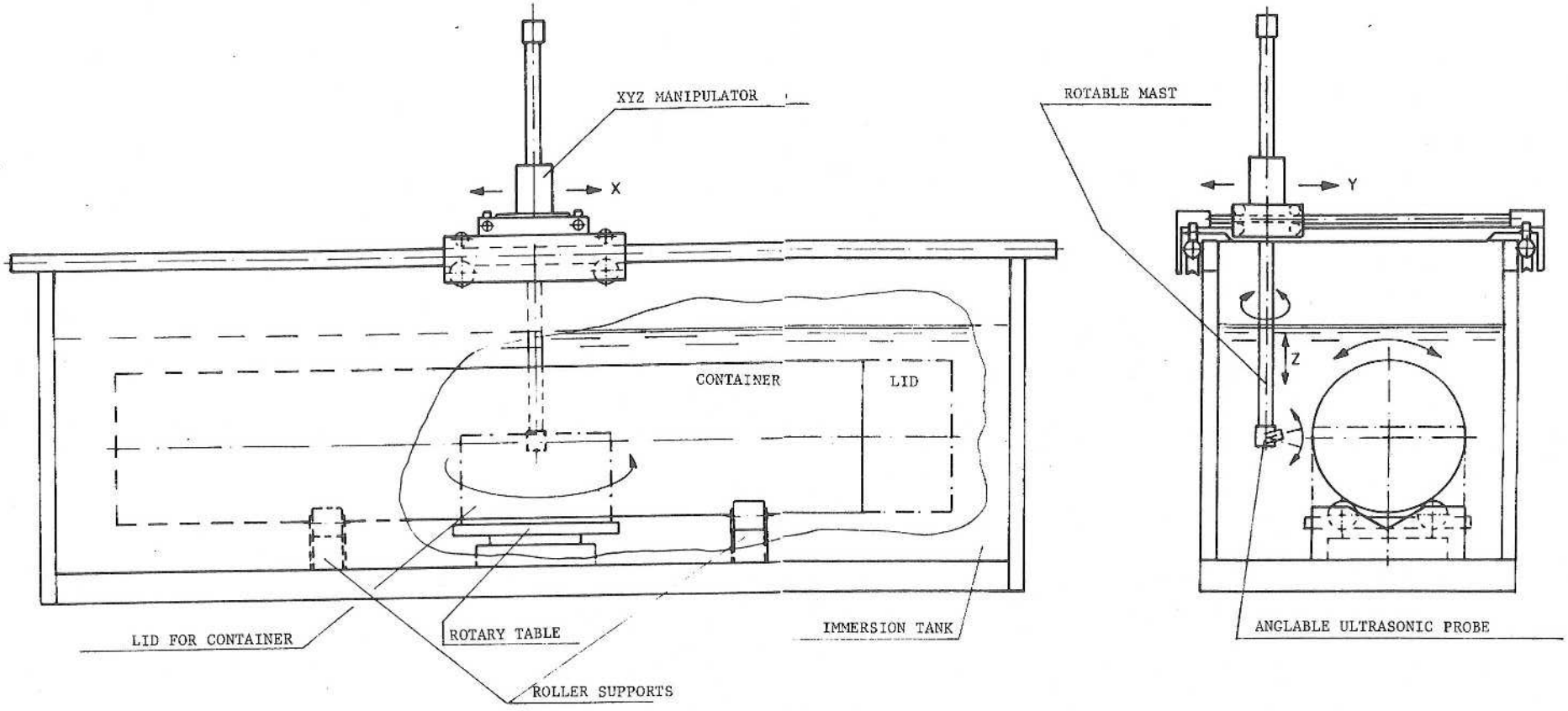

Der.-nr	Ant	Benämning	Material	Mod.-nr. Ämne Dimension	Anm
Konstr	Ritad BRC	Kop	Kontr.	Stand.	Godk.	Skala	Ersatter	Ersatt av
								Dat

TRC
TEKNISKA RÖNTGENCENTRALEN AB

IMMERSION TESTING EQUIPMENT FOR NUCLEAR FUEL CONTAINER
SCHEMATIC DRAWING

DRAWING No 31634

Stress distribution during proof testing of full-scale ceramic canister for WCP

Bertil Larsson

Summary

A calculation of the transient stress distribution during the proof testing of a full-scale canister has been performed. Due regard has been paid to residual stresses occurring during the cooling down after the pressing, and a temperature difference giving σ_z = 112 MN/m^2 in the outer surface of the synthetic corundum, at some distance from the ends, has been used as load. The assumed heating cycle takes about 2.5 h until steady-state conditions are reached.

The results show that σ_z = 112 MN/m^2 is obtained 290 mm from the open end and that σ_{zmax} = 126 MN/m^2 about 250 mm from the bottom surface. No stress components exceed their steady-state values during the heating stage.

The stress distribution obtained is fully acceptable for the proof testing with respect to the residual stresses occurring during the sealing of the cainster.

Introduction

This report presents calculated temperatures and the stress during the proof testing of ceramic canisters for WCP. The calculations have been made with the ALEXANDER and LUCAS programs for a two-dimensional, rotation symmetrical model.

Computing model

The figure in Appendix 1 shows the geometry of the canister. The computing model has been divided into two parts, one upper ($z > 1490$ mm) and one lower part ($z < 1490$ mm).

The following material data have been used for the calculations:

Al_2O_3	λ	$= 27.2 \times 10^{-3}$ W/(mm °C)
	α	$= 6.45 \times 10^{-6}$ $(°C)^{-1}$
	E	$= 390{,}000$ N/mm^2
	ν	$= 0.27$
	ρ	$= 3.98 \times 10^{-6}$ kg/mm^3
	c_p	$= 930$ Ws/kg °C
Steel	λ	$= 67 \times 10^{-3}$ W/(mm °C)
	α	$= 12 \times 10^{-6}$ $(°C)^{-1}$
	E	$= 205{,}000$ NOmm^2
	ν	$= 0.30$
	ρ	$= 7.80 \times 10^{-6}$ kg/mm^3
	c_p	$= 464$ Ws/kg °C

For the transient temperature calculations the temperatures of the inside and outside have been assumed to vary with time according to Appendix 2. The steady-state temperature difference corresponds to an axial stress in the outer surface of the corundum of σ_z = 112 MN/m^2. The actual temperature in the inner surface of the corundum has been assumed to be +150°C. To take into account residual stresses, occurring during the cooling down after the pressing, and the temperature drop across the steel jackets, the steady-state temperatures of the inner and outer surfaces have been set at -17.7°C and -106.4°C.

Results

The temperature calculation shows that steady state was reached after 2.5 h with the surface temperature according to Appendix 2. Appendices 3 and 4 show the steady-state temperature distribution in the upper and lower part. The power input during steady state was 76 kW and the maximum power required during the heating was about 84 kW. Appendix 5 shows the power input during the entire heating cycle.

Appendices 6 to 11 show stress distributions in the form of level diagrams for σ_z, σ_φ and the largest principal stress σ_{max}. These diagrams apply for a steady-state temperature distribution. The calculation shows that no tensile stresses, exceeding the steady-state ones, occur during the heating according to Appendix 2. At some distance from the ends σ_z = 112 MN/m^2 and σ_φ = 116 MN/m^2 are obtained.

Owing to imperfections in LUCAS the calculated stress in the nodes lying on the limit between zones with different material properties will be incorrect. The level diagrams are therefore incorrect for a 2-mm-thick layer along the inside and outside of the corundum (only on the inside of the upper part) and within a zone up to 20 mm from the open end. The solution in the other parts has not been influenced by this.

Appendix 12 shows the stresses σ_z and σ_φ in the outside of the corundum versus the distance from the end surface, while Appendix 15 shows the stresses in the zone close to the bottom. The stresses are influenced by end effects about 650 mm from the open end and 450 mm from the bottom surface.

σ_z reaches a value of 112 MN/m^2 290 mm from the open end and 200 mm from the bottom surface. After this there is a maximum value of σ_z lying 4 per cent above the desired value at the open end and 13 per cent above this close to the bottom. σ_φ shows a similar tendency, except that it increases by the open end.

The largest calculated tensile stress is σ_z = 126 MN/m^2 close to the bottom. At the open end σ_φ can be larger within a small zone, but it has not been able to prove this owing to the problems mentioned earlier with LUCAS. (For the 1/3-scale canister σ_φ in the end surface became 51 per cent higher than the value at som distance from the end.)

The diagrams in Appendices 13, 14, 16 and 17 show the distribution of σ_z and σ_φ at different times during the heating.

Comments

The residual stresses after the sealing of the canister will have their maximum value 450 to 530 mm from the joint according to an earlier report (Appendix EI). The calculations show that σ_z during the proof testing is influenced by end effects within this zone, but that the stress exceeds the desired value by 0 to 4 per cent. The proof testing will therefore be somewhat conservative.

The maximum value of σ_z close to the bottom (13 per cent too high) should preferably be reduced by lowering the temperature difference in this zone. The residual stresses after the sealing will be small here and no high proof testing stress is needed.

The hoop stress, σ_φ , is slightly larger than σ_z at some distance from the ends. This means that if the surface defects in the corundum are randomly oriented, any failures in most cases will take place through axially propagating cracks. Cracks initiated from defects perpendicular to the longitudinal axis can also be deflected and propagate axially.

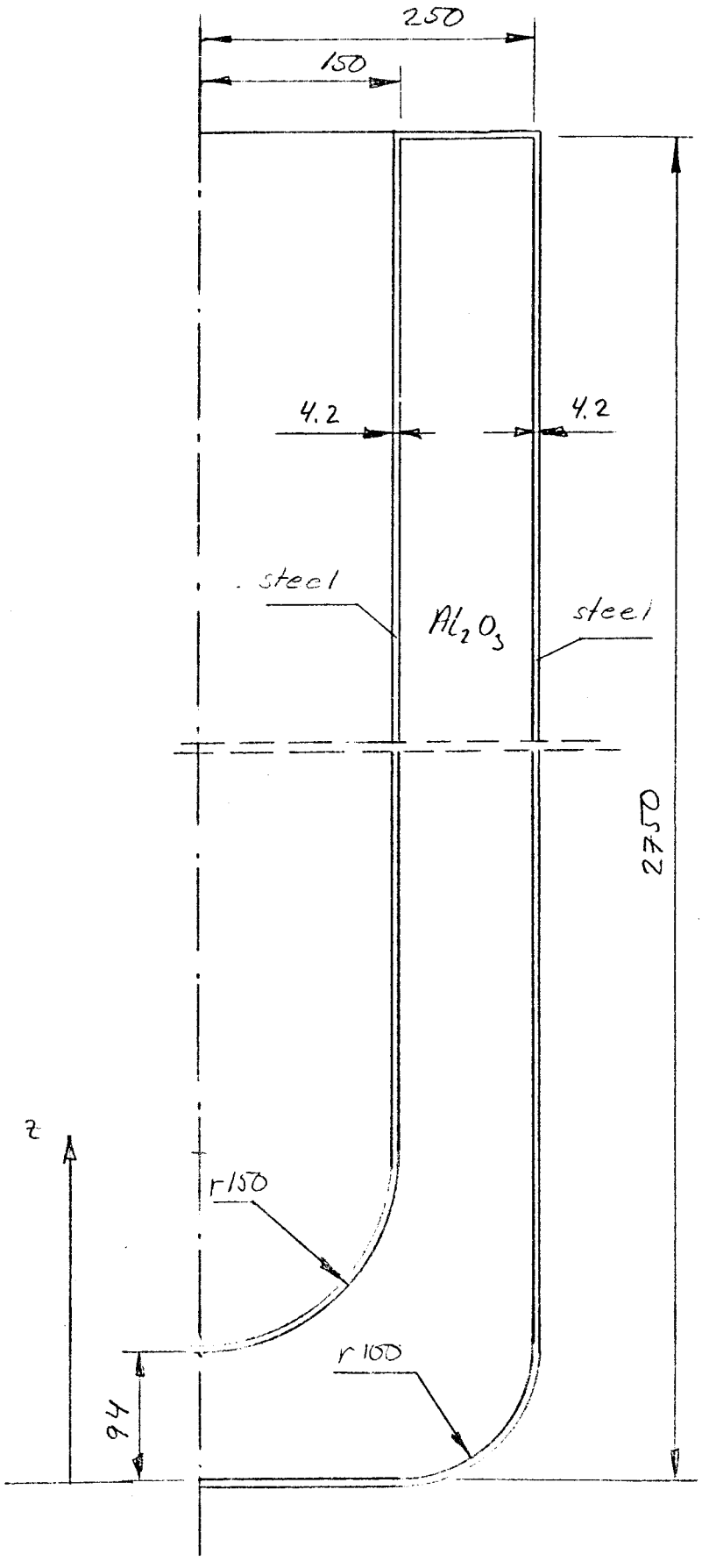

1526B/58B

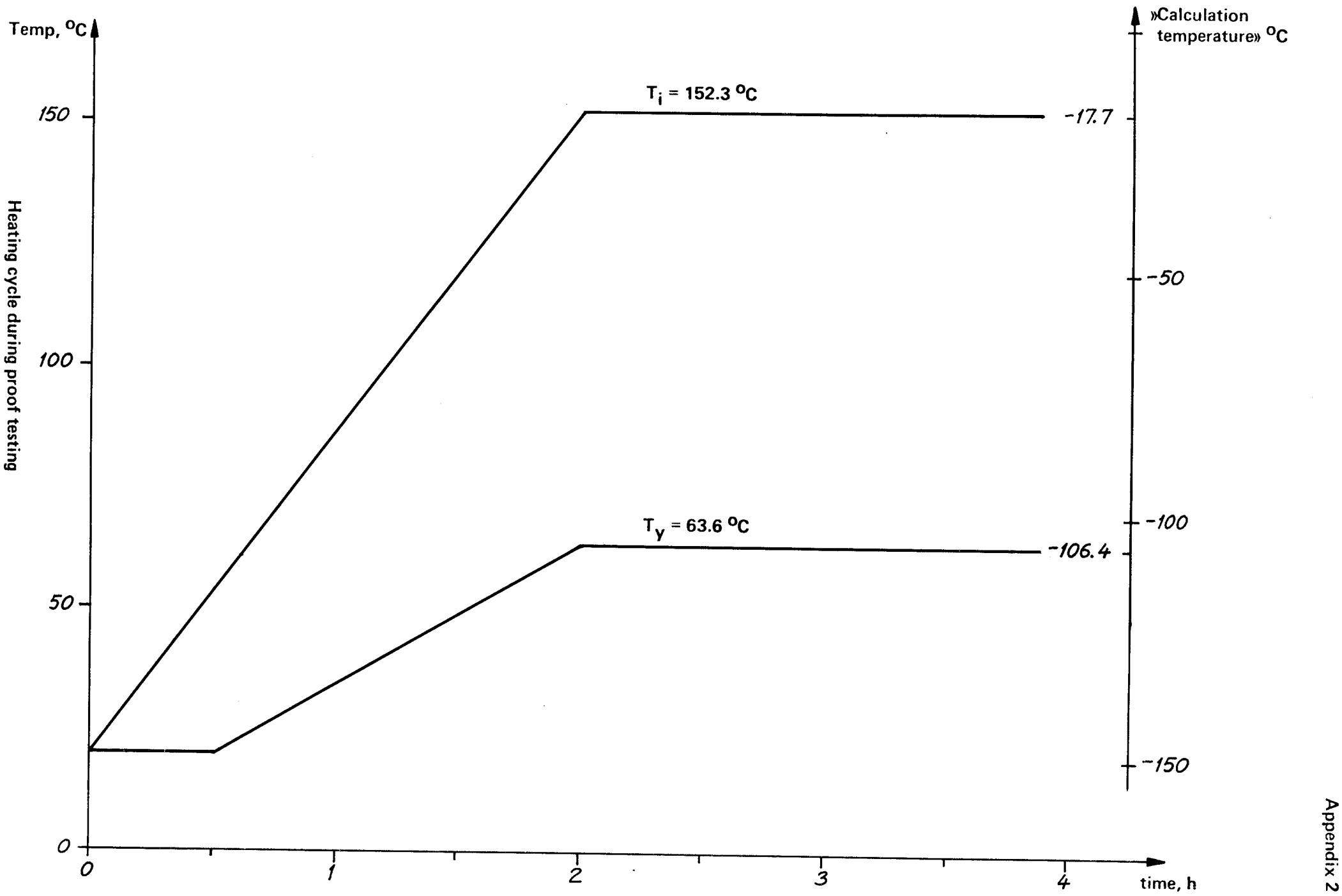
Temp, °C
150
100
50
0
Heating cycle during proof testing
T_i = 152.3 °C
T_y = 63.6 °C
»Calculation temperature» °C
-17.7
-50
-100
-106.4
-150
0
1
2
3
4
time, h

Appendix 2

Steady-state temperature distribution

Temp. = (Level − 26) 10 deg C

Appendix 3

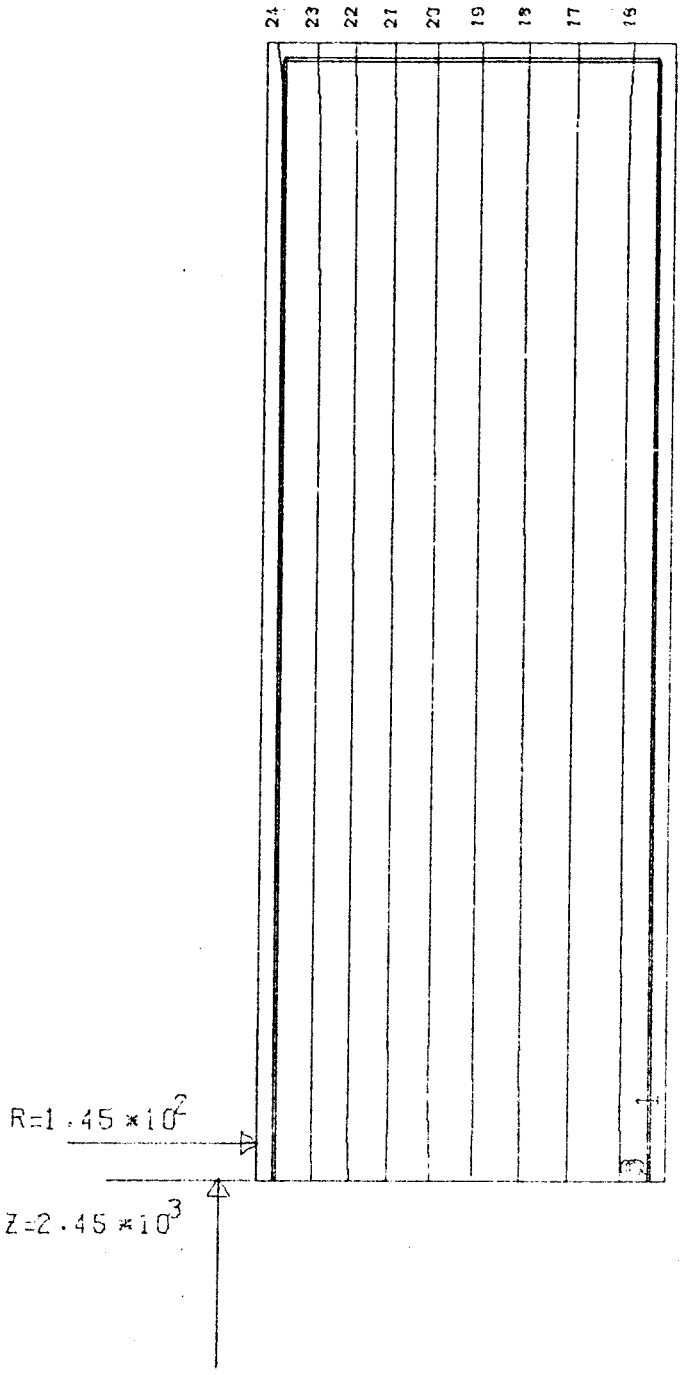

Steady-state temperature distribution.

Temp. = (Level - 96) / 10 deg. C

Appendix 4

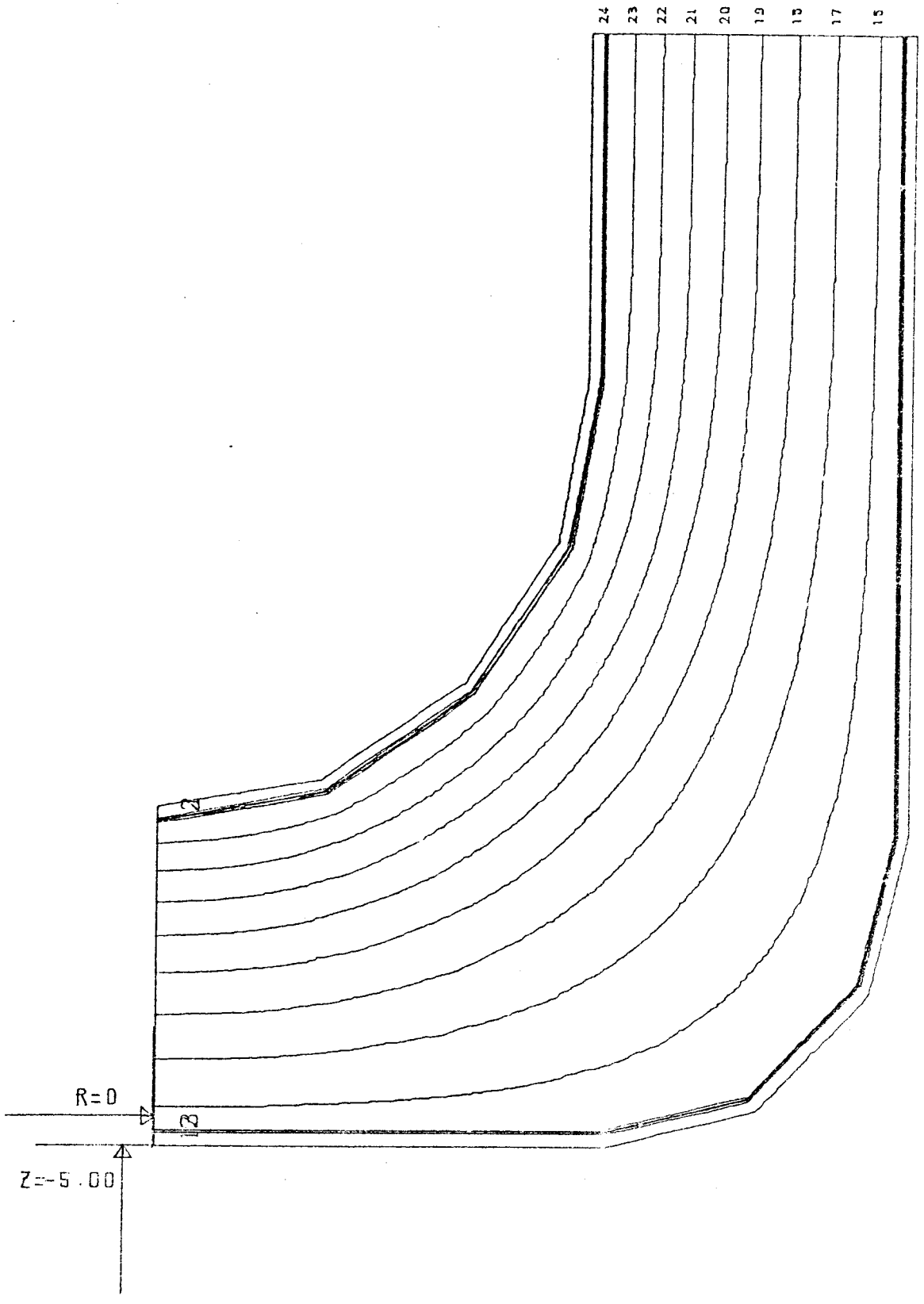

Power input during heating

Time h	Upper part kW	Lower part kW	Total kW
0.5	16.0	17.8	33.8
1.0	24.5	27.0	51.5
1.5	32.0	35.5	67.5
2.0	39.5	43.8	83.3
2.5 (steady-state)	36.0	40.0	76.0

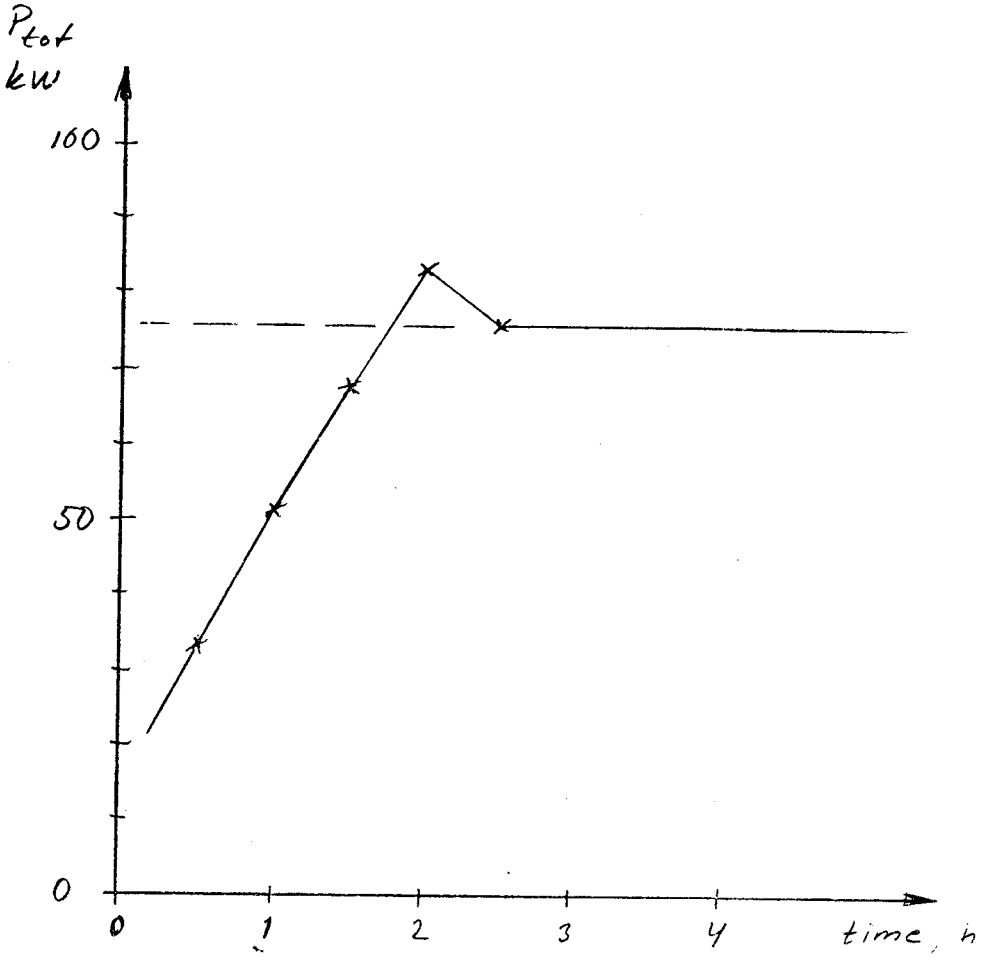

... stress distribution

1CM ≙ 20 UNITS

Stress = (Level) × 25 MN/m^2

Appendix 6

EQUISTRESSPLOT OF SIGMA-Z

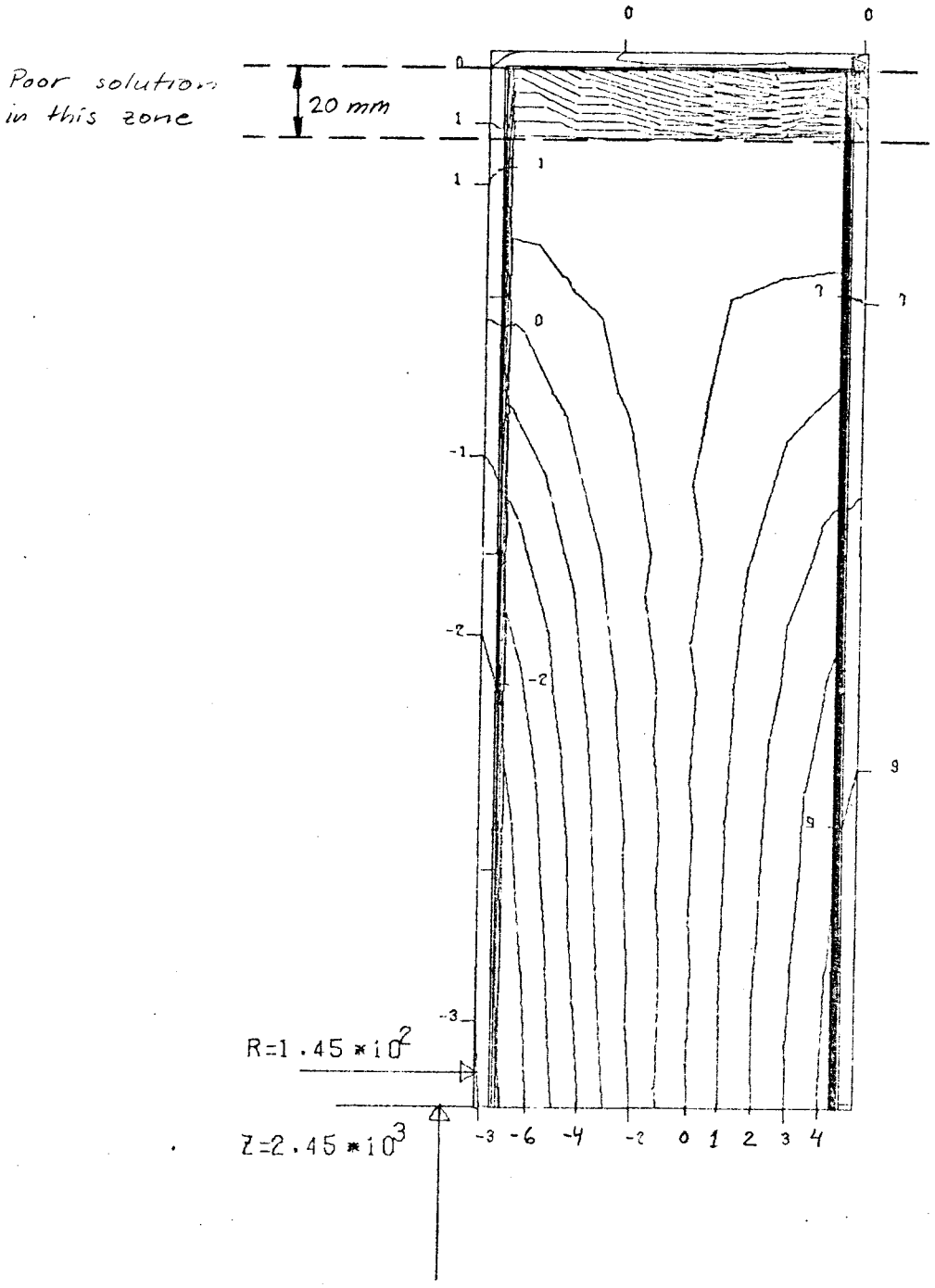

Steady-state stress distribution

Stress = (Level) × 25 MN/m²

1CM ≙ 20 UNITS

Appendix 7

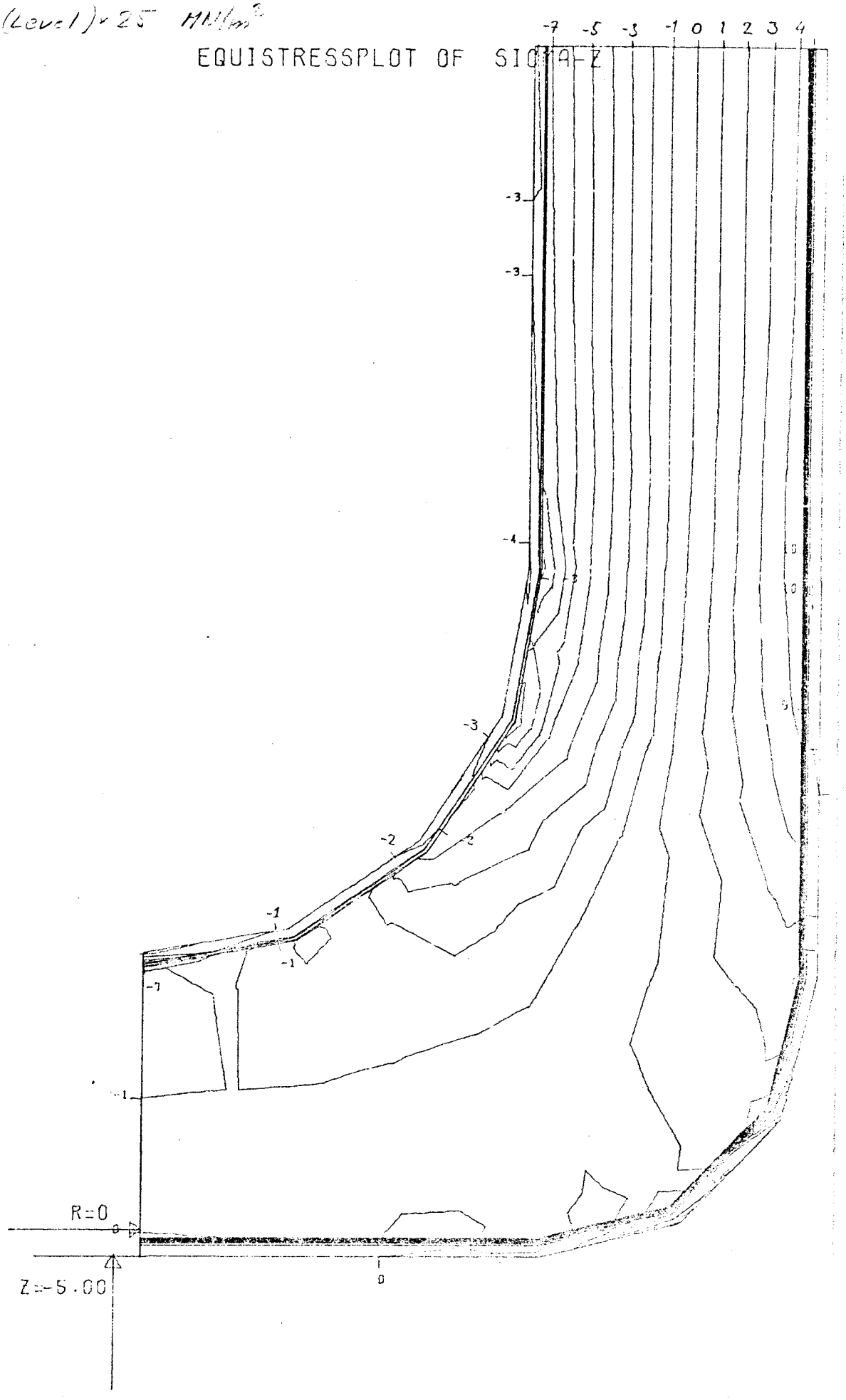

Stress-wave stress distribution

1CM ≙ 20 UNITS

Appendix C

Stress = (Level) × 25 MN/m²

EQUISTRESSPLOT OF SIGMA-FI

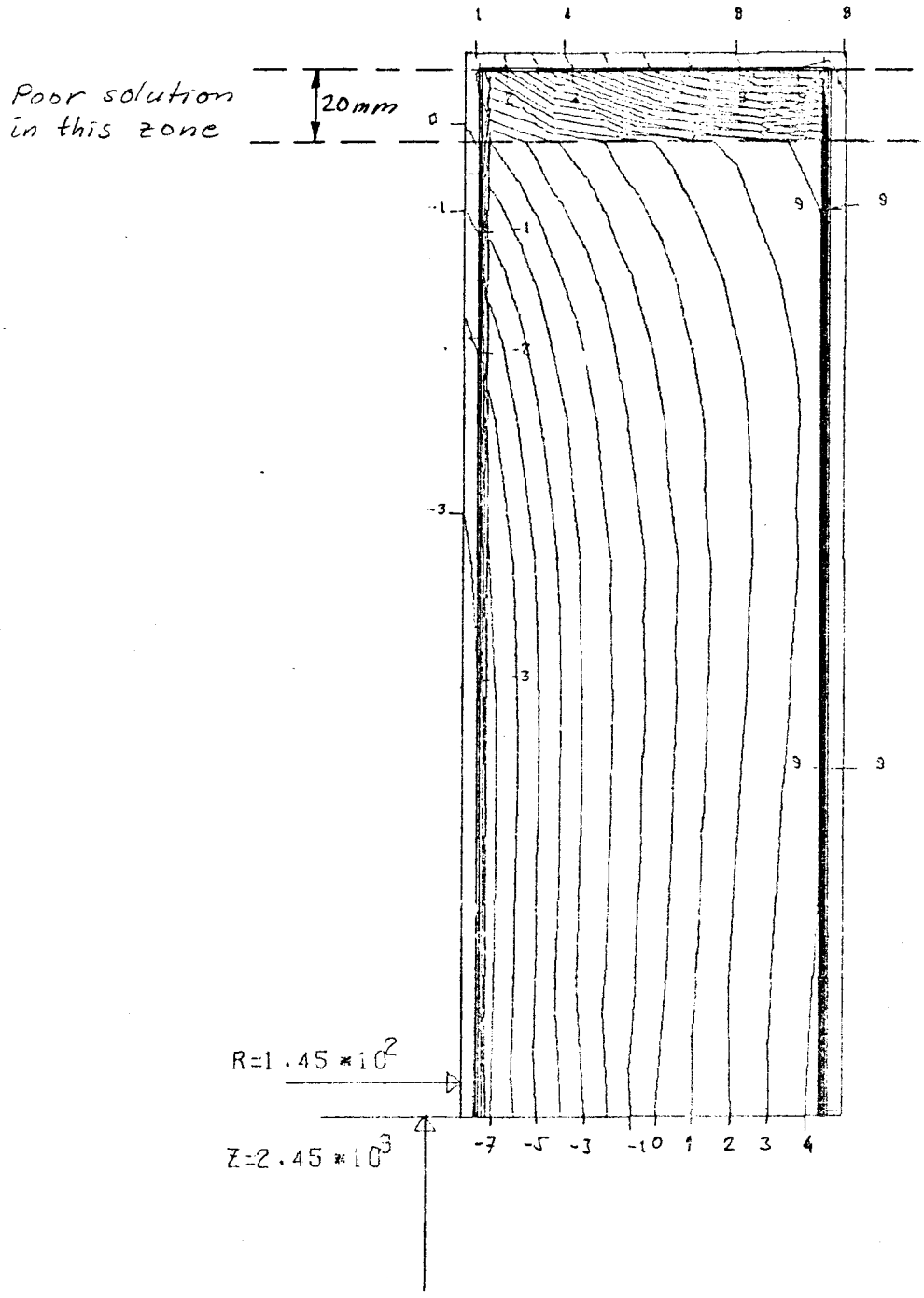

Steady-state stress distribution

Stress = (Level) × 15 MN/m^2

1CM ≙ 20 UNITS

Appendix 9

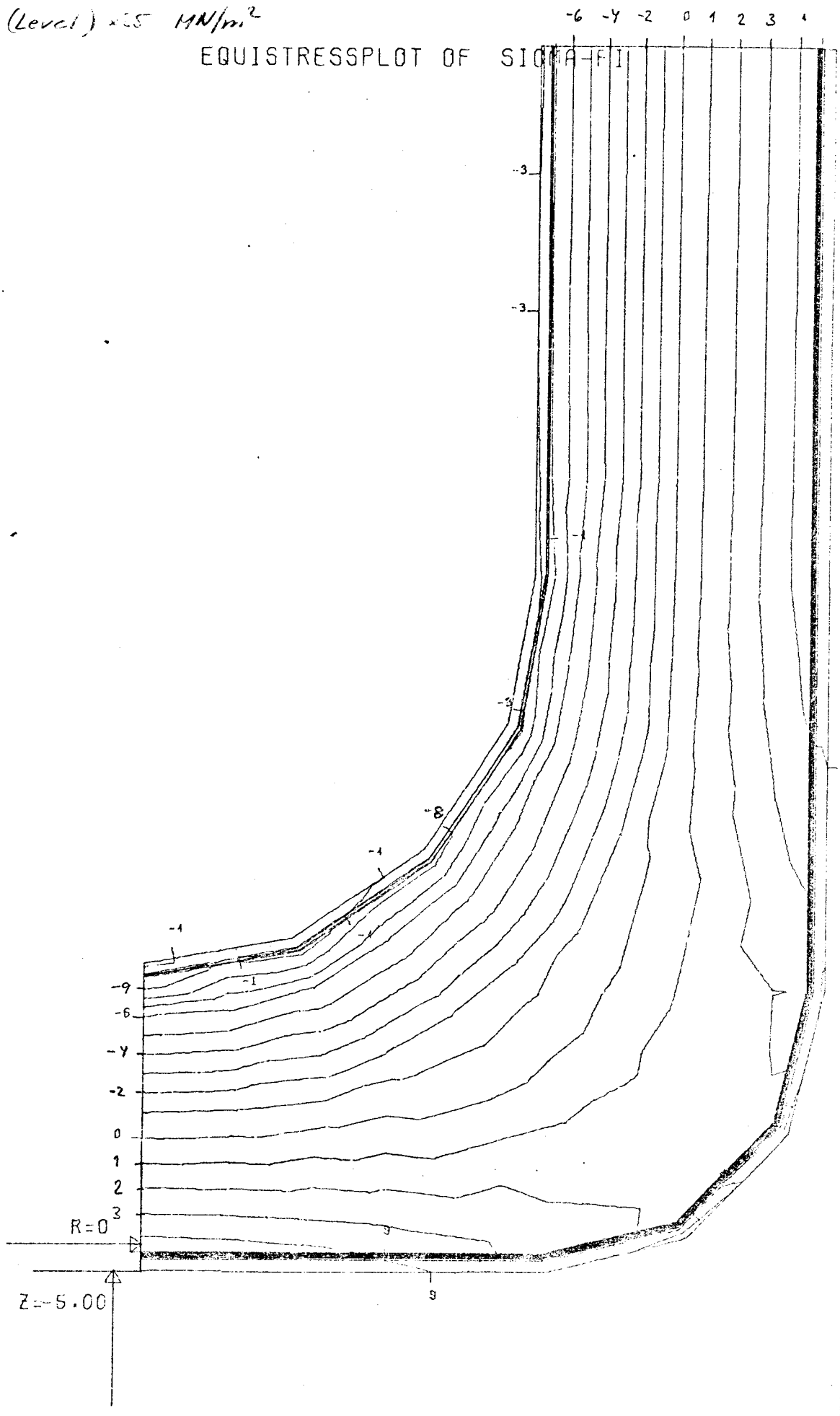

Steady-state stress distribution

1CM ≙ 20 UNITS

Appendix D

Stress = (Level) × 25 MN/m²

EQUISTRESSPLOT OF MAX. PRINCIPAL STRESS

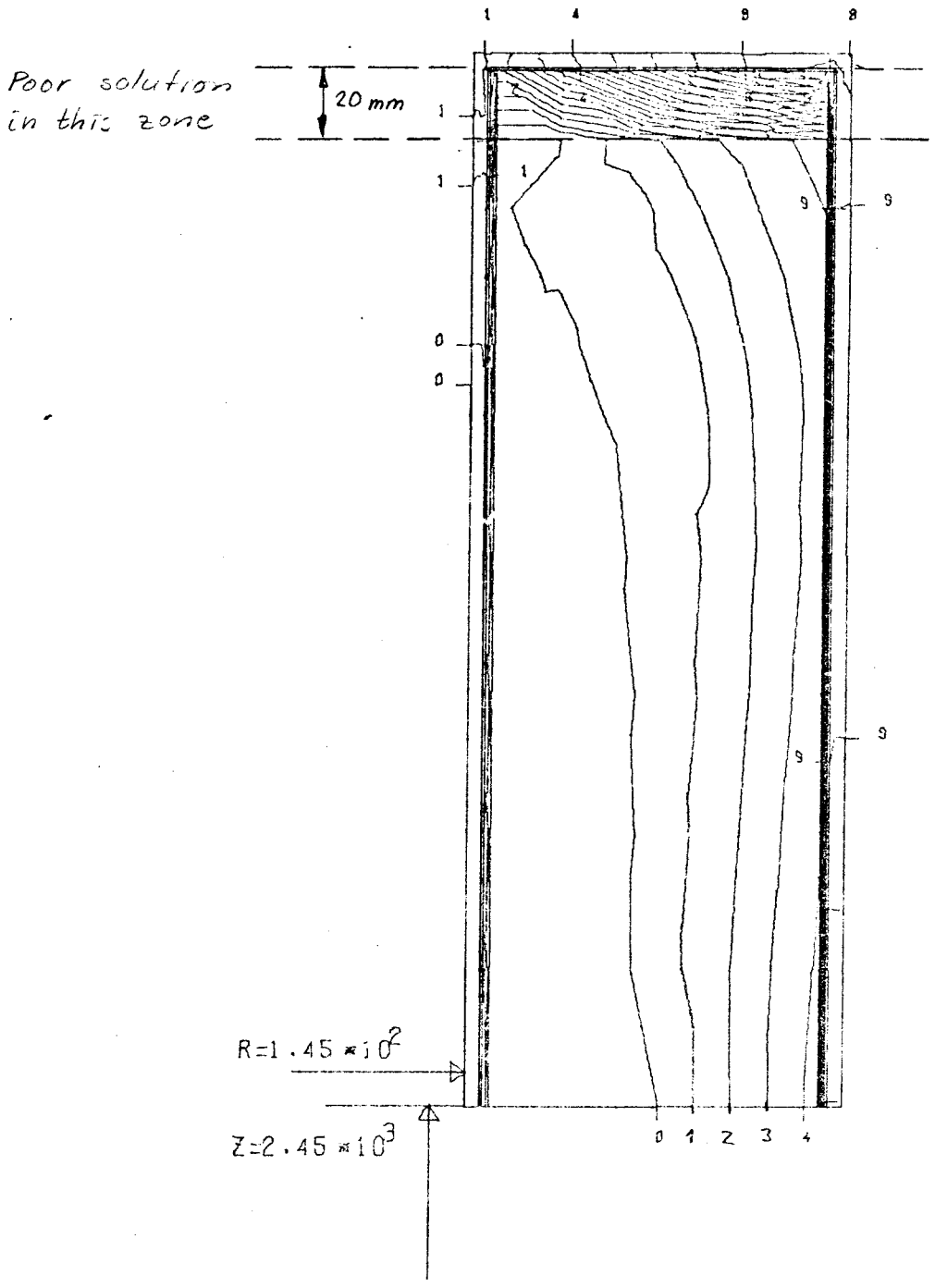

St ay-state stress distributio.

1CM ≙ 20 UNITS

Appendix

Stress = (Level) × 25 MN/m²

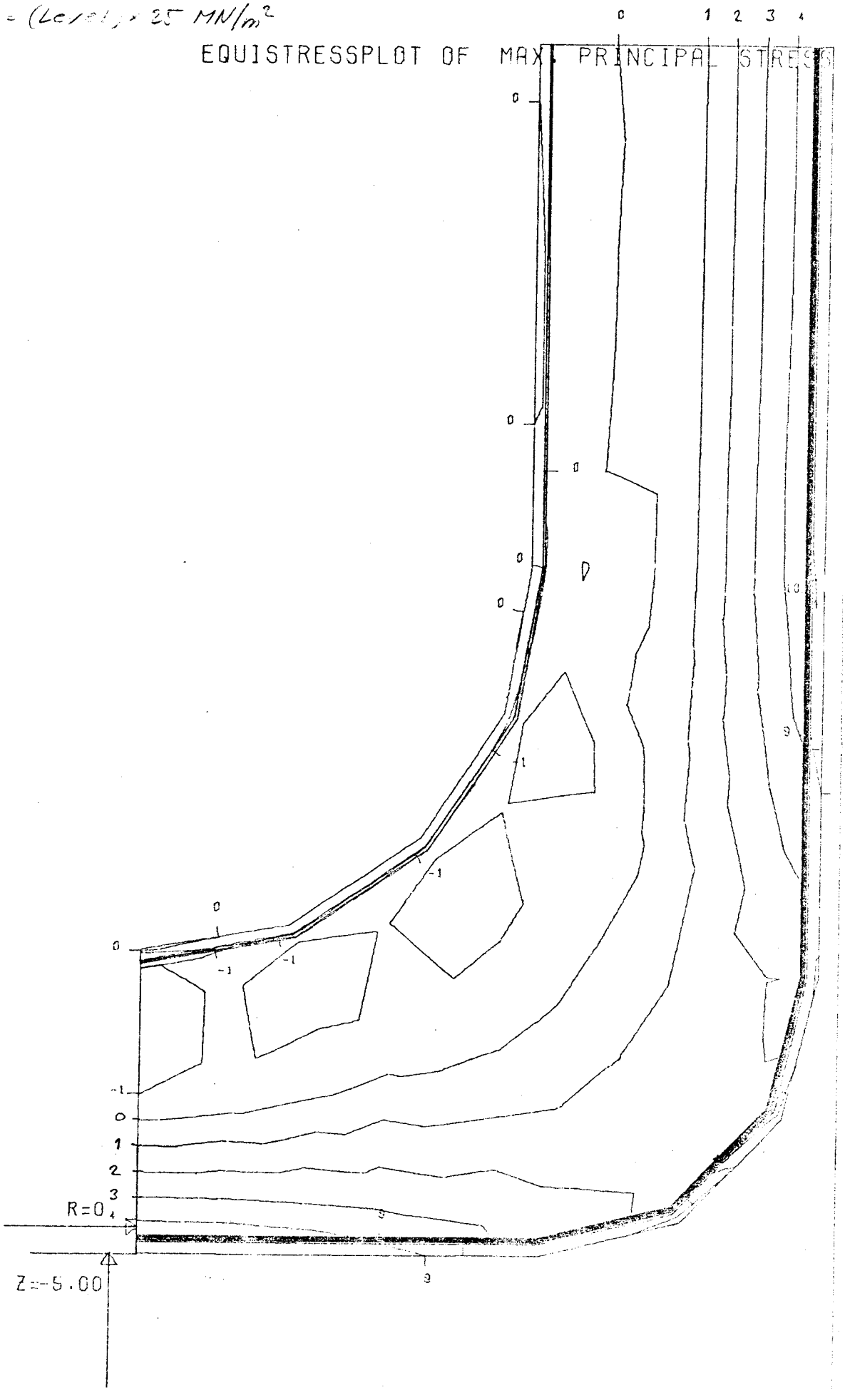

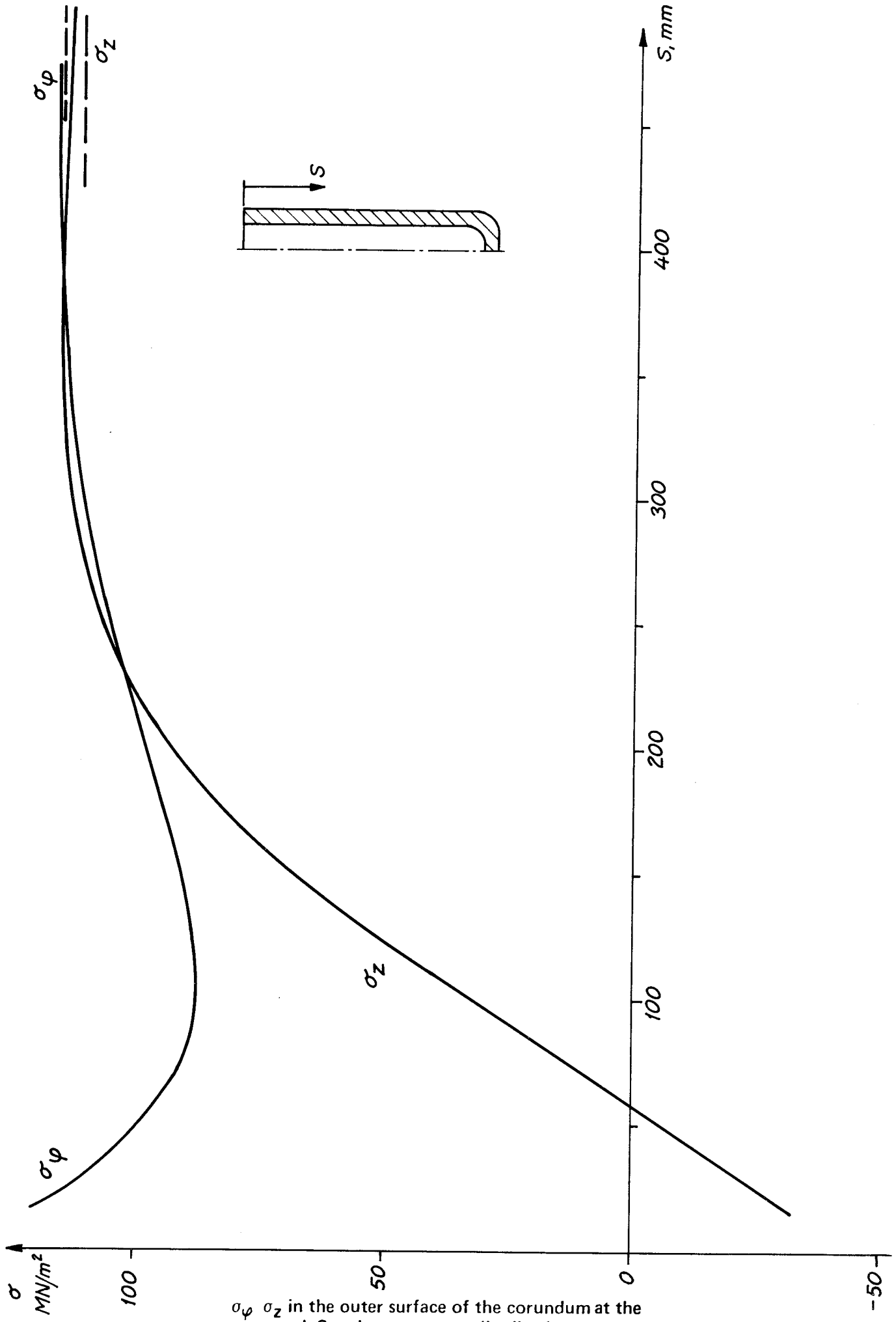

σ_φ σ_z in the outer surface of the corundum at the open end. Steady-state temp. distribution.

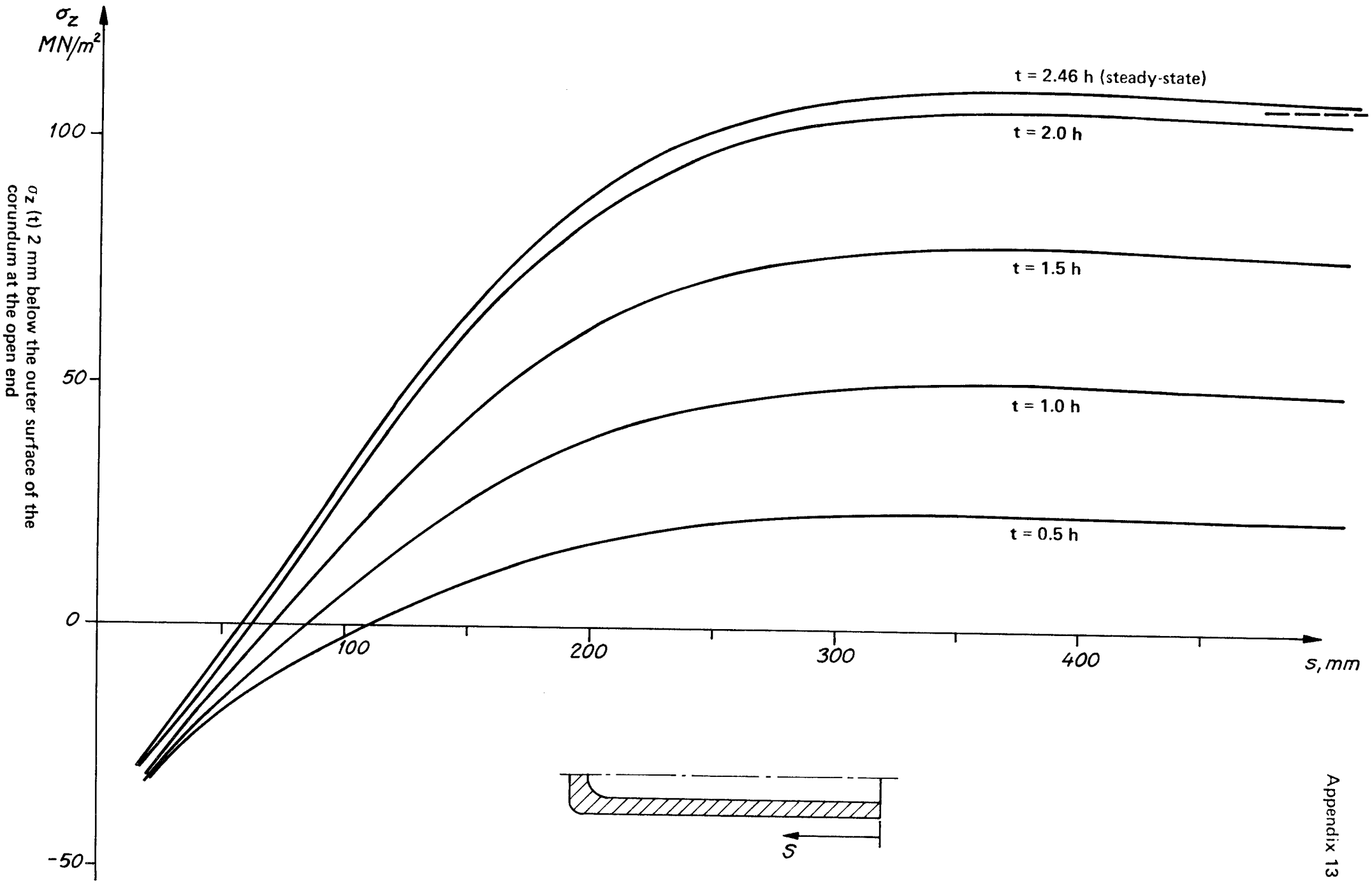

σ_z (t) 2 mm below the outer surface of the corundum at the open end

Appendix 13

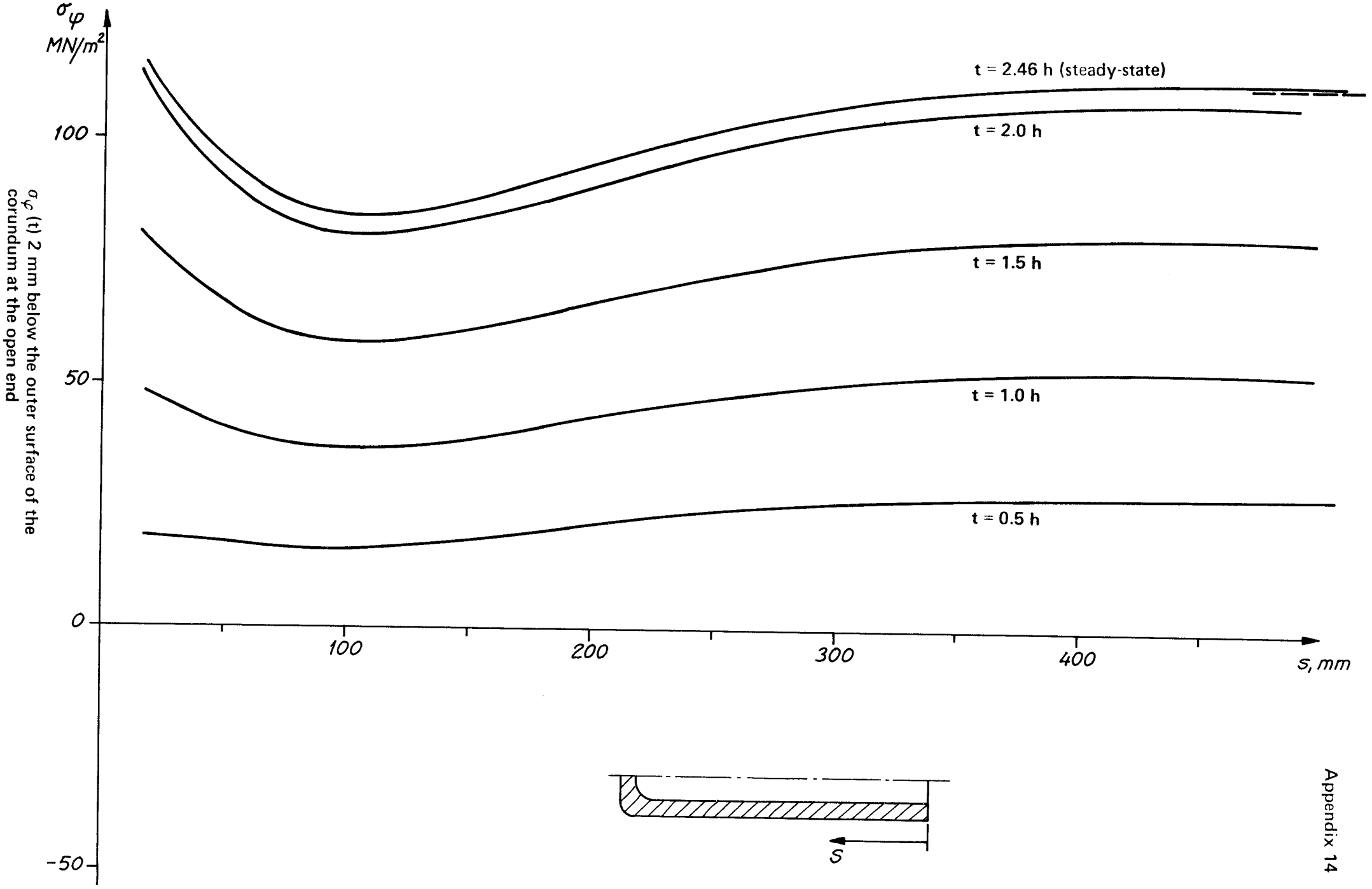
σ_φ
MN/m²
100
50
0
-50
100
200
300
400
s, mm
t = 2.46 h (steady-state)
t = 2.0 h
t = 1.5 h
t = 1.0 h
t = 0.5 h
σ_φ (t) 2 mm below the outer surface of the corundum at the open end
s

Appendix 14

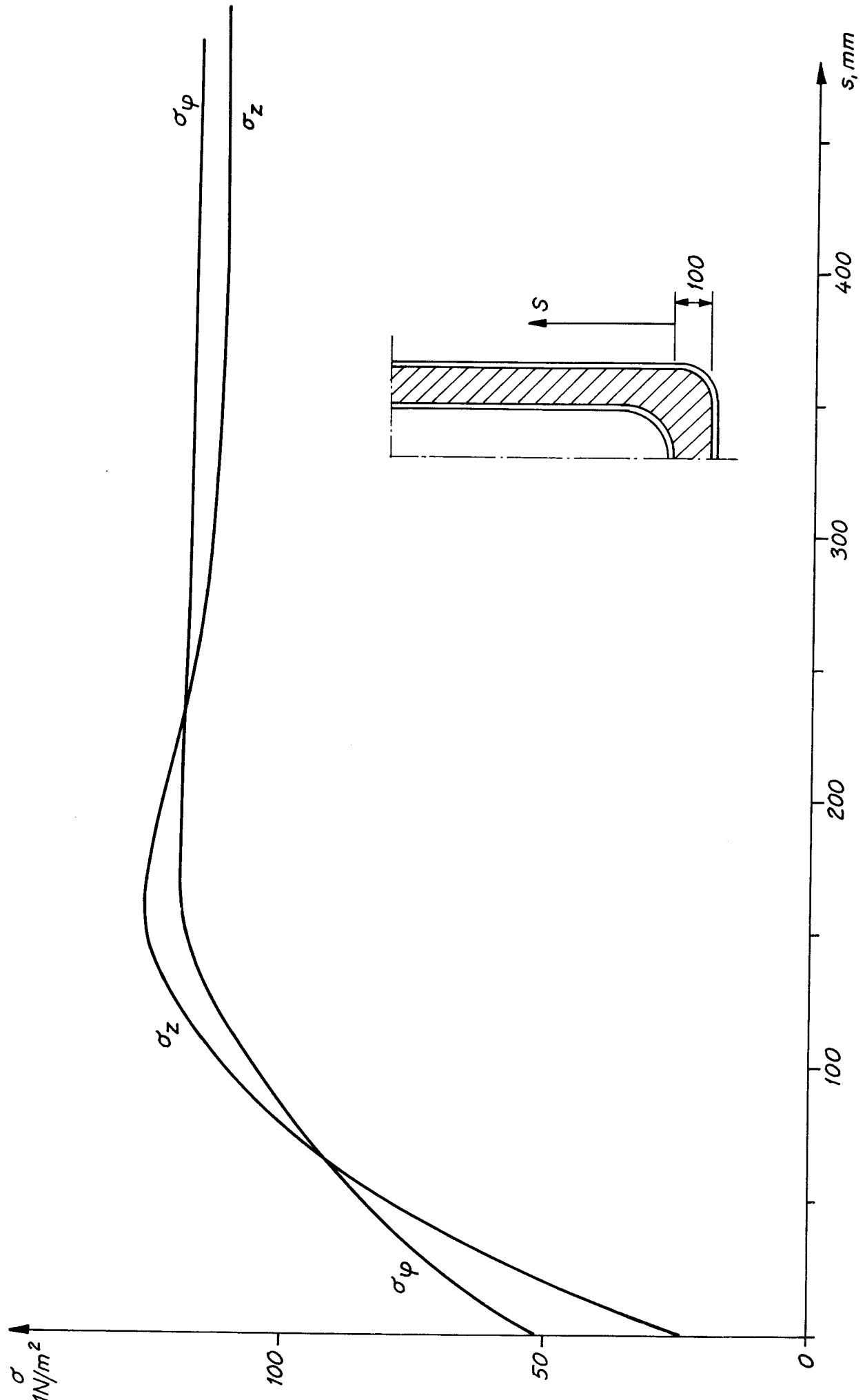

σ_z, σ_φ in the outer surface of corundum close to the bottom.
Steady-state temp. distribution

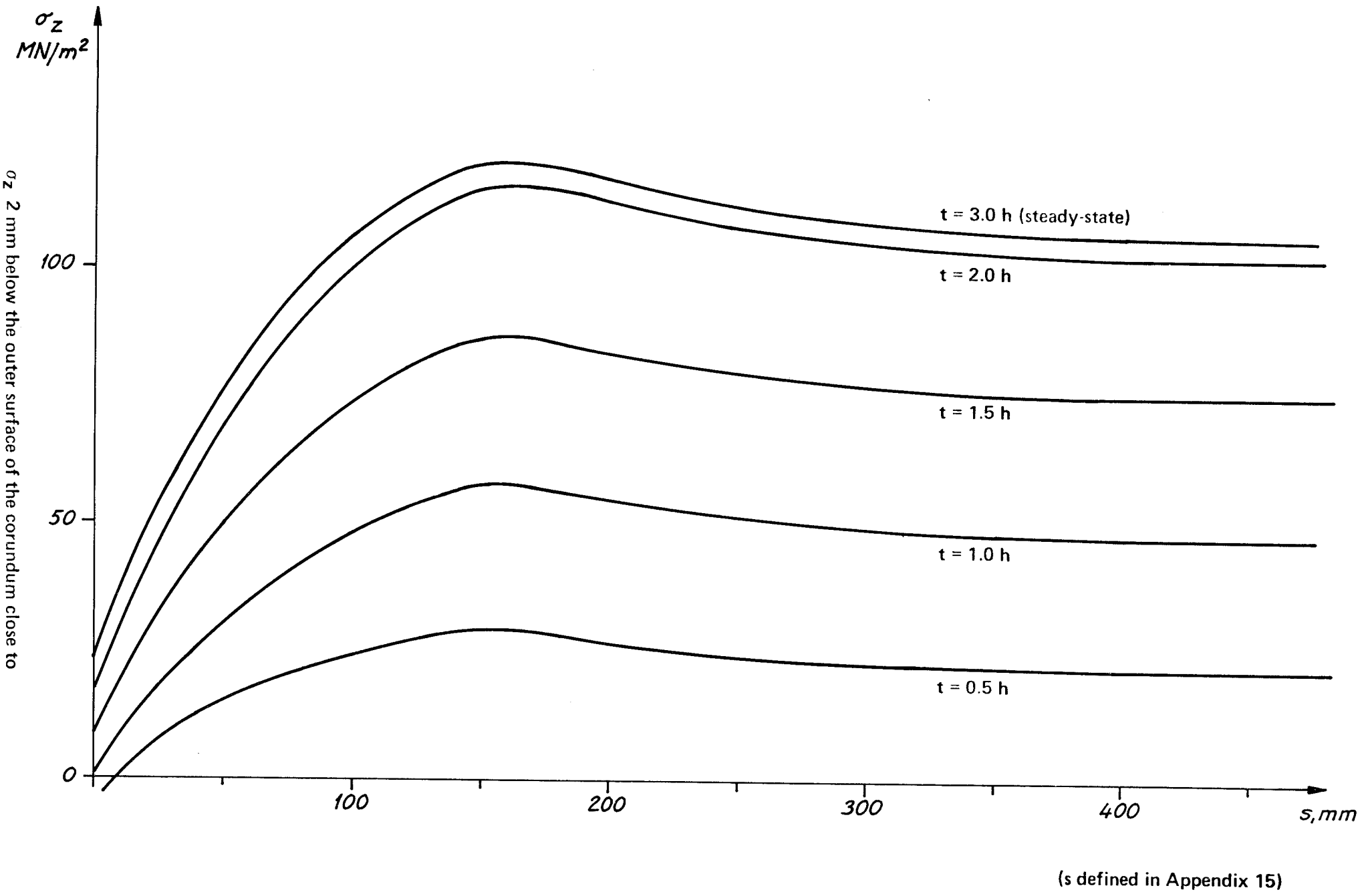

σ_z 2 mm below the outer surface of the corundum close to the bottom

(s defined in Appendix 15)

Appendix 16

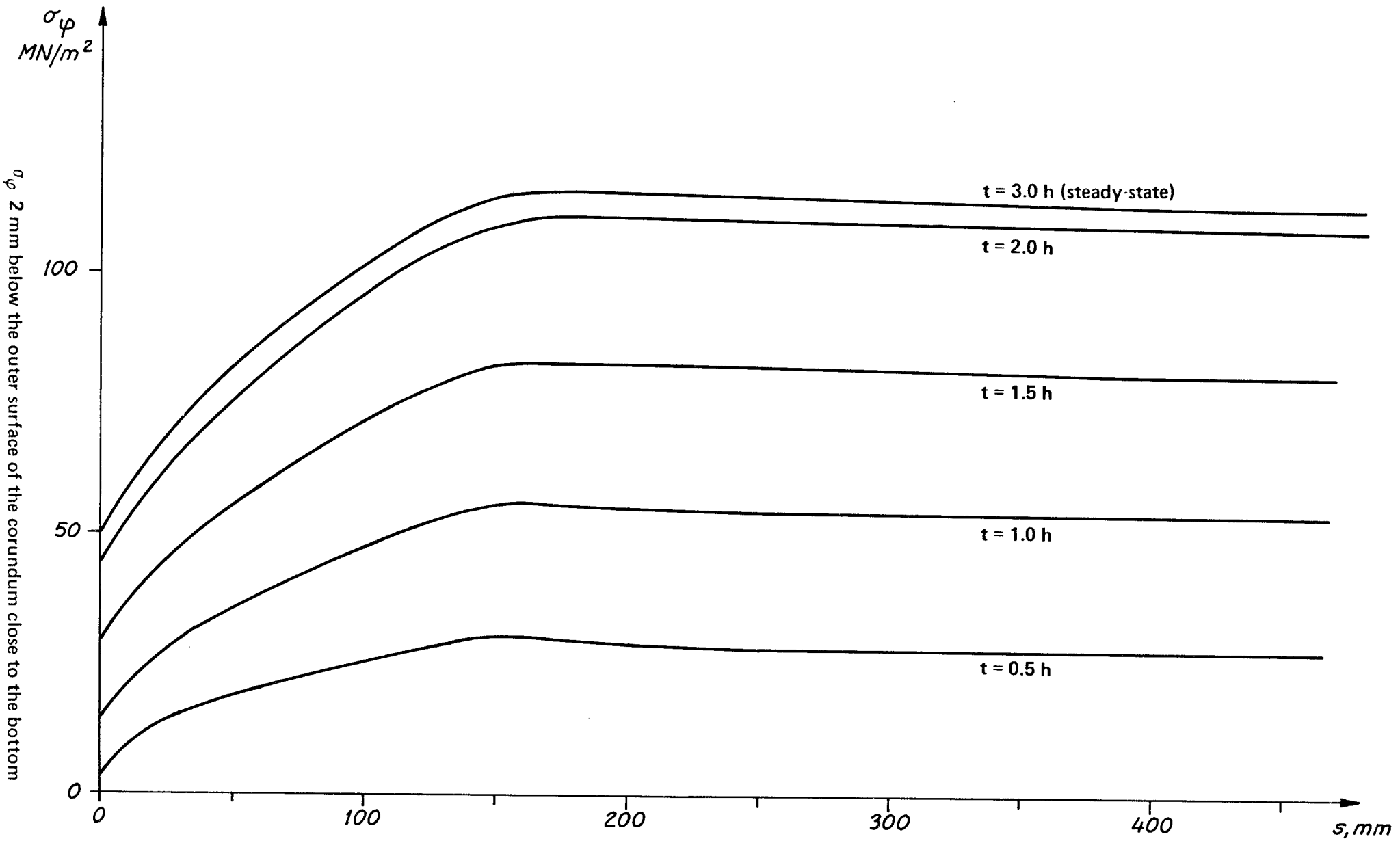

(s defined in Appendix 15)

Appendix 17

Reference Group, Corrosion of
Encapsulation Material for
Nuclear Waste
Attention: Lars Ekbom, Lic. Eng.
The Swedish Corrosion Institute
Box 5607
S-114 86 STOCKHOLM
Sweden

"Calculated life of container of aluminium oxide"

The stress calculation and the fracture mechanics analysis carried out in the above-cited report are, as far as I have been able to determine by means of careful examination, correct. The fracture mechanics analysis has been carried out in accordance with accepted practice, to the extent that such exists in a young science as fracture mechanics. The most recent findings within this field have been used in the analysis.

The calculations of container life are, in many respects, conservative, which means that the time to fracture obtained strictly on the basis of theory and experimental data is longer than the reported time at the given stress and initial crack length.

Despite the fact that the calculations and the conclusions that are drawn from them are formally beyond criticism, their reliability may be questioned. The reason for this is the extrapolation that was done of the measured crack growth data.

The measurements were carried out with a minimum growth velocity of the order of centimetres per year, while the design case involves mean velocities as low as nano (10^{-9}) metres/year. Strictly in terms of fracture mechanics, an application of the law of propagation $v = A K_I^n$ to these velocities does involve an overestimation of the crack velocity. But the question must be posed as to whether other phenomena of importance for material destruction do not dominate crack growth at these long lives. However, I am not competent to judge the question of the long-time stability of materials of this type.

It is my opinion that an attempt should be made to determine whether a threshold value for crack growth exists or, alternatively, to measure the crack velocity at very low K_I values.

Stockholm 1978-12-15

Janne Carlsson

SWEDISH INSTITUTE FOR SILICATE RESEARCH
Gothenburg
Roger Carlsson and Leif Hermansson

STATEMENT OF COMMENT ON ASEA'S STUDY ENTITLED "RESIDUAL STRESSES, DEFECTS AND CALCULATED LIFE OF ALUMINIUM OXIDE CONTAINER" (APPENDIX E)

Introduction

Since the end of the last century, it has been qualitatively known that the measured strength of glass in a normal room atmosphere is considerably lower under long-term loads than under instantaneous loads (1). This phenomenon has been called static fatigue, but the concepts of slow crack growth or subcritical crack growth leading to delayed failure (delayed fracture) are used more often nowadays (2). This phenomenon occurs especially in the presence of water. It has been found that all oxide-based ceramics can exhibit delayed failure in an aqueous environment. The largest body of experimental data is available for glass, where a permissible maximum stress in the material equivalent to 1/3 of the fracture limit determined in a moist environment or 15-20% of the fracture limit determined in a vacuum is normally assumed in order to avoid delayed failure (1-4).

Slow crack growth has been studied quantitatively since the 1960s. In the case of ceramics, intensified research has been conducted since the mid-60s (5, 6). A further increase in the intensitity of research in the field of the fracture mechanics of ceramics has taken place since the beginning of the 1970s in connection with, among other things the study of high-temperature ceramics for combustion engines (7, 8). The method used by ASEA, with load relaxation utilizing double-torsion (DT) specimens to determine K_I-V diagrams, dates back to 1972, with further refinement in the following years (9). Other methods for the study of slow crack growth include the double cantilever beam (DCB) technique, constant moment (CM) technique, compact tension (CT) technique and controlled flaw technique (CFT or SCB = surface crack bend technique) (10-13).

Discussion

In general, it can be said that ASEA's report is based on well-established technique employing DT specimens and that generally accepted theoretical relationships are used. No criticism can be raised against the manner in which ASEA has carried out the reported calculations. In our judgement, however, there are certain points (premises) for the reported calculations which require commentary.

A) Extrapolation of K_I-V diagrams to regions far beyond those with experimental backing and the influence of temperature.

B) The validity of the measured factor n for service life calculations.

C) The geometric constant Y in the general expression $K_I = \sigma Y \sqrt{\pi a}$.

D) Calculated K_I values using an analytical expression for DT specimens.

A

In determining the K_I-V diagrams, values of V down to 10^{-9} ms^{-1} have been recorded by ASEA. Within the V interval 10^{-4}-10^{-9} ms^{-1}, linear relationships of log V to log K_I have been obtained. The very low crack velocity at actual K_I values cannot be determined experimentally. Instead, ASEA has linearly extrapolated the curve obtained for measurements at higher velicities down to lower velocities, i.e. using the same n and A values. This procedure is conservative at an unchanged or increased slope of the curve.

The mechanism for slow crack growth in oxide-based ceramics in an aqueous environment within region 1 of the K_I-V curve, that is generally accepted has been described by Charles and Hillig (5). Oxide-based ceramics are always subject to corrosion (hydration, dissolution) in an aqueous environment. If there is a crack in the material and a sufficiently high tensile stress is present, the corrosion rate at the tip of the crack will increase compared with the sides of the crack, whereby the crack will slowly grow. It has been shown that the process is thermally activated and that the chemical reaction at the crack tip at low crack velocities is velocity-determining (3, 5, 14). At higher velocities, the diffusion of the ions or molecules participating in the reaction can be velocity-determining (3).

According to the Charles-Hillig theory, there is a certain minimum stress below which the velocity of slow crack growth is zero (5). When the stress drops below the limit value, the crack is rounded off and ceases to grow. Such limit values have been found experimentally for glass, insulator porcelain and Pb-Zr-titanate ceramic (3,14,15,16). However, for many ceramic materials, including aluminium oxide, it has not been possible to carry out measurements to low enough crack velocities to permit limit values to be generally verified. Experimental support for the Charles-Hillig theory is provided by the fact that glass stored in a moist environment under stresses below the limit value possesses a higher strength, which is believed to be due to the rounding-off of existing crack tips (3).

Measured activation energies for slow crack growth agree with what applies for chemical reactions (3). 59kJ $mole^{-1}$ has been measured for aluminium oxide (17,18), which can be compared with the 60 kJ $mole^{-1}$ reported by Fyfe (19) for the general corrosion of aluminium oxide. Other postulated mechanisms, such as vacancy diffusion and plastic flow, correspond to activation energies that are considerably higher than measured values (3). Furthermore, mechanisms that have been shown to exist within range III of K_I-V curves have always corresponded to higher n values than those obtained within region I.

For the chemical mechanism, Doremus (4) has proposed a simplification of the Charles-Hillig theory, and Lawn (20) recently presented an atomic model to explain slow crack growth. A limit value below which crack growth does not occur is obtained with this theory as well (3).

As far as temperature is concerned, ASEA's K_I-V measurements were carried out at 21°C, while the temperature on the canister surface has been given at 70°C, and after 1 000 years, 50°C. Since a chemical corrosion reaction in the crack tip is involved at slow crack velocities, a higher crack velocity can be expected at temperatures higher than 21°C. Relevant data for Al-oxide have not been found in the literature. However, increases in crack velocity by up to two powers of ten at a temperature increase of 50°C have been reported for glass and Pb-Zr-titanate ceramic (3,21,16). The n value appears to be affected only marginally by a temperature increase. Furthermore, in the case of soda-lime glass, the limit value for slow crack growth is not affected by the temperature, which is also supported by theoretical models (22).

In lieu of relevant data for Al oxide, an increase of the crack velocity in Al oxide at 70°C as compared with 21°C by a factor of 100 should be assumed. This, however, corresponds to a shift of the K_I-V curve of only 0.1 MN $m^{-3/2}$. However, measurements should be carried out by ASEA at 70°C in order to provide a more reliable basis for judgement with regard to the possible change of the n value.

In summary, we feel that the linear extrapolation of available measurement results used by ASEA provides a conservative assessment of the crack velocity. No additional mechanism is reported in the literature which could give lower values of n at lower crack velocities. On the contrary, it appears probable that a limit value exists below which slow crack growth ceases. An adjustment of the K_I-V curve by 0.1 MN $m^{-3/2}$ towards a lower K_I value should, however, be done for the temperature 70°C.

B

The material constant n and the associated factor A in the K_I-V relationship can be determined by means of two independent methods: either using fracture mechanics through examination of the propagation of a macrocrack or by means of conventional measurements of flexural or tensile strength. In the latter case, existing micro cracks in the material give a certain fixed life under static load and a varying ultimate strength under different loading rates (14,3,23). ASEA has determined values of n only by means of the fracture mechanics method.

In order to be able to use measured n values with certainty to predict the lives of ceramic engineering materials, however, it is currently considered necessary to demonstrate that the same n values are obtained in measurement by means of both methods (3,23,24). There are, namely, examples where the kinetics have been different in connection with the growth of macroscopic cracks as compared with microscopic cracks (3,24). At very low crack growth in region I,

there should be no such difference, but this ought to be demonstrated by ASEA, especially since the given n value is the highest reported for any ceramic material in an aqueous environment.

C

In general, the stress state can be described by the expression $K_I = \sigma Y \sqrt{a \pi}$. For different test configurations and appearances of the crack, different Y values are obtained, e.g.:

a) For a crack with a length of 2a in an infinitely large plate subjected to tensile stresses perpendicular to the crack, Y=1.0 is obtained.

b) For a circular crack in an infinitely large plate subjected to tensile stresses, Y=0.64 is obtained.

c) For surface cracks, the Y factor has been determined by several researchers (28-31). For a plane stress state, a value of 1.12 is obtained with a margin of error of no more than a percent or so.

The chosen value Y=1.12 in the ASEA study applies for surface cracks where the crack depth is large compared with the radius of curvature of the crack. If the crack has a slightly "rounder" appearance, lower values of Y are obtained. Y=1.12 should therefore be a conservative value.

D

ASEA has used K_I values calculated according to $K_I = P W_m (3(1+\nu)/W d^3 d_n \xi)^{1/2}$. K_I is considered to be independent of crack length with DT specimens. This should be demonstrated experimentally by ASEA. Some comments should be made concerning DT specimens in order to shed light on the validity of the above expression.

a) DT specimens are treated as two independent elastic specimens subjected to torsion, utilizing the approximate relationship $\theta = Y/W_m \simeq 6 T a/W d^3 G$ (32).

   All deformations are ascribed to torsion. Changes caused by shear or fluctual stresses are neglected.

b) The velocity of the crack front varies, owing to the fact that the crack grows faster on the bottom of the specimen than in other parts. ASEA's correction gives realistic values - not conservative.

c) The stress pattern in DT specimens is such that opening mode III could exist (9). However, Evans has shown that the opening mode for glass is exclusively I. The same should apply for Al oxide.

By means of a compliance calibration procedure, calculated K_I values can be compared with experimentally measured values. For steel, Evans obtained a discrepancy of about 8% (32). Compliance calibration should be carried out for Al oxide.

In comparing K_I and K_{Ic} values determined by means of different methods, a somewhat unclear picture is obtained. According to certain studies (32), very good agreement is obtained for DT, DCB and flexural specimens, especially for glass. A comparison of K_{Ic} values for Al oxide (33) shows, however, that discrepancies of slightly more than 10% can exist for similar materials. However, let it be noted directly here that large variations can be caused by microstructural differences (34). ASEA's value for K_{Ic} (6.2 MN $m^{3/2}$) is the highest that has been reported for Al oxide.

A study of K_{Ic} values for densely sintered α-SiC produced by means of different methods from the same material was presented at the Autumn meeting of the American Ceramic Society in 1977, and shows large differences in K_{Ic} values obtained (35).

Method	Performed by	K_{Ic} (MN $m^{-3/2}$)	Remark
DT	Penn State Univ	4.6	
DCB	Nat Res Lab	3.4	
SENB	Carborundum Co	5.4	
SCB	Carborundum Co	2.8	Probably faulty specimen preparation
IFF	Carborundum Co	4.7	

(IFF=Intrinsic flaw fractorgraphy)

A standard method for K_{Ic} values was called for at the meeting, since K_{Ic}, which is theoretically a material constant, appears to be dependent upon the test method. Since the same analytical expressions apply for K_I as for K_{Ic}, this should also be true of K_I values.

Conclusions

1. In order to eliminate any remaining uncertainties, the following supplementary work should be carried out by ASEA on hot isostatically pressed Al oxide.

a) Recording of K_I-V diagrams, using DT specimens, at 70°C in rock water in order to check the slope (n value) of the K_I-V curves.

b) Determination of n by varying the ultimate strength with the loading rate at 21°C and 70°C in rock water.

c) Experimental confirmation that K_I is independent of crack length by means of calibration.

d) Execution of a compliance calibration.

e) Measurement of K_{Ic} values by means of the DCB and CFT methods.

2. In view of all of the shortcomings mentioned above, we consider it justified to write down ASEA's K_I values by up to 30% in order to obtain a reliably conservative assessment. According to the relationship $(a_{o1}/a_{o2})^{-(n/2-1)} = A_1/A_2\ (Y_1/Y_2)^n$, where log $A_1 = -120$, $n_1 = n_2 = n = 210$, $Y_1 = Y_2$, a decrease of the maximum permissible crack length a_o is obtained according to:

K_I value	Maximum initial crack length
K_I calc (ASEA)	a_o
0.9 K_I calc	0.80 a_o
0.8 K_I calc	0.63 a_o
0.7 K_I calc	0.48 a_o

ASEA's own calculations for the container life of 10^6 years gives an initial crack depth of 1.6 mm. In to our more conservative judgement, this value should be adjusted to 0.8 mm until existing uncertainties have been eliminated.

3. A crack depth of 0.8 mm is of the same order of magnitude as that considered by the Technical X-ray Centre to be detectible. In our judgement, a proof testing of each canister must be carried out in order to be able to guarantee a service life of 10^6 years.

Bibliography

(1) Adamson B and Backman HE: "Glas i hus" ("Glass in houses"), Lund 1975, p. 43.

(2) Kingery WD, Bowen HK and Uhlmann DR: "Introduction to Ceramics", 2 ed, New York 1976

(3) Wiederhorn SM: Mechanisms of subcritical crack growth in glass, ref 8, vol 4 (1978), 549.

(4) Doremus RH in "Corrosion Fatigue" ed by McEvily AJ and Staehle RW, Nat Ass Corr Eng, Houston 1972, 743.

(5) Hillig WS and Charles RJ: "High Strength Materials" ed by Zackay VF, New York 1965, 682.

(6) Wiederhorn SM: J Am Ceram Soc 50 (1967) 407.

(7) ASTM, STP 513 "Stress Analysis and Growth of Cracks" (1972).

(8) "Fracture Mechanics of Ceramics", ed by Bradt RC, Hasselman DPH and Lange FF, New York, Vol 1-2 (1974), Vol 3-4 (1978).

(9) Evans AG: Int J Fract 9 (1973) 267.

(10) Wiederhorn SM and Baltz LH: J Am Ceram Soc 53 (1970) 543.

(11) Freiman SW et al: J Mat Sci 8 (1973) 1527.

(12) Wiederhorn SM et al: J Appl Phys 39 (1968) 1569

(13) Wills et al: J Mat Sci 11 (1976) 1330.

(14) Wiederhorn SM: Subcritical crack growth in ceramics, ref 8, vol 2 (1974) 613.

(15) Matsui M, Soma T and Oda I: Subcritical crack growth in electrical porcelains, ref 8, vol 4 (1978) 711.

(16) Bruce JG, Gerberich WW and Koepke BG: Subcritical crack growth in PZT, ref 8, vol 4 (1978) 687.

(17) Charles RJ and Shaw RR: Delayed failure of polycrystalline and single-crystal alumina, General Electric Research Laboratory Report No 62-RL- 3081 M July 1962.

(18) Chen CP and Knapp WJ: Fatigue fracture of an alumina ceramic at several temperatures, ref 8, vol 2 (1974) 691.

(19) Fyfe WS: Corrosion rate of Al_2O_3 in aqueous solutions from 25-350°C, Report 1978.

(20) Lawn BR: J Mat Sci 10 (1975) 469.

(21) Wiederhorn SM and Bolz LH: Stress corrosion and static fatigue of glass, J Am Ceram Soc 53 (1970) 543.

(22) Brown SD: A multibarrier rate process approach to subcritical crack growth, ref 8, vol 4 (1978) 597.

(23) Ritter JE: Engineering design and fatigue failure of brittle materials, ref 8, vol 4 (1978) 667.

(24) Pletka BJ and Wiederhorn SM: Subcritical crack growth in glass-ceramics, ref 8, vol 4 (1978) 745.

(25) Richter H: Unterkritische Rissausbreitung in keramischen Werkstoffen, Ber Deut Ker Ges 54 (1977) 405.

(26) ASTM STP 381 (1964) 35.

(27) Sneddon IN: Proc Roy Soc London 187 (1946) 229.

(28) Bowie OL: ASME J Appl Mech 31 (1964) 208

(29) Gross et al, enligt ASTM, STP 381 (1964) 44

(30) Smith, enligt ASTM STP 513 (1972) 26

(31) Bansal GK: J Am Ceram Soc 59 (19769 87

(32) Williams DP and Evans AG: J Testing and Evaluation 1 (1973) 264

(33) Barker LM: Short rod K_{Ic} measurements of Al_2O_3, ref 8, vol 3 (1978) 483

(34) Freiman SW, McKinney KR and Smith HL: Slow crack growth in polycrystalline ceramics, ref 8, vol 2 (1974) 659

(35) Kraft EH and Smoak RH: Crack propagation in sintered alpha SiC, Bull Am Ceram Soc 56 (1977) 734

SWEDISH INSTITUTE FOR SILICATE RESEARCH
Gothenburg
Roger Carlsson and Leif Hermansson

SUPPLEMENTARY STATEMENT CONCERNING DELAYED FAILURE IN ALUMINIUM OXIDE CONTAINERS

In reference to the discussion of 28 August 1979 in Stockholm between the Swedish Corrosion Institutes reference group and Professor A. G. Evans of the University of California, as well as Professor Evans' later statement - Appendix I - we wish to add the following comments and clarifications to our previous statement of comment - Appendix G1.

1. At the meeting, Evans was of the opinion that the values of K_I and K_{Ic} measured by ASEA are probably correct, but that the possibility that systematic errors of a maximum of 20% may exist cannot be excluded.

Evans therefore proposed that supplementary measurements be carried out, using the increasingly widely accepted SCB, or as it is also called CFT - technique (SCB = Surface Crack Bending, CFT = Controlled Flaw Technique; it is important that the plastic zone at the indentation has been removed). The measurement should be carried out at varying loading rates and temperatures.

This proposal also includes the demands for supplementary measurements presented by us earlier (APPENDIX G1), except that Evans' assessment of the maximum error in K_{Ic} is somewhat more optimistic than ours.

2. Evans' written statement (APPENDIX I) has brought into focus a new aspect that was only briefly touched upon at the meeting, namely the possibility of a more certain assessment with the use of a higher proof test ratio. This requires some comments.

By increasing the proof test ratio to 4.0, it is possible to determine whether cracks larger than 0.4 mm exist. This means that the stress intensity factor for each container that passes the proof test will have a maximum value of 1.5 MN $m^{3/2}$. The stress intensity factor will thereby be a maximum of 25% of the K_{Ic} value measured in the environment in question. This is less than or on a level with the K_o values reported for ceramics in the literature (Table 1). This means that no slow crack growth at all should occur in the aluminium oxide.

Table 1 (data for wet environment)

Material	K_{Ic} (MN $m^{-3/2}$)	K_O (MN $m^{-3/2}$)	$\frac{K_O}{K_{Ic}}$ (%)	Reference
Glass	0.75	0.29	39	1
	0.75	0.19	25	2
	0.75	0.25	33	3
Porcelain	1.3	0.6	46	1
			80	6
Pb-Zr-titanate	0.8	0.45	56	5
Al-oxide	5.4	< 2.5	< 46	4

(1) Wiederhorn SM: "Subcritical crack growth in ceramics", "Fracture Mechanics of Ceramics" ed by Bradt el al, Vol 2 (1974) 630.

(2) Williams DP and Evans AG, J Testing and Evaluation 1 (1974) 267.

(3) Wiederhorn SM and Bolz LH, J Am Ceram Soc 53 (1970) 543.

(4) Evans AG, Int J Fract 9 (1973) 267.

(5) Bruce et al: "Subcritical crack growth in PZT" etc enl ref 1, Vol 4 (1978) 687.

(6) Matsui et al: "Subcritical crack growth in electrical porcelains" osv enl ref 1, Vol 4 (1978) 711.

In this connection, it is appropriate to point out the very rapid decline of the crack velocity with declining K_I value, which, due to a very high n value, applies for the hot isostatically pressed aluminium oxide in question. If it is assumed that the general corrosion rate of the material is 10^{-9} m/year, the crack velocity in connection with delayed failure will be lower than the general corrosion rate already at K_I values lower than 3.1 MN $m^{-3/2}$ x).

The calculated maximum K_I value (1.5 MN $m^{-3/2}$) for material that has passed proof testing with a proof testing ratio of 4.0 corresponds to a crack velocity of 10^{-83} m/s (10^{-65} Å/year)! In other words, there is room for a number of unknown mechanisms within the K_I interval 1.5-3.1 MN $m^{3/2}$ before the crack velocity reaches such a magnitude that it can begin to be compared with the material's general corrosion rate!

Naturally, this line of reasoning leads to the conclusion that the K_O value for the hot isostatically pressed aluminium oxide in question is considerably higher than 25% of the K_{Ic} value. This in turn means that the necessity of using such a high proof testing ratio as 4.0 can be questioned.

x) (i.e. 52% of the K_{Ic} value)

UNITED STATES DEPARTMENT OF COMMERCE
National Bureau of Standards
Washington, D.C. 20234

March 19, 1979

562.00

Dr. Einar Mattsson
Swedish Corrosion Institute
Box 5607
S-114 86 Stockholm
Sweden

Dear Dr. Mattsson:

I am afraid that I will not be able to attend your meeting in Stockholm at the end of April because of prior commitments in the United States. I am, however, very interested in the subject of the meeting. Extrapolation of crack growth, or strength data to predict failure after long periods of time is a question of great concern, which will have to be solved before ceramic materials can be used for waste disposal. Using our present base of data, I am convinced extrapolations for hundreds or thousands of years are not reliable. For your information, I have included, several recently published articles that bear on this subject, and may be of value in your deliberations.

Thank you for inviting me to visit Stockholm. I have always enjoyed my visits to your city and am sorry that I cannot accept your invitation at this time.

Sincerely,

Sheldon M. Wiederhorn
Fracture and Deformation Division

Enclosure

FROM: Prof. A.G. Evans
UNIVERSITY OF CALIFORNIA
LAWRENCE BERKELEY LABORATORY
1 CYCLOTRON ROAD
BERKELEY, CALIFORNIA 94720 USA

LIFE PREDICTION OF ALUMINA CANISTERS

GENERAL CONCLUSION

The alumina canister concept is basically viable, within the confines of available knowledge, provided that various optimum precautionary measures are adopted, as discussed below.

DETAILS

The prevention of failure in the alumina canisters requires consideration of two potential fracture sources: (a) the direct extension of pre-existent defects, (b) the extension of cracks formed by corrosion reactions with the canister environment. It is convenient to consider these separately.

a) Pre-existent Defects

Failure from pre-existent defects could occur by slow crack growth in the presence of stress (residual + external). For the very long lifetimes required in this application it will never be possible to obtain crack growth data at the requisite low levels of stress intensity factor. Some extrapolation scheme must, therefore, be adopted. The extrapolation of data, obtained within the accessible velocity range, is the only plausible approach. The premise of the extrapolation is that new mechanisms, which yield an accelerated growth rate at low K, are unlikely: based on available knowledge. Any difficulties which may arise from this presumption diminish greatly if the proof test ratio is designed to be as large as possible, because the initial stress

intensity factor is then more likely to be below the threshold for crack growth. This concept is illustrated in Fig. 1.

The present test results and analysis indicate that the crack growth susceptibility of the material and the level of total stress are sufficiently low that the assured integrity of the canister appears plausible. However, further studies should emphasize additional safeguards against unknown regimes of crack growth by augmenting the proof ratio, as noted above. This can be achieved by optimizing the diffusion bonding process (e.g., by numerical simulation) in order to minimize the residual stress. Then, proof testing should be conducted at the maximum possible stress level compatible with the strength of the material (e.g., $\sim$ 1 proof test failure in 10 or 10^2). Ideally, proof ratios up to 4 might be possible (the present estimate of 2.13 must, of course, be an absolute minimum requirement). Continuous monitoring of the proof test with acoustic emission is mandatory to ensure that crack growth does not occur (in the proof test survivors) during the unstressing cycle.

b) Corrosion Induced Cracks

A potential source of time dependent failure can emerge if there is a preferred chemical reaction of inclusions within the material with the environment. This is a significant effect when the reaction involves the inward diffusion of the environmental species to create a reaction product with a larger volume than the original inclusion; a volume change that is constrained by the matrix. Tangential stresses develop within

the matrix, around the inclusion, which can initiate radial cracks. These cracks are then susceptible to extension, motivated by the general stress within the canister. The magnitude of radial cracks generated by this mode of corrosion reaction is related to the size of the initial inclusion (usually $\tilde{<}$ 3 times the inclusion size). The assurance that the canister will not fail if subject to this type of corrosion induced cracking is thus contingent upon the exclusion of inclusions above the size that would yield cracks larger than those that remain after proof testing. This size can only be subjectively estimated at this juncture, in the absence of any knowledge concerning possible corrosion reactions. However, it is unlikely that the maximum permissable inclusion size will be less than 100 μm (a radial crack size $\tilde{<}$ 300 μm). It is proposed, therefore, that near surface inclusions, larger than 100 μm be classified as unacceptable: a conservative requirement that could certainly be relaxed as more information becomes available. It is only necessary to detect inclusions of this size located $\tilde{<}$ 100 μm beneath the surface, because the diffusion distances would be too large to involve inclusios at greater sub-surface depths. Inclusions of this type could be detected by surface acoustic wave examination of the canister or, perhaps, by optical methods (taking advantage of the translucency of the material). The adoption of surface acoustic wave examination procedures is thus recommended. This type of inspection could also be used as an extra precautionary measure to confirm the effectivity of the proof test.

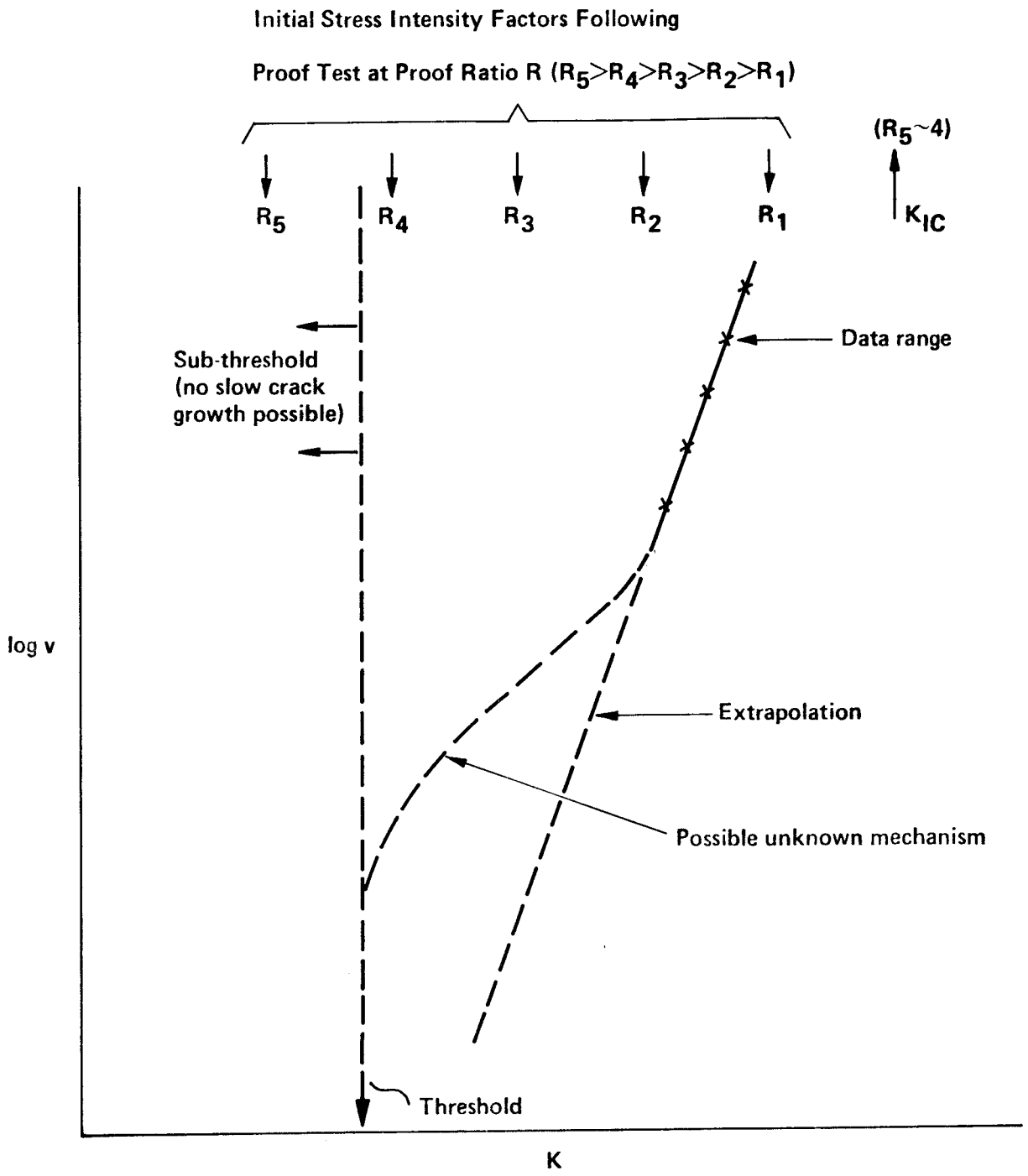
Initial Stress Intensity Factors Following
Proof Test at Proof Ratio R ($R_5>R_4>R_3>R_2>R_1$)
(R_5~4)
R_5
R_4
R_3
R_2
R_1
K_{IC}
Sub-threshold
(no slow crack
growth possible)
Data range
log v
Extrapolation
Possible unknown mechanism
Threshold
K

Lawrence Berkeley Laboratory
University of California
Berkeley, California 94720
Telephone 415/843-2740

December 13, 1979

Dr. Einar Mattsson
Korrosionsinstitutet
Swedish Corrosion Institute
Box 5607
S0114 86 Stockholm
SWEDEN

Dear Dr. Mattsson:

Thank you for your recent letter. In response to your request, let me firstly indicate my willingness to consult for you on the delayed failure of titanium canisters. However, I have had less experience with Ti than Al_2O_3 and my judgement might not, therefore, be as broadly based as that already professed on the Al_2O_3 canister.

I will again be in Europe during August. If it is possible for you to wait until then, I will visit you in Stockholm. Otherwise, I would be happy to receive one of your committees at Berkeley.

Your questions regarding the ultrasonic techniques for inspecting the Al_2O_3 are again responded to in the sense of feasibility, rather than already demonstrated viability. Transducers capable of generating high frequency ultrasonic pulses that detect small (<25μm) defects in fine grained ceramics have been made and demonstrated by Gordon Kino at Stanford University (Edward Ginzton Lab), Palo Alto, California. The technology for making these transducers and the associated electronic circuitry is now well-established and, thus, entirely capable of being reproduced. As yet, there is no commercial manufacturer . However, it would be possible to quite readily duplicate the high frequency system by employing Kino or his associates as consultants, with regard to the purchase and assembly of the appropirate components.

Such a system should be able to detect defects at least as small as 100μm in the fine grained, isostatically pressed Al_2O_3 for the proposed canister concept. However, its application to the canister geometry would require some development. Certainly, the ultrasonic waves could be introduced via the machined surfaces at the canister ends. However, beam spreading effects occurring as a result of the large length of the canister, which would yield extraneous reflections from the iron/Al_2O_3 interface, must be minimized. It is probable that a focussing method or an imaging approach can be developed to suit the special requirements of the canister. Such approaches have already been applied to components of more complex geometry than the canister, and I am, therefore, encouraged by such possibilities.

I hope that this information has been useful to you. Let me know if you require further details.

Yours sincerely,

Anthony G. Evans

The ASEA Canister for Final Disposal of Spent Nuclear Fuel

Special statement
by
Professor Gösta Wranglén
Royal Institute of Technology, Stockholm 70

concerning

"Aluminium oxide as an encapsulation material for unreprocessed nuclear waste - evaluation with respect to corrosion" (Report from Reference Group Encapsulation Material for Nuclear Waste" of the Swedish Corrosion Institute)

Summary

1. According to a guiding principle in the international debate concerning waste from nuclear reactors, the long-term toxicity of the waste, after the fission products have decayed, should not be allowed to exceed the toxicity of the uranium ore from which the waste originally stems. In consideration of this principle, French and American researchers have found it to be "indispensable" to further separate plutonium from conventional high-level waste from reprocessing, from which 99.5% of the plutonium in the spent fuel has already been separated, so that only 0.01-0.05% of the original amount of plutonium remains.

2. The direct disposal of spent fuel would entail that all of the plutonium would be allowed to remain in the waste. As a result, it will be 10 million years before the hazard index for the spent fuel decreases to a value which corresponds to 30% uranium ore and which is therefore 1000 times higher than that of the Swedish Ranstad ore with 0.03% uranium.

3. The direct disposal of spent nuclear fuel would also entail the risk of criticality accidents, owing to the large quantities of plutonium which are stored. Following a canister failure, uranium can be dissolved by carbonate-bearing groundwater and the plutonium thereby enriched so that an uncontrolled nuclear reaction occurs, rapidly leading to additional canister failures and the escape of large quantities of radioactive material from the waste repository. The risk of criticality persists for some 100 000 years.

4. The foundation of the safety analysis on which the Nuclear Fuel Safety Project (KBS) is based, namely the existence of a virtually unfractured and watertight rock massif, has been shattered completely since the Geology Group appointed by the Swedish Nuclear Power Inspection Board (SKI's Geologist Group) found in March of 1979 1) that the rock 3) considered to be best by KBS, 2) on the Sternö Peninsula outside of Karlshamn, 4) does not meet the established requirements. However, the dispersal of radioactive material to the biosphere will increase with the square of the permeability of the rock,

since both the corrosion of the canister material + the waste and the further transport of the corrosion products can be considered to be proportional to the permeability of the rock.

5. Even if the existence of a rock massif possessing the characteristics necessary for a waste repository could be demonstrated, the conditions that exist at the time of deposition with respect to the fracturing and water content of the rock and the composition, flow rate and flow direction of the ground water cannot be expected to persist for all future time, especially not during the next ice age, which, according to geological experts, may occur as soon as within 1 000 - 10 000 years.

6. 1) The short-term tests 3) of the material 2) on corrosion 4) in the ASEA canisters that have been reported have not simulated actual conditions with respect to pressure and radiation and the strongly oxidizing conditions caused by radiolysis. Nor have the testing conditions reproduced actual temperatures in question with respect to delayed failure.

7. Calculation of the life of the canisters with respect to delayed failure, stemming from the slow growth of the small cracks that already exist in newly fabricated canisters, has been carried out with the aid of a theory developed by Dr. Sh. M. Wiederhorn, USA. Lives of hundreds of thousands and millions of years have been arrived at in this manner. However, in reply to a direct question from the Reference Group for Corrosion, Dr. Wiederhorn has stated that he is convinced that his own theory is not reliable even for calculations that extend to hundreds or thousands of years.

8. The risk of delayed failure due to the slow growth of cracks generated during the storage period by intercrystalline corrosion has not been taken into account, despite the fact that this form of corrosion has been verified in two independent studies commissioned by ASEA. The intercrystalline corrosion that has been found in connection with leaching in air-saturated water at 80-90°C and normal pressure can be expected to be incomparably larger under the conditions prevailing in the repository, namely high pressures and strongly oxidizing conditions due to radiolysis.

9. Aluminium oxide cylinders for the encapsulation of spent unreprocessed nuclear fuel can therefore not be guaranteed a very long life, 100 000 years or more. At the present time, lives beyond a few decennia cannot be regarded as "absolutely certain".

10. The direct disposal of spent nuclear fuel would seem to be a morally irresponsible act towards future generations and towards future life on earth in general.

11. It should be up to us, the generations now living, to destroy our own long-lived radioactive wastes, such as plutonium and other transuranium elements. This would appear to be possible by means of the reprocessing of spent fuel with the separation of transuranium elements and their use as new fuel in fast reactors (so called breeders. The storage problem is thereby limited to the storage of fission products for a relatively short period of time, 500-1000 years, which should be possible even from the point of view of corrosion.

12. The storage of the nuclear ash with a low content of transuranium elements from both conventional and fast reactors can be accomplished entirely without risk in containers of fireproof steel deposited in dry rock caverns or concrete bunkers (possibly decommissioned nuclear power plants) for a period of 500-600 years, after which final disposal can be effected.

13. For the direct disposal of vitrified nuclear waste with a low content of transuranium elements, a thick walled copper canister would appear to be far superior to the lead-titanium canister proposed in KBS Report I.

14. The so-called Synroc method, involving the chemical binding of reprocessed waste in synthetic minerals based on insoluble and weathering-resistant titanates would appear to entail great advantages over the vitrification of nuclear ash. Owing to the insolubility of the waste material, both the encapsulation and the imperviousness of the rock will be of subordinate importance.

15. In the same manner as reprocessed waste, spent nuclear fuel can be stored without risk in steel containers in dry rock caverns above the groundwater level for hundreds of years, but reprocessing is eventually necessary.

Contents

1. Requirements on the service life of the canisters

1.1 With reference to the toxicity of the waste (hazard index)

No precise requirements concerning the service life of the canister material for the two alternatives of spent fuel and vitrified waste have been specified to serve as a guideline for the judgement of the reference group. But such requirements on service life can be derived from a principle which has long been a guiding one in the international debate concerning nuclear waste, namely that the long-term toxicity of the waste, after the fission products have decayed, should not be permitted to exceed the toxicity of the uranium ore from which the waste originally stems. The waste in question is vitrified waste with a low transuranium content, deriving from conventional reprocessing followed by the separation of transuranium elements. Swedish nuclear power specialists (1, 2), including the leader of the encapsulation group within the KBS project (2), have also backed up this principle. Such a safety requirement based on comparison with uranium ore has the advantage of being well-defined and unambiguous, something which cannot be said of the risk analysis (or safety analysis) practiced within the KBS project which was formerly used in the American space program and for nuclear reactors. A risk analysis can be of value in comparing similar systems or designs over relatively short periods of time. But making estimates of absolute risks over the long periods of time in question here is obviously a questionable approach. It has been found that the results can vary by several powers of 10, according to the assumptions which are made.

Figure 1, taken from a KBS report (3), is a comparison between the toxicity of spent fuel and that of uranium ore which shows how the hazard index for spent fuel decreases with time, whereby an index of 1 tonne of uranium in ore is chosen as the basic unit. This diagram gives the impression that the toxicity of the spent fuel has dropped to the level of the ore after only some 30 000 years. But this is grossly misleading, since the ore in the comparison is 100% uranium ore, while most uranium deposits only contain 0.2-0.3% uranium, and, for example, the Ranstad deposit in Sweden contains only 0.03% uranium. In a comparison of spent fuel with 100% ore, only the concentration of radioactivity in time by the nuclear power activities has been taken into account, not the concentration of radioactivity in space, which is the result of numerous enrichment processes in the fabrication of the fuel.

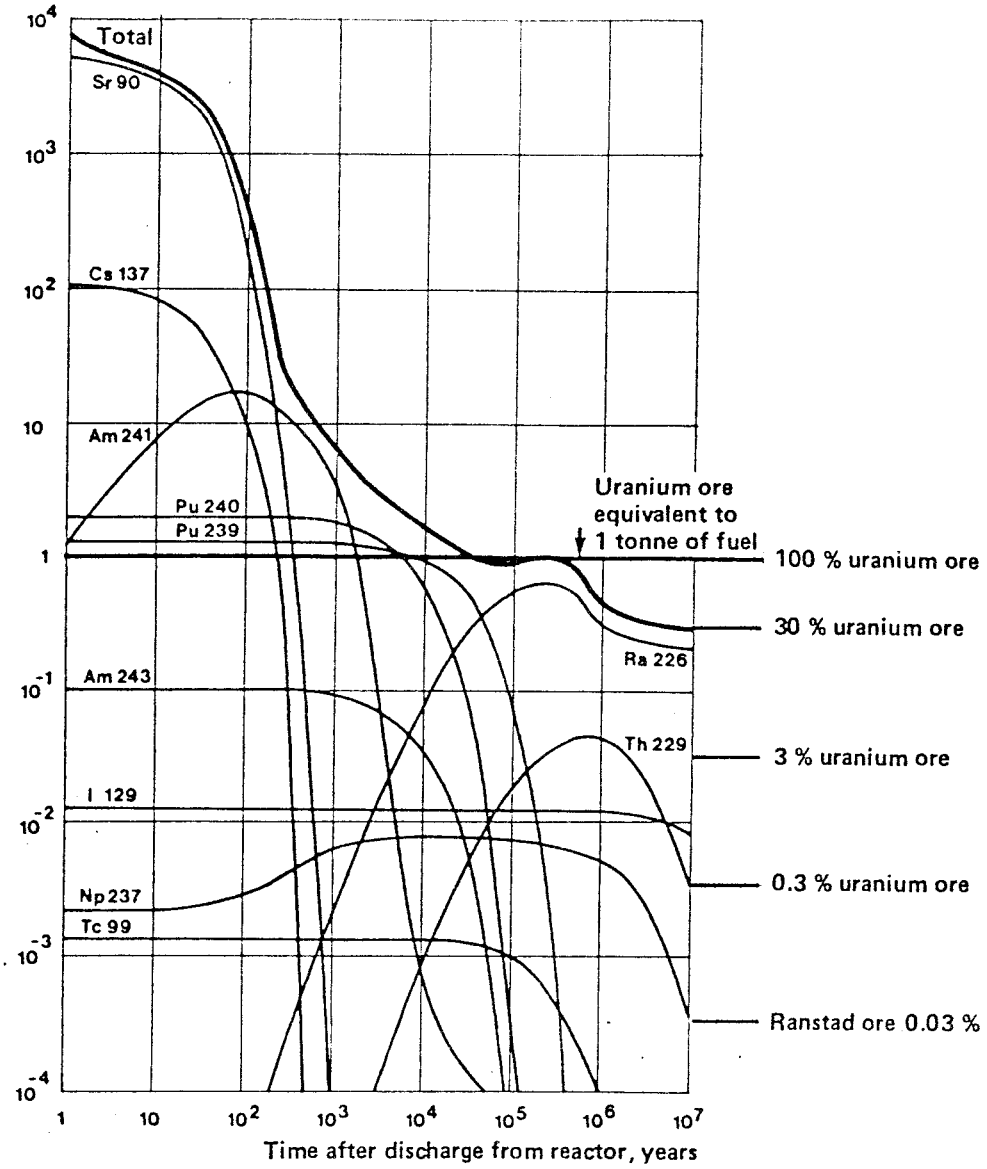

Fig. 1

Potential hazard index for different nuclides in 1 ton of spent fuel in relation to the quantity of uranium ore which is equivalent to 1 ton of fuel. Actual hazard is also dependent upon the exposure pathways of the elements to man (see chapter 6). The fuel has a burnup of 33 000 MWd(t)/tU, a power density of 34.4 MW(t) tU and an enrichment of 3.1% uranium 235.

The importance of the concentration of the radioactivity in space is emphasized in a recently published work by French geologists (4), from which the following quote is taken: "But for the evaluation of the safety of a repository, it is important to notice that the effect of the geological disposal is to concentrate 3530 tons of natural radioactive material in about 0.26 ton of glass. Besides, an enormous dilution is necessary to meet the safety requirements. For instance, approximately 1/30 of all France's groundwater resources would be required to dilute the cumulated quantity of waste

produced in the country up to the year 2000. The high density of radioactive material stored in a repository makes any comparison with natural radioactivity unacceptable until hundreds of thousands of years have passed, when radioactive decay will have reduced this density to natural levels in the ground." In this connection criticism is levelled at the American nuclear physicist B.L. Cohen, who disregards the concentration effect and who furthermore is cynical enough to calculate the number of human lives which are saved over a period of 1 million years (!) due to the fact that the amount of uranium in the world is reduced by uranium fission in nuclear reactors (5).

Other foreign calculations of the hazard index of waste and ore have taken into account the high dilution of the uranium in the ore. One example is provided by figure 2 from Bond, Claiborne and Leuze (6). While the hazard index of the high-level waste, calculated as the volume of water of maximum permissible concentration per volume of waste, has dropped to the level of the hazard index for 100% uranium ore after some 5000 years, it has been found that the hazard index of the waste will never, not even after dilution in 10 times the amount of glass, be reduced to the level of the hazard index of 0.2% uranium ore. Since an intact and effective encapsulation cannot be guaranteed for all future time, the authors draw the conclusion that it is necessary to separate the heavy nuclides U, Np, Pu, Am and Cm from the waste. Based on the requirement that the hazard index for the undiluted waste after the fission products have decayed should not exceed the hazard index for 3% uranium ore, the following degrees of separation are necessary:

99.9% for uranium, americium and curium
95.0% for neptunium
99.95% for plutonium

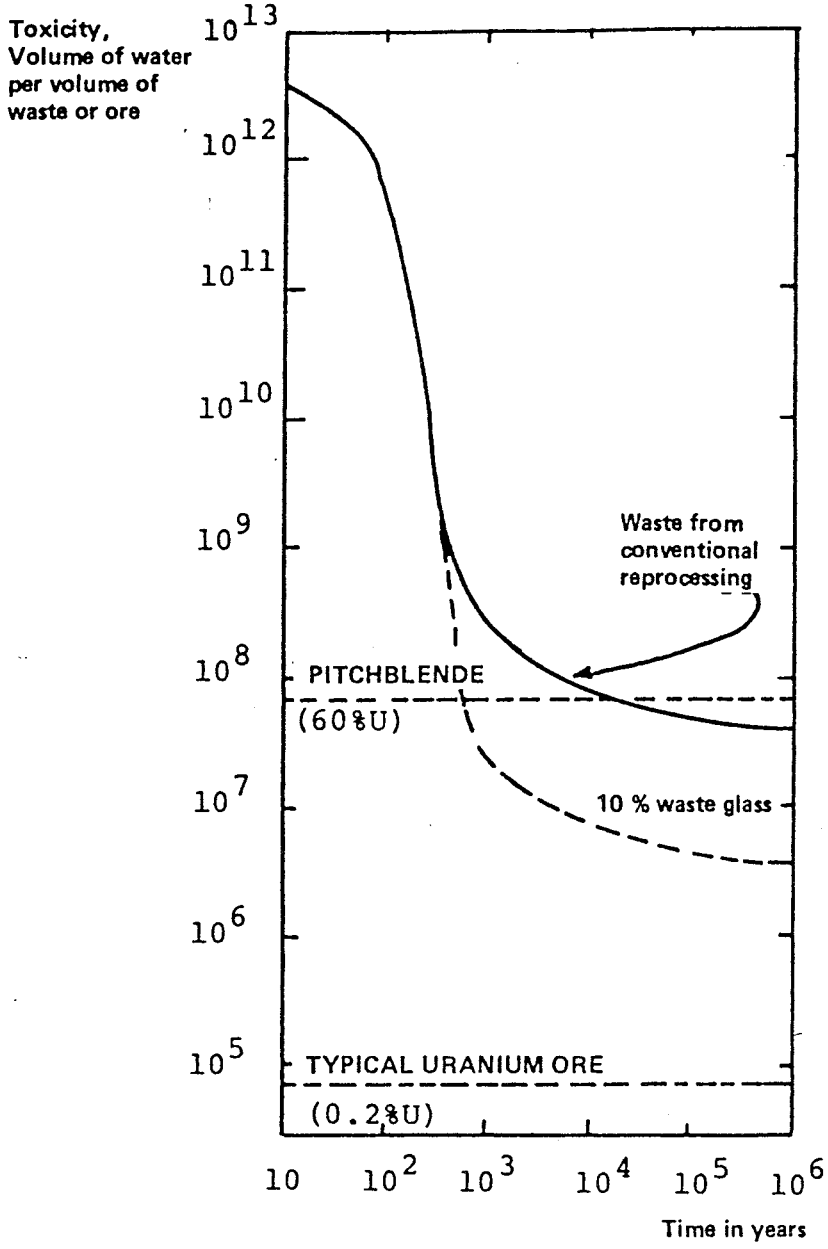

Fig. 2

Toxicity for high-level waste in comparison with uranium ore, from W.D. Bond, H.C. Claiborne and R.E. Leuze, Nuclear Technology 24 (1974) 362.

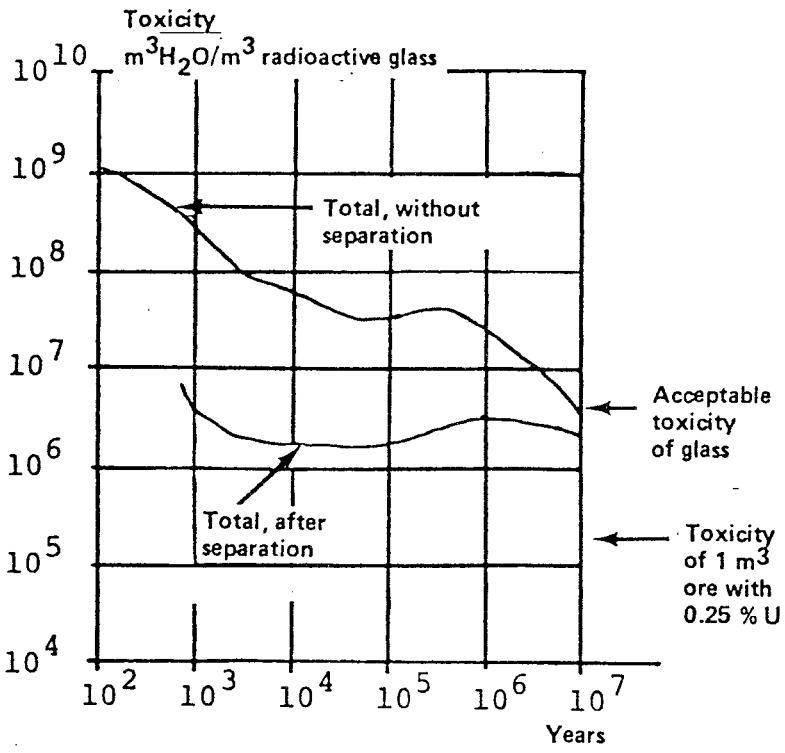

Fig. 3

Toxicity index of high-level waste glass in comparison with uranium ore, from B. Guillaume, B.I.S.T., CEA, No. 217. Sept. 1976, p. 31.

A French study published one year ago (7) arrived at similar results. Based on the leaching rate for French waste glass, combined with the maximum permissible concentration (MPC) for different nuclides, an acceptable toxicity index has been calculated for waste glass: $3 \cdot 10^6$ $m^3 H_2O/m^3$ glass. As is evident from figure 3, it takes 10^7 years for conventional waste glass to decay to this value. From this, the conclusion is again drawn that it is necessary to separate the trans-uranium elements from the high-level waste so that the above-mentioned limit is reached after only 1000 years, which is a reasonable service life for an effective encapsulation. The following degrees of separation have been calculated:

99.5% for americium and curium
95.0% for neptunium
99.99% for plutonium

It is thus concluded in both of these studies that the disposal of conventional high-level waste glass is not possible, since the encapsulation materials do not have a sufficient life span.

The solution is to separate long-lived nuclides, especially transuranium elements. Such a separation is termed in the French report to be "indispensable".

This French attitude is of special interest in view of the existing reprocessing agreement which Sweden has with France, under the terms of which French waste glass will be finally stored in Sweden. The fact that a country with such a positive attitude towards nuclear power as France takes such a hard line in the question of waste that they demand that 99.99% of the plutonium be removed from the waste makes the Swedish plans to allow all of the plutonium remain in the waste seem particularly heroic. Up until a couple of years ago, even Swedish nuclear power specialists considered the direct disposal of spent fuel to be "entirely unacceptable", not only from the energy point of view but also in view of safety requirements (ref. 1, page 93). If it is nevertheless decided that it is desirable to try to dispose of spent fuel directly without first separating plutonium and other transuranium elements, then in order to meet the aforementioned requirements, it is necessary to make sure that the spent fuel is kept effectively encapsulated until its toxicity has declined to that of the original uranium ore. A glance at fig. 1 shows that this can never be possible. While the ore can be assumed to have contained 0.3% uranium (in the case of the Ranstad ore, 0.03%), the hazard index for the spent fuel after 10 million years has only decreased to a value corresponding to 30% uranium ore. Even after 10 million years, the toxicity index of the spent fuel is still 100 - 1000 times greater than that of the ore from which it was produced. It is already evident from what has been said above that the direct disposal of spent nuclear fuel in accordance with KBS II must be regarded as out of the question, regardless of the encapsulation material (e.g. copper or aluminium oxide) used. Such a direct disposal of spent fuel gets us literally "out of the ashes and into the fire". Besides, discarding the nuclear fuel after only a few % of its energy content has been utilized is an unreasonable and indefensible waste of an energy source which is, for the time being and perhaps for the foreseeable future, unavoidably necessary. The only available alternative appears to be reprocessing and use and thereby destruction of plutonium and other transuranium elements as fuel in breeder reactors or other fast reactors. I shall return to this later.

1.2 With reference to the risk of criticality

With the direct disposal of spent fuel, one doesn't have the extra safety barrier in the form of low solubility which can be obtained with vitrified waste. The following quote from the report of the Aka Committee (the Swedish Government Committee on Radioactive Waste), part II (10), pages 115-116 illustrates this:
Naturally occurring uranium is effectively dissolved by oxidation by carbonate-containing groundwater, forming uranyl-

carbonate complex. - Uranium concentrations of up to 1800 µg per tonne have been measured in the groundwater in bedrock with a high water content from the Masugnsby district in Norrbotten, where a single spring (7.2 m^3 water per hour) is estimated to precipitate more than 6 kg uranium per year."

Strongly oxidizing conditions resulting from radiolysis are automatically obtained in the event of a canister failure. Strongly oxidizing conditions resulting from radiolysis are automatically obtained in the event of a canister failure. According to calculations by ASEA-ATOM (8), the water even around an undamaged canister will, after only a few years, be saturated with oxygen at 50 bar, which at 50°C gives about 1250 ppm. This oxygen content is about 250 times higher than in warm surface water and about 10 000 times higher than outside the most strongly radiation-absorbing canisters of lead-titanium and copper. Additional species that are oxidizing for the Al_2O_3 canister must also be considered, especially metal ions at a higher oxidation state, which are not taken into account in the calculations.

Groundwater normally contains high levels of carbonate. Thus, Forsmark water from a depth of 450 m has been found to contain 400 ppm HCO_3^-, which is about 10 times higher than the level in surface water. In addition, the basically reacting clay (bentonite) in which the canister is proposed to be embedded contains some 2% organic matter, which will be radiolytically oxidized to carbonate. Carbonate solutions are, incidentally, used to leach uranium out of uranium ores. It even seems that the richest uranium ores in nature were formed by precipitation from carbonate solutions, which had taken up uranium on their passage through uranium-bearing bedrock. If the uranium, which makes up most (95%) of the spent fuel, is leached out, plutonium and other transuranium elements (combined about 1%) will remain in the form of a poorly soluble sludge. Under such circumstances, there is a definite risk that plutonium could accumulate in sufficient quantity to trigger a nuclear reaction. Only 0.5 kg of fissionable plutonium is required for this purpose (11). A suitable moderator, water, is always available. The risk of such criticality accidents in connection with the direct disposal of spent nuclear fuel is pointed out by the Aka Committee Report (9): "However, terminal storage of spent fuel places greater demands due to factors such as risk of criticality in the presence of plutonium." The Aka Committee Report pointed out the risk of criticality accidents during storage for the reprocessing alternative as well: "It would entail special problems if it became necessary in any situation to include large quantities of plutonium in the waste. In such a case, the risks of criticality in connection with storage over very long periods of time would have to be carefully examined" (ref. 10, page 99.) In the direct disposal of spent fuel, all of the plutonium is incorporated in the waste. A nuclear reaction in the middle of a waste repository would be a catastrophe with unforeseeable consequences. New canister failures could then occur in rapid sequence and large quantities of radioactive material could escape.

According to the direct disposal alternative proposed by the KBS project, each ceramic canister would contain ca 1 ton of uranium in the form of spent fuel. This would contain 0.7% or some 7 kg of plutonium-239. The time required for this to decay to 0.5 kg is some 100 000 years. Such a long period of time would certainly embrace one or more ice ages and would thereby entail unforeseeable conditions in the waste repository.

2. The importance of slow-acting and unknown material destruction processes and the lack of relevant test results.

The long time perspective involved in the terminal storage of nuclear waste creates problems which were previously unknown in technical contexts. The long periods of time which are necessary for the waste to decay lead to a high degree of uncertainty in extrapolations of test results and experiences obtained over short periods of time. The entire history of science shows that scientific exploration normally begins with practical observations for which an explanation is then sought, in the beginning (in classical antiquity) by purely speculative means, later (after the breakthrough of the scientific method) by means of systematic experimental procedures, which have gradually been facilitated by an ever-growing theoretical understanding of certain fundamental phenomena. In many cases, this has made it possible for us to learn to master the problems which gave the impetus to the research work. In the case at hand, time does not permit this natural process of development. Even within, for example, the technologically highly advanced field of space exploration, it has been possible to work with both simulations and practical trials from which conclusions could be drawn for the continued work. But it is not possible to simulate or study by means of practical trials the effects of time spans which are far beyond those of human experience. In selecting materials and designs for waste canisters, it is patently impossible to take into account processes whose nature is unknown, but whose existence cannot rightfully be excluded. Allowance must be made, for example, for the existence of heretofore unknown processes of ageing and material destruction. The possibility cannot be excluded that a canister will, after a thousand years or so, begin to be destroyed by a slowly-acting ageing process XYZ, the nature of which, due to the necessarily long periods of time required for testing, may not have been elucidated until long after.

In the absence of test results and practical experiences, even fundamentally well-known phenomena and processes can easily be overlooked. Thus, the Aka Committee (9, 10) completely overlooked the radiolysis effect.

After the undersigned, in his statement of comment (12) on the findings of the Aka Committee, called attention to this effect, well-known within reactor technology, it has been found to be of fundamental importance for the entire disposal technique and is the reason why a copper canister with a wall thickness of 200 mm

has also been proposed for spent fuel. For vitrified waste, the original proposal was a titanium canister with an "inner radiation shield" of 250 mm steel, which in the final version was replaced by 100 mm lead. With such wall thicknesses, penetrating radiation and thereby radiolysis effects are reduced to negligible levels, compared with the case with Al_2O_3 canisters, around which the environment will be strongly oxidizing for the foreseeable future, including saturated with oxygen at high pressure, about 50 bar (cf. ref. 8, point 1.2 above).

3. Geohydrogical conditions in the repository

3.1 Requirements on the bedrock in accordance with the KBS safety analysis

As a basis for the work of the reference group, an Appendix A, dated 29 September 1978, has been submitted. This appendix contains the following introductory text under the above heading:
Test drillings and measurements at three different sites in Sweden to a depth of about 500 m (a total of 7 boreholes) have demonstrated that rock with a permeability of about 10^{-9} m/s is available at the intended depth (2).

The hydraulic gradient (i.e. slope of an isobar surface) at the depth in question is only one or a few promille. At a hydraulic gradient of 3 o/oo and a permeability of 10^{-9} m/s, a flow of 0.1 litre per year is obtained per m^2 cross-section of the rock.

The above conditions pertain to the time before the repository has been excavated and the time after the water table has been reestablished after closure of the repository. During the intervening period, an inflow towards the repository will take place that compensates for drainage pumping and later for recharging of the aquifer. The regional flow pattern of the groundwater should be largely restored 100 years after closure of the repository. Disturbances of the groundwater flow due to heating of the repository are, on the whole, neglible.

The storage holes in the repository will, as has already been indicated, not be located in or immediately adjacent to existing zones of weakness in the bedrock, in which any future rock movements will be concentrated. However, stress changes of tectonic origin, e.g. caused by a glaciation, may conceivably give rise to fractures and minor displacements in the rock around the repository. Only small movements will be involved here, and the buffer material will, thanks to its swelling capacity and plasticity, act as a mechanical cushion for the canisters. Any fractures created by these movements will not be so large that the buffer material is carried away with groundwater. Hence, the canisters will always be surrounded by conditions of unchanged low permeability."

This constitutes a brief review of two of KBS's previous geological reports, namely:
"Handling of Spent Nuclear Fuel and Final Storage of High-Level Reprocessing Waste. II Geology", Dec. 1977 (13) "Handling and Final Storage of Unreprocessed Spent Nuclear Fuel. II Technical", p. 83-126, August 1978 (14).

After test drillings at a number of sites - Finnsjö, Forsmark, Kråkemåla, Torö and Karlshamn (Sternö) - KBS has concluded that only Karlshamn meets the requirements on low fracture content and low permeability for water that must be imposed on a final repository.

3.2 The Government's requirements on a supplementary geological study

As is known, the Government rejected on 5 October 1978 the Swedish State Power Board's application of 6 December 1977 to fuel Ringhals II and required a supplementary geological study. In explaining its decision, the Government stated the following:

"The Stipulations Act does not require that the applicant specify a definite site for the final repository. In the present case, however, the law is interpreted as requiring the applicant to demonstrate that an area or areas possessing such characteristics that a final disposal of nuclear waste can be effected in accordance with the requirements imposed by law exists in Sweden.

The supplementary geological study should therefore demonstrate the existence of a sufficiently large rock formation at the depth in question and possessing the other characteristics on which the KBS safety analysis is based."

In connection with the Government's rejection of the Swedish State Power Board's fuelling application and the subsequent Government crisis, leading politicians made statements based on the assumption that the waste issue had been 99% solved and that the demand for additional boreholes was "politically motivated". In retrospect, such statements appear to be deeply irresponsible.

KBS concentrated the study requested by the Government to the Sternö Peninsula near Karlshamn and presented a report entitled "Handling of Spent Nuclear Fuel and Final Storage of Vitrified High-Level Reprocessing Waste. VI Supplementaty geological studies" in February of 1979 (15) as a basis for a renewed application of 20 February 1979 to fuel Ringhals II, at the same time as the "Forsmarks Kraftgrupp AB"

3.3 Review of the supplementary geological study ("the borehole report") through SKI's Geologist Group

3.3.1 Bedrock conditions and rock volumes

In order to evaluate the supplementary studies called for by the Government, the Swedish Nuclear Power Inspection Board (SKI) appointed an advisory consultant group for geology matters, referred to in the following as the SKI Geologist Group, in November of 1978.

As is generally known, in its statement (SKI's Geologist Report) of 12 March 1979 (16), the SKI Geologist Group subjected KBS Report VI to a point-by-point scathing criticism and declared it to be completely unsatisfactory.

Introductorily, the SKI Geologist Group observes that the new boreholes (Ka 2, Ka 3, Ka 4 and Ka 5) were all positioned incorrectly in order to achieve their purposes. With regard to the boreholes Ka 4 and Ka 5, this is demonstrated by Fig. 4 below, reproduced from the SKI Geologist Report (ref. 16, Fig. 3.1.1, page 11).

Boreholes Ka 4 and Ka 5

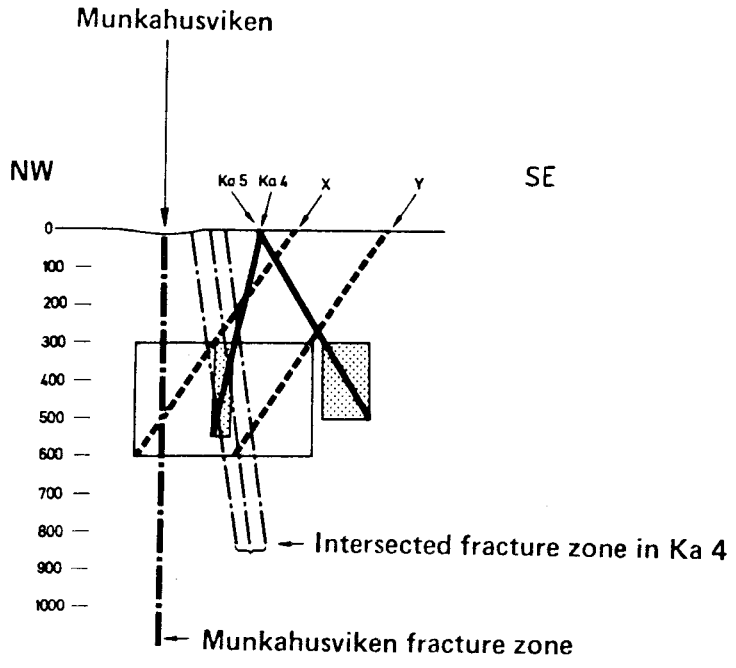

Figure 4. The dashed lines X and Y show how drilling should have been carried out in order to cover as large a portion of the area as possible SE of the fracture zone between the depths of 300 and 600 m. The dotted rectangles show what was sampled and the white rectangle shows what would have been sampled with the right borehole positioning.

In spite of this, some of the information obtained is indicative enough. Fig. 5 below is a reproduction from the SKI Geologist Report, Fig. 3.1:5, supplemented with a symbol key from Fig. 3.1:3 and a text passage from page 45 (ref. 16). Even a layman can see that a rock massif containing a number of water-bearing fracture zones (crush zones) up to 25 m wide, four of which are in direct connection with the water in Munkahusviken Bay, cannot be suitable for the storage of radioactive waste.

With regard to its review of the supplementary geological study as far as bedrock conditions and rock volumes are concerned, the SKI Geologist Report states in conclusion (ref. 16, page 40): "The Sternö study has not demonstrated that a repository for high-level waste in accordance with KBS I can be effected in Sweden".

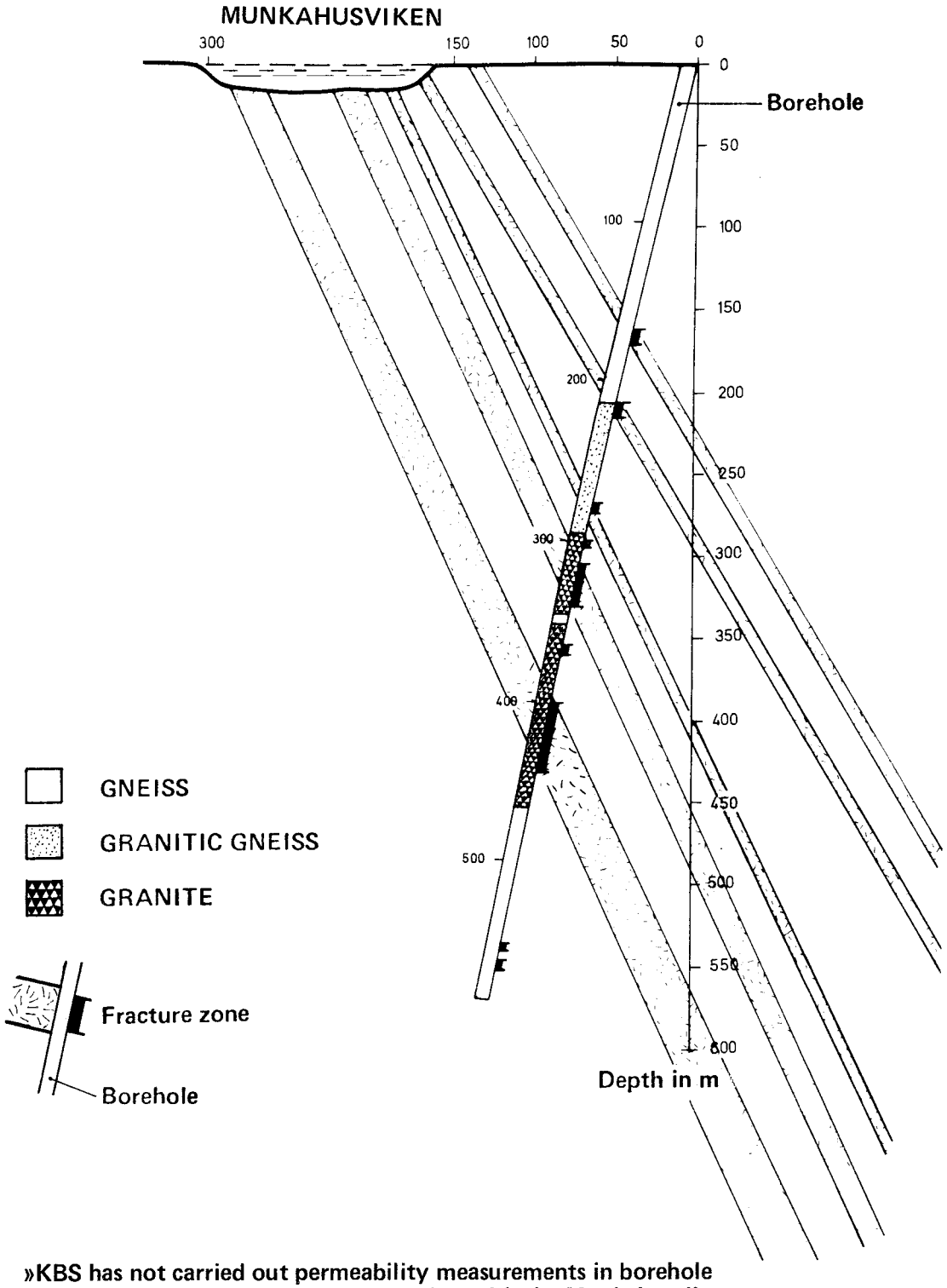

»KBS has not carried out permeability measurements in borehole Ka4, which is drilled in direct connection with the Munkahusviken fracture zone B. High permeability values would probably have been obtained there.»

SKI Geologist Report (Ref.16), page 45

Figure 5. Fracture zones below Munkahusviken on the Sternö Peninsula outside Karlshamn, intersected by KBS borehole Ka 4.

3.3.2 Permeability conditions and groundwater movements

Under the above heading, the SKI Geologist Report states the following with regard to the theoretical potential (flow-technical) calculations on which the KBS safety analysis is based:

"Since fracture zones can be expected to have a much higher permeability than the surrounding, less pervious rock, the potential theory calculations carried out by KBS give erroneous results as long as the fracture zones are not taken into account. Fracture zone A, which cuts right through the final repository in figs. 3.2:5 and 3.2:6, has, according to SGU February 1979, a measured permeability of between $1 \cdot 10^{-9}$ and $1.5 \cdot 10^{-6}$ m/s. KBS has not performed permeability measurements in borehole Ka 4, which is drilled in direct connection with the Munkahusvikens fracture zone B. High permeability values would probably have been obtained there."

To this may be added the fact that a higher permeability than that which is assumed has double, or rather a quadratic effect. If, for example, the permeability is ten times higher than that which has been assumed, the effect will be 10.10 = 100 times higher, since both the corrosion attack on the canister material plus the eventually exposed fuel or waste glass and the dispersal of dissolved radioactivity can be assumed to be proportionate to the flow rate of the water through the repository.

3.3.3 Composition of the groundwater

Concerning the two probably decisive factors in the composition of the groundwater, namely chloride content and oxygen content, the SKI Geologist Report states the following:

With regard to the chloride content:

"Regardless of whether the water is salt or fresh in rock at a depth of 500 m on the Sternö peninsula, the risk must be considered to be very great that salt water will come to constitute part of the pumped water quantity after a few years of pumping in the repository.

On the basis of the water sample taken in the Baltic Sea at the water intake to the Karlshamn station, the chloride content in parts of the repository can be expected to rise to about 4 000 mg/l, as compared to the maximum value of 400 mg/l assumed by KBS."

With regard to oxygen content:

"The concentration of free oxygen normally declines with increasing depth (TR 88). However, fracture zones with a high water turnover could conceivably carry oxygen-containing water down to great depth. Evidence for this is provided by the signs of groundwater circulation far below the level of the valley bottoms found in certain mines, e.g. the Nyäng Mine at Hofors and Kristinaberg in Västerbotten county (situation report, AKA Committee, 24 June 1974). In the Ställberg Mine as well, the iron-manganese ore is oxidized to a depth of 700 m in the fracture zones (STU, Ser Ca No 35), as well as in the Garpenberg sulphide ore mine at Hedemora, where parts of the ore are oxidized to a depth of 500 m. (Wesslén, Internal Report, AB Zinkgruvor)."

It is also worth mentioning that the environment immediately surrounding the Al_2O_3 canister in particular will be strongly oxidizing due to radiolysis in the foreseeable future, including saturation with oxygen at high pressure, about 50 bar (cf ref. 8 and points 1.2 and 2 above).

3.3.4 Conclusions of SKI's Geologist Report

The conclusions at which the Consultant Group for Geology Matters appointed by SKI has arrived on the basis of its review are reproduced here in extenso:

"The additional four boreholes drilled by KBS on the Sternö Peninsula and the geological studies carried out by SGU have shown that the bedrock is intersected by a number of crush and fracture zones. Upon examining the drill core mapping results, the group has also found additional fracture zones of importance, and has been able to illustrate how, e.g., the Munkahusviken fracture zone intersects the repository. The few boreholes that have been drilled leave large portions unsampled and the fracture frequency in these portions cannot be estimated.

Merely the fact that a broad NNE running fracture zone divides the repository area into two parts keeps this area from fullfilling the geological conditions established by KBS for an absolutely safe repository. The additional fracture zones located within the repository area show conclusively that the Sternö area does not meet the established geological requirements. Nor can it therefore be used as a reference area to demonstrate that such a repository may be effected.

Due to the existence of fracture zones in and around the Sternö peninsula, the flow paths of the groundwater in the intervening, less pervious rock are judged to be short. In order for the transit time of the water to be 400 years, homogeneous rock with a permeability of about 10^{-12} m/s must extend around the repository and to a

distance of ten or several tens of metres around the storage holes and the tunnels. In order for the groundwater flow around the storage holes to be no more than 0.2 l/m^2 and year, a permeability of about 10^{-10} m/s is required. It is not possible to conclude with certainty on the basis of the data presented by KBS that rock fullfilling the above requirements has been found on the Sternö peninsula. This uncertainty can largely be explained by the absence of scientific evidence for the contention that the measuring methods used provide a representative picture of the permeability conditions existing in a large rock mass.

The water chemistry studies performed cannot be considered to be sufficient to verify the supposition that the chemical properties of the groundwater that are of importance for the safety of the repository lie within the variation range postulated in previous KBS reports.

The Consultant Group is therefore of the opinion that the Sternö area

- cannot be used for the repository proposed by KBS,
- cannot be used as a reference area for a final repository.

The Consultant Group would none the less like to state its confirmed opinion that the Sternö studies have not demonstrated that it is impossible to effect a repository for vitrified waste from reprocessing in crystalline bedrock in Sweden.

A special statement has been submitted by Professor Sven Hjelmqvist."

Following is the final paragraph of the special statement submitted by Professor emeritus Hjelmqvist, which in detail does not appear to contradict the opinion of the majority:

"My conclusion is that the rock as such on Sternö is quite usable for the disposal of nuclear waste, but that it is uncertain whether its extent is sufficient for 9 000 waste canisters on one level."

In view of the reservation expressed by Professor Hjelmqvist in his statement, it would seem to be more fitting to characterize the majority ratio within the SKI Geologist Group as 7 1/2:1/2 rather than 7:1.
It should be observed that the SKI Geologist Group studied the current situation, but not the unforeseeable factors which could come into play in connection with a future glaciation (17).

3.3.5 The importance of the conclusions in the SKI Geologist Report

Through their conclusions, the SKI Geologist Group have shattered the foundation of the entire KBS project, since one of the premises for the project is impervious rock with virtually stationary groundwater. As is known, the Board of SKI chose to disavow its own Geologist Group. When the Chairman of the Board of SKI, Governor Netzén, appeared on TV late in the evening of 27 March 1979 (ironically enough the day before the Harrisburg accident!), he characterized, using an expression which was more apt than he probably intended, the meeting in question as a "long day's journey into night" and justified the position of the Board by saying that the Geologist Group was not unanimous (!).

Unfortunately, the Ullsten Government followed the decision of the Board of SKI and thereby put itself above the judgement of the Geologist Group as well, despite the fact that this judgment was based on facts that were quite clear and understandable even for the layman. That this could occur could only be explained by the anti-intellectualism and the contempt for knowledge which has permeated Swedish society in recent years, destroying our schools, returning us to illiteracy, ruining our universities and undermining our research potential. Nevertheless, the scientists in the Corrosion Institute Reference Group should refrain from following in the footsteps of the politicians. Instead, the Reference Group should respect what another group of scientists, the SKI Geologist Group, has arrived at after careful consideration and thereby reject the premises set up by KBS, which were clearly based on ignorance and wishful thinking. In actuallity, it should be the Reference Group's duty, in the light of the results arrived at by the SKI Geologists Group, to revise its previous statements on the expected life of both the lead-titanium and the copper canisters. The general public cannot be expected to be familiar with the premises upon which and the reservations with which the Reference Group has predicted lives of thousands and hundreds of thousands of years. If, however, the premises are false, the conclusions are also false. For my own part, I have also rejected the metal canisters in special statements, in the case of the copper canister with reference primarily to geological arguments.

4. Corrosion testing

4.1 Testing conditions

Corrosion testing in water of approximately the composition that can be expected in the final repository has been performed on both unloaded and loaded specimens of isostatically compressed Al_2O_3. The testing of unloaded specimens was done to study general corrosion as well as types of local corrosion that are not affected by the state of mechanical stress, e.g. intercrystalline corrosion (intergranular corrosion) and pitting. The tests of mechanically loaded specimens were aimed at studying the risk of stress corrosion cracking (spontaneous cracking, delayed failure), which has been found to be a commonly occurring phenomenon in ceramics.

While the time factor can never be simulated, corrosion testing should otherwise be conducted under the conditions of actual use. Corrosion was studied on unloaded specimens at different temperatures, whereby an elevated temperature, which appears to be accelerating, can compensate to some extent for the time factor. The studies of delayed failure, however, took, place at 20° C instead of 70° C, as recommended by the Reference Group for Corrosion.

Above all, however, neither of the testings took place under realistic conditions as far as radiation and resultant strongly oxidizing conditions due to radiolysis of the surrounding water are concerned. Radiolysed water is the strongest oxidant known to man. Even if Al^{3+} in Al_2O_3 cannot be oxidized to a higher valence, impurities of e.g. Cr, Mn and B present at the grain boundaries could be oxidized to water-soluble chromate, permanganate and perborate, respectively. There is therefore reason to suspect that the intercrystalline corrosion that has been found in irradiated water by means of two independent methods will be incomparably greater under conditions of radiolysis. Since intergranular corrosion can give rise to microcracks, which then grow to critical size and led to failure, the same should apply to stress corrosion cracking.

Tests of the types of corrosion which appear to be of special importance for the life of the canisters are described below.

4.2 Intercrystalline corrosion

The corrosion of the aluminium oxide in a stressless state has been studied on small specimens (3 x 3 x 50 mm) in chloridic water buffered by sodium hydrogen carbonate at 80° C and pH 8.5 in a study by Nils Ingri and Lars-Olof Öhman at the University of Umeå (18). The summary of this report is reproduced below in extenso (this author's underlinings):

"Polycrystalline δ-Al_2O_3 was leached at 80° C in flowing sodium-hydrogen-carbonate-buffered chloridic water, and with pH = 8.5 for 75 days. By means of continuous addition of leachant solution, the solution was kept unsaturated with respect to Al (aq) in order to maximize corrosion.

The corrosion rate for Al_2O_3 was determined in two independent ways : first by means of regular weighing of the test body, second by spectro fluorometric Al analysis of the leachant solution. After 10 days of leaching, a constant corrosion rate was obtained in accordance with both methods. The values that were obtained were:

$(68 \pm 6).10^{-9}$ m.year^{-1} according to the gravimetrical anaylsis method
$(16 \pm 1).10^{-9}$ m.year^{-1} according to the fluorometric method

The specified error limits correspond to a significant level of 99%.

A probable explanation of the difference is that the gravimetric method measures a combined chemical and mechanical corrosion, while the fluorometric method only measures the chemical portion, i.e. the Al_2O_3 quantity that has been dissolved and has come out into the leaching solution.

The results are summarized in Fig. 6. below, which is a reproduction of the original report's Fig. 3. The authors make the following comments to this diagram:

"After about 10 days of leaching, a state has been reached where the corrosion rate is constant. According to the gravimetric method of analysis, a corrosion rate of $(68 \pm 6).10^{-9}$ m.year^{-1} is obtained, while the fluorometric method gives a corrosion rate of $(16 \pm 1).10^{-9}$ m.year^{-1}. The given error limits correspond to a significance level of 99%.

The difference in the corrosion rate cannot be explained by reference to statistical or technique-related factors. A reasonable explanation is that the gravimetric method measures a combined chemical and mechanical corrosion, while the fluorometric method only measures the chemical portion, i.e. the Al_2O_3 that has been disolved and has come out into the leaching solution. The mechanical portion of the corrosion would consist of undissolved Al_2O_3 particles that have come loose from the test body and have accompanied the leaching solution out into the collection vessel."

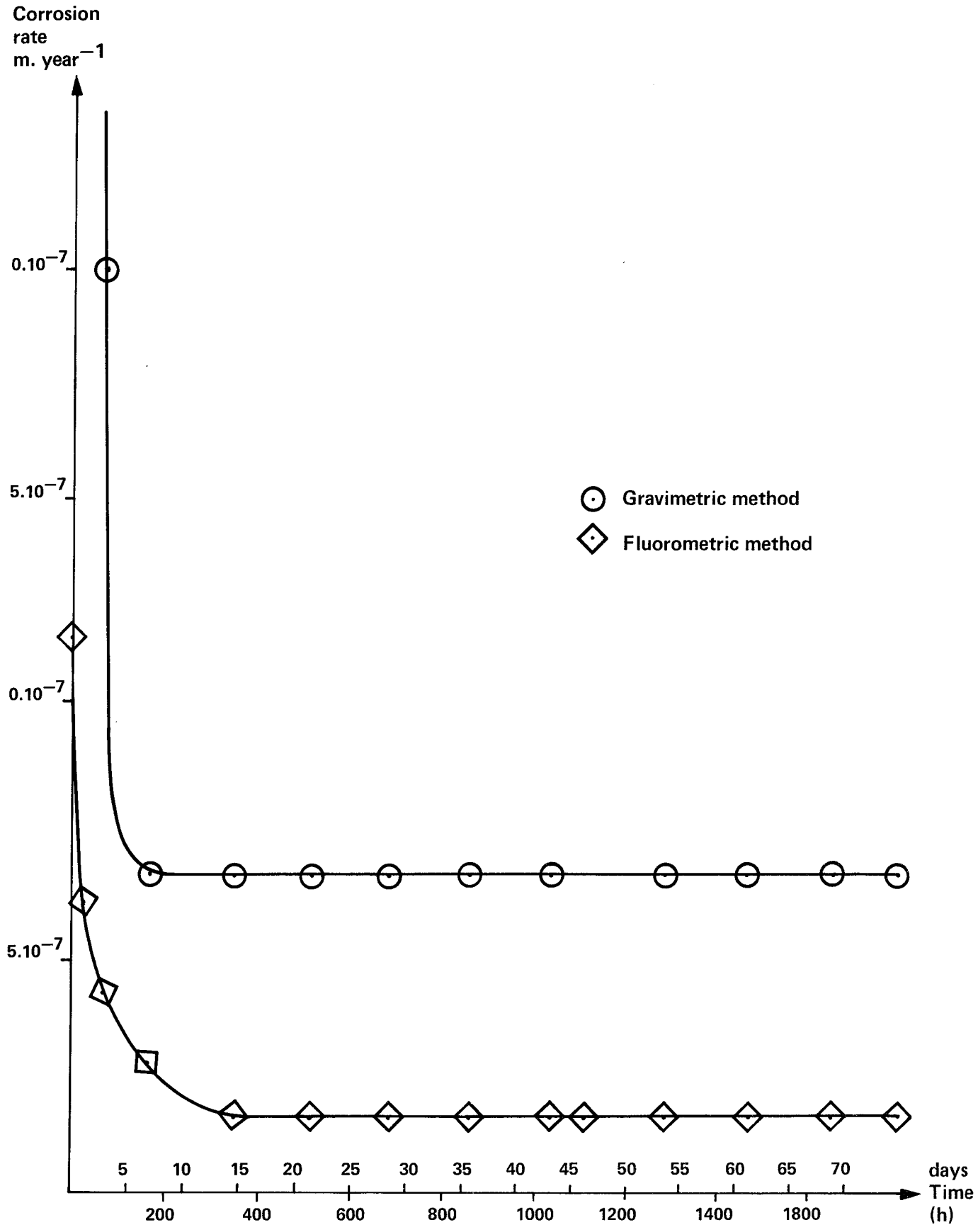

Figure 6. The rate of corrosion of the test body as a function of the leaching time.

The interpretation which lies nearest at hand is that the Al_2O_3 material (with an average particle size of 3 µm) is attacked (etched) preferentially at the grain boundaries so that some grains fall off the test bodies. While weighing the test bodies records the total material loss, the fluorometric method only records the chemical portion thereof.

The supposition that the corrosion attack on isostatically pressed Al_2O_3 is of an intercrystalline nature is confirmed in a study by A. Bäcklin, A. Johansson, Bo Sandqvist and Lars Westerberg at the Tandem Accelerator Laboratory at the University of Uppsala (19). The purpose of this study was to determine, by methods of nuclear physics, how deeply hydrogen penetrates into aluminium oxide. This was accomplished by measuring the depth distributions of hydrogen in specimens leached for different periods of time in water. Comparison was thereby made with a single crystal of sapphire. With reference to a diagram in report (19), the authors write (on page 6):

"The points for the sapphire specimen do not deviate significantly from a horizontal line. With this method, we can therefore not demonstrate any attack on the saphire. For the two polycrystalline specimens, at pH 9.3 and 7, straight lines have been adjusted by means of the least squares method resulting in slopes of 220 ± 90 Å/year, and 340 ± 90 Å/year respectively.

"The fact that the attack takes place at a faster rate in the polycrystalline material indicates that the attack takes place along the grain boundaries."

It may be argued that the intercrystalline attack takes place very slowly. But it must be remembered that the attack can be expected to proceed more rapidly in materials subjected to both mechanical stresses and radiation and that local intergranular attacks can give rise to stress-raisers (micro cracks) which first grow slowly (subcritical crack growth), but then after reaching a given critical size, rapidly grow to failure in accordance with what is said below under 4.3.

4.3 Delayed failure (delayed fracture, stress corrosion cracking, spontaneous cracking) in Al_2O_3 material

As in other ceramic materials, there is a risk in Al_2O_3 of delayed failure, owing to the fact that small cracks existing from the beginning grow slowly under the influence of tensile stress and water or moist air, until they reach a critical size, whereby failure occurs rapidly. This phenomenon can be regarded as a case of stress corrosion. If the tensile stresses consist of residual stresses from the fabrication process, which is often the case, the term spontaneous cracking is appropriate.

The theory of delayed failure in ceramic materials, short-term tests based on this theory and the means of making service life predictions for e.g. electrical insulators of Al_2O_3 have been developed over the past 15 years above all by the American S. M. Wiederhorn (20-26), active at the National Bureau of Standards, Washington, D.C., USA. Experience of the applicability of the theory in practice extends back only ten years or so.

The following empirical relationship holds for slow-sub-critical crack growth for relatively short periods of time:

$$V = A \cdot K_I^n \qquad (1)$$

where V = the crack growth velocity in m/s
A and n are constants
K_I = the stress intensity factor in MN . $m^{-3/2}$

defined by

$$K_I = \sigma_a \cdot Y \cdot \sqrt{a} \qquad (2)$$

where σ_a = tensile stress in MN . m^{-2}
a = crack depth in m
Y = a geometric factor, which in this case is assumed to be 1.12 $\sqrt{\pi} \simeq 2$.

Equation (1) is usually illustrated schematically in a log-log diagram, as shown in Fig. 7. The equation corresponds to the straight line designated I in the figures. The slope of this line constitutes the exponent n.

By integration of equation 1, an expression for the life of τ (s) the canister is derived in ref. 24:

$$\tau = \frac{2}{(n-2)A} \, 2^{-2} \cdot \sigma_a^{-2} \cdot K_I^{2-n} \qquad (3)$$

corresponding to equation (5) in ref. 24. By inserting K_I according to equation (2) in equation (3) the following is obtained:

$$\tau = \frac{2}{(n-2)A} \, 2^{-n} \cdot \sigma_a^{-n} \cdot a_i^{-\frac{n-2}{2}} \qquad (4)$$

where a_i = the depth of the deepest crack in the initial phase.

Solution for a_i gives

$$a_i = \left(\frac{n-2}{2} \cdot A \cdot \tau\right)^{-\frac{2}{n-2}} \cdot \left(2 \sigma_a\right)^{-\frac{2n}{n-2}} \qquad (5)$$

an expression well-suited for taking the logarithm of.

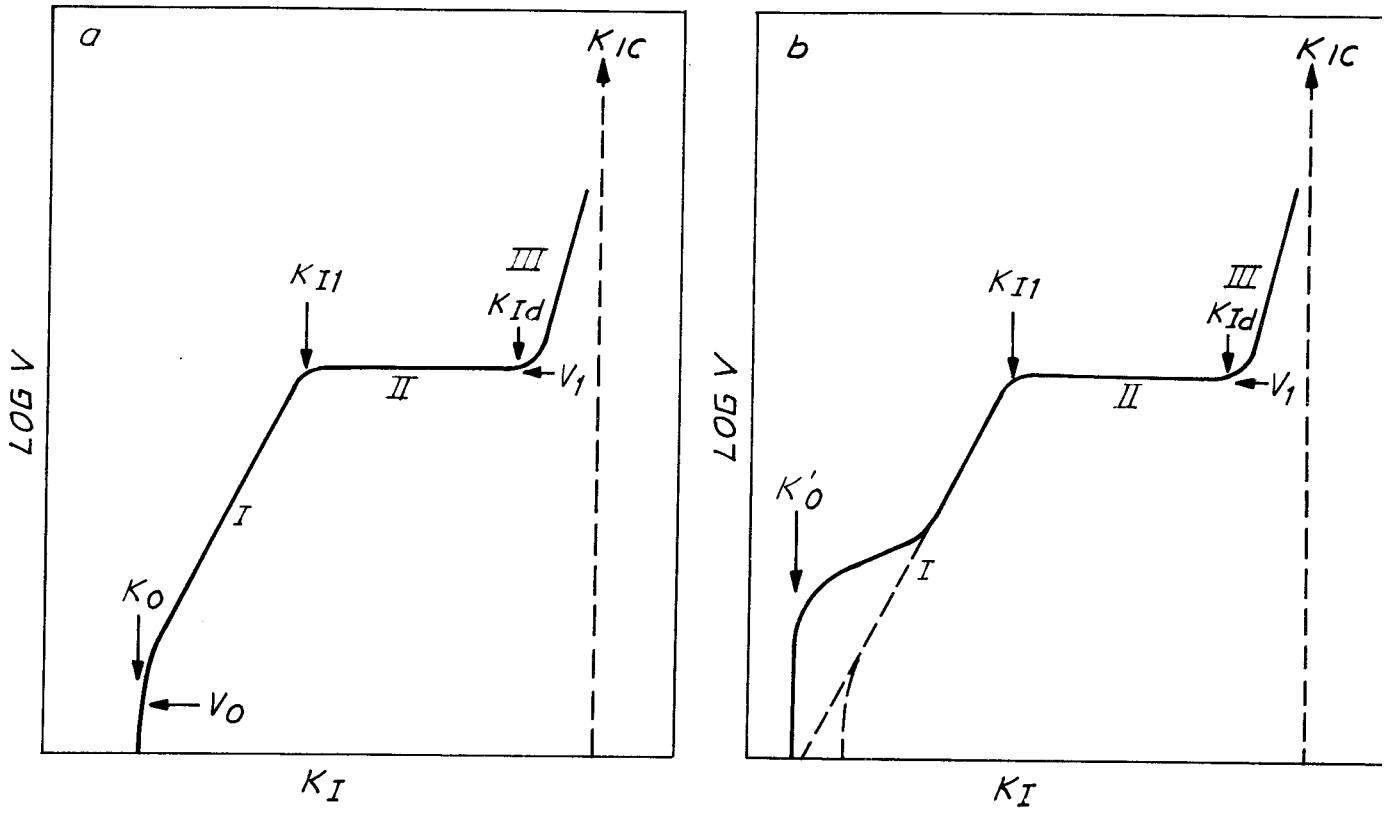

Figure 7. Schematic K-V diagrams

a. According to what is known now

b. With now unknown accelerated cracking mechanism at low crack propagation velocity

Since n is a large number, it will be seen that the permitted crack depth a_i varies only insignificantly with assumed canister life. ASEA has mainly carried out calculations for 10^6 years = $3.1536 \cdot 10^{13}$ s. However, it is of the utmost importance to carry out calculations for shorter times as well. The easiest way to do this is to calculate the factor with which a_i can be permitted to increase if the service life requirement is reduced by one power of ten. It will be seen that this factor, here designated the decade factor (d), is $10^{\frac{2}{n-2}}$.

While, according to information in the literature (27), it has been found that for single crystals of Al_2O_3 $n \simeq 30$, 1) ASEA has found, 3) with isostatically pressed aluminium oxide 2) in preliminary tests 4) in rock water, a stronger dependence on K_I, $\frac{1}{109}$ namely with the exponent n = 210, whereby $d = 10^{\frac{1}{109}} = 1.021$. The corresponding value for log A is given to be -120.

In table 1, the permitted crack depth has been calculated according to equation (5) for the times 1, 10, 100, 10^3, 10^4 and 10^6 years, expressed in seconds. σ_a is expressed in MPa = MN/m^2. a_i is then obtained in m, but is expressed in the table in mm.

The values for 10^6 years were first calculated. These values agree well with those calculated by ASEA. For shorter times, a_i has been obtained by multiplication by the decade factor d.

Table 1. Largest permitted initial defect for ASEA's isostatically pressed Al_2O_3 material. Calculation of a_i in accordance with equation (5), whereby n = 210. log A = -120. The decade factor $d = 10^{\frac{1}{109}} = 1.021$

Tensile stress, σ_a		Maximum permitted crack depth, a_i mm, at a calculated canister life of						
MPa=MN/m^2	kgf/mm^2	1 yr	10 yrs	100 yrs	10^3 yrs	10^4 yrs	10^5 yrs	10^6 yr
38[a]	3.87	1.80	1.76	1.72	1.69	1.66	1.63	1.60
50[b]	5.09	1.07	1.05	1.03	1.01	0.99	0.97	0.95
80[c]	8.15	0.393	0.385	0.377	0.370	0.363	0.357	0.350
150[c]	15.3	0.112	0.110	0.108	0.106	0.104	0.102	0.100

a estimated maximum residual stress

b maximum residual stress + tensile stress, caused by uneven swelling of the bentonite

c proposed proof tests in order to be able to reject canisters with unpermitted initial crack depth in advance.

4.4 Discussion of test results with respect to delayed failure

Materials that are sensitive to cracking resulting from stress corrosion should not even be considered for use for very long periods of time. This should apply to aluminium oxide as well as titanium.

Furthermore, it would appear to be extremely chancy to extrapolate from short-term measurements of crack velocity over a few days to very long periods of time. In connection with measurements during short periods of time, the crack growth may be diffusion-limited (ref. 28), which is very unlikely to be the case when long periods of time are available, at least in the liquid phase in the cracks. Extrapolation of short-term measurements to long periods of time can therefore give excessively low values for crack growth. If, on the other hand, diffusion in the solid phase is velocity-limiting, it should not be possible to disregard the effect of radiation on diffusion in the solid phase and thereby on crack growth.

It is also evident from table 1 that the service life for the ASEA material drops very steeply at only an insignificant increase of initial crack depth. The difference in permitted crack depth per power of 10 of service life is only 2% and the difference between 1 million years and 1 year is only 12%.

Originally, it had been planned to detect unpermitted initial crack depths by means of ultrasonic testing. However, according to a report from the "Tekniska Röntgen Centralen" (Technical X-ray Centre), the detectability limit on a bare canister surface is 0.6 mm. In practice, however, the canister is enclosed by a steel shell, whereby the detectability limit rises to about 2 mm. Instead it has therefore been found necessary to proof test each canister at a proof stress amounting to 2-4 times the expected maximum residual stress (38 MPa). The underlying theory for this testing methodology is the same, however. While, in principle, unpermitted crack depths deriving from the fabrication procedure can be detected in this manner, there remains a risk of defects of unpermitted size arising due to local corrosion.

4.5 Summary of criticism of ASEA's corrosion tests and the Reference Group's review thereof

The main points in my criticism of ASEA's corrosion tests on isostatically pressed aluminium oxide for waste canisters and the Reference Group's evaluation of these tests can be summarized in brief as follows:

a) The corrosion tests were not carried out under realistic conditions with respect to pressure and radiation and resultant strongly oxidizing conditions due to radiolysis. As far as the tests of delayed failure are concerned, they were carried out at 20° C instead of at the proposed temperature of 70° C.

b) The Reference Group has not given sufficient consideration to two independent reports indicating intercrystalline (intergranular) corrosion in the Al_2O_3 material, instead preferring to regard this as harmless general corrosion, whereas intercrystalline corrosion can be expected to lead to spontaneous cracking (delayed failure).

c) The Reference Group has accepted predictions of service lives of hundreds of thousands and millions of years, obtained by the application of a theory developed by Dr. S. M. Wiederhorn for the delayed failure of ceramic materials, despite the fact that Dr. Wiederhorn himself has said that his theory is not reliable for even hundreds or thousands of years.

5. Revisions of the Reference Group's final report

The Reference Group's final report existed in the form of three drafts (dated 23.10.1978, 10.1.1979 and 9.1.1980) before it achieved its final form. As soon as the Reference Group had held a preparatory discussion on the first version, ASEA rushed out to the mass media with an assurance that the aluminium oxide canister would last for 1 million years and that the waste problems of nuclear power were thereby solved. I was requested in this context to comment on ASEA's claims (appendices 1, 2). I thereby contended that service lives of millions of years had been calculated after measurements concerning short periods of time in the laboratory and with the application of a theory that could only actually be depended upon for 10-20 years, a procedure which I regarded as impossible and, to say the least, of doubtful validity. In the light of what the originator of the theory (Wiederhorn) later stated in reply to a question from the Reference Group namely that not even extrapolations to hundreds and thousands of years are reliable (appendix 3), what I said in the TV interview appears to be very balanced and well-founded.

The Reference Group's second version of the final report (dated 10.1.1979) contained demands for a number of supplementary studies as follows:

"a) Recording of K_I-V diagrams using DT specimens at 70° C in rock water to check the slope (n value) of the K_I - V curves.

b) Determination of n from the variation of the ultimate strength with the loading rate at 21° C and 70° C in rock water.

c) Experimental confirmation of the contention that K_I is independent of crack length through calibration.

d) Execution of compliance calibration.

e) Measurement of K_I values by means of the DCB and CFT methods."

These demands are based on a review of ASEA's fracture mechanics analysis by the Reference Group's ceramic experts (Roger Carlsson and co-worker Leif Hermansson, Appendix G, dated 5.1.1979).

In what was assumed to be a final discussion of the finally revised report of 18.1.1979, it was resolved that "in determining the service life of the canister, reservations shall be made in view of the fact that the fracture mechanics theories on which the evaluation is based are of relatively recent origin and of the fact

that supplementary tests have been recommended whose results can effect the evaluation". (Minutes from the meeting of the Reference Group of 18.1.1979, transcribed 24.8.1979.) However, after KBS was informed of the conclusions of the Reference Group with the attendant reservations, KBS expressed a "desire that the enquiry be deepened so that the uncertainty expressed in the reservations in the conclusion of the Reference Group can be eliminated, if possible".

In a letter to the members of the Reference Group dated 26.1.1979, its chairman states:

"Due to the uncertainty which was the cause of the reference group's reservations, the following work should be undertaken:

- ASEA should carry out the supplementary studies proposed by Roger Carlsson and Leif Hermansson in their review statement

- suitable foreign experts on the fracture mechanics of ceramics should be summoned for further discussions of delayed failure over extremely long time perspectives: Dr. Wiederhorn of the National Bureau of Standards has been mentioned as a suitable expert in this respect."

6. Consulting of American experts

The supplementary work called for by the reference group never appears to have been done. On the other hand, a letter was written to Dr. Sheldon M. Wiederhorn of the National Bureau of Standards, Washington, D.C., originator of the theory on which ASEA based it extrapolations from short-term measurements to hundreds of thousands and millions of years. Dr. Wiederhorn was invited to a discussion in Stockholm at the end of April, 1979. His reply (Appendix 3) was a disappointment, not so much because he explained that he could not come on the proposed date, which would certainly have been worse, but more because of an opinion in the matter at hand which he took the opportunity to express in his reply (Appendix 3):

Extrapolation of crack growth, or strength data to predict failure after long periods of time is a question of great concern, which will have to be solved before ceramic materials can be used for waste disposal. Using our present base of data, I am convinced extrapolations for hundreds or thousands of years are not reliable.

In other words, the originator of the theory on which ASEA has based its calculations of service lives of hundreds of thousands and millions of years himself believes that his theory cannot even be used for service life calculations of hundreds or thousands of years!

Instead of Dr. Wiederhorn, one of his former younger colleagues, Dr. Anthony G. Evans of the University of California, was then invited to a discussion of delayed failure in Al_2O_3 material of 28 August 1979 in Stockholm. Dr. Evans was able to come and also submitted a written statement.

In the draft of its report of 23.10.1978, the Reference Group, like ASEA previously, had assumed that permitted initial defects in the canister would be to detect ultrasonically. Later, the reference group found that permitted defects were too small to be able to be demonstrated in this manner 1), especially if the Al_2O_3 canisters, 3) are assumed to be surrounded by the metal shell in which they are fabricated, 2) during the ultrasonic testing procedure. In its report of 10.1.1979, the Reference Group instead ordained proof testing of all canisters to a stress of at least 100 MN/m^2. In this manner, canisters containing microcracks of unpermitted size would be induced to fail so that they could be discarded.

In his written statement, Dr. Evans recommended proof testing to 150 MN/m^2. Since proof testing can only reveal already existing cracks and Evans assumes the possibility of crack-generating local corrosion reactions around inclusions in the aluminium oxide material, he has further recommended that such inclusions be detected by acoustic means. Canisters with inclusions with a diameter > 100 µm, which could be assumed to give rise to cracks of a depth of about three times as great, would then be rejected. An assumption that only inclusions of the aforementioned size would give rise to dangerous cracks is, naturally, completely arbitrary.

In its final report, the Reference Group has concurred with Dr. Evans' recommendations. At the same time, it has, without explanation, omitted the previous requirements for supplementary studies (as per points a)-e) above).

7. Alternative methods of waste storage

7.1 Proposals presented by KBS

In my special statements concerning the KBS project, I have thus been forced, on scientific grounds, to reject all of its proposals for the final disposal of nuclear fuel waste, namely:

a) Final disposal of vitrified waste in lead-titanium canisters according to KBS I (KBS Technical Report No. 107, ref. 29)

b) Final disposal of spent nuclear fuel in copper canisters according to KBS II (KBS Technical Report No. 90, ref. 30)

c) Final disposal of spent nuclear fuel in aluminium oxide canisters according to ASEA, as set forth in the present special statement.

My analysis of the various proposals for waste disposal is based partly on geological arguments, partly on the relative impermanence of the canister materials and, finally, partly on the too high solubility of both the vitrified waste and the spent nuclear fuel. While both the titanium canister and the ASEA canister of aluminium oxide are sensitive to delayed failure due to hydrogen embrittlement and stress corrosion cracking, this is not the case with the copper canister, which is therefore the best of the proposals put forth by KBS. Although far from adequate for spent nuclear fuel, the copper canister may prove to be usable for reprocessed, vitrified waste with a low content of transuranium elements.

7.2 Storage in dry rock caverns

As I have contended repeatedly, for instance in a newspaper article (Appendix 4) 2 1/2 years ago, I believe that the waste problems of nuclear power are possible to solve, provided that the waste is subjected to reprocessing with the separation of plutonium and other transuranium elements and that these separated elements are destroyed in fast reactors (so-called burners). This reduces the problem of final storage to the storage of high-level waste (fission products, nuclear ash) with a low content of transuranium elements for a period of 500-600 years, for example in dry rock caverns above the water table. This is not a new proposal, but rather the method sketched several years ago by Professor Gerholm (31), Dr. Kåre Hannerz (2), Pelle Isberg (1) and many other capable scientists and engineers.

For the time being, both spent nuclear fuel and vitrified waste can be stored in a simple and fully safe manner in containers of heat-resistant steel in dry rock caverns or concrete bunkers (possibly decommissioned nuclear power plants) above the water table. Since the containers stay hot and dry for centuries, there is no risk of corrosion. The vitrified waste can then be deposited in final repositories. The spent nuclear fuel must, in any case, be unconditionally subjected to reprocessing. Owing to the continuous decline in radioactivity, this is more convenient the longer the spent fuel is allowed to cool.

7.3 The Synroc method

The waste glass intended as a binder for reprocessed nuclear fuel waste (nuclear ash) has been found by numerous studies in recent years not to have the low solubility that had originally been assumed. On the other hand, it has been found that certain ceramic waste bodies, based on titanates, are virtually insoluble in water. In contrast to the silicates in glass, they do not undergo weathering. A method to chemically bind the nuclear ash in insoluble synthetically fabricated materials based on titanates has been presented by the prominent Australian geochemist Professor A. E. Ringwood, who has coined the term Synroc (acronym for "Synthetic rock") for this material. Through correspondence with Professor Ringwood (Appendix 5) and after having listened to his presentation of the method in connection with his visit to Sweden in December of 1978, I have personally become convinced that there is reason here to hope for a method to bind the nuclear ash so safely in an insoluble solid body that both the incapsulation material and the imperviousness of the rock will be of subordinate importance. Professor Ringwood's preliminary results show that the synthetic minerals have a structure coinciding with that of equivalent natural, decomposition-resistant minerals and an equally high chemical resistance, determined by accelerated tests in aggressive solutions at high temperatures. Even if the synthetic waste bodies upon deposition are enclosed in the metal shells in which they are fabricated, the service life predicted for these metal shells does not have to be particularly long. If, moreover, the waste ceramic can be regarded as being insoluble in water, both present and future fractures in the rock and the flow of the groundwater will be without importance. Since it appears to be possible to bind securely not only fission products such as cesium and strontium, but also small quantities of plutonium and other transuranium elements in the minerals in question, it is possible that we have a method here for the final disposal of conventional high-level waste without the necessity of separating transuranium elements, something which the French have found to be "indispensably necessary" when it comes to borosilicate glass. Of particular Swedish interest is the fact that Professor Westermark of the Royal Institute of Technology in Stockholm has conducted fundamental studies for a number of years concerning the binding of fission products in titanates with results which confirm and complement Professor Ringwood's findings, as well as the fact that the synthetic minerals are produced by hot isostatic high-pressure compaction, a technique in which ASEA occupies a leading position in the world. In contrast to what is the case with the waste canisters of aluminium oxide advocated by ASEA and produced in accordance with this method, cracking of the waste bodies does not matter, since the material is virtually insoluble in water.

8. Declaration of voting intention in the nuclear referendum on 23 March 1980

Despite what I have said in this and earlier special statements concerning the various proposals of the KBS project for waste proposal, I would like to declare openly that I intend to vote yes to a continued expansion of nuclear power in Sweden in the nuclear referendum scheduled for 23 March, 1980, more specifically in accordance with line 1. My reasons for this are:

a) that safe methods for the handling and final storage of nuclear fuel waste will be developed, even if the KBS project has not been able to demonstrate such a method in the short time available

b) that reactor safety today is incomparably better than it was one year ago, thanks to the warning signal provided by the Harrisburg incident and the general tightening of standards to which it led.

Bibliography

1. P. Isberg, Svensk Kärnkraft, (Swedish Nuclear Power), Natur och Kultur 1976, p. 95.

2. K. Hannerz, Kärnkraftens radioaktiva avfall, ("Radioactive waste from nuclear power"), 2nd edition, ASEA-ATOM, p. 7.

3. Handling of Spent Nuclear Fuel and Final Storage of Vitrified High Level Reprocessing Waste, IV, Safety Analysis, KBS Nuclear Fuel Safety Project, fig. 3-8, p. 30.

4. G. de Marsily, E. Ledoux, A. Barbreau & J. Margat, Nuclear waste disposal: Can the geologist guarantee isolation? Science 197, No. 4303, p. 519, Aug. 5, 1977.

5. B. L. Cohen, High-level radioactive waste from lightwater reactors, Reviews of Modern Physics 49 (1977) 1.

6. W. D. Bond, H. O. Claiborne & R. E. Leuze, Methods for the removal of actinides from high-level wastes, Nuclear Technology 24 (1974) 362.

7. G. Guillaume, Problèmes posés par la présence d'éléments transuraniens dans les détachets du retraitement de combustible nucléares, Bulletin d'Information Scientifiques et Techniques, No. 217, Sept. 1976, p. 31 Commissariat à l'Energie Atomique.

8. K. Lundgren, Deponerad strålningsenergi utanför Al_2O_3-kapsel med utbrända bränslestavar, ("Deposited radiant energy outside Al_2O_3 canister with spent nuclear rods"), ASEA-ATOM, PMRF 77-445, dated 20.10.77, distributed to the meeting of the Reference Group of 9.6.78.

9. Spent nuclear fuel and radioactive waste, Part I, Statens Offentliga utredningar (SOU) 1976:30, Liber Förlag 1976, p. 35.

10. Spent nuclear fuel and radioactive waste, Part II, Statens Offentliga Utredningar (SOU) 1976:31, Liber Förlag 1976, p. 115-116.

11. J. Rydberg, Introduktion till Kärnkemin, ("Introduction to Nuclear Chemistry"), Natur och Kultur 1967, p. 253.

12. G. Wranglén, Statement of comment on findings of Aka Committee, October 1976.

13. NUCLEAR FUEL SAFETY, Handling of Spent Nuclear Fuel and Final Storage of Vitrified High Level Reprocessing Waste, II Geology, Solna 1977.

14. NUCLEAR FUEL SAFETY, Handling and Final Storage of Unreprocessed Spent Nuclear Fuel, II Technical, Solna 1978.

15. NUCLEAR FUEL SAFETY, Handling of Spent Nuclear Fuel and Final Storage of Vitrified of High Level Reprocessing Waste, VI Supplementary geological studies, Solna 1979.

16. Review statement concerning the KBS study Handling of Spent Nuclear Fuel and Final Storage of Vitrified High Level Reprocessing Waste, VI Supplementary Geological Studies. Prepared for the Swedish Nuclear Power Inspection Board by the Consultant Group for Geology Matters (S. Andersson, A. Eriksson, S. Hjelmqvist, S Huseby, P.O. Nielsen, K. Rankama, A. Wesslén, B. Åberg), Stockholm 1979.

17. N-A. Mörner, Rörelser och instabilitet i den Svenska berggrunden, ("Movements and instability in the Swedish bedrock"), KBS Technical Report No. 18, Sept. 1977.

18. N. Ingri & L-O. Öhman, Bestämning av korrosionshastigheten for Al_2O_3 i natriumväte-karbonatbuffrat, kloridhaltigt vatten vid 80°C och pH = 8.5, ("Determination of the corrosion rate for Al_2O_3 in sodium hydrogen carbonate-buffered, chloridic water at 80°C and pH = 8.5"). University of Umeå, Department of Inorganic Chemistry, 31.8.1978.

19. A. Bäcklin, A. Johansson, B. Sundqvist & L. Westerberg, Bestämning av väteprofiler i aluminiumoxid med kärnfysikaliska metoder, ("Determination of hydrogen profiles in aluminium oxide by means of nuclear physics methods"), Tandem Accelerator Laboratory University of Uppsala, 14.9.1978.

20. S. M. Weiderhorn, J. Am. Ceram. Soc. 50 (1967) 407.

21. S. M. Wiederhorn et al, J. Appl. Phys. 39 (1968) 569.

22. S. M. Wiederhorn, J. Am. Ceram. Soc. 52 (1969) 99.

23. S. M. Wiederhorn & L. H. Botz, J. Am. Ceram. Soc. 53 (1970) 543.

24. A. G. Evans & S. M. Wiederhorn, Int. J. of Fracture 10 (1974) 379.

25. S. M. Wiederhorn, "Subcritical crack growth in ceramics" in "Fracture Mechanics of Ceramics, Ed. by R. C. Bradt, DPH Hasselman & F. F. Lange, New York, Vol. 2 (1974) 613.

26. S. M. Wiederhorn, "Subcritical crack growth in glass, op cit. Vol. 4 (1978) 549.

27. A. G. Evans, Int. J. of Fracture 9 (1973) 267.

28. R. Dutton, "The propagation of cracks by diffusion", op cit. Vol. 2 (1978) 647.

29. KBS Technical Report No. 107, "Blyinfodrad titankapsel för upparbetat och glasat kärnbränsleavfall - Bedömning ur korrosionssynpunkt", ("Lead-lined titanium canister for reprocessed and vitrified nuclear fuel waste - Evaluation from the viewpoint of corrosion"). The Swedish Corrosion Institute and its reference group. Final report 25.5.1978.

30. KBS Technical Report No. 90, "Copper as an Encapsulation material for unreprocessed nuclear waste - Evaluation from the viewpoint of corrosion". The Swedish Corrosion Institute and its reference group. Situation report 31.3.1978.

31. T. R. Gerholm, Varför Kärnkraft? ("Why Nuclear Power?") KREAB, Stockholm 1977.

Appendix 1

Notes for interview statement by
Professor Gösta Wranglén, Royal Institute of Technology,
on TV news programme "Aktuellt" on 22.11.1978.

Aluminium oxide is an excellent material for many engineering applications, for example as an insulator material in spark plugs. But to guarantee a life time of millions of years, i.e. through one or more ice ages, would appear impossible to me. We are, after all, dealing with a ceramic material, in other words a porcelain-like material. It is generally known that such materials are brittle and sensitive to impact. It is also known that ceramic materials that may have held for many years can suddenly fail due to spontaneous cracking. This is due to the fact that a ceramic material always contains small cracks. These cracks grow, first slowly and unnoticeably. When a crack has reached a certain critical size, it grows rapidly and leads to failure through spontaneous cracking (a phenomenon known scientifically as "delayed failure"). The material contains small cracks from the start. Cracks can also be created during transport and handling, and perhaps also during storage through the action of groundwater. Studies at the University of Umeå have shown that a slow process of corrosion takes place in groundwater which causes pulverization of the material on the surface. This could lead to small cracks, which could then grow.

What has now been done is that various measurements have been made on the material over the space of a few months. Then, with the help of certain mathematical formulae, a life span of millions of years has been calculated for the material. Even if the calculation formulae have been shown to hold true for ten or twenty years, extrapolation to millions of years seems to be of doubtful validity, to say the least. Over this long period of time, the material is also exposed to intense atomic radiation. We still know very little about the effects of radiation on materials over long periods of time.

Stockholm 78-12-04

Appendix 2

The Reference Group - Corrosion of Incapsulation material for nuclear fuel waste
Attention Professor Einar Mattsson
The Swedish Corrosion Institute
Box 5607
S-114 86 Stockholm, Sweden

Spontaneous cracking of Al_2O_3 canister.

With this epistle, testimony is hereby submitted on the 4th of December in this year of our Lord 1978, whereby I once again declare myself an apostate from the latest prophecy of the Reference Group - a prophecy which ASEA, with its even greater strength of faith, has already managed to extend by a power of ten.

If, in this case, under some fatigue, I extend myself beyond the limit of my formal competence, this is due to the fact that I have been called a "material expert" by the far-seeing oracle at Oxenstiernsgatan i.e. the Swedish TV. I prefer to call myself a Professor of Corrosion Science, but the oracle spoke and said that Professor sounded to fancy and corrosion was too difficult a word ("what is it, do you spell it with one or two r's? The viewers have to know what we are talking about") and then it turned out as it did and in the beginning of the seance, the oracle got the idea that I was the prophet Larker.

This epistle and testimony is being sent to the same congregation who received my last, also not entirely serious letter of the 29th ult and to two brethren with special talents within the Strength of Materials.

With unreserved greetings,
I remain your
Gösta Wranglén
Professor, but not prophet.

Appendix: "Delayed failure (stress corrosion, spontaneous cracking) in Al_2O_3". Draft of 4.12.78.

Copy of letter with appendix to the member of the Reference Group and to P.-E. Ahlström, G. Blomqvist, K. Hannerz, L. Hydén, A. Johansson, H. Larker, L.-B. Nilsson, B. Widell, Prof. Janne Carlsson and Dr. Fred Nilsson, Department of Strength of Materials and Solid Mechanics, Royal Institute of Technology, Stockholm.

UNITED STATES DEPARTMENT OF COMMERCE
National Bureau of Standards
Washington, D.C. 20234

March 19, 1979

562.00

Dr. Einar Mattsson
Swedish Corrosion Institute
Box 5607
S-114 86 Stockholm
Sweden

Dear Dr. Mattsson:

I am afraid that I will not be able to attend your meeting in Stockholm at the end of April because of prior commitments in the United States. I am, however, very interested in the subject of the meeting. Extrapolation of crack growth, or strength data to predict failure after long periods of time is a question of great concern, which will have to be solved before ceramic materials can be used for waste disposal. Using our present base of data, I am convinced extrapolations for hundreds or thousands of years are not reliable. For your information, I have included, several recently published articles that bear on this subject, and may be of value in your deliberations.

Thank you for inviting me to visit Stockholm. I have always enjoyed my visits to your city and am sorry that I cannot accept your invitation at this time.

Sincerely,

Sheldon M. Wiederhorn
Fracture and Deformation Division

Enclosure

Arbetarbladet, August 11, 1977 (Swedish Newspaper)

The problems of nuclear power can be managed
by Professor Gösta Wranglén,
Royal Institute of Technology Stockholm. (Syndicated newspaper article in the Swedish Social-Democratic press)

In its present form, the Nuclear Power Stipulations Act is as constraining as a straight jacket, rendering the efficient management of nuclear waste impossible from both the technical and environmental points of view. It sets up conditions for the management of nuclear waste which are impossible to meet, but whose purpose - an absolutely safe terminal isolation of the waste - can be achieved in another manner. However, the environmental risks envolved with the nuclear waste, as well as the country's energy supply, are much too important questions to be dealt with by such an unserviceable and arbitrary instrument as the Stipulations Act. Fortunately, this hastily pieced-together legislation is, in contrast to the laws of nature, neither eternal nor inalterable. It also lacks counterparts in other countries. In the application of the Act, in so far as it can and should be applied at all, the requirements on waste management imposed by the laws of nature, should, in any case, be accorded decisive importance.

According to the Stipulations Act adopted by the Swedish Parliament in April of 1977, those nuclear reactors which are currently under construction may not be loaded with nuclear fuel unless certain conditions are fulfilled. The owner of the reactor may not begin fueling until he has:

either: "produced an agreement which adequately satisfies the requirement for the reprocessing of spent nuclear fuel and has demonstrated how and where an absolutely safe final storage of the high-level waste obtained from reprocessing can be effected,"

or: "has demonstrated how and where an absolutely safe final storage of spent unreprocessed nuclear fuel can be effected."

In actual fact, neither "spent unreprocessed nuclear fuel" nor "the high-level waste obtained from reprocessing" is suitable for "final storage". With the large quantities involved in both cases, it is impossible to accomplish such a final storage in an "absolutely safe" manner within reasonable economic limits.

The laws of nature, which must always guide our actions, demand, in contrast to the Stipulation Act:

1) supervised storage of at least most of the spent fuel or high-level waste

2) separate storage of different components of spent fuel or high-level waste

3) dry storage instead of the wet storage, which is always the result of a final disposal

4) that the final storage of hazardous waste be eliminated entirely or at least limited to the minimum possible fraction of the waste.

REPROCESSING IS PREFERABLE

Like all other handling of spent nuclear fuel and nuclear waste, final storage should be supervised to as great an extent as possible. This is the only way that any problems that arise can be corrected and that new technological developments can be put to use. The reprocessing of spent nuclear fuel, the separation of transuranium elements, the operation of breeder reactors, etc are supervised processes that can be mastered and, when necessary, modified and improved. Waste management should be therefore be based on reprocessing, whereby uranium and plutonium are separated and reused as new fuel. In addition, transuranium elements should be separated from the high-level waste. If the transuranium elements can be destroyed in, for example breeder reactors or hydrogen fusion reactors, then the storage requirement is reduced to a supervised storage of nuclear ash (fission products) for about 500 years.

SUPERVISION

The need for supervision is generally motivated by the fact that the radioactive material is just that - active. Final storage can therefore not be regarded as a one-time measure, which humanity can then ignore. Although the process of radioactive decay follows strict laws and is, unlike other processes, completely independent of external conditions, its multifarious and long-range consequences are difficult, not to say impossible, to predict. The radiation causes changes in the active material itself, in the encapsulation material and in the immediate environment, especially if it is wet.

Separate storage involves treating and storing different components in the spent fuel separately, each according to its nature. Table 1 shows a typical case (boiling water reactor with burnup 28 500 MWd per tonne of uranium) with quantity and toxicity for various components in the spent fuel, corresponding to 1 tonne of uranium in the original fuel. Toxicity is expressed as the number of possible cancer cases per year caused by ingestion or inhalation. The following conversion factors have been used: 1 cancer dose = 2 500 m^3 of water of maximum permissible concentration (MPC). The cancer risk per rem = 1:100 000.

Table 1. Quantity (weight) and toxicity of different components of spent nuclear fuel, figured per tonne of uranium in the original fuel.

Component	Weight	Toxicity in cancer doses per year			
		after 2 years following ingestion 1)	inhalation 2)	after 500 years following ingestion 1)	inhalation 2)
Plutonium					
Other transuranium elements					
Nuclear ash					

milj = mill. Fresh nuclear fuel 1000 kg

1) Source E. Guillaume, BIST, No. 217, Sept. 1976 2) Source B. Cohen, Scientific American, June 1977

UNSUITABLE MIXTURE

It is obviously unsuitable to store large quantities of uranium, with relatively very low toxicity together with very small quantities of other components, each of which is highly toxic in its own way. Nor is it appropriate to store together with the nuclear ash plutonium and other transuranium elements which, if they cannot be destroyed, must be kept in safely isolated for all future time.

In conventional reprocessing, uranium and plutonium are separated virtually completely. Because these components are used as new fuel, they are destroyed and do not have to be terminally isolated. The high-level waste obtained from reprocessing consists (per tonne of uranium) of 29 kg of nuclear ash + 1 kg of uranium + 1 kg of transuranium elements.

Transuranium elements (also called actinides) should be separated from this high-level waste and destroyed or stored separately, Guillaume (reference according to footnote to table 1) considers separation of transuranium elements from the high-level waste to be "indispensably necessary". From this, it follows that direct disposal of fuel must be regarded as out of the question.

SUITABLE MEASURES

The present Swedish nuclear power programme with 13 reactors will, when completed, consume 300 tonnes of uranium per year. After reprocessing and separation of transuranium elements, the quantities given in table 2 are obtained. Suitable measures for each component are also specified there.

Table 2. Quantity (weight) and suitable measure for different components of spent nuclear fuel, corresponding to 300 tonnes of uranium in new fuel per year.

Components	Quantity per year	Suitable measure
Uranium	288.3 t	Use as new fuel
Plutonium	2 700 kg	Use as new fuel
Other		
Transuranium elements	300 kg	Destruction in breeders or final storage.
Nuclear ash for	8.7 t = 100 t	Supervised storage
	waste glass	500 years.

The reprocessing of spent nuclear fuel and separation and destruction of transuranium elements is planned to be carried out on a commercial scale in both Western Europe and the Soviet Union, and will therefore be able to be contracted for there. The latter alternative (Soviet Union) appears to be preferable, since land transports can then be relied on. Sea transports always entail a

risk of shipwreck and thereby an unintentional final disposal under unacceptable conditions. One year's production of Swedish nuclear waste corresponds to the maximum permissible concentration (MPC) in the entire Baltic Sea and would, due to the enrichment of, e.g. strontium-90 in bone tissue, probably make fishing impossible for hundreds of years. Pending the construction of plants for reprocessing etc., spent nuclear fuel should be stored dry in rock caverns or concrete bunkers.

ABSOLUTELY SAFE FINAL DISPOSAL

The nuclear ash, which does not remain hazardous for all future time, should under all circumstances be stored dry and under supervision. It can be mixed with molten glass and cast into containers of fireproof steel, which are then placed in drained rock caverns. The radiation from the nuclear ash would keep these steel containers hot and dry for centuries so that they would not rust. (Consider, for example, the 1600 year old, non-rusting iron column in Delhi in India, which, thanks to solar heating during the day in combination with its large mass, stays hot and dry during the night as well.) After 500 years, the nuclear ash will be virtually harmless and can be deposited in the bedrock without risk. With early final disposal in the bedrock, however, radiation will cause radiolysis of the surrounding water and thereby corrosion of the storage containers. This will give rise to the risk of dispersal of the initially extremely hazardous contents. Thus, radiation prevents corrosion in the case of dry storage, but causes corrosion in the case of wet storage. The choice of storage method is therefore obvious.

THE AUSTRALIAN NATIONAL UNIVERSITY
RESEARCH SCHOOL OF EARTH SCIENCES
INSTITUTE OF ADVANCED STUDIES · P.O. BOX 4 · CANBERRA 2600
TELEPHONE : CANBERRA 49 3406 · TELEGRAMS : NATUNIV · TELEX 62693

Professor Östa Wranglén, Director,
Department of Applied Electrochemistry & Corrosion Science,
Royal Institute of Technology,
100 44 STOCKHOLM 70,
SWEDEN.

18 September, 1978

Dear Professor Wrangler,

Thank you for your letter and the enclosures which I found most interesting and instructive - particularly the discussions of corrosion of metallic lining. I think that we are in essential agreement on many issues, particularly with regard to direct disposal of spent fuel rods. I do not believe that this policy will survive.

I am, however, more optimistic than you about burying waste at very great depths in suitable geological environments, even if they do permit limited access of water. This is because the mineral assemblage within which we proposed to incorporate radwaste is much more stable and insoluble than borosilicate glasses.

The booklet which I prepared was at a semi-popular level and was written partially with the objective of trying to achieve a more rational level of discussion of this subject in Australia. The radwaste disposal issue raises strong emotions here on both sides of the fence and the country seems to be almost hopelessly polarized about nuclear power.

I have a considerable amount of experimental data on SYNROC and will be preparing a technical paper around November. We have now settled upon a fairly narrow range of chemical and mineralogical compositions, very different from anything the Americans have come up with, despite some claims to the contrary. Currently we are testing SYNROC and borosilicate glasses under accelerated leaching conditions including subjecting to water at high pressure and temperatures (e.g. 400°C, 100-1000 bars). We find that glasses are very unstable under these conditions and that the mechanisms of breakdown differ from those which are involved in the conventional water-leaching experiments at 100°C. Although our results are preliminary, it looks as if SYNROC will prove to be greatly superior to glass.

I am now proposing to make SYNROC by hot-pressing near the solidus. Under such conditions, all loss of Ru, Cs and I can be prevented, whilst a well crystallized, mechanically strong synthetic rock of low porosity can be produced.

The leading organisation for this kind of hot-pressing technology is of course, ASEA and I would like to explore the possibility of collaborative research with them. It seems to me that their background in this area and our experience with the relevant phase equilibria could be complementary. I would be grateful if you could let me know the name of the appropriate ASEA executive to approach; indeed, I would welcome the opportunity to visit Sweden to lecture on the subject and to consult with those working in the field.

Yours sincerely,

Ted Ringwood

A.E. Ringwood
Director
Research School of Earth Sciences

FÖRTECKNING ÖVER KBS TEKNISKA RAPPORTER

1977-78

TR 121 KBS Technical Reports 1 - 120.
Summaries. Stockholm, May 1979.

1979

TR 79-28 The KBS Annual Report 1979.
KBS Technical Reports 79-01--79-27.
Summaries. Stockholm, March 1980.

1980

TR 80-01 Komplettering och sammanfattning av geohydrologiska undersökningar inom sternöområdet, Karlshamn
Lennart Ekman
Bengt Gentzschein
Sveriges geologiska undersökning, mars 1980

TR 80-02 Modelling of rock mass deformation for radioactive waste repositories in hard rock
Ove Stephansson
Per Jonasson
Department of Rock Mechanics
University of Luleå

Tommy Groth
Department of Soil and Rock Mechanics
Royal Institute of Technology, Stockholm
1980-01-29

TR 80-03 GETOUT - a one-dimensional model for groundwater transport of radionuclide decay chains
Bertil Grundfelt
Mark Elert
Kemakta konsult AB, January 1980

TR 80-04 Helium retention
Summary of reports and memoranda
Gunnar Berggren
Studsvik Energiteknik AB, 1980-02-14

TR 80-05 On the description of the properties of fractured rock using the concept of a porous medium
John Stokes
Royal Institute of Technology, Stockholm
1980-05-09

TR 80-06 Alternativa ingjutningstekniker för radioaktiva jonbytarmassor och avfallslösningar
Claes Thegerström
Studsvik Energiteknik AB, 1980-01-29

TR 80-07 A calculation of the radioactivity induced in PWR cluster control rods with the origen and casmo codes
Kim Ekberg
Studsvik Energiteknik AB, 1980-03-12

TR 80-08 Groundwater dating by means of isotopes
A brief review of methods for dating old groundwater by means of isotopes
A computing model for carbon - 14 ages in groundwater
Barbro Johansson
Naturgeografiska Institutionen
Uppsala Universitet, August 1980

TR 80-09 The Bergshamra earthquake sequence of December 23, 1979
Ota Kulhánek, Norris John, Klaus Meyer, Torild van Eck and Rutger Wahlström
Seismological Section, Uppsala University
Uppsala, Sweden, August 1980

TR 80-10 Kompletterande permeabilitetsmätningar i finnsjö-området
Leif Carlsson, Bengt Gentzschein, Gunnar Gidlund, Kenth Hansson, Torbjörn Svenson, Ulf Thoregren
Sveriges geologiska undersökning, Uppsala, maj 1980

TR 80-11 Water uptake, migration and swelling characteristics of unsaturated and saturated, highly compacted bentonite
Roland Pusch
Luleå 1980-09-20
Division Soil Mechanics, University of Luleå

TR 80-12 Drilling holes in rock for final storage of spent nuclear fuel
Gunnar Nord
Stiftelsen Svensk Detonikforskning, september 1980

TR 80-13 Swelling pressure of highly compacted bentonite
Roland Pusch
Division Soil Mechanics, University of Luleå
Luleå 1980-08-20

TR-80-14 Properties and long-term behaviour of bitumen and radioactive waste-bitumen mixtures
Hubert Eschrich
Eurochemic, Mol, October 1980

TR 80-15 Aluminium oxide as an encapsulation material for unreprocessed nuclear fuel waste - evaluation from the viewpoint of corrosion
Final Report 1980-03-19
Swedish Corrosion Institute and its reference group

TR 80-16 Permeability of highly compacted bentonite
Roland Pusch
Division Soil Mechanics, University of Luleå
1980-12-23

TR 80-17 Input description for BIOPATH
Jan-Erik Marklund
Ulla Bergström
Ove Edlund
Studsvik Energiteknik AB, 1980-01-21

TR 80-18 Införande av tidsberoende koefficientmatriser i BIOPATH
Jan-Erik Marklund
Studsvik Energiteknik AB, januari 1980

TR 80-19 Hydrothermal conditions around a radioactive waste repository
Part 1 A mathematical model for the flow of groundwater and heat in fractured rock
Part 2 Numerical solutions
Roger Thunvik
Royal Institute of Technology, Stockholm, Sweden
Carol Braester
Israel Institute of Technology, Haifa, Israel
December 1980

TR 80-20 BEGAFIP. Programvård, utveckling och benchmarkberäkningar
Göran Olsson
Peter Hägglöf
Stanley Svensson
Studsvik Energiteknik AB, 1980-12-14

TR 80-21 Report on techniques and methods for surface characterization of glasses and ceramics
Bengt Kasemo
Mellerud, August 1980

TR 80-22 Evaluation of five glasses and a glass-ceramic for solidification of Swedish nuclear waste
Larry L Hench
Ladawan Urwongse
Ceramics Division
Department of Materials Science and Engineering
University of Florida, Gainesville, Florida
1980-08-16

TR 80-23 Exact solution of a model for diffusion in particles and longitudinal dispersion in packed beds
Anders Rasmuson
Ivars Neretnieks
Royal Institute of Technology, August 1979

TR 80-24 Migration of radionuclides in fissured rock - The influence of micropore diffusion and longitudinal dispersion
Anders Rasmuson
Ivars Neretnieks
Royal Institute of Technology, December 1979

TR 80-25 Diffusion and sorption in particles and two-dimensional dispersion in a porous media
Anders Rasmuson
Royal Institute of Technology, January 1980